6223490

Robust Reed Solomon Coded MPSK Modulation

by

Emir Mauludi Husni

Thesis submitted to the University of Surrey
for the degree of
Doctor of Philosophy

Centre for Communication Systems Research
University of Surrey
Guildford, Surrey
United Kingdom

July 1997

SUMMARY

Much work has been done on design of efficient coded modulation schemes since the publication of [Ungerboeck, 1982] for trellis coded modulation and [Imai & Hirakawa, 1977] for block coded modulation. Recently, increasing interest in digital mobile radio and indoor wireless systems has led to the consideration of coded modulation designs for combating fading channels.

In this research, it is intended to present results of an investigation of the construction of Reed Solomon coded MPSK modulation which is robust for the Gaussian channel and a Rayleigh fading channel. Two approaches have been applied to Reed Solomon coded modulation. First, a Reed Solomon code was combined with MPSK signal set using Gray code mapping; this was called Reed Solomon coded modulation not based on set partitioning. This approach was the baseline scheme which would be compared with the proposed approach, namely Reed Solomon coded modulation based on set partitioning.

The second approach to coded MPSK with $M = 2^m$ was multilevel Reed Solomon coding. In this case, each of the m bits defining an MPSK symbol was coded and decoded by different Reed Solomon codecs. The set partitioning principle was applied to define subsets with distances Δ_i, $(i = 1$ to $m)$ that were nondecreasing with i. Each of the m bits defined a subset and was decoded in multistage decoding schemes. The novel idea here was that in the receiver, we used a rotated 2^{m+1}-PSK detector if the transmitter used a 2^m-PSK modulator.

The designs of Reed Solomon coded modulation schemes for the Gaussian channel and a Rayleigh fading channel (i.e. choice of the code configurations which were suitable for this channel) have been studied. The performance of Reed Solomon coded modulation based on set partitioning was compared with Reed Solomon coded modulation not based on set-partitioning, then with multilevel Reed Solomon coded modulation using Gray mapping and finally with coded modulation schemes using binary codes, Reed Muller codes.

It has been shown that over the Gaussian channel and a Rayleigh fading channel, Reed Solomon coded modulation based on set partitioning is better than several alternatives, such as schemes not based on set partitioning, multistage Reed Solomon coded

modulation based on Gray mapping and Reed Muller coded modulation. It was found that good codes for a Rayleigh fading channel have configurations in which all component codes have the same minimum Hamming distance because the fading phase is uniformly distributed random process. Therefore, by matching configurations of component codes with the channel characteristics, it was shown that Reed Solomon coded modulation based on set partitioning was robust for the Gaussian and a Rayleigh fading channel.

Reed Solomon coded modulation schemes were applied to Orthogonal Frequency Division Multiplexing (OFDM) transmissions. The main disadvantage of OFDM systems is that they have high Peak-to-Mean Envelope Power Ratio (PMEPR). A scheme for reducing the PMEPR of OFDM systems was investigated. Multiphase complementary code pairs of length 2 are proposed to reduce the PMEPR of MPSK and QAM OFDM. Concatenated codes with Reed Solomon coded modulation as an inner code and an RS(511, 443) code as an outer code are proposed as coding schemes for OFDM systems.

ACKNOWLEDGEMENTS

TABLE OF CONTENTS

CHAPTER 1

INTRODUCTION

In today's highly competitive communication industry great emphasis is placed upon the reliable and economical transmission of digital data. From this underlying necessity there has developed the need for reliable communication systems and efficient modulation and coding schemes. Error control coding has played an important role since Shannon's paper [Shannon, 1948] presented a statistical formulation of the communication problem. If the rate of information transmission is over a certain limit, the so-called channel capacity, then successful data transmission cannot be reliably achieved. To counteract the effects of the channel, redundancy is often introduced into the transmissions, or error control coding used, to deliver the information with a minimum number of errors.

The purpose of the error control is to detect or to detect and correct errors and this can be achieved using two traditional techniques: Forward Error Correction (FEC) and Automatic Repeat reQuest (ARQ). In FEC the data is transmitted and in the presence of errors an attempt is made to correct the errors at the receiving end. In an ARQ system, if the errors are detected a re-transmission is requested from the message transmitter. One of the differences between the two systems is that in FEC the transmission is one way whilst an ARQ system requires a two way path to exist. Also, ARQ systems which require error detection only are much simpler than FEC systems which require error correction. In this thesis only FEC systems will be considered.

1.1. CODING SYSTEMS

The channel encoder performs all the digital processing needed to prepare the source data for modulation. We define the encoder here in a general way to encompass a variety of possible operations. In the simplest case, where no redundancy is to be added and the transmission in the physical channel is to use a binary signalling alphabet, the encoder has no function. But if the transmission alphabet is to be non-binary, the encoder performs the necessary binary-to-non-binary symbol conversion.

In a system using error control coding, the encoder accepts information bits and adds redundancy, producing encoded data. For encoding with a binary block code, the encoder accepts information in successive k-bit blocks and for each k bits generates a block of n bits, where $n \geq k$. The n-bit block is called a codeword. If the block coding is non-binary, M-ary where $M = 2^m$, and m is an integer greater than 1, the encoder accepts information bits in block of km bits each and produces encoded block of n M-ary symbols each.

For encoding with a binary convolutional code, the information stream is fed to the encoder k bits at a time, the encoder operates on the current k-bit input and some number of immediately preceding k-bit inputs to produce n output bits; a convolutional code encodes the information in a manner where the output is dependent on a number of previous blocks.

We define the dimensionless ratio

$$R = \frac{k}{n}$$

as the rate of the code, or simply the *code rate*. The code rate in practice usually lies between one half and near unity [Farrell, 1990] and is always less than unity.

A block diagram of a general coding system is shown in Figure 1.1. Raw data enters the encoder which adds redundancy to the data to be transmitted in a well-defined manner. This is done to allow the decoder at the receiver site to correct errors that may have been caused by the transmission channel. The encoded data is then used to modulate a carrier for transmission over the channel. The modulation scheme varies according to the application.
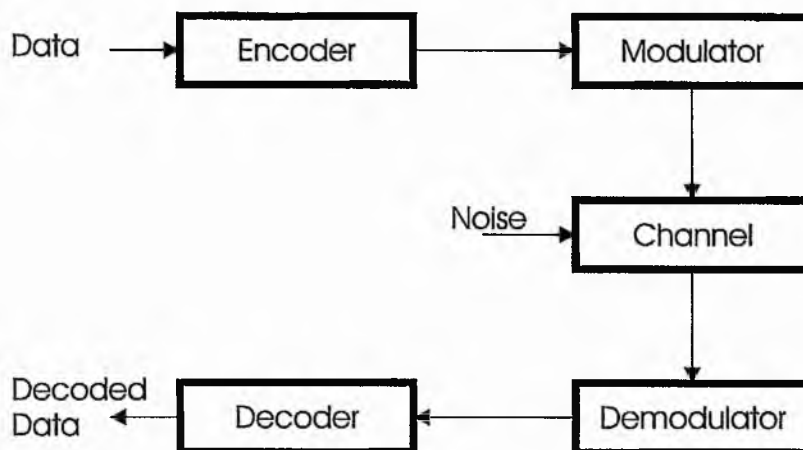
Figure 1.1 Coding system

The channel can suffer from a variety of noise effects which result in either a Gaussian channel or in non-Gaussian error channels including a bursty error channel. In a Gaussian error channel the noise amplitude is a normally (Gaussian) distributed random variable, and the errors which occur on the channel are independent from one symbol to the next. For a burst error channel, the noise is usually impulsive and the errors will occur in bursts of varying lengths followed by long intervals of no or relatively few errors.

At the receiver, the demodulator will attempt to recover the transmitted waveform from the channel output and can also give additional information to the decoder which may assist it in decoding. The decoder will generate an estimate of the original information data. In the absence of errors the received word is decoded back into the original transmitted data. However, if errors are occurred and detected by the decoder, then the decoder will attempt to correct them.

1.2. MODULATION

The digital modulation process transforms digital symbols into waveforms that are compatible with the characteristics of the channel. For bandpass modulation, the desired information signal modulates a sinusoid called a carrier which is converted to an electromagnetic field for propagation to the desired destination by radio transmission. A sinusoid has just three features that can be used to distinguish it from other sinusoids:

amplitude, frequency, and phase. Thus digital bandpass modulation can be defined as the process whereby the amplitude, frequency, or phase of an RF carrier, or a combination of them is varied in accordance with the digital information to be transmitted.

When the receiver exploits knowledge of the carrier's phase to detect the signals, the process is called coherent demodulation; such as phase shift keying (PSK), frequency shift keying (FSK), amplitude shift keying (ASK), continuous phase modulation (CPM), and hybrid combinations. PSK has the advantage of a constant envelope and in comparison with frequency shift keying (FSK) it provides better spectral efficiency (number of transmitted bit $\sec^{-1}$ per unit of radio-frequency bandwidth). Spectral efficiency is an important parameter in the choice of modulation type: the benefit increases as spectral occupation decreases and the number of such bandwidth users increases, that is the throughput is high.

When the source-emitted symbols are used to change the phase of a bandpass signal of period T, we have a digital phase modulation in which a sequence of K messages is represented by the signal:

$$v_\xi(t) = \text{Re}\left\{ \sum_{k=0}^{K-1} \xi_k s(t - kT) e^{j2\pi f_0 t} \right\}, \qquad 0 \le t < KT \qquad (1.1)$$

where $\xi_k = e^{j\varphi_k}$ and φ_k takes values in the set

$$\left\{ \frac{2\pi}{M}(i-1) + \Phi \right\}_{i=1}^{M},$$

and Φ is an arbitrary constant phase. When $s(t)$ is a rectangular pulse of amplitude A, that is $s(t) = Au_T(t)$, the modulation is called PSK, and the signal of (1.1) becomes

$$v_\xi(t) = A \sum_{k=0}^{K-1} u_T(t - kT)\cos(2\pi f_0 t + \varphi_k) = I(t)\cos 2\pi f_0 t - Q(t)\sin 2\pi f_0 t,$$

where

$$I(t) = A \sum_{k=0}^{K-1} \cos\varphi_k u_T(t - kT),$$

$$Q(t) = A \sum_{k=0}^{K-1} \sin \varphi_k u_T (t - kT).$$
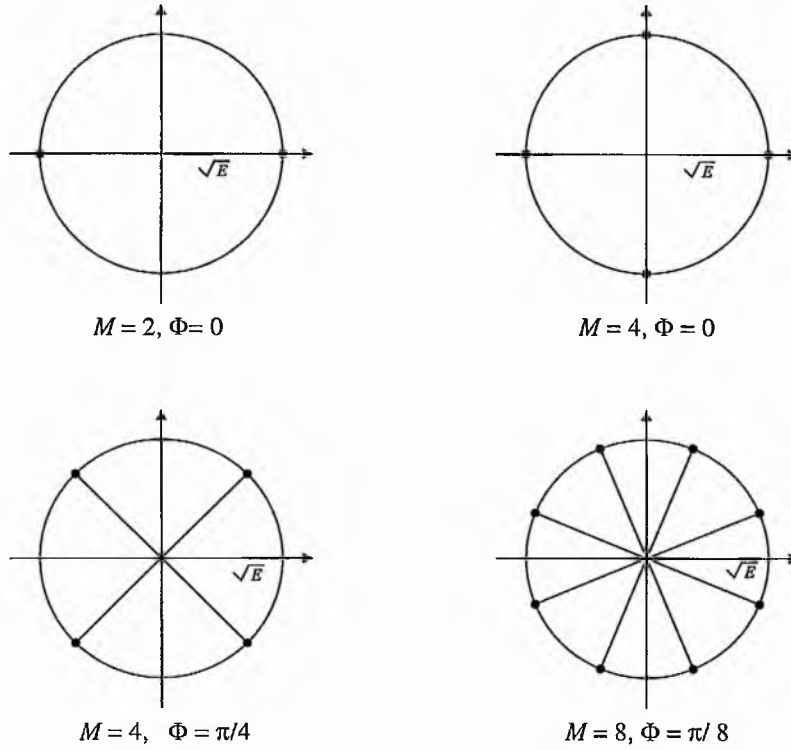
Figure 1.2 Geometrical representation of PSK signal constellations

The signal waveforms that are used by the transmitter have equal energy $E = A^2 T / 2$. The geometric representation of several MPSK signal sets is shown in Figure 1.2. The signals lie on a circle. As M increases the dimensionality of the signal space does not change, and this means a bandwidth efficiency increasing with M. On the other hand the radius of the circle depends on the signal energy. Therefore, when M is increased the signals get closer if the energy is kept constant. Consequently, the same error performance can be maintained only with an increase of the transmitted energy.

The simplest case in PSK modulation is binary PSK (BPSK). In BPSK modulation, the modulating data signal shifts the phase of the carrier to one of two states, either zero or π (180º). Figure 1.3 shows a BPSK modulator.

In a quaternary PSK (QPSK) modulation, the modulator takes two input bits at a time and produces one of the four possible phases of the carrier $A\cos 2\pi f_0 t$. Therefore, a signalling rate reduction of one-half is achieved. The QPSK modulator is shown in Figure 1.4. This modulator can be considered as made up of two BPSK modulators whose output are added together. The two quadrature channels are usually denoted as the I channel (in-phase channel) and the Q channel (quadrature channel), respectively.
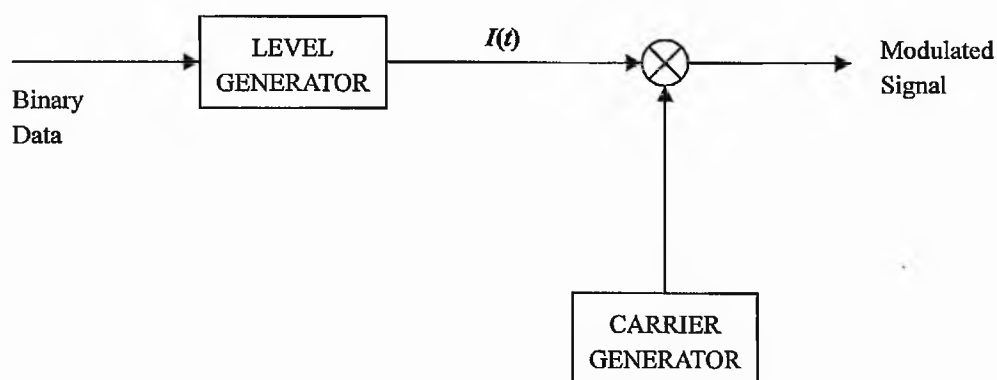
Figure 1.3 BPSK modulator
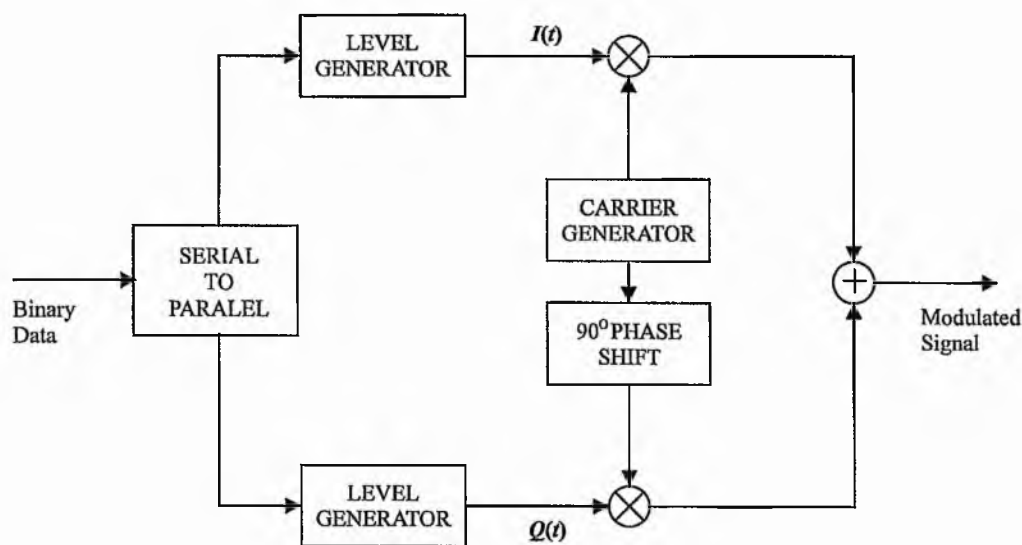
Figure 1.4 QPSK modulator

The theoretical spectral efficiency of BPSK modulation is 1 bit sec^{-1} Hz^{-1}. For QPSK modulation, it is 2 bit sec^{-1} Hz^{-1}. In practice, taking account of the imperfections of the transmission channel (such as non-optimal filtering and non-linearities), the spectral efficiency is of the order of 0.7 - 0.8 bit sec^{-1} Hz^{-1} for BPSK and 1.4 - 1.6 bit sec^{-1} Hz^{-1} for QPSK [Maral and Bousquet, 1993].

Bandpass modulation can provide other important benefits in signal transmission. If more than one signal utilises a single channel, modulation may be used to separate the different signals. In such a technique, known as frequency-division multiplexing (FDM), the bandwidth of a channel is divided into sub-bands; each sub-band is assigned to the carriers transmitted at different frequencies.

In the mobile communication environment simultaneously containing multiple paths, interference and impulsive parasitic noise, transmission of high bit-rates (several Mbit sec^{-1}) is a risky process. An approach consists in splitting the information to be transmitted into a large number of elementary sub-channels each carrying a low bit-rate. This transforms a highly-selective wide band channel into a large number of non-selective narrow-band channels which are frequency-multiplexed (FDM).

In a normal FDM system, the many carriers are spaced apart in such a way that the signals can be received using conventional filters and demodulators. This results in a lowering of spectral efficiency. The principles of an FDM system which is particularly effective from the point of view of the spectrum is known as Orthogonal FDM (OFDM). It is possible, however, to arrange the carriers in OFDM signals so that the sidebands of the individual carriers overlap and the signals can still be received without adjacent carrier interference. In order to do this the carriers must be mathematically orthogonal. OFDM systems will be described more fully later in chapter 6.

1.3. MULTILEVEL MODULATIONS

Multilevel modulations are used to carry several bits in a single signal without bandwidth penalties in which the transmitted signal can take M different values (M = 4, 8, 16, 32, etc.). Two popular ways to expand the signal constellation without bandwidth penalties are to adopt **M-ary Phase Shift Keying (MPSK)** and **Quadrature Amplitude Modulation (QAM)**.

In MPSK, a single transmitted signal can take M different phase values, and the bandwidth depends on the signalling rate, not on the number of levels. Figure 1.5 shows the signal space diagram for MPSK. The shortest distance from a signal point to the edge of a demodulator decision boundary is proportional to $\sin(\pi/M)$. The value of signal energy which is required to maintain the symbol error rate increases substantially as the number of levels increases. In the case where the predominant errors are corruptions from the transmitted point to one of its nearest neighbours (i.e. at low error rates), it needs to be increased by a factor of $1/\sin^2(\pi/M)$. For large M, this amounts to an increase of 6 dB each time M is doubled [Proakis, 1995].
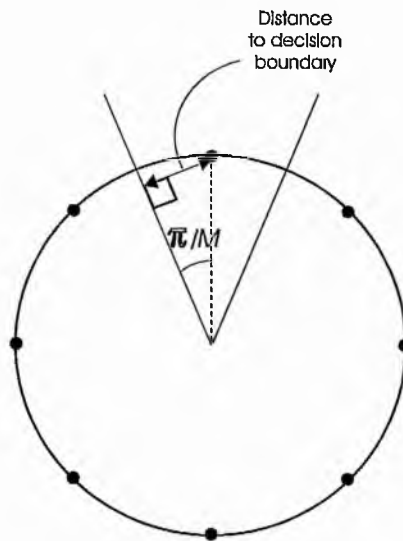
Figure 1.5 Demodulator decision boundaries for MPSK

We also can use QAM to expand the signal constellation without bandwidth penalties. Two signals in phase quadrature are combined such that the resultant can take a large number of discrete amplitude and phase combinations. Figure 1.6 shows a 16-level QAM signal constellation. Then in Figure 1.7 the number of points in the constellation are doubled with approximately the same mean symbol energy by insertion of a number of intermediate points. The distance between the points is now reduced by a factor of √2, so that signal energy must be doubled to maintain the same symbol error rate. In other words, each doubling of M requires a 3 dB increase in E_b/N_0 for the same symbol error rate, i.e. a 3 dB coding loss, in the limit of large M [Proakis, 1995].
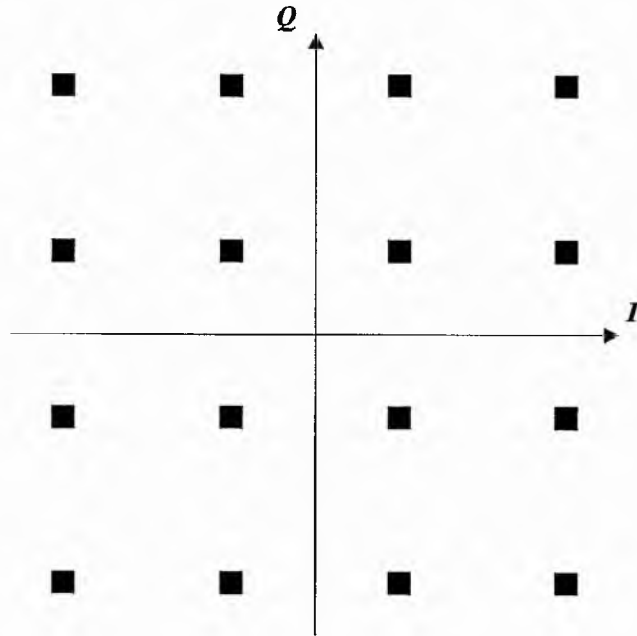
Figure 1.6 A 16-level QAM constellation
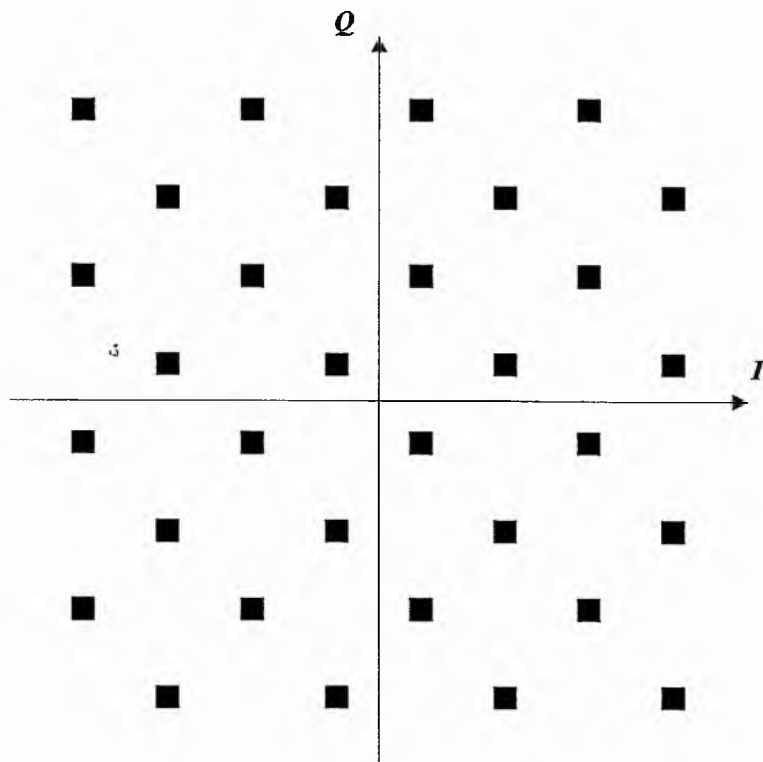
Figure 1.7 A 32-level QAM constellation

It can be seen that the losses of expanding the signal set using QAM are less severe than those resulting from the use of MPSK. On the other hand, MPSK has a constant envelope signal, which may pose fewer problems in many applications.

In this thesis, error control coding and modulation are combined to improve the reliability of a digital transmission system without increasing the transmitted power or the required bandwidth. The basic idea of combined coding and modulation will be discussed in chapter 2.

Here, Reed Solomon codes, which are an important subclass of non-binary Bose-Chaudhuri-Hocquenghem (BCH) codes, are used for error control coding because they can cope with a range of error conditions and they have been widely implemented for communication purposes. Multilevel MPSK modulations are used to expand the signal constellation without bandwidth penalties.

1.4. THESIS OUTLINE

Following the introduction chapter, this thesis will show how the Reed Solomon coded modulation was developed. Chapter 2 describes the fundamental principles of combined coding and modulation. These include a basic introduction to trellis coded modulation, block coded modulation and multistage decoding methods for block coded modulation decoding. Reviews of Reed Solomon codes and Reed Muller codes which were used for combined coding and modulation are also given.

To develop Reed Solomon coded MPSK modulation schemes, two approaches are considered: Reed Solomon coded modulation not based on set partitioning and Reed Solomon coded modulation based on set partitioning which is proposed as a robust block coded MPSK modulation. Chapter 3 describes three methods generalising the first approach, followed by the explanation of the second approach. The encoding and the decoding designs are included in the descriptions. In the decoding section, the novel idea is proposed that in the receiver, a rotated 2^{m+1}-PSK detector should be used if the transmitter uses a 2^m-PSK modulator. This section also discusses the multistage decoding procedure used for this approach and Reed Solomon approaches for multistage decoding. Finally, distance considerations for the second approach are given.

Chapter 4 studies the designs of coded modulation schemes over the Gaussian channel (i.e. choose the code configurations which are suitable for this channel) and analyses the error performance over the Gaussian channel of two approaches as stated above. These schemes will be compared with multilevel Reed Solomon coded modulation using Gray mapping and with coded modulation schemes using binary codes, Reed Muller codes.

A design study of coded modulation schemes (i.e. choice of the code configurations which are suitable for this channel) and the error performance analysis for a Rayleigh fading channel are given in chapter 5. The basic principles and simulation model of a Rayleigh fading channel are given in this chapter. Then the schemes' designs for this channel are studied. Finally the error performance of those schemes as stated above is analysed. These schemes are compared with multilevel Reed Solomon coded modulation using Gray mapping and with coded modulation schemes using binary codes, Reed Muller codes. The results of these schemes are also compared with bit-interleaved coded modulation which is proposed in [Zehavi, 1992] and with robust coded modulation proposed in [Sundberg & Seshadri, 1993].

The applications of Reed Solomon coded modulation are given in chapter 6: Reed Solomon coded modulation is used as an inner code for concatenated schemes which are also using Reed Solomon codes as the outer code. Then concatenated schemes is applied to OFDM systems. Chapter 6 describes several approaches of OFDM system, studies the designs of Reed Solomon-Reed Solomon concatenated schemes which are applied to an OFDM system then, studies the approach to OFDM problem in mobile communications which is peak-to-mean envelope power ratio. Here complementary code pairs of length 2 are proposed as an approach to this problem.

The thesis ends with a conclusion chapter which looks back on the contributions made in this thesis. The second part of the chapter reflects upon the possible future avenues for research.

1.5. ORIGINAL WORK

The original work in this thesis can be summarised as follows:

- Development of Reed Solomon coded modulation based on set partitioning: the encoder, a multistage decoding approach, the demodulator, and the detector.

- Development of a multistage decoding approach for Reed Solomon coded modulation based on set partitioning.

- Novel idea of the detector; a rotated 2^{m+1}-PSK detector is used if the transmitter uses a 2^m-PSK modulator.

- The designs for Reed Solomon coded modulation based on set partitioning over the Gaussian channel.

- The designs for Reed Solomon coded modulation based on set partitioning over a Rayleigh fading channel.

- Development of robust Reed Solomon coded modulation.

- Establishment of performance relative to other baseline schemes.

- Development of peak-to-mean envelope power ratio reduction using complementary code pairs of length 2.

- Development of concatenated schemes using Reed Solomon coded modulation and a Reed Solomon outer code.

Publications and presentations include:

Fifth ESA International Workshop on Digital Signal Processing Techniques Applied to Space Communications, Sitges, Barcelona-Spain, September 1996.

IMSC'97, International Mobile Satellite Conference 1997, Pasadena, California-USA, June 1997.

Fourth International Symposium on Communication Theory and Applications, Charlotte Mason College, Lake District-UK, July 1997.

Sixth IMA Conference on Cryptography and Coding, Royal Agricultural College, Cirencester-UK, December 1997.

CHAPTER 2

COMBINED CODING
AND MODULATION

System trade-offs are fundamental to all digital communication designs. Some goals of the designer are (1) to maximise transmission bit rate; (2) to minimise error rate; (3) to minimise required power, or equivalently, to minimise information bit energy to noise power spectral density ratio, E_b/N_0; (4) to minimise required system bandwidth. However, goals 1 and 2 are clearly in conflict with goals 3 and 4.

Figure 2.1 illustrates the system trade off and an approach to this problem, where data from a source is emitting two information bits every T second. Figure 2.1 (a) shows a very simple system, where uses no coding and 4 PSK modulation. However, to minimise error rate we need to use coding as shown in Figure 2.1 (b), where the system uses $R = 2/3$ encoder and 4 PSK modulator. The consequence is that the bandwidth increases by factor 3/2 (compared with uncoded). If we keep the bandwidth constant, thus the transmission bit rate will be decreased; alternatively, if we maintain the error rate without coding, the required power will be increased. It can be seen that there is a system trade off to achieve those goals.

Figure 2.1 (c) gives us an approach to this problem; the system uses $R = 2/3$ encoder and 8-PSK modulator, each signal carries two information bits and occupies the same bandwidth as (a). We see that in this approach, we can use coding without bandwidth expansion. The use of a higher-order signal constellation would involve a power penalty

with respect to 4 PSK. Thus the coding gain achieved by the rate 2/3 code should be more than needed to offset this penalty, the net result being some coding gain at no price in bandwidth.
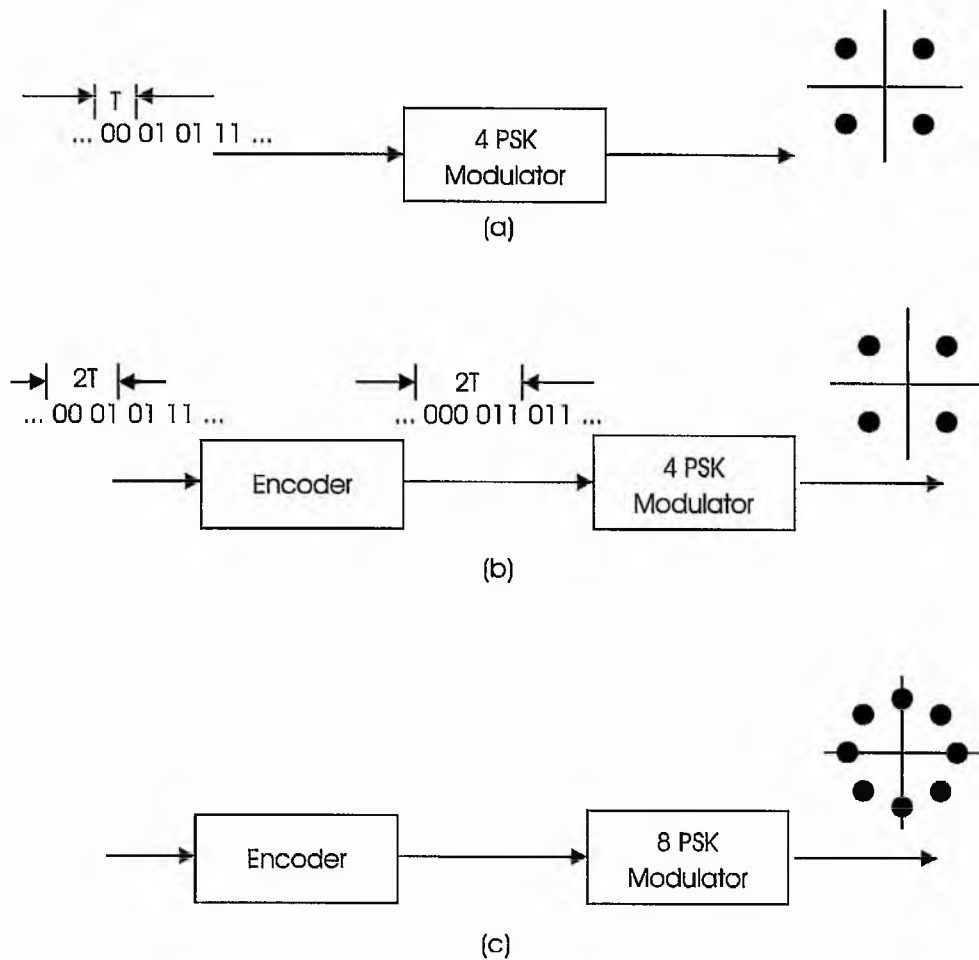
Figure 2.1 Three digital communication schemes transmitting 2 bits every T seconds: (a) uncoded transmission with QPSK; (b) QPSK with a rate 2/3 code; (c) 8-PSK with a rate 2/3 code

The approach explained above is the basis of any combined coding and modulation scheme; that is to improve the reliability of a digital transmission system without increasing the transmitted power or the required bandwidth.

The origins of combined coding and modulation date back to 1974, when Massey published a paper [Massey, 1974] in which he suggested that the performance of a digital communications system could be improved by looking at coding and modulation as a combined entity rather than two separate operations. The results from this work unfortunately did not make people interested in using combined coding and modulation schemes.

It was not until 1982 that Ungerboeck published a paper [Ungerboeck, 1982] in which he showed that significant improvements in performance over uncoded modulation could be obtained by combining the operations of channel encoder and modulator. Using the technique of set partitioning, in which the basic modulation signals are partitioned into subsets, Ungerboeck constructed a variety of trellis coded modulation schemes.

Actually, the idea of trellis coded modulation had already been presented in an earlier conference [Ungerboeck and Csajka, 1976], and at about the same time a paper had also been published [Imai and Hirakawa, 1977] in which block and convolutional codes had been combined with modulation. These also failed to stimulate interest, but they formed the basis from which today's combined modulation and coding has developed.

2.1. TRELLIS CODED MODULATION (TCM)

TCM uses signal-set expansion to provide redundancy for coding, and to design coding and signal-mapping functions jointly so as to maximise directly the *free distance* (minimum Euclidean distance) between coded signal sequences. This allows the construction of modulation codes whose free distance significantly exceeds the minimum distance between uncoded modulation signals, at the same information rate, bandwidth, and signal power. These schemes can be described by a state-transition (trellis) diagram similar to the trellis diagrams of binary convolutional codes. The difference is that in TCM schemes, the trellis branches are labelled with redundant non-binary modulation signals rather than with binary code symbols. The asymptotic coding gain of a TCM scheme can be defined as [Biglieri *et al.*, 1991]:

$$\gamma = \frac{d_{\text{free}}^2/E}{d_{\text{min}}^2/E'}$$

where E' and E denote the average signal energies of the uncoded and coded schemes respectively. d_{free} is the free Euclidean distance of an error event and d_{min} is the minimum distance of the uncoded constellation used for comparison.

Ungerboeck [Ungerboeck, 1982] provided a method which is called set partitioning for mapping the coded bits into signal points in such a way as to maximise the minimum Euclidean distance.

As can be seen in Figure 2.2, by the set partitioning method, the M-ary constellation is successively partitioned into 2,4,8,..., subsets with size $M/2$, $M/4$, $M/8$, ..., having larger minimum Euclidean distances, $\Delta_0 < \Delta_1 < \Delta_2 < \cdots$, between the signal points of these subsets.

We will consider uncoded QPSK transmission and a 4-state TCM scheme employing an 8-PSK redundant modulation scheme. An 8-PSK signal set can be seen in Figure 2.2.

From Figure 2.3 we have:

$$\sin\left(\frac{\pi}{4}\right) = \frac{d_{\text{min}}/2}{\sqrt{E}} \Rightarrow \frac{d_{\text{min}}^2}{E} = 4\sin^2\left(\frac{\pi}{4}\right) = 2$$
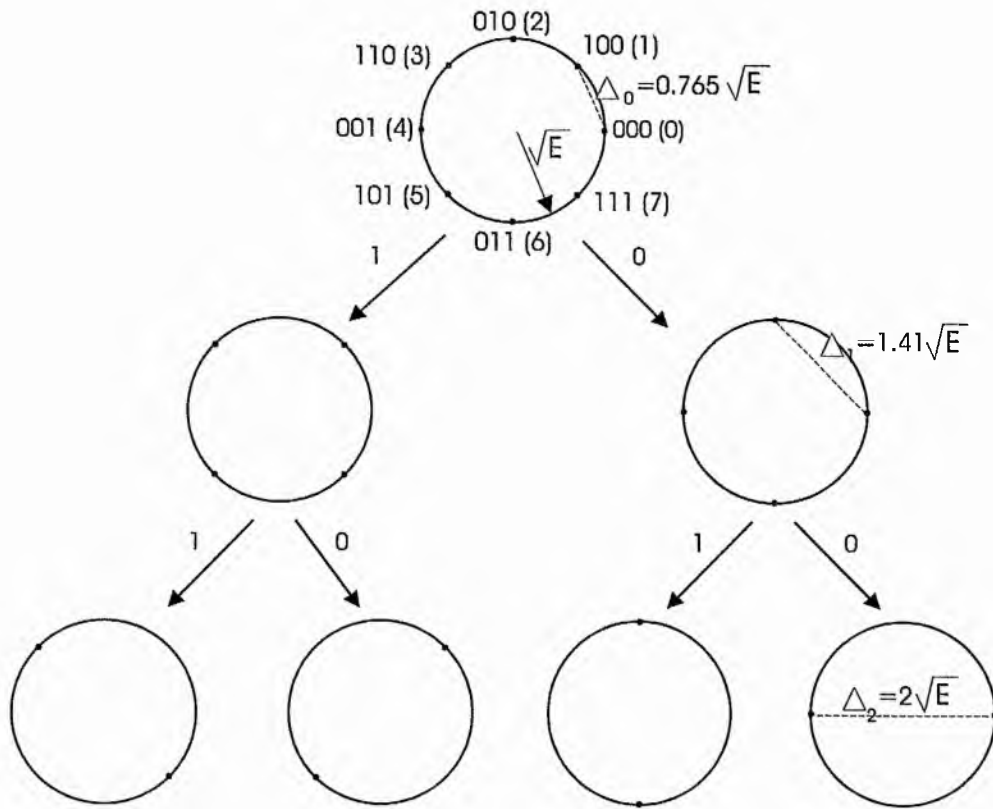
Figure 2.2 Set partitioned 8-PSK signal set
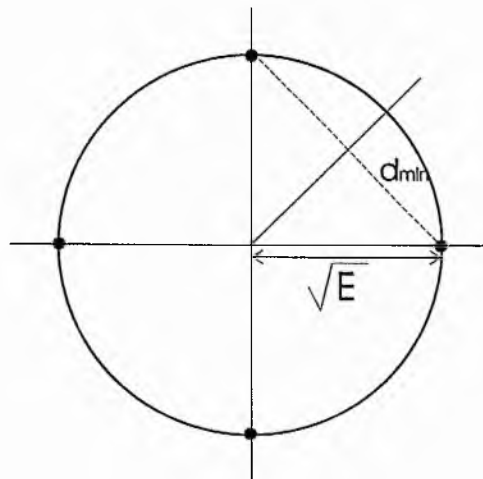
Figure 2.3 Minimum distance for QPSK constellation

From the trellis diagram in Figure 2.4 (an example taken from [Ungerboeck, 1982]), we can easily compute the free Euclidean distance. The error event is determined by the parallel transition (0 and 4) and the free Euclidean distance will be:

$$\frac{d_{free}^2}{E} = d^2[0,4] = 4$$

The asymptotic coding gain is:

$$\gamma = \frac{4}{2} = 2 = 3\,\text{dB}.$$

Therefore, a four-state Trellis Code for 8-PSK modulation technique can improve the robustness of digital transmission against noise by 3 dB compared with conventional uncoded modulation. With more complex TCM schemes, the coding gain can reach 6 dB.
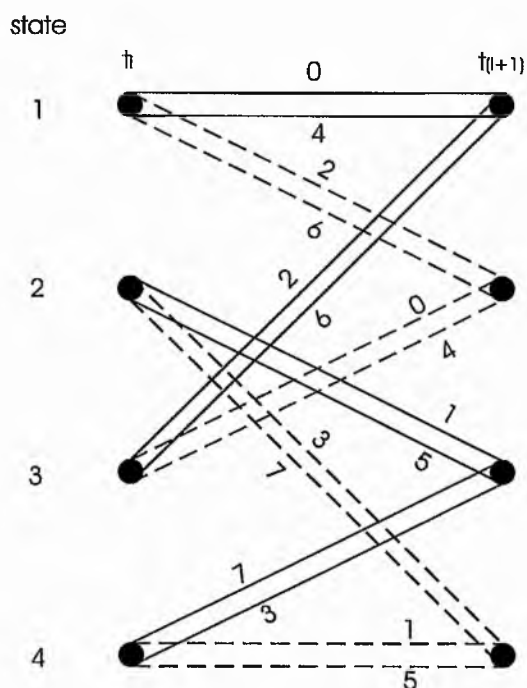
Figure 2.4 Trellis diagram for the four states 8-PSK TCM

2.2. BLOCK CODED MODULATION (BCM)

A block diagram of a block coded modulation encoder using an 8-PSK signal constellation is shown in Figure 2.5. The block coded modulation encoder consists of 3 binary codes (called binary component codes) of length n shown as $(n, k_i, d_{\min i})$, $i = 1, 2, 3$, where k_i and $d_{\min i}$ are the information length and the minimum Hamming distance of the i-th code respectively.
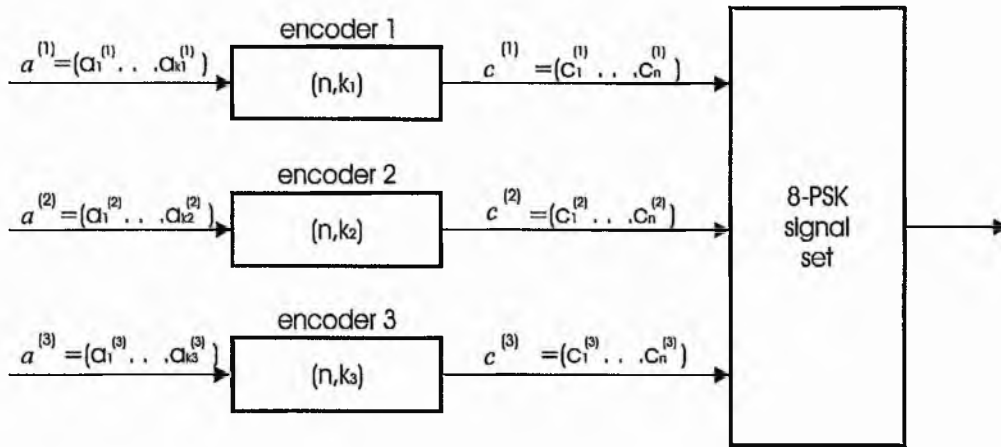
Figure 2.5 block coded modulation encoder using 8-PSK constellation

The output of 3 component code encoders can be expressed as a binary array with n columns and 3 rows

$$
\begin{array}{ll}
\mathbf{c}^{(1)}: & c_1^{(1)}c_2^{(1)}\ldots c_n^{(1)} \\
\mathbf{c}^{(2)}: & c_1^{(2)}c_2^{(2)}\ldots c_n^{(2)} \\
\mathbf{c}^{(3)}: & c_1^{(3)}c_2^{(3)}\ldots c_n^{(3)}
\end{array}
\qquad 2.1
$$

Binary digits are assigned to each point in the signal space according to Ungerboeck's set partitioning scheme [Ungerboeck, 1982], as illustrated in Figure 2.2. Thus each column of this array will correspond to a signal point in the 8-PSK signal space with the bit in the first row corresponding to the leftmost digit and the bit in the last row corresponding to the rightmost digit in the representation of the signal space points. The array will be

transmitted one column at a time, each column being represented by the corresponding signal space point.

The array in Equation 2.1 contains $3n$ bits of which $3 \cdot n \cdot R_c$ bits are information bits. Denoting the number of information bits in the i-th row by k_i, we can write

$$k_1 + k_2 + k_3 = 3R_c n, \qquad\qquad 2.2$$

where R_c is the rate of the block coded modulation scheme. For a given rate R_c, the values of k_i's are chosen subject to the above conditions in such a way as to maximise the minimum Euclidean distance between the codewords of the code.

The array in Equation 2.1 is a codeword in the signal space code if and only if each row of the array is a codeword in its corresponding binary code. Consider two different codewords in the binary code $(n,\ k_1,\ d_{\min 1})$ of the first row. For each one of the positions where these two codewords differ, the corresponding points in the signal space (regardless of the values in row 2 and 3) will be at a Euclidean distance of at least Δ_0 (see Figure 2.2). Since the two codewords must differ in at least $d_{\min 1}$ positions, we conclude that the squared Euclidean distance, D^2, between two codeword arrays whose first rows are different is:

$$D^2 \geq \Delta_0^2 \cdot d_{\min 1}.$$

If the two codewords in the first row are the same, we examine the second row. By the same reasoning, we conclude that the squared Euclidean distance between two different codewords in the second row is lower bounded as

$$D^2 \geq \Delta_1^2 \cdot d_{\min 2}.$$

Finally, the two codewords with binary arrays which only differ in the third row has the lower bound on the squared Euclidean distance

$$D^2 \geq \Delta_2^2 \cdot d_{\min 3}.$$

Therefore, we conclude that the squared Euclidean distance, D^2, between the codewords of the signal space 8-PSK code must satisfy

$$D^2 \geq \min\left(\Delta_0^2 \cdot d_{\min 1}, \Delta_1^2 \cdot d_{\min 2}, \Delta_2^2 \cdot d_{\min 3}\right).$$

By looking at all possible pairs of codewords, then

$$D_{\min}^2 = \min\left(\Delta_0^2 \cdot d_{\min 1}, \Delta_1^2 \cdot d_{\min 2}, \Delta_2^2 \cdot d_{\min 3}\right). \qquad 2.3$$

In our example, the codes used are denoted by the triple $(n, k_i, d_{\min i})$:

$$\begin{bmatrix} (8,1,8) \\ (8,7,2) \\ (8,8,1) \end{bmatrix}$$

The top row is an 8-bit repetition code with the minimum Hamming distance of $d_{\min 1} = 8$. The second row is a binary parity check code with the minimum Hamming distance of $d_{\min 2} = 2$. The third row is uncoded codeword, and therefore has the lowest Hamming distance of $d_{\min 3} = 1$. Using Equation 2.2 the rate of this block coded modulation scheme can be obtained as

$$R_c = \frac{k_1 + k_2 + k_3}{3n} = \frac{1 + 7 + 8}{3 \times 8} = \frac{2}{3}.$$

which translates to 2 bit s^{-1} Hz^{-1} throughput (comparable with uncoded QPSK). Finally the overall minimum squared Euclidean distance of this scheme is obtained as

$$\begin{aligned} D_{\min}^2 &= \min\left(0.586E \cdot d_{\min 1}, 2E \cdot d_{\min 2}, 4E \cdot d_{\min 3}\right) \\ &= \min\left(0.586E \cdot 8, 2E \cdot 2, 4E \cdot 1\right) \\ &= 4E \end{aligned}$$

which translates to an asymptotic coding gain of

$$\gamma = \frac{4E}{2E} = 2 = 3\,\text{dB}$$

compared to uncoded QPSK.

2.2.1. BCM Decoding

The multistage structure allows the use of multistage decoding methods similar to the algorithms developed in a paper [Imai and Hirakawa, 1977] for binary codes. In these methods component codes are decoded sequentially stage by stage and with decoded information passed from one stage to the next stage.

Multistage decoding of multilevel trellis modulation codes has been recently studied and analysed in a number of papers. In [Taubin and Trofimov, 1990], a multistage decoding scheme, called pipeline decoding, is proposed for a class of multilevel trellis codes devised in another paper [Yamaguchi and Imai, 1987]. In [Woerz and Hagenauer, 1990], multistage soft-decision decoding for multilevel trellis MPSK modulation codes was analysed. In [Rajpal *et al.*, 1991], a class of multilevel multidimensional trellis MPSK modulation codes is investigated which is constructed based on multilevel concatenation and multidimensional MPSK signal space. In [Takata *et al.*, 1993] several types of multistage decoding are devised and analysed, including a suboptimum soft-decision decoding scheme and hard-decision minimum distance measure decoding. The algorithm most commonly adopted was suggested in paper [Sayegh, 1986], and will be discussed below.

The optimum decoding strategy (assuming equal a *priori* probabilities) is maximum likelihood decoding. This would involve correlating the received waveforms with each of the $2^{\sum k_i}$ waveforms corresponding to the codewords of the signal space code. If the value of $\sum k_i$ is large, this method becomes prohibitively complex. Instead, the suboptimum scheme partitions all the possible codewords (arrays) into 2^{k_1} sets. All the elements within a set are arrays that have the same codeword in the first row. The first step in the decision process to assign (in optimum fashion) the received waveform to one of those 2^{k_1} sets. Once this decision is made, we assume it to be correct and look into the 2^{k_2} subsets of the chosen set. All the elements of a subset are arrays that have the same codeword in the second row (as well as having the same codeword in the first row). The received waveform is then assigned to one of those 2^{k_2} subsets. The above procedure is

carried out as many times as there are rows in the array. This algorithm is illustrated in Figure 2.6.

Received Array
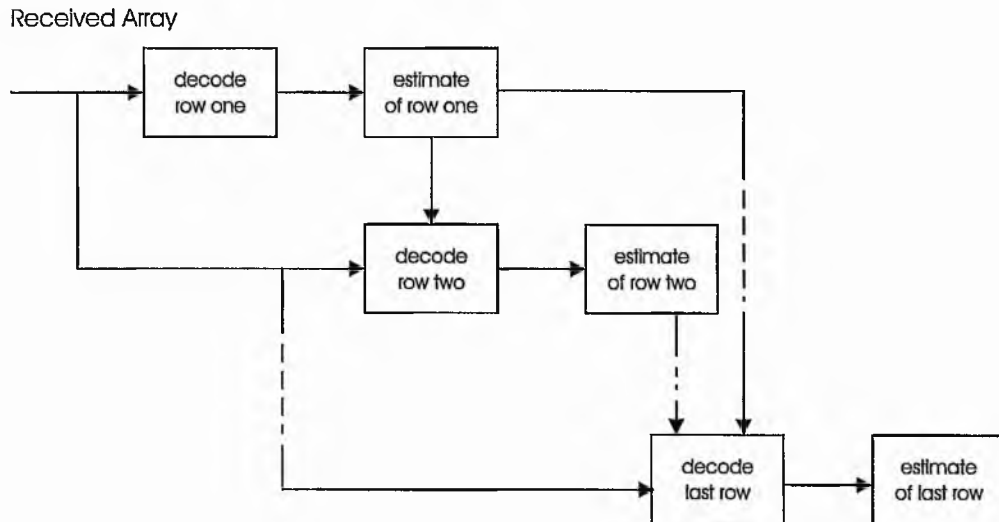
Figure 2.6 Multistage decoding procedure

In this thesis, the multistage decoding procedure explained above is used. Non-binary codes, Reed Solomon codes, are used as component codes for block coded modulation. The complete explanation will be given in chapter 3.

2.3. REED SOLOMON CODES

In this thesis, Reed Solomon codes are proposed to construct robust block coded MPSK modulation. There are several reasons for using Reed Solomon codes, such as:

- These codes are maximum distance separable codes, and hence, they make highly efficient use of the redundancy; this will be discussed further in this section.

- Reed Solomon codes are burst error correcting codes, which are suitable for non-Gaussian channels.

- The block lengths and symbol sizes of Reed Solomon codes can be readily adjusted to match the MPSK constellation.

- Reed Solomon codes provide a wide range of code rates that can be chosen such that the coded scheme has bandwidth efficiency compatible with the reference uncoded system.

Reed Solomon codes are an important subclass of non-binary Bose-Chaudhuri-Hocquenghem (BCH) codes. They were discovered in 1960 [Reed and Solomon, 1960] and are possibly the only multilevel codes to have been widely implemented for communication purposes. They have been used in a variety of applications including CD player and CD ROMs [Arai, 1984], digital audio tape [Watkinson, 1988], teletext broadcasting [Mortimer *et al.*, 1987], space communications [Hodgart, 1992], [Liu and Lee, 1984] and have been proposed for use in Mobile Speech Communications [Atungsiri *et al.*, 1991].

In non-binary BCH codes the code symbols are chosen from $GF(q)$, called the symbol field, with generator polynomial having roots in $GF(q^m)$, called the locator field. The Reed Solomon codes are obtained by choosing the locator field to be the same as the symbol field, i.e. $m = 1$. A systematic Reed Solomon code word defined in $GF(2^m)$ has the code word structure shown in Figure 2.7.
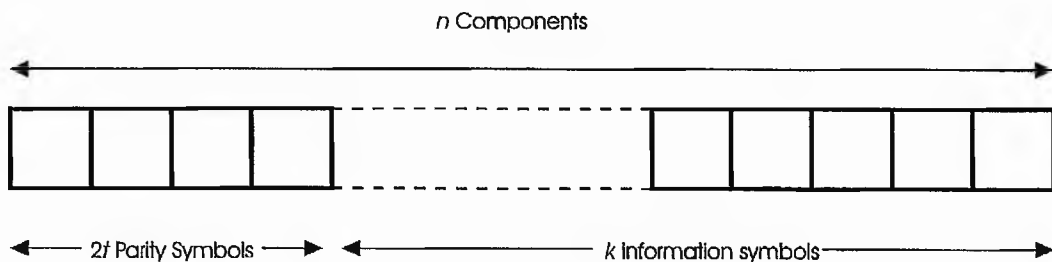
Figure 2.7 Reed Solomon code word.

Block Length	$n = 2^m - 1$
Information Symbols	k
Parity Symbols	$2t = n - k$
Minimum Distance	$d_{\min} = 2t + 1$

Reed Solomon codes are the only non-trivial codes meet the Singleton bound [Singleton, 1964] with equality, that is

$$d_{\min} = n - k + 1$$

Codes that satisfy this inequality are termed maximum distance codes. This implies that a Reed Solomon code word can be reconstituted from any k symbols. Each symbol in $GF(2^m)$ is represented by m-bit characters. The structure of the code word is such that the $2t$ parity check symbols may be placed as a block at any position in the code word, but for purposes of convenience, they are usually placed in the first $2t$ positions.

There are two main Reed Solomon coding techniques available now. The first technique was historically developed in the time domain using the generator polynomial approach. The second one was invented when Fourier transforms were defined over a finite field [Pollard, 1971]; this is usually called the frequency domain coding technique.

In this following subsections the time and frequency domain approaches for the coding process will be shown generally.

2.3.1. Time Domain Coding Technique

As stated above, Reed Solomon codes are non-binary BCH codes where the symbol field and locator field are the same. As a consequence all minimum polynomials have degree 1 and the generator polynomial of the Reed Solomon codes can be constructed as the least common multiple of consecutive powers of the primitive elements of $GF(2^m)$:

$$g(x) = \left(x + \alpha^{m_0}\right)\left(x + \alpha^{m_0+2}\right)\cdots\left(x + \alpha^{m_0+d-2}\right)$$

where m_0 is an arbitrary integer.

One of advantages using this method is a capability of producing the code in a systematic form [Blahut, 1983]. Let $c(x)$ be the code word polynomial corresponding to the information polynomial $a(x)$. To encode Reed Solomon codes in a systematic manner a code word polynomial is generated

$$c(x) = x^{n-k}a(x) + b(x)$$

where $b(x)$ is the remainder polynomial of degree less than $(n - k)$ of the division of $x^{n-k}a(x)$ by the generator polynomial $g(x)$

$$b(x) = x^{n-k}a(x) \bmod g(x)$$

The polynomial $b(x)$ is generated by a feedback shift register. Hence an encoder circuit for this technique can be implemented as shown in Figure 2.8.

It can be seen that when all the data has entered the channel, the parity check symbols have been generated in the registers and are ready to be transmitted over the channel.
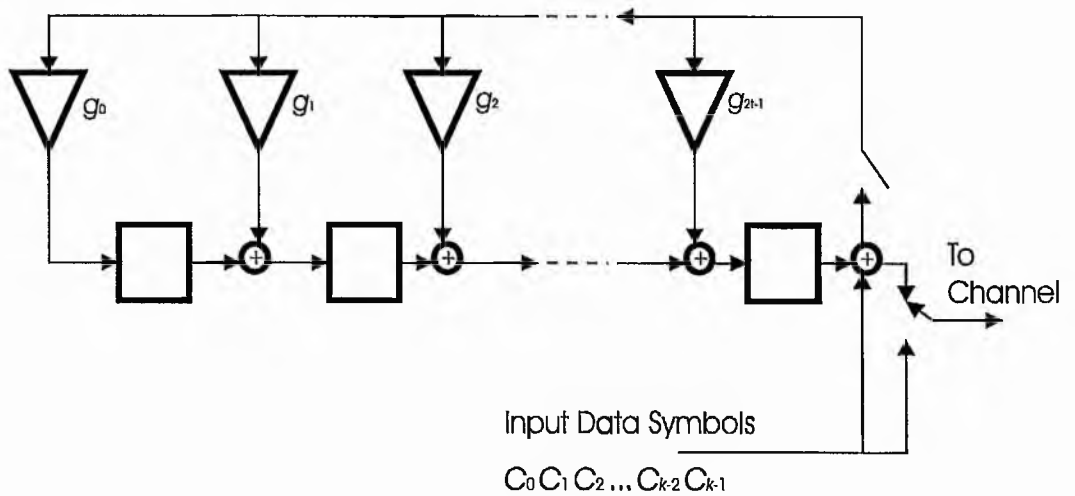
Figure 2.8 Encoder circuit.

After the data has been encoded it is ready to be transmitted over the channel. The effects of the channel may cause the received sequence to become erroneous. Thus the received polynomial $r(x)$ can be represented as

$$r(x) = c(x) + e(x)$$

where $e(x)$ is the error pattern introduced by the channel. Accordingly it can be said that the objective of the Reed Solomon decoder is to find the number of errors, their positions and their values.

The time domain decoding approach requires the initial step of computing the $2t$ syndrome components. The syndrome values are obtained by reapplying the encoding rules to the received word. This is done by evaluating $r(x)$ at the prescribed roots of the generator polynomial, α^k for $k = 1,2,3,...,2t$, that is

$$
\begin{aligned}
S_k &= r\!\left(\alpha^k\right) \\
&= c\!\left(\alpha^k\right) + e\!\left(\alpha^k\right) \\
&= e\!\left(\alpha^k\right)
\end{aligned}
$$

Each erroneous symbol produces its own syndrome and the syndrome of the received word is the sum of the syndromes of each of the erroneous symbols. Hence the syndrome values can be written as

$$S_k = \sum_{i=1}^{t} Y_i X_i^k$$

where X_i is the error locator for the i-th error and Y_i is its value. As stated above the decoding task is, given the S's, find the X's and Y's.

2.3.2. Frequency Domain Coding Technique

In this approach, it is assumed that the data block or code symbol sequence fed into the encoder is in the frequency domain. The first point which can be made is that, in the frequency domain, the parity check symbols are constrained to the zero element in the finite field, and can be placed anywhere in the code word as long as they are in a continuous $2t$ block. But for the sake of simplicity the first $2t$ positions are usually chosen. The inverse finite field Fourier transform is taken to produce the code word $c(x)$

and this results in the time domain code word $C(z)$ which is ready to be transmitted over the channel.

At the decoder end a forward finite field Fourier transform is performed on the received sequence resulting in $2t$ parity check symbols (syndrome). If the syndrome is equal to zero (in the finite field) then it is assumed that no errors have occurred during transmission, otherwise errors have occurred and an error correction routine must be invoked to try and extract the original transmitted code word. This coding procedure is summarised in Figure 2.9.
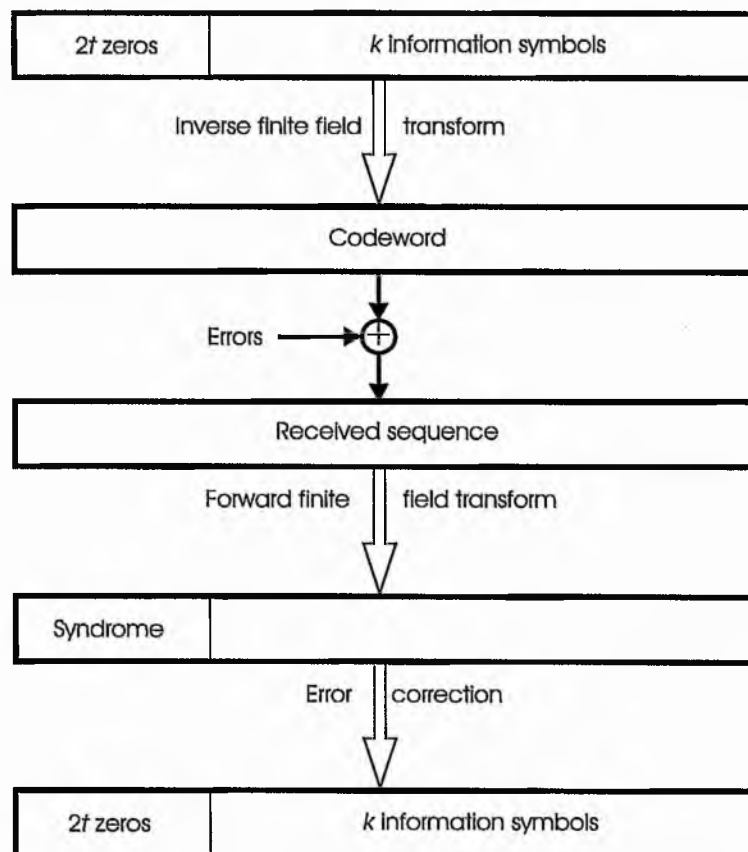
Figure 2.9 Frequency domain coding procedure for Reed Solomon codes.

2.4. REED MULLER CODES

In this thesis, Reed Muller codes are used to construct binary block coded MPSK modulation schemes. The error performances of these schemes will be compared with those of Reed Solomon coded MPSK modulation in chapter 4.

Reed Muller codes are among the earliest block codes to be defined. The great merit of Reed Muller codes is that they are relatively easy to decode, using majority-logic circuits. However, except for first order Reed Muller codes and codes of modest block lengths, their minimum distance is lower than that of BCH codes. For any m and r, $0 \le r \le m$, there is a binary r^{th} order Reed Muller code RM(r, m) with the following properties:

Code length	$n = 2^m$
Information bits	$k = 1 + \binom{m}{1} + \cdots + \binom{m}{r}$
Minimum distance	$d_{\min} = 2^{m-r}$

Reed Muller codes can be defined very simply in terms of Boolean functions. To define codes of length $n = 2^m$, we need the set of all binary m-tuples, $v = (v_1, \ldots, v_m)$. The rth order binary Reed Muller code of length $n = 2^m$, for $0 \le r \le m$, is the set of all vectors f, where $f(v_1, \ldots, v_m)$ is a Boolean function which is a polynomial of degree at most r.

In general the rth order Reed Muller code consists of all linear combinations of vectors corresponding to the products

$$1, v_1, \ldots, v_m, v_1 v_2, v_1 v_3, \ldots, v_{m-1} v_m, \ldots \text{ (up to degree } r)$$

which form a basis for the code. There are k linearly independent basis vectors. Figure 2.10 shows 16 possible basis vectors for Reed Muller codes of length 16, $m = 4$.

A generator matrix G of the second-order Reed Muller code of length 16, RM(2, 4) can be taken from the first 11 rows of Figure 2.14. Thus the information bits

$$a = a_0 a_4 a_3 a_2 a_1 a_{34} a_{24} a_{14} a_{23} a_{13} a_{12}$$

are encoded into the codeword

$$x = aG = a_0 \mathbf{1} + a_4 v_4 + \cdots + a_1 v_1 + a_{34} v_{34} + \cdots + a_{12} v_{12}$$
$$= x_0 x_1 \cdots x_{15}$$

This is a single-error-correcting code. A simple decoding approach for Reed Muller codes is that using majority logic decoding. The received bits

$$y = y_0 y_1 \cdots y_{15}$$

are decoded step by step. The first step is to recover the 6 bits $a_{12}, \ldots, a_{34}$. Observe from Figure 2.10 that if there are no errors,

$$
\begin{aligned}
a_{12} &= y_0 + y_1 + y_2 + y_3 \\
&= y_4 + y_5 + y_6 + y_7 \\
&= y_8 + y_9 + y_{10} + y_{11} \\
&= y_{12} + y_{13} + y_{14} + y_{15}
\end{aligned}
\qquad 2.4
$$

$$
\begin{aligned}
a_{13} &= y_0 + y_1 + y_4 + y_5 \\
&= y_2 + y_3 + y_6 + y_7 \\
&= y_8 + y_9 + y_{12} + y_{13} \\
&= y_{10} + y_{11} + y_{14} + y_{15}
\end{aligned}
\qquad 2.5
$$

. . . .

$$
\begin{aligned}
a_{34} &= y_0 + y_4 + y_8 + y_{12} \\
&= y_1 + y_5 + y_9 + y_{13} \\
&= y_2 + y_6 + y_{10} + y_{14} \\
&= y_3 + y_7 + y_{11} + y_{15}
\end{aligned}
$$

Equation 2.4 gives 4 votes for the values of a_{12}, Equation 2.5 gives 4 votes for a_{13}, and so on. So if one error occurs, the majority vote is still correct, and thus each a_{ij} is obtained correctly.

31

1	1	1	1	1	1	1	1	1	1	1	1	1	1	1	1	1
v_4	0	0	0	0	0	0	0	0	1	1	1	1	1	1	1	1
v_3	0	0	0	0	1	1	1	1	0	0	0	0	1	1	1	1
v_2	0	0	1	1	0	0	1	1	0	0	1	1	0	0	1	1
v_1	0	1	0	1	0	1	0	1	0	1	0	1	0	1	0	1
v_3v_4	0	0	0	0	0	0	0	0	0	0	0	0	1	1	1	1
v_2v_4	0	0	0	0	0	0	0	0	0	0	1	1	0	0	1	1
v_1v_4	0	0	0	0	0	0	0	0	0	1	0	1	0	1	0	1
v_2v_3	0	0	0	0	0	0	1	1	0	0	0	0	0	0	1	1
v_1v_3	0	0	0	0	0	1	0	1	0	0	0	0	0	1	0	1
v_1v_2	0	0	0	1	0	0	0	1	0	0	0	1	0	0	0	1
$v_2v_3v_4$	0	0	0	0	0	0	0	0	0	0	0	0	0	0	1	1
$v_1v_3v_4$	0	0	0	0	0	0	0	0	0	0	0	0	0	1	0	1
$v_1v_2v_4$	0	0	0	0	0	0	0	0	0	0	0	1	0	0	0	1
$v_1v_2v_3$	0	0	0	0	0	0	0	1	0	0	0	0	0	0	0	1
$v_1v_2v_3v_4$	0	0	0	0	0	0	0	0	0	0	0	0	0	0	0	1

Figure 2.10 Basis vectors for Reed Muller codes of length 16.

To find the bits $a_1,\ldots,a_4$, y must be subtracted

$$\mathbf{y'} = \mathbf{y} - \left(a_{34}\mathbf{v}_3\mathbf{v}_4 + \cdots + a_{12}\mathbf{v}_1\mathbf{v}_2\right)$$
$$= y_0' y_1' \cdots y_{15}'$$

Using that result, again from Figure 2.10 we observe that

$$a_1 = y_0' + y_1'$$
$$= y_2' + y_3'$$
$$\cdots$$
$$= y_{14}' + y_{15}'$$

$$\cdots\cdots\cdots\cdots$$

$$a_4 = y_0' + y_8'$$
$$= y_1' + y_9'$$
$$\cdots$$
$$= y_7' + y_{15}'$$

Now, there are 8 votes for each a_i, and so if there is one error the majority vote certainly gives each a_i correctly. It remains to determine a_0. We have

$$\mathbf{y}'' = \mathbf{y}' - \left(a_{34}\mathbf{v}_3\mathbf{v}_4 + \cdots + a_{12}\mathbf{v}_1\mathbf{v}_2\right)$$
$$= a_0\mathbf{1} + \text{error}$$
$$= y_0'' y_1'' \cdots y_{15}''$$

and $a_0 = 0$ or 1 according to the number of 1's in $\mathbf{y}''$.

This scheme is called the *Reed decoding algorithm*, and will work for any Reed Muller code.

Many properties of Reed Muller codes are best stated in the language of finite geometries. The Euclidean geometry EG(m, 2) of dimension m over GF(2) contains 2^m points, whose coordinates are all the binary vectors $v = (v_1, \ldots, v_m)$.

We can find which components of the codeword x are to be used in the parity checks, such as Equations 2.4 and 2.5, using a geometric description of the algorithm for decoding RM(r, m). We first find a_σ, where $\sigma = \sigma_1 \cdots \sigma_r$. The corresponding row of the generator matrix $v_{\sigma_1} \cdots v_{\sigma_r}$, is the incidence vector of an $(m - r)$-dimensional subspace S of EG(m, 2). For example, the dash line in Figure 2.11 shows the plane S corresponding to a_{12}. Let T be the complementary subspace to S with incidence vector $v_{\tau_1} \cdots v_{\tau_{m-r}}$, containing a 1 in those components $s \in S$ and zeros elsewhere. where $\{\tau_1, \ldots, \tau_{m-r}\}$ is the complement of $\{\sigma_1, \ldots, \sigma_r\}$ in $\{1, 2, \ldots, m\}$. Clearly T meets S in a single point, the origin.

Let $U_1, \ldots, U_{2^{m-r}}$ be all the translates of T in EG(m, 2), including T itself (these are shaded in Figure 2.11). Each U_i meets S in exactly one point.

Theorem 1.   *If there are no errors, a_σ is given by*

$$a_\sigma = \sum_{P \in U_i} x_P, \qquad i = 1, \dots, 2^{m-r}$$

These equations are a generalisation of Equations (2.4), (2.5), and give 2^{m-r} votes for a_σ.

The theorem was proved in [MacWilliams & Sloane, 1977]. It implies that, if no more than $\left\lfloor \frac{1}{2}\left(2^{m-r} - 1\right) \right\rfloor$ errors occur, majority logic decoding will recover each of the symbols v_σ correctly, where σ is any string of r symbols. The rest of the v's can be recovered in the same way, as shown in the previous example. Thus the error-correcting capability of the Reed decoding algorithm is

$$\left\lfloor \tfrac{1}{2}(d_{\min} - 1) \right\rfloor = \left\lfloor \tfrac{1}{2}\left(2^{m-r} - 1\right) \right\rfloor$$

where $\lfloor c \rfloor$ means the largest integer no greater than c.
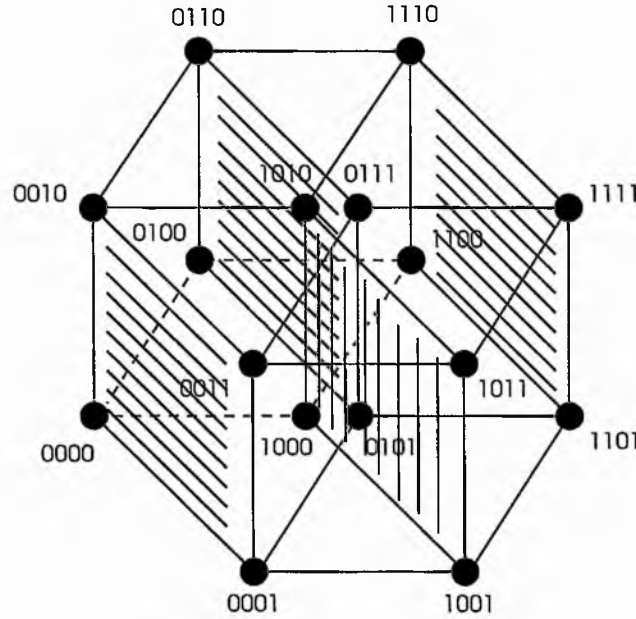
Figure 2.11 EG(4, 2) showing subspace S (dash line) and $U_1, \dots, U_4$ (shaded).

2.5. ROBUST SOLUTIONS

Coded modulation is an attractive proposition for improving the performance of digital transmission systems since Ungerboeck published his landmark paper on trellis coded modulation [Ungerboeck, 1982]. More recently, the increasing interest for digital mobile-radio systems or indoor wireless systems has led to the consideration of coded modulation for fading channels in order to cope with the severe performance degradation effects associated with fading. Analysis of coded modulation for fading channels has shown that the code performance depends strongly, rather than on the minimum Euclidean distance of the code (as it does over the AWGN channel), on its minimum Hamming distance (the *code diversity*) [Biglieri *et al.*, 1996].

Several results followed this discovery: Zehavi achieves improved theoretical time diversity by means of one encoder and built in interleaving creating random modulation [Zehavi, 1992]. He mentioned that the error performance of the proposed coding scheme raises the question whether the standard TCM approach is the best for obtaining a bandwidth efficient coding scheme with such a channel. In [Sundberg and Seshadri, 1993] they constructed schemes which are based on multilevel trellis coded modulation and utilise maximum free Hamming distance binary convolutional codes as a building block. Subsequently Jamali and Le-Ngoc designed codes for the Rayleigh fading channel so as to maximise their diversity by means of one encoder using Gray mapping [Jamali and Le-Ngoc, 1994].

In mobile radio or indoor wireless transmission, the channel model is not stationary, as it fluctuates in time between the extremes of Rayleigh and AWGN. Thus, a code designed to be optimum for a fixed channel model might perform poorly when the channel varies, and hence a code optimal for the AWGN channel may be actually not optimum for the Rayleigh fading channel. And also, an optimum code for the Rayleigh fading channel may be not optimum for the AWGN channel. In these conditions, the search for a *robust* solution should be regarded as a viable alternative.

In this thesis, Reed Solomon coded MPSK modulation schemes are proposed as robust coded modulation schemes for the AWGN channel and the Rayleigh fading channel. The main case of interest here is multi-level Reed Solomon coding. In this case each of the m bits defining an MPSK symbol, $M = 2^m$, is coded and decoded by different Reed Solomon codecs. The set partitioning principle is applied to define subsets with distances

Δ_i, ($i = 1$ to m) that are nondecreasing with i. Each of the m bits defines a subset and is decoded in multistage decoding schemes.

These schemes are designed to be robust block coded MPSK modulation by matching the configurations of component codes with channel characteristics: the code performance over the AWGN channel depends strongly on the minimum Euclidean distance of the code; but over a Rayleigh fading channel, the code performance depends on its minimum Hamming distance. This will be discussed in chapter 4.

CHAPTER 3

REED SOLOMON CODED MODULATION

Much work has been done on design of efficient coded modulation schemes for band-limited channels since the publication of [Ungerboeck, 1982] which showed that significant improvements in performance over uncoded modulation could be obtained by combining the operations of channel encoder and decoder [Imai and Hirakawa, 1977] in which block and convolutional codes had been combined with modulation.

The main area of interest here is that Reed Solomon codes are used to construct block coded modulation schemes. As mentioned before in section 2.3 that there are several reasons for using Reed Solomon codes, such as:

- These codes are maximum distance separable codes, and hence, they make highly efficient use of the redundancy.

- Reed Solomon codes are burst error correcting codes, which are suitable for non-Gaussian channels.

- The block lengths and symbol sizes of Reed Solomon codes can be readily adjusted to match the MPSK constellation.

- Reed Solomon codes provide a wide range of code rates that can be chosen such that the coded scheme has bandwidth efficiency compatible with the reference uncoded system.

To develop Reed Solomon coded MPSK modulation schemes, two approaches are considered. First, a Reed Solomon code is combined with an MPSK signal set using Gray code mapping: this approach is called Reed Solomon Coded modulation (RSCM) not based on set partitioning.

The second approach to coded MPSK with $M = 2^m$ is multilevel Reed Solomon coding. In this case each of the m bits defining an MPSK symbol is coded and decoded by different Reed Solomon codecs. The set partitioning principle is applied to define subsets with distances Δ_i, ($i = 1$ to m) that are nondecreasing with i. Each of the m bits defines a subset and is decoded in multistage decoding schemes. The following sections will discuss the two approaches as stated above.

3.1. REED SOLOMON CODED MODULATION NOT BASED ON SET PARTITIONING

This approach was firstly proposed in [Sweeney, 1991] as a bandwidth-efficient block-coded technique, over the Gaussian channel. This approach is only using one Reed Solomon encoder and one decoder with Gray labelling. Here, there are three methods generalising this approach in which methods 2 and 3 are taken from [Jamali and Le-Ngoc, 1994].

3.1.1. Method 1

This method uses a Reed Solomon code, defined over $GF(2^\nu)$, having code rate $R_c = \dfrac{m-1}{m}$ combined with a 2^m-PSK signal set. In this combination the code rate is chosen such that the rate of the coded scheme is the same as the uncoded one (2^{m-1}-PSK). In this case the MPSK signal set used for modulation does not correspond with the finite field over which the code is defined.

For example, a Reed Solomon code defined over $GF(2^5)$ may be combined with QPSK signalling. The rate of code is chosen such that the overall coded QPSK throughput is comparable to that of uncoded BPSK, i.e., 1 bit sec^{-1} Hz^{-1}. The (30, 15) Reed Solomon code with a symbol rate $R_c = {}^{15}\!/_{30} = {}^{1}\!/_{2}$ is chosen, which translates into a throughput of 1 bit sec^{-1} Hz^{-1}.

3.1.2. Method 2

In the second method, a Reed Solomon code, defined over $GF(2^m)$, is combined with a 2^m-PSK signal set. In this combination the code rate is chosen such that the rate of the coded scheme is the same as the uncoded one (usually 2^{m-1}-PSK). Here, the time diversity of the coded scheme is determined by the minimum Hamming distance of the Reed Solomon code.

As the first example we construct a Reed Solomon coded 8-PSK scheme with a (7, 5) Reed Solomon code which can be shortened by omitting one of the information symbols. The resulting scheme is the (6, 4) Reed Solomon code, defined over GF(8), which is used with 8-PSK signalling. The (6, 4) Reed Solomon code has a symbol rate $R_c = \frac{4}{6} = \frac{2}{3}$, which translates into a throughput of 2 bit sec^{-1} Hz^{-1}, uncoded QPSK throughput.

A second example is that a Reed Solomon (14, 7) code, which is a shortened Reed Solomon (15, 8) code defined over GF(16), is combined with a 16-PSK signal set. This yields a coded scheme with minimum Hamming distance 8 and a throughput of $4 \cdot \frac{7}{14} = \frac{28}{14} = 2$ bit sec^{-1} Hz^{-1}, the same bandwidth efficiency as the uncoded QPSK..

3.1.3. Method 3

The symbols of a Reed Solomon code, defined over $GF(2^{ym})$, are mapped to the signal points of a 2^m-PSK signal set such that each symbol of the Reed Solomon code consists of the concatenation of y channel symbols. The proposition given in [Jamali and Le-Ngoc, 1994] indicates that the effective order of time diversity in such a mapping is at least $d_{\min}$, the minimum Hamming distance of the Reed Solomon codes. This method allows us to enhance the order of time diversity by using more powerful low rate codes. Increasing y gives more powerful coded schemes.

As an example of constructing the Reed Solomon coded MPSK schemes based on the third method, we considered a Reed Solomon (63, 42) coded 8-PSK scheme. The code is defined over $GF(2^6)$, and hence, each code symbol consists of two concatenated 8-PSK symbols. The rate of the Reed Solomon code is $\frac{42}{63}$ which translates into 2 bit sec^{-1} Hz^{-1} throughput when combined with an 8PSK signal set.

3.2. REED SOLOMON CODED MODULATION BASED ON SET PARTITIONING

Block coded modulation based on set partitioning was first proposed in [Cusack, 1984]. She constructed block codes using Reed Muller codes and QAM signal sets. Later, [Sayegh, 1986] generalised Cusack's work to other signal constellations by using known binary codes. The main case of interest here is using non-binary BCH codes, Reed Solomon codes, for block coded modulation based on set partitioning.

A block diagram of a Reed Solomon coded modulation based on set partitioning using a 2^m-PSK signal constellation is shown in Figure 3.1.
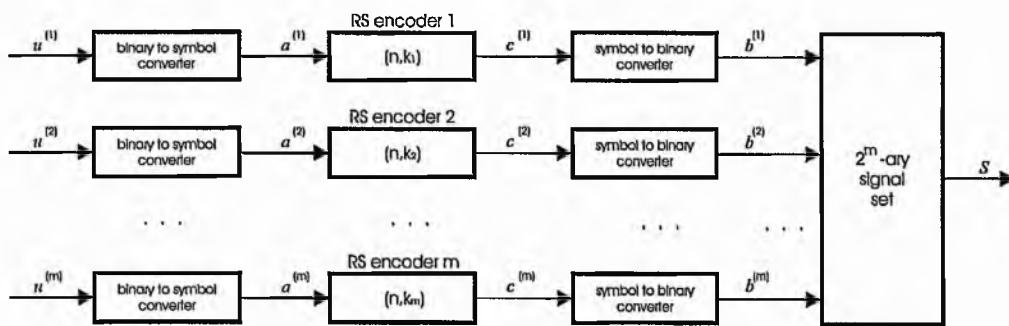
Figure 3.1 A Reed Solomon coded modulation encoder

The block coded modulation encoder consists of m Reed Solomon codes (called Reed Solomon component codes), defined over $GF(2^v)$, with length n shown as (n, k_i), $i = 1, 2, ..., m$, where k_i is the information length.

The input bits are partitioned into m blocks with $v \cdot k_i$ bits in the i-th block

$$u^{(i)} = \left(u_1^{(i)}, u_2^{(i)}, \cdots, u_{v \cdot k_i}^{(i)} \right) \qquad 3.1$$

where $u_h^{(i)} \in \{0,1\}$ for $1 \le h \le v \cdot k_i$. The input bits are converted to symbols $a^{(i)}$ before they are fed to encoders

$$a^{(i)} = \left(a_1^{(i)}, a_2^{(i)}, \cdots, a_{k_i}^{(i)}\right)$$ (3.2)

where $a_x^{(i)} \in GF\left(2^v\right)$ for $1 \le x \le k_i$. Thus every symbol consists of v input bits which are the binary representation of a finite field element.

The i-th block is encoded by a Reed Solomon encoder (n, k_i) which generates a codeword with n symbols

$$c^{(i)} = \left(c_1^{(i)}, c_2^{(i)}, \cdots, c_n^{(i)}\right)$$ (3.3)

where $c_y^{(i)} \in GF\left(2^v\right)$ for $1 \le y \le n$. After symbol to binary converting, the outputs of m encoders can be expressed as a binary array with $v \cdot n$ columns and m rows

$$
\begin{array}{cccc}
b_1^{(1)} & b_2^{(1)} & \cdots & b_{v\cdot n}^{(1)} \\
b_1^{(2)} & b_2^{(2)} & \cdots & b_{v\cdot n}^{(2)} \\
\cdots & \cdots & \cdots & \cdots \\
b_1^{(m)} & b_2^{(m)} & \cdots & b_{v\cdot n}^{(m)}
\end{array}
$$ (3.4)

where $b_q^{(i)} \in \{0,1\}$ for $1 \le q \le v \cdot n$. Hence the encoder's output of the i-th component code in binary sequence is

$$b^{(i)} = \left(b_1^{(i)}, b_2^{(i)}, \cdots, b_{v\cdot n}^{(i)}\right)$$ (3.5)

Binary digits are assigned to each point in the signal space according to Ungerboeck's set partitioning scheme [Ungerboeck, 1982]. Thus each column of this array, b_q, will correspond to a signal point in the 2^m-PSK signal space, S, with the bit in the first row

corresponding to the leftmost digit and the bit in the last row corresponding to the rightmost digit in the representation of the signal space points. The array will be transmitted one column at a time, each column being represented by the corresponding signal space point.

$$b_q = b_q^{(1)} b_q^{(2)} \ldots b_q^{(m)} \qquad\qquad 3.6$$

Let $s(\cdot)$ be the mapping defined on b_q such that $s\left(b_q^{(1)} b_q^{(2)} \ldots b_q^{(m)}\right)$ gives a unique signal point in S.

$$S_q = s(b_q), \qquad\qquad 3.7$$

where $S_q \in \left\{2^m - \text{PSK signal points}\right\}$

Table 3.1 gives binary-string values of length 2, $m = 2$, which are labeling signal points in S [see Figure 3.2], Table 3.2 for $m = 3$ and signal points in S can be seen Figure 3.3, and finally Table 3.3 for $m = 4$ and signal points in S are illustrated in Figure 3.4.

$b_q^{(1)}$	$b_q^{(2)}$	S_q
0	0	S_0
1	0	S_1
0	1	S_2
1	1	S_3

Table 3.1 Binary-string values for $m = 2$.
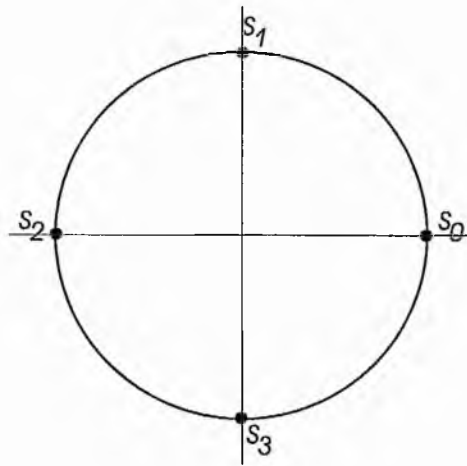
Figure 3.2 QPSK signal set

$b_q^{(1)}$	$b_q^{(2)}$	$b_q^{(3)}$	S_q
0	0	0	S_0
1	0	0	S_1
0	1	0	S_2
1	1	0	S_3
0	0	1	S_4
1	0	1	S_5
0	1	1	S_6
1	1	1	S_7

Table 3.2 Binary-string values for $m = 3$.
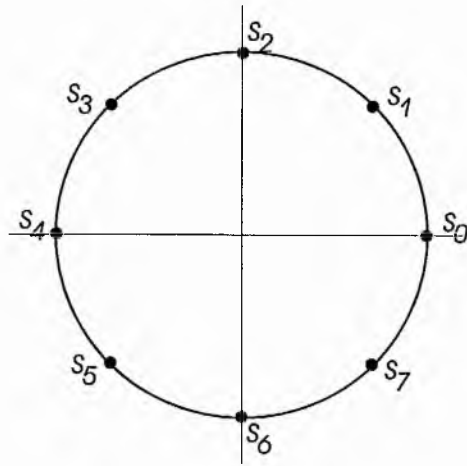
Figure 3.3 8-PSK signal set

$b_q^{(1)}$	$b_q^{(2)}$	$b_q^{(3)}$	$b_q^{(4)}$	S_q
0	0	0	0	S_0
1	0	0	0	S_1
0	1	0	0	S_2
1	1	0	0	S_3
0	0	1	0	S_4
1	0	1	0	S_5
0	1	1	0	S_6
1	1	1	0	S_7
0	0	0	1	S_8
1	0	0	1	S_9
0	1	0	1	S_{10}
1	1	0	1	S_{11}
0	0	1	1	S_{12}
1	0	1	1	S_{13}
0	1	1	1	S_{14}
1	1	1	1	S_{15}

Table 3.3 Binary-string values for $m = 4$
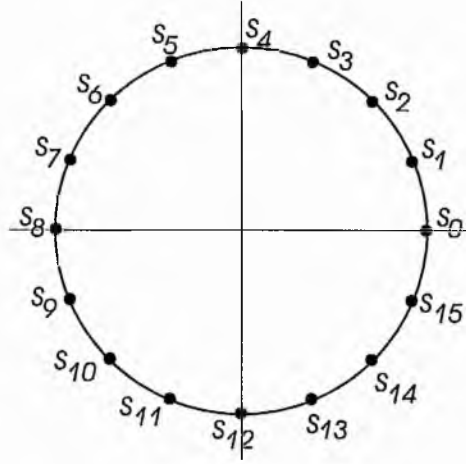
Figure 3.4 16-PSK signal set

The array in Equation 3.4 contains $v \cdot n \cdot m$ bits of which $v \cdot n \cdot m \cdot R_c$ bits are information bits. Denoting the number of information bits in i-th row by $v \cdot k_i$, we can write

$$v \cdot k_1 + v \cdot k_2 + \cdots + v \cdot k_m = m \cdot v \cdot n \cdot R_c \qquad 3.8$$

Equation 3.8 can be simplified to find R_c

$$R_c = \frac{\sum\limits_{i=1}^{m} k_i}{m \cdot n} \qquad 3.9$$

3.3. MULTISTAGE DECODING

Multistage decoding of multilevel trellis modulation codes has been recently studied and analysed in a number of papers. As previously mentioned, in [Taubin and Trofimov, 1990], [Woerz and Hagenauer, 1990] and [Rajpal et al, 1991] they used multilevel trellis codes for multistage decoding. In [Takata et al, 1993] several types of multistage decoding are devised and analysed, including a suboptimum soft-decision decoding scheme and hard-decision minimum distance measure decoding.

The main case of interest here is using a block encoder and a block decoding algorithm for each component code of a multilevel modulation code.

The novel idea here is that in the receiver, a rotated 2^{m+1}-PSK detector will be used if the transmitter uses a 2^m-PSK modulator. This is illustrated in Figure 3.5, a detector of a QPSK modulator, and Figure 3.6, a detector of an 8-PSK modulator.

The reason for the use of this scheme may be seen by considering the two obvious alternatives, namely using a detector corresponding exactly to the transmitted constellation and using an expanded detector without rotation. Suppose for QPSK transmission we use a QPSK detector as in Figure 3.7 and the point corresponding to 00 is received. Suppose the leftmost bit is first decoded and the decoder decides that it was in error, i.e. that it should take value 1. For the second stage of decoding, the receiver must choose between points 10 and 11, but the detected point is on the decision boundary between those values. Thus every decoder correction in the first stage of decoding results in an erasure in the second stage of decoding. Using a non-rotated 8-PSK detector would not solve this problem if one of the QPSK points was received and the intermediate points lie on the decision boundaries for the leftmost bit, causing an erasure in the first stage decoding.

Using the rotated, expanded detector ensures that the detector output does not fall on a decision boundary when the detector decodes any of the bits in the symbol. In this case, the advantage of using the rotated 2^{m+1}-PSK signal set is that the signal point gives additional information of direction to determine the closest 2^m-PSK region if a decoder detects a bit error.

For example we assume that signal S_0 (label 00) of the QPSK signal set was transmitted and because of noise the detector receives a signal point of the rotated 8-PSK signal set (Figure 3.5) which is in the decoding region of S_3 (label 11), on the side close to S_0. If we

46

assume that the first bit decoding can correct the error, the receiver can estimate that S_0 is the transmitted signal because it is the closest QPSK region with the decoded value of the first bit. A more complete example of multistage decoding using a rotated 16-PSK detector will be given in subsection 3.3.3.
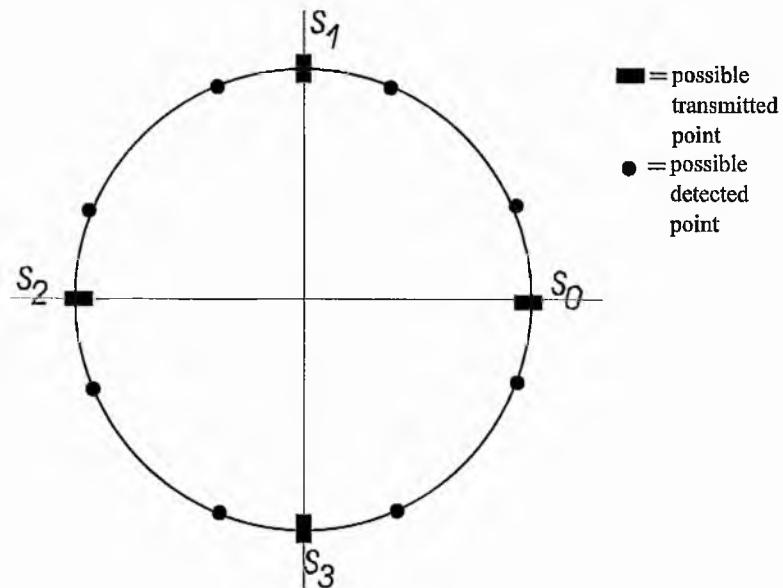
Figure 3.5 A rotated 8-PSK signal set for a QPSK modulator
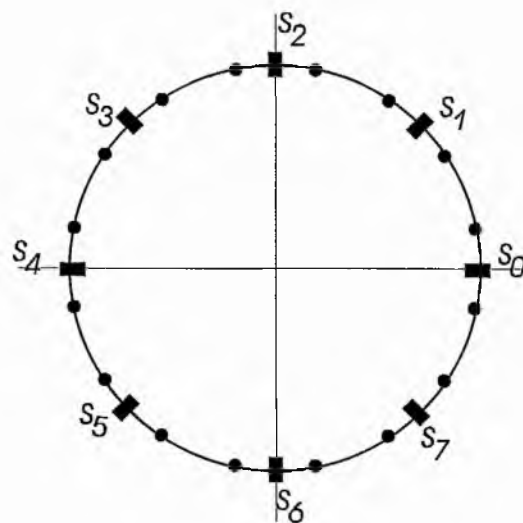
Figure 3.6 A rotated 16-PSK signal set for an 8-PSK modulator

47
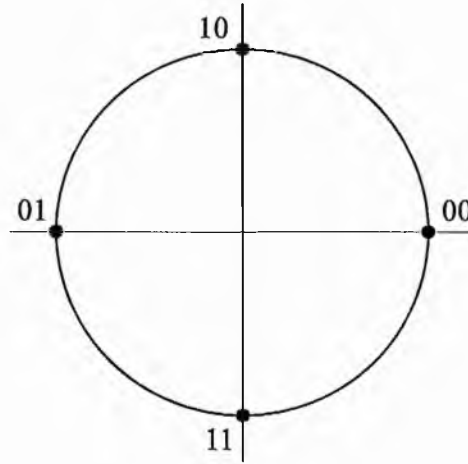
Figure 3.7 A QPSK detector

3.3.1. A Multistage Decoding Procedure

Suppose a codeword in a binary sequence, $b = (b_1, b_2, \cdots, b_{v \cdot n})$, is transmitted and $z = (z_1, z_2, \cdots, z_{v \cdot n})$ is the received sequence at the output of the detector, where $z_q \in \{\text{rotated } 2^{m+1} - \text{PSK signal points}\}$.

At each stage of decoding, the following process is carried out. Based on z, the demodulator gives a binary sequence,

$$H_i\left(z, b_D^{(1)} \cdots b_D^{(i-1)}, b_D^{(i+1)} \cdots b_D^{(m)}\right),$$

as discussed in the next subsection. Then the decoder performs a decoding process for $c^{(i)} = \left(c_1^{(i)}, c_2^{(i)}, \cdots, c_n^{(i)}\right)$, where $1 \le i \le m$. If the decoding is successful, the decoder puts out a decoded codeword in binary sequence $b_D^{(i)} = \left(b_{D1}^{(i)} b_{D2}^{(i)} \cdots b_{v \cdot n}^{(i)}\right)$ to the demodulator and a flag = 1. Otherwise, the decoded codeword in binary sequence is a null string with a report that an uncorrectable error has been detected (this is a decoding failure), a flag = −1.
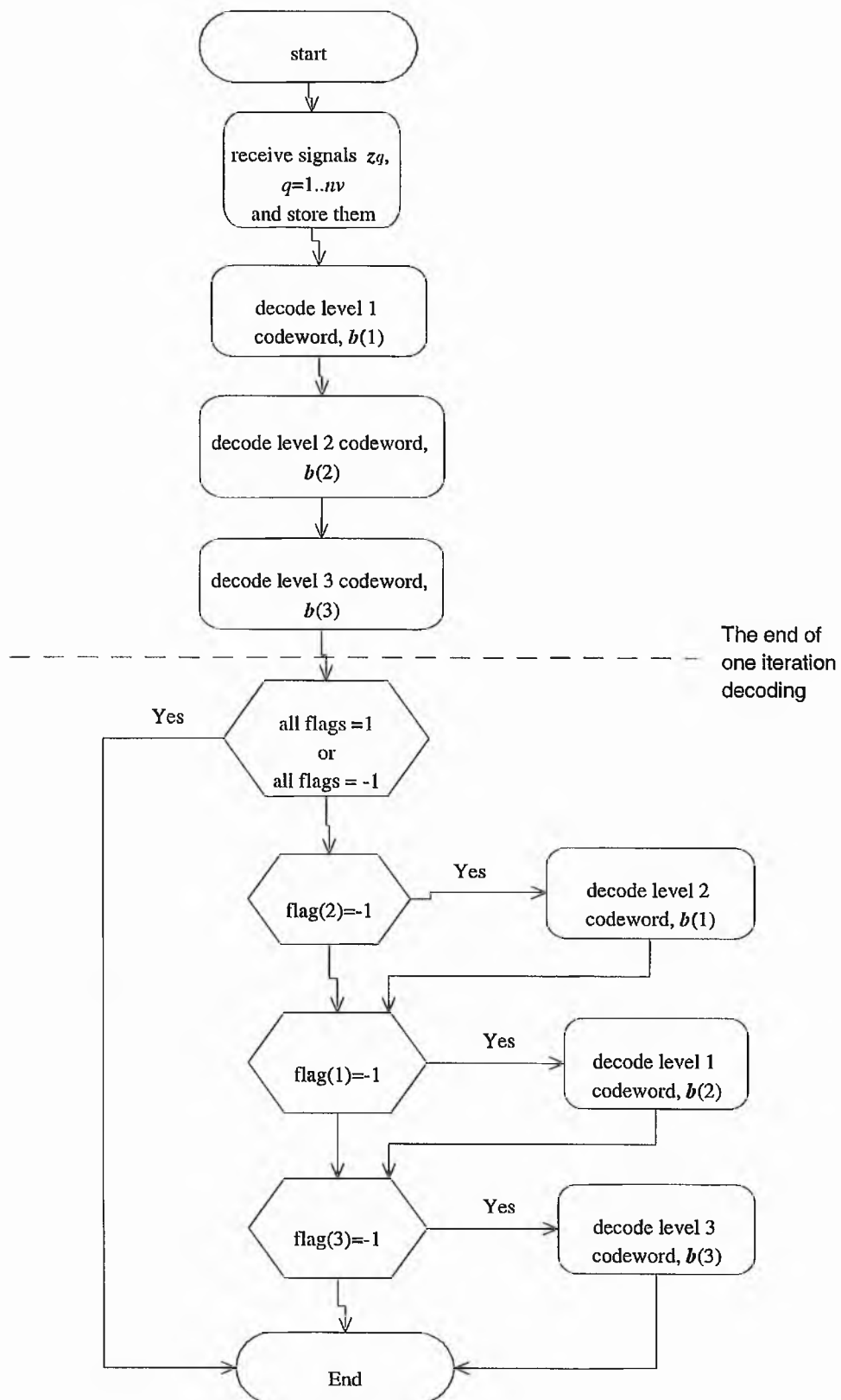
Figure 3.8 A multistage decoding procedure for the coded 8-PSK modulation

Either one or two iterations may be used for decoding. In one iteration decoding, the decoder performs decoding processes starting from the first stage until the m-th stage, once for each stage. For two iteration decoding, at the end of the first iteration the decoder checks the flags: if all flags are 1, the decoding is successful; if all flags are –1, the decoding fails. In either case, the second iteration is not needed, and the decoding is stopped. Otherwise, the decoder checks each stage's flag and performs a decoding process at the stage whose flag = –1, starting from the $(m-1)$-th until the first component codes and finish at m-th component code. Finally, when the decoding is finished, if there are decoding failures in at least at one stage, then the decoding has failed. The flow diagram of a multistage decoding procedure for the coded 8-PSK modulation is illustrated in Figure 3.8.

In one iteration decoding of Reed Solomon coded 8-PSK modulation schemes, the decoding process progresses from the first stage until the third stage. If the decoding process continues to the second iteration, the decoder will check each stage's flag and perform a decoding process at the stage whose flag = –1, starting from the second component code then the first component code and finishing at the third component code.

In the second iteration decoding, the decoding process starts from the penultimate component code, proceeds towards the first component code and finishes with the last component code. The reason for this sequence can be explained using Figure 3.9 which illustrates Ungerboeck's partitions of signal set to subset [Ungerboeck, 1982].

We assume that we use two iteration decoding and, in the first iteration decoding, the first and the second component codes have flag = –1 but the third component code has flag = 1. The decoding process therefore continues to the second iteration decoding. The third decoder puts out a codeword which gives the values of the bit 3 sequence to the demodulator. Using each bit 3 value, $b_{Dq}^{(3)}$ and a given received point, z_q, the demodulator finds the appropriate values for bit 2.

We can see from Figure 3.9 that for a given value of a bit 3, there are 0 and 1 subsets of bit 2; therefore, the demodulator can find a value for bit 2 by choosing one of the 1 subsets based on the given bit 3 value. Also we can see that on a bit 2 subset there are 0 and 1 subsets of bit 1; therefore, the demodulator will find a bit 1 value by choosing one of the 1 subsets of bit 1 based on the given bit 2 value.

It is also shown in Figure 3.9 that for a given value of bit 3, there are two 0 and two 1 subsets of bit 1. If we find a bit 1 based on a given bit 3 only, the demodulator must find a

bit 1 value by choosing one of two 0 and two 1 subsets of bit 1. Thus, we can say that it is better to find a value of bit 1 based on a given bit 2 value rather than a given bit 3 value. For this reason, the second iteration decoding starts from the $(m-1)$-th until the first component codes and finishes at the m-th component code.

Bit 1

Bit 2

Bit 3
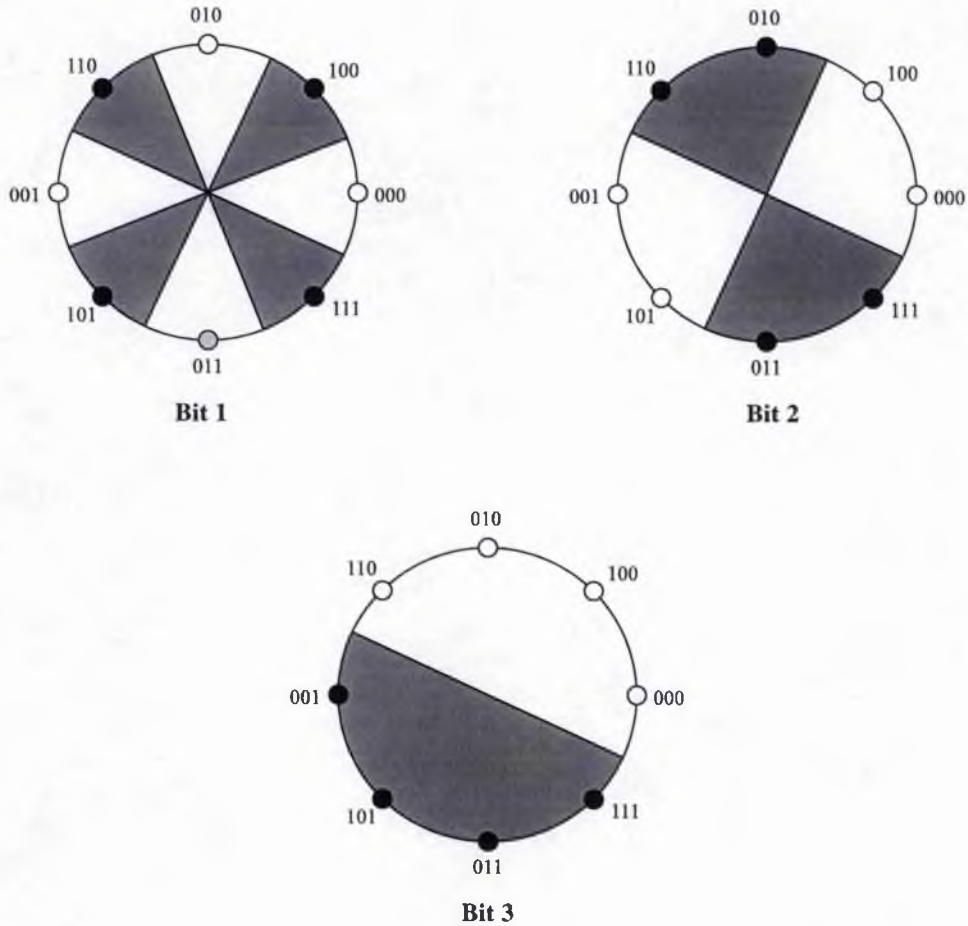
Figure 3.9 Partitions of signal set to subset for Ungerboeck's set partitioning

3.3.2. Hard-Decision Output of the Demodulator at the i-th Stage

Suppose a signal point from a signal set S is transmitted. Let $z_q \in \left\{ \text{rotated } 2^{m+1} - \text{PSK signal points} \right\}$, $z_q \in z$ where $z = (z_1, z_2, \cdots, z_{v \cdot n})$, be the

corresponding received point at the input of demodulator. The demodulator makes a hard decision (quantisation) as follows.

For the given received point z_q and decoded sublabels $b_{Dq}{}^{(j)} \in b_D{}^{(j)}$, where $1 \le j < i$ and $i < j \le m$, find the label

$$b_q = b_{Dq}{}^{(1)} b_{Dq}{}^{(2)} \ldots b_{Dq}{}^{(i-1)} b_q{}^{(i)} b_{Dq}{}^{(i+1)} \ldots b_{Dq}{}^{(m)}$$

with $b_{Dq}{}^{(1)} b_{Dq}{}^{(2)} \ldots b_{Dq}{}^{(i-1)}$ as a prefix and $b_{Dq}{}^{(i+1)} \ldots b_{Dq}{}^{(m)}$ as suffix such that

$$\text{the norm } \left\| z_q - s(b_q) \right\| \text{ is minimised,}$$

where $s(b_q)$ denotes the signal point in 2^m-PSK represented by b_q. $b_D{}^{(j)}$ is a decoded codeword in binary sequence, $b_D{}^{(i)} = \left(b_{D1}{}^{(i)} b_{D2}{}^{(i)} \ldots b_{Dv \cdot n}{}^{(i)} \right)$, as the output of the i-th stage decoder if the decoding at that stage is success, otherwise the $b_D{}^{(j)}$ is a null string. If all sub-labels, $b_{Dq}{}^{(1)} b_{Dq}{}^{(2)} \ldots b_{Dq}{}^{(i-1)}$ and $b_{Dq}{}^{(i+1)} \ldots b_{Dq}{}^{(m)}$, are null, then b_q is all signal points of 2^m-PSK. The i-th sub-label, $b_q{}^{(i)}$, of b_q is the hard-decision output of the demodulator.

This process is denoted by

$$H_i \left(z_q, b_{Dq}{}^{(1)} \ldots b_{Dq}{}^{(i-1)}, b_{Dq}{}^{(i+1)} \ldots b_{Dq}{}^{(m)} \right).$$

The hard-decision codeword output of the demodulator at the i-th decoding stage is denoted by $H_i \left(z, b^{(1)} \ldots b^{(i-1)}, b^{(i+1)} \ldots b^{(m)} \right)$, where $z = (z_1, z_2, \cdots, z_{v \cdot n})$ is the received sequence of the detector. If there is no decoded codeword in binary sequence at i-th sub-label, $b^{(i)} = \lambda$ where λ is a null string.

As a conclusion, we can formulate the whole hard-decision output of a demodulator at the i-th stage as follows.

For $1 \leq j < i$ and $i < j \leq m$, $b_D{}^{(j)} = \left(b_{D1}{}^{(j)} b_{D2}{}^{(j)} \ldots b_{Dv \cdot n}{}^{(j)} \right)$ is the decoded codeword in binary sequence at the j-th stage, and $b_D{}^{(j)} = \lambda$ if there is no decoded codeword. At i-th stage

$$H_i\left(z, b_D{}^{(1)} \ldots b_D{}^{(i-1)}, b_D{}^{(i+1)} \ldots b_D{}^{(m)} \right) \qquad 3.10$$

denote the $v \cdot n$-tuples output of demodulator whose the q-th element of Equation 3.10 is the output of $H_i\left(z_q, b_{Dq}{}^{(1)} \ldots b_{Dq}{}^{(i-1)}, b_{Dq}{}^{(i+1)} \ldots b_{Dq}{}^{(m)} \right)$.

3.3.3. An Example of Multistage Decoding

Here an example of multistage decoding for Reed Solomon coded 8-PSK modulation based on set partitioning is given. The scheme consists of 3 Reed Solomon component codes. The outputs of the 3 encoders can be expressed as a binary array with $v \cdot n$ columns and 3 rows

$$
\begin{array}{cccc}
b_1{}^{(1)} & b_2{}^{(1)} & \ldots & b_{v \cdot n}{}^{(1)} \\
b_1{}^{(2)} & b_2{}^{(2)} & \ldots & b_{v \cdot n}{}^{(2)} \\
b_1{}^{(3)} & b_2{}^{(3)} & \ldots & b_{v \cdot n}{}^{(3)}
\end{array}
$$

We assume that the encoder gave output:

$$
\begin{array}{cc}
0 & \ldots \\
0 & \ldots \\
0 & \ldots
\end{array}
$$

Here, we consider only the first coloumn of the array. As mentioned before, each coloumn of the array is assigned to each point in the 8-PSK signal space according to Ungerboeck's set partitioning scheme [Ungerboeck, 1982]. We can see in Table 3.2 that the first coloumn of the array corresponds to S_0 in Figure 3.3.

Assume that at the detector, the received signal point, z_1, is f_a in Figure 3.10. The demodulator makes a hard decision output at the first stage as follows:

For the given received point, z_1, find the label $b_1 = b^{(1)} b^{(2)} b^{(3)}$ such that the norm $\| z_1 - s(b_1) \|$ is minimised, where $s(b_1)$ denotes the signal point in 8-PSK represented by b_1. We find that the label b_1 which minimises the norm $\| z_1 - s(b_1) \|$ is 111, where $s(111)$ is S_7 in Figure 3.10. Therefore, the demodulator gives the first stage output $b^{(1)} = 1$ to the first stage Reed Solomon component code decoder.

We assume that the decoding is successful and the decoder puts out a decoded codeword $b_D^{(1)}$ with $b_{D1}^{(1)} = 0$ to the demodulator. Using the result of the Reed Solomon decoder at the first stage, the demodulator makes a hard decision output at the second stage as follows:

For the given received point z_1 and decoded sublabel $b_{D1}^{(1)} = 0$, find the label $b_1 = 0 b^{(2)} b^{(3)}$ such that the norm $\| z_1 - s(b_1) \|$ is minimised. The demodulator finds that the label b_1 which minimises the norm $\| z_1 - s(b_1) \|$ is 000, where $s(000)$ is S_0 in Figure 3.10. Thus, the hard decision output of the second stage of the demodulator is $b^{(2)} = 0$. The demodulator gives the second stage output $b^{(2)} = 0$ to the second stage Reed Solomon component code decoder.
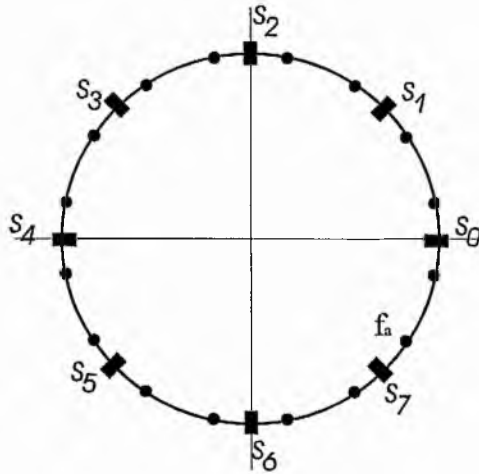
Figure 3.10 A rotated 16-PSK signal set for an 8-PSK modulator

We also assume that the decoding is successful and the decoder puts out a decoded codeword $b_D^{(2)}$ with $b_{D1}^{(2)} = 0$. to the demodulator. Using the result of the Reed Solomon decoder at the first and second stages, the demodulator makes a hard decision output at the third stage as follows:

For the given received point z_1, decoded sublabel $b_{D1}^{(1)} = 0$ and $b_{D1}^{(2)} = 0$, find the label $b_1 = 00b^{(3)}$ such that the norm $\|z_1 - s(b_1)\|$ is minimised. The demodulator finds that the label b_1 which minimises the norm $\|z_1 - s(b_1)\|$ is 000, where $s(000)$ is S_0. Thus, the hard decision output of the second stage of the demodulator is $b^{(3)} = 0$. The demodulator gives the third stage output $b^{(3)} = 0$ to the third stage Reed Solomon component code decoder.

The decoder will put out a decoded codeword $b_D^{(3)}$ if the decoding is successful to the demodulator. $b_D^{(1)}$, $b_D^{(2)}$ and $b_D^{(3)}$ are decoded codewords of the first iteration multistage decoding. If the second iteration is needed, the demodulator will continue.

3.3.4. Reed Solomon Coded Approaches for Multistage Decoding

If the Viterbi algorithm is used for multistage decoding, then the estimated information bit sequence is liable to contain error bursts. This sequence is re-encoded and fed into the decoder of the next level. Thus, the re-encoded sequence also contains error bursts. If this decoder also uses the Viterbi algorithm then it is very sensitive to these error bursts, because the algorithm is designed to deal with independent errors in the input stream.

Reed Solomon codes, on the other hand, have powerful error detection capability which distinguishes them from binary convolutional codes. In the simulations, if the decoder detected the errors but it could not correct the errors, the decoder passed the input sequence to the decoder output. Therefore, the possibility of an error propagation effect, in multistage decoding, because of undetected errors is very small.

As previously mentioned, there are two main Reed Solomon decoding techniques that can be used for multistage decoding The first approach is the frequency domain decoding technique and the second one is time domain decoding.

In the frequency domain decoding technique, we assume that a code sequence at the i-th stage $c^{(i)}(X)$ in the time domain is transmitted and that it is received with the addition of an error sequence $e^{(i)}(X)$. Then the decoder transforms the received sequence to the frequency domain, giving

$$Z^{(i)}(z) = C^{(i)}(z) + E^{(i)}(z)$$

where $Z^{(i)}(z)$, $C^{(i)}(z)$ and $E^{(i)}(z)$ are the transforms of the received sequence, the codeword and the error sequence at the i-th stage respectively. If errors in the received sequence are not beyond correction capability, the sequence polynomial of $E^{(i)}(z)$ can be obtained. Finally $C^{(i)}(z)$ is found from

$$C^{(i)}(z) = Z^{(i)}(z) - E^{(i)}(z).$$

If the decoding is successful, the decoder puts out a decoded codeword to the demodulator for use in the decoding process at other stages. This means that a decoded codeword must be in the time domain, and thus an inverse transform must be done to a decoded codeword

$$\mathbf{c}_D^{(i)}(X) = F^{-1}\left\{C^{(i)}(z)\right\}$$

This procedure is illustrated in Figure 3.11, in which $A(z)$ is a frequency domain polynomial. If the decoding is successful, all parity check symbols which are located in the first $2t$ positions will be zero. Thus, we can have an information polynomial from a code polynomial by using

$$A(z) = z^{-(n-k)}C(z).$$

In other words, the decoded information symbols are found in the last k positions.

In the time domain technique, the decoder at the i-th stage receives the sequence

$$z^{(i)}(x) = c^{(i)}(x) + e^{(i)}(x)$$

where $z^{(i)}(x)$, $c^{(i)}(x)$ and $e^{(i)}(x)$ are the received sequence, the codeword and the error sequence at the i-th stage respectively. In this case we assume that a code sequence at the i-th stage $c^{(i)}(x)$ is transmitted.

If errors in the received sequence are not beyond correction capability the sequence polynomial of $e^{(i)}(x)$ can be obtained. Finally $c^{(i)}(x)$ is found from

$$c^{(i)}(x) = r^{(i)}(x) - e^{(i)}(x).$$

Similar to a frequency domain technique, if the decoding is successful, the decoder puts out a decoded codeword to the demodulator for the decoding process at other stages. However in this technique, the codeword $c^{(i)}(x)$ is in the same domain as $z^{(i)}(x)$. Thus

$$\mathbf{c}_D^{(i)}(x) = c^{(i)}(x).$$

This procedure is illustrated in Figure 3.12, in which $a(x)$ is a time domain polynomial. As explained in section 2.3, the time domain coding technique used here will produce the code in a systematic form. The systematic Reed Solomon code is represented by:

$$c(x) = x^{n-k} a(x) + b(x)$$

where $b(x)$ is a parity check polynomial. Parity check symbols are placed in the first $(n-k)$ positions and information symbols are placed in the last k positions. Therefore, the decoded information symbols are found symbols in the last k positions of the decoded codeword.

For this reason, if we assume that the frequency domain and the time domain techniques have the same degree of computational complexity, the time domain technique will be better than the frequency domain technique for multistage decoding.
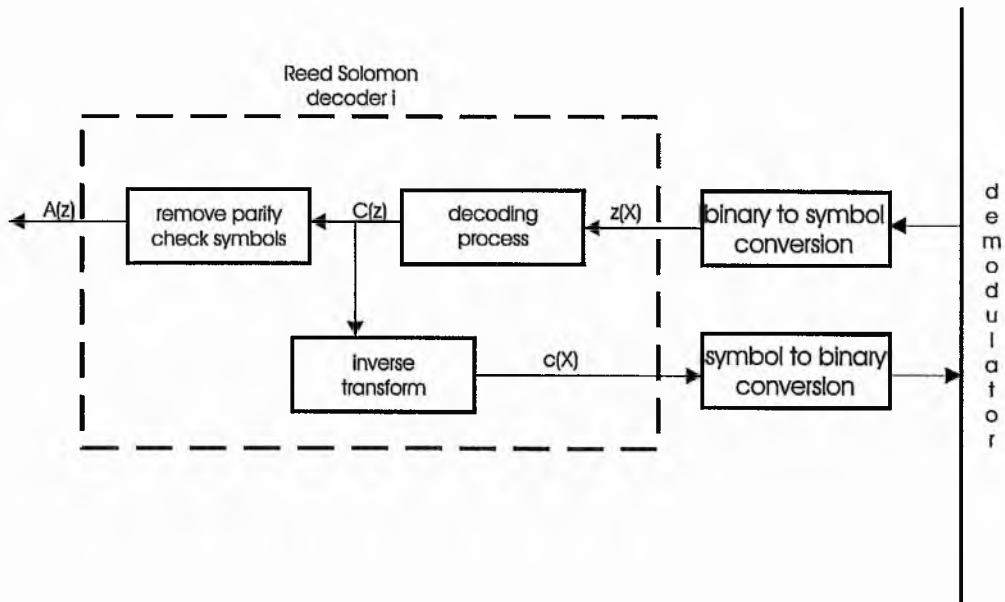
Figure 3.11 A frequency domain technique decoder for multistage decoding
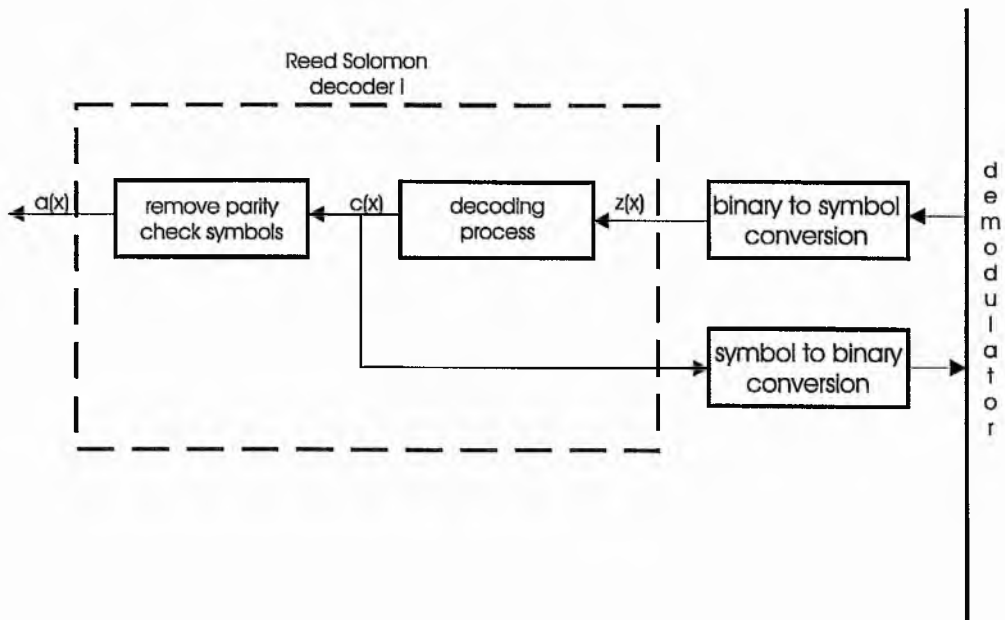
Figure 3.12 A time domain technique decoder for multistage decoding

58

3.4. DISTANCE CONSIDERATIONS FOR REED SOLOMON CODED MODULATION BASED ON SET PARTITIONING

Consider a block-coded 8-PSK scheme consisting of three binary component codes C_{b1}, C_{b2} and C_{b3} with minimum Hamming distances d_{min1}, d_{min2} and d_{min3}, respectively. The minimum Euclidean distance between two distinct codewords of this block-coded scheme can be evaluated by considering their binary arrays.

The minimum squared Euclidean distance, D_{min}^2, of binary block coded 8-PSK scheme is obtained as

$$D_{min}^2 = \min\left(\Delta_0^2 \cdot d_{min1}, \Delta_1^2 \cdot d_{min2}, \Delta_2^2 \cdot d_{min3}\right).$$ 3.11

This is illustrated in Figure 3.13. Thus in a binary block coded scheme design, the minimum Hamming distance of each component code can be determined by setting

$$\Delta_0^2 d_{min1} \cong \Delta_1^2 d_{min2} \cong \Delta_2^2 d_{min3}$$ 3.12

where $\cong$ is the same or almost the same.

It is difficult to determine the minimum Hamming distance of each component code of Reed Solomon coded modulation based on set partitioning for the following reasons:

Firstly Reed Solomon codes are non-binary codes, so Equation 3.11 is no longer valid for this code.

Secondly, in multistage decoding the first stage decoding gives a decoded codeword to the second stage decoding, the second stage decoding gives a decoded codeword to the third stage decoding and so on. Thus the second stage decoding depends on and takes advantages from the first stage decoding, the third stage decoding depends on and takes advantages from the second and first stage decoding and so on.

Thirdly, Equation 3.11 is valid for a Gaussian channel only. Thus, the Equation of the minimum squared Euclidean distance, D_{min}^2, of binary block coded 8-PSK scheme in other channels can be different.

Consequently, the minimum Hamming distance of each component code can not be exactly determined using Equation 3.12.
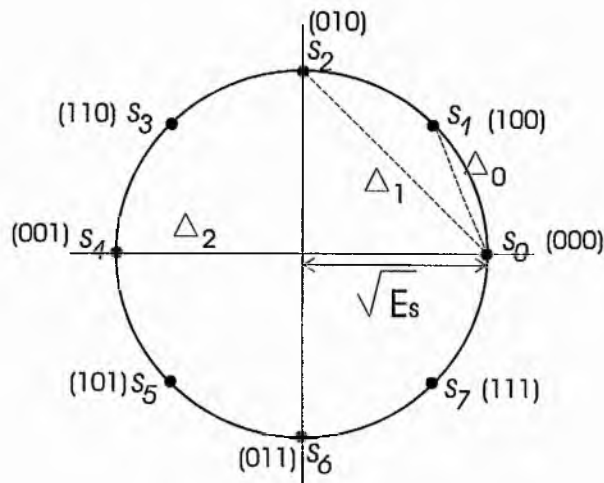
$$\Delta_0^2 = 0.586E_s$$
$$\Delta_1^2 = 2E_s$$
$$\Delta_2^2 = 4E_s$$

Figure 3.13 8PSK signal set.

3.5. THE IMPLEMENTATIONS OF REED SOLOMON CODED MODULATION

A variety of Reed Solomon coded modulations based on set partitioning and not based on set partitioning schemes, as explained in this chapter, have been implemented for the Gaussian channel and a Rayleigh fading channel. In chapter 4, the designs of coded modulation schemes over the Gaussian channel (i.e. the choice of code configurations which are suitable for this channel) are studied and the error performance over the Gaussian channel of the two approaches as stated above is analysed.

In chapter 5, a design study of coded modulation schemes (i.e. choice of code configurations which are suitable for this channel) and the error performance analysis over a Rayleigh fading channel are given. These schemes, as explained in this chapter, will be compared with other coded modulation schemes in chapters 4 and 5.

CHAPTER 4

CODE DESIGN AND PERFORMANCE FOR THE GAUSSIAN CHANNEL

In this chapter, the designs of coded modulation schemes for the Gaussian channel (i.e. choice of the code configurations which are suitable for this channel) are studied and the error performance over the Gaussian channel of Reed Solomon coded modulation schemes is analysed. The performance of Reed Solomon coded modulation based on set partitioning is compared with Reed Solomon coded modulation not based on set-partitioning, then with multilevel Reed Solomon coded modulation using Gray mapping and finally with coded modulation schemes using binary codes, Reed Muller codes. We need to establish comparisons between the many different methods previously described to see if there are any general conclusions to be drawn about which is best.

In order to analyse the performance of Reed Solomon coded modulation, the simulation package COSSAP has been used. COSSAP is an integrated design and simulation environment for communication system modelling. Using the programming language C it has been possible to produce various models for Reed Solomon coded modulation simulations in COSSAP. More explanation about the simulation package COSSAP is given in Appendix A.

For all simulations, we assume perfect carrier phase tracking at the receiver. In the simulation results, bit error rate (BER) is plotted versus the parameter E_b/N_0, where E_b

is the average energy per information bit and N_0 single-sided power spectral density. We have

$$\frac{E_b}{N_0} = \frac{1}{m \cdot R_c} \frac{E_s}{N_0}$$

where m is the number of bits per transmitted symbol, R_c a code rate used by an encoder and E_s the average energy of the signals representing the symbols.

In the following sections, we analyse the error performance of the proposed schemes, Reed Solomon coded modulation based on set-partitioning. These schemes will be compared with Reed Solomon coded modulation not based on set-partitioning, then with multilevel Reed Solomon coded modulation using Gray mapping and finally with coded modulation schemes using binary codes, Reed Muller codes.

Here, we will discuss the partitioned Reed Solomon coded modulation design over the AWGN channel and compare it with other schemes. Then in the next chapter, we will analyse the design of partitioned Reed Solomon coded modulation over a Rayleigh fading channel, also compared with other schemes.

4.1. THE GAUSSIAN CHANNEL

We assume that the signals are transmitted on a channel where the only impairment is additive white Gaussian noise with single-sided power spectral density N_0. The output of the channel becomes

$$r_q = x_q + w_q$$

where x_q is the transmitted complex-valued discrete channel signal transmitted at modulation time $q \cdot T$, and w_q is an independent normally distributed noise sample with zero-mean and variance

$$\sigma^2 = \frac{N_0}{2}$$

along each dimension. The symbol interval is T.

4.1.1. M-ary Phase Shift Keying

Figure 4.1 shows the configuration of the simulation to establish the performance of the MPSK scheme. This simulation is using Gray code mapping, the mapping or assignment of m information bits to the $M = 2^m$ possible signal points in which the adjacent signal points differ by one binary digit.
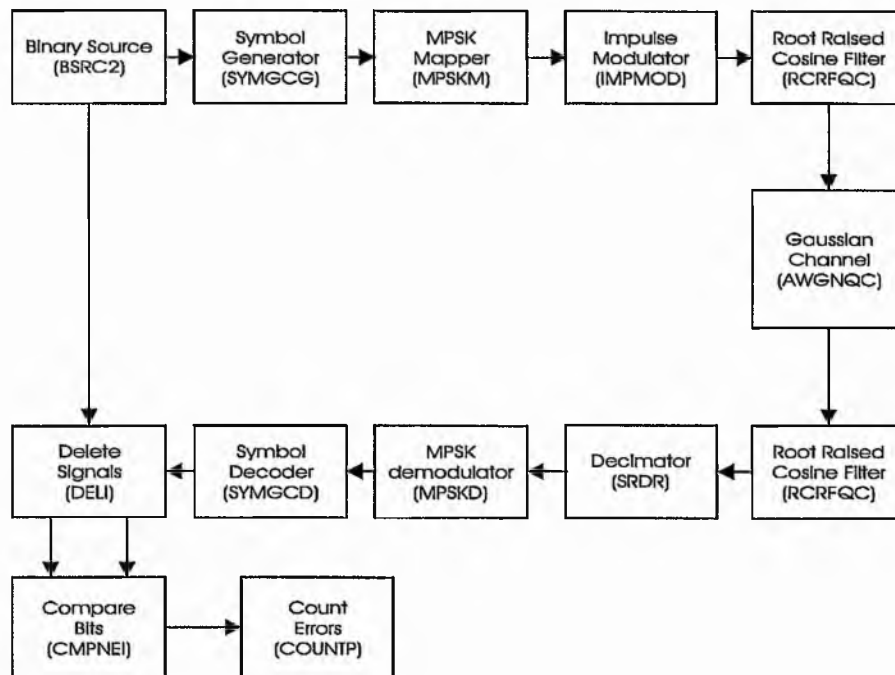
Figure 4.1 A COSSAP system diagram for an MPSK simulation configuration.

In a COSSAP system, the impulse modulator (IMPMOD) generates impulses which are weighted by the incoming signal elements and have a sampling rate of

$$\frac{1}{\text{Sampling Time}} = \text{Rate Factor} * \text{Symbol Rate}.$$

Thus, the model multiplies each input signal element by 1/(Sampling Time) and inserts (Rate Factor − 1) zeros after each result. The inverse operation of the impulse modulator is the sampling rate decimation (SRDR). The decimator writes each (Decimator Factor)-th signal element to the output.

Block DELI in Figure 4.1 is used to delete a certain number of signals (the same as the fast Fourier transform length) because the filter needs time to settle down. In other words, COSSAP filters out the transient errors in the fast Fourier transform computation.

The error performances of QPSK and 8-PSK can be seen in Figure 4.2. The performance of QPSK from the simulation is similar to that from theory.
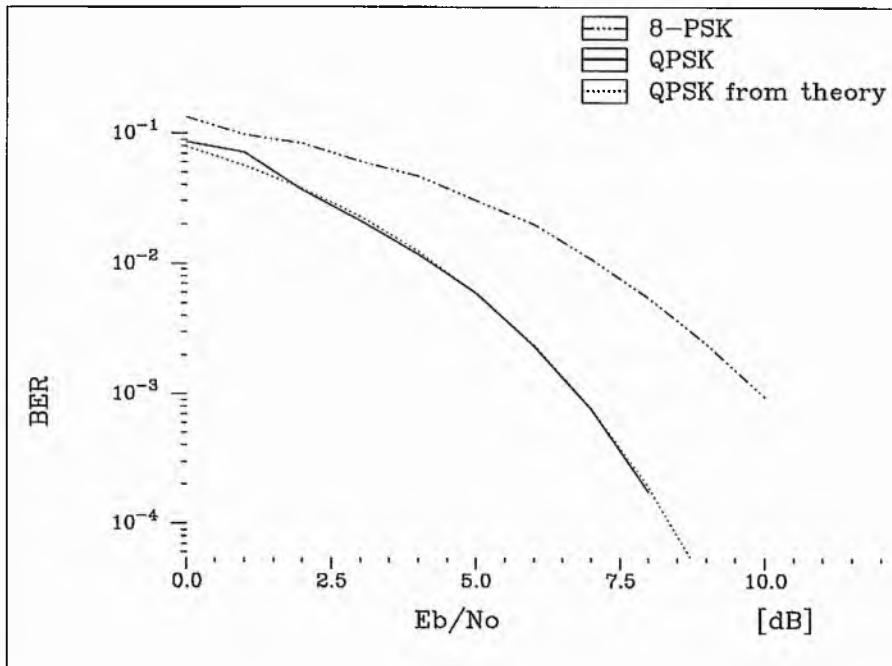
Figure 4.2 The error performances of QPSK and 8-PSK.

4.2. REED SOLOMON CODED MPSK MODULATION NOT BASED ON SET PARTITIONING

These schemes are using Gray code mapping to assign m coded bits to the $M = 2^m$ possible signal points. Several Reed Solomon codes are used in these simulations. Figure 4.3 shows the error performances of RS(31, 17) and RS(63, 33) codes combined with a QPSK signal set.
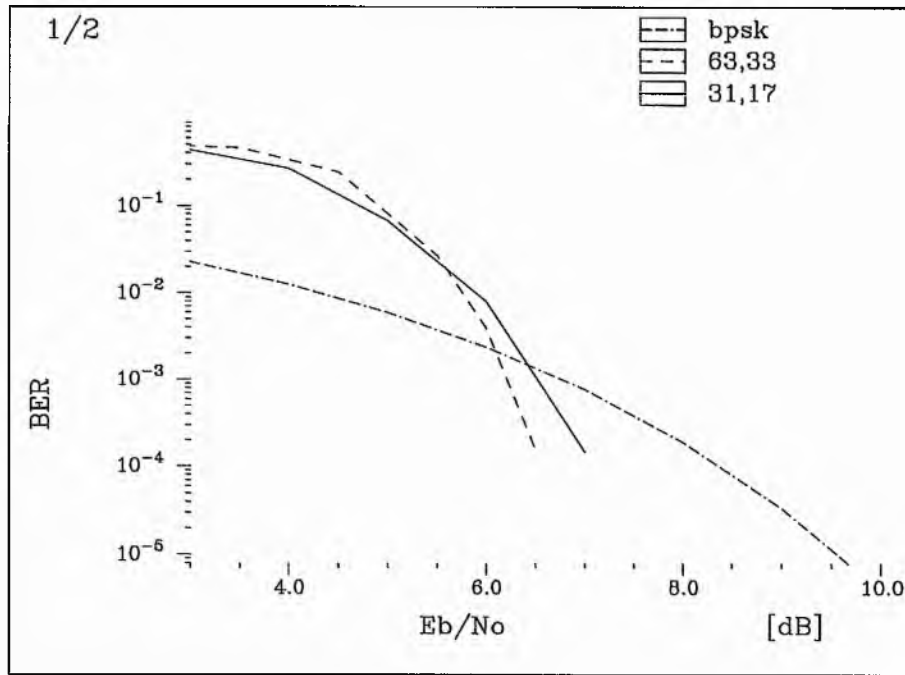
Figure 4.3 The error performances of RS(31, 17) and RS(63, 33) codes combined with a QPSK signal set.

The first code is an implementation of the first method discussed in section 3.1 in which the MPSK signal set used for modulation does not correspond with the finite field over which the code is defined. This code has code rate $R_c = {}^{17}\!/_{31}$, which translates into a throughput of 1.1 bit sec^{-1} Hz^{-1} which is comparable to that of uncoded BPSK. The second code is an implementation of the third method. The code rate is 33/63 which translates into a throughput of 1.05 bit sec^{-1} Hz^{-1}.

Figure 4.4 shows the error performances of RS(63, 43) and RS(127, 85) codes combined with an 8-PSK signal set. The first code rate is 43/63 which translates into a throughput of 2 bit sec^{-1} Hz^{-1}, comparable to that of uncoded QPSK. The second code has code rate $R_c = {}^{85}\!/_{127}$, which translates into a throughput of 2.008 bit sec^{-1} Hz^{-1}, again comparable to that of uncoded QPSK.

The first code is an implementation of the third method and the second code is an implementation of the first method discussed in section 3.1. In the first method, the MPSK signal set used for modulation does not correspond with the finite field over which the code is defined. In the third method, each symbol of the Reed Solomon code consists of the concatenation of y channel symbols. The results show that the longer the code we use the better the performance becomes.
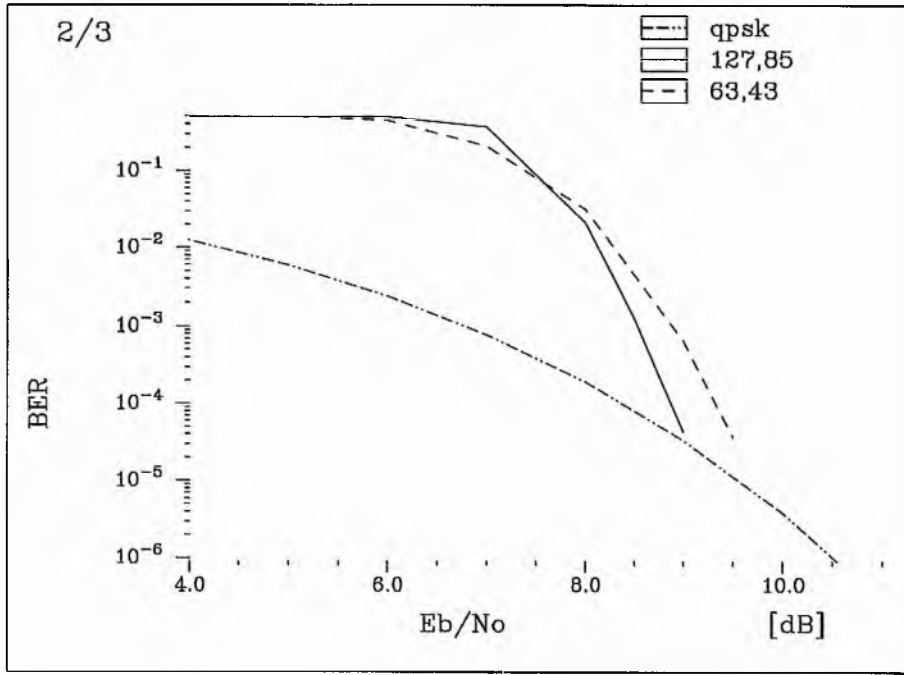
Figure 4.4 The error performances of RS(63, 43) and RS(127, 85) codes combined with an 8-PSK signal set.

4.3. REED SOLOMON CODED MPSK MODULATION BASED ON SET PARTITIONING

In this approach, each level of the *m* bits defining an MPSK symbol is coded and decoded by different Reed Solomon codecs. The set partitioning principle is applied to define subsets with distances Δ_i, ($i = 1$ to m) that are nondecreasing with i. Each stage of the *m* bits defines a subset and is decoded using multistage decoding. Figure 4.5 shows a block diagram for multistage decoding of partitioned Reed Solomon coded 8-PSK modulation. The complete explanation of this approach was given in section 3.2.

As previously mentioned in section 3.4, in binary coded schemes the minimum Hamming distance of each level component-code over the Gaussian channel can be determined by setting

$$\Delta_0{}^2 d_{\min 1} \cong \Delta_1{}^2 d_{\min 2} \cong \Delta_2{}^2 d_{\min 3} \qquad 4.1$$

67

for coded 8-PSK modulation, and

$$\Delta_0{}^2 d_{\min 1} \cong \Delta_1{}^2 d_{\min 2} \qquad\qquad 4.2$$

for coded QPSK modulation.

However, it is difficult to determine the minimum Hamming distance of each component code of partitioned Reed Solomon coded modulation for the following reasons:

- Reed Solomon codes are non-binary codes.
- In multistage decoding the first stage decoding gives a decoded codeword to the second stage decoding, the second stage decoding gives a decoded codeword to the third stage decoding and so on. Thus the second stage decoding depends on and takes advantages from the first stage decoding, the third stage decoding depends on and takes advantages from the second and first stage decoding and so on.
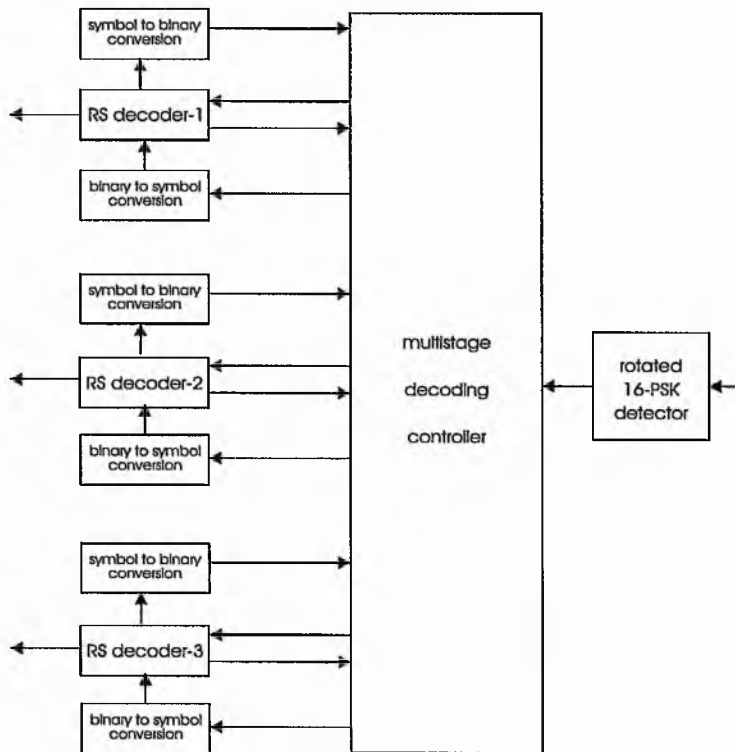
Figure 4.5 Multistage decoding block diagram

Thus, we should do many simulations to find a good configuration for a specific code length which is measured in symbols rather than bits. Reed Solomon codes provide a wide range of code rates, therefore there are many configurations of component codes for partitioned Reed Solomon coded modulation, Figures 4.6 - 4.9 show error performances of a selection of schemes. Table 4.1 gives a list of component-code configurations, which have the best error performance for specific code length, for coded 8-PSK modulation and Table 4.2 for coded QPSK modulation.

Figure 4.6 shows the error performances of Reed Solomon codes with code length of 31 combined with QPSK modulation using various component-code configurations, and Figure 4.7 shows the error performances of Reed Solomon codes with code length of 63 combined with QPSK modulation also using various component-code configurations. Label k_1, t_1; k_2, t_2 denotes that the first level component-code has information length of k_1 and t_1 error-correcting capability, and the second level component-code has information length of k_2 and t_2 error-correcting capability.

The relation of k_1 and t_1 of an RS(n, k_1) code is

$$t_1 = \frac{n - k_1}{2}.$$

And the minimum Hamming distance of an RS(n, k_1) code is

$$d_{\min} = n - k_1 + 1$$

or

$$d_{\min} = 2t_1 + 1$$

The overall code rate of partitioned Reed Solomon coded QPSK modulation, whose first level component code is an RS(n, k_1) code and the second level component code an RS(n, k_2) code, is

$$R_c = \frac{\sum\limits_{i=1}^{m} k_i}{\sum n} \qquad\qquad , m = 2 \text{ for coded QPSK modulation}$$

$$= \frac{k_1 + k_2}{2n}$$

where each level component-code has the same code length, n, and m is number of bits defining a MPSK symbol, assuming all component codes have same size symbols. Finally, the throughput of partitioned Reed Solomon coded QPSK modulation is $m \cdot R_c$ bit sec^{-1} Hz^{-1}.

For example, the curve with label 7, 12; 25, 3 in Figure 4.6 is the error performance of partitioned Reed Solomon coded QPSK modulation with code length of 31 whose the information length and error-correcting capability of the first level component code are 7 and 12, the information length and error-correcting capability of the second level component code are 25 and 3. The first level component-code has minimum Hamming distance of $2t_1 + 1 = 2 \times 12 + 1 = 25$ and the second level component code has minimum Hamming distance of $2t_2 + 1 = 2 \times 3 + 1 = 7$. This scheme gives a code rate of $R_c = \frac{(7+25)}{31 \times 2} = 0.516$ which translates into a throughput of $2 \times R_c = 2 \times 0.516 = 1.03$ bit sec^{-1} Hz^{-1} which is comparable to that of uncoded BPSK.

It is seen that the best error performance of partitioned Reed Solomon coded QPSK modulation with code length of 31 in Figure 4.6 is the error performance with label 7, 12; 25, 3. The properties of this component-code configuration have been explained in the previous paragraph.

The best error performance of partitioned Reed Solomon coded QPSK modulation with code length of 63 in Figure 4.7 is the error performance with label 11, 26; 53, 5. The information length and error-correcting capability of the first level component code are 11 and 26, the information length and error-correcting capability of the second level component code are 53 and 5. The first level component-code has minimum Hamming distance of $2t_1 + 1 = 2 \times 26 + 1 = 53$ and the second level component code has minimum Hamming distance of $2t_2 + 1 = 2 \times 5 + 1 = 11$. This scheme gives a code rate of $R_c = \frac{(11+53)}{63 \times 2} = 0.508$ which translates into a throughput of $2 \times R_c = 2 \times 0.508 = 1.01$ bit sec^{-1} Hz^{-1} which is comparable to that of uncoded BPSK.
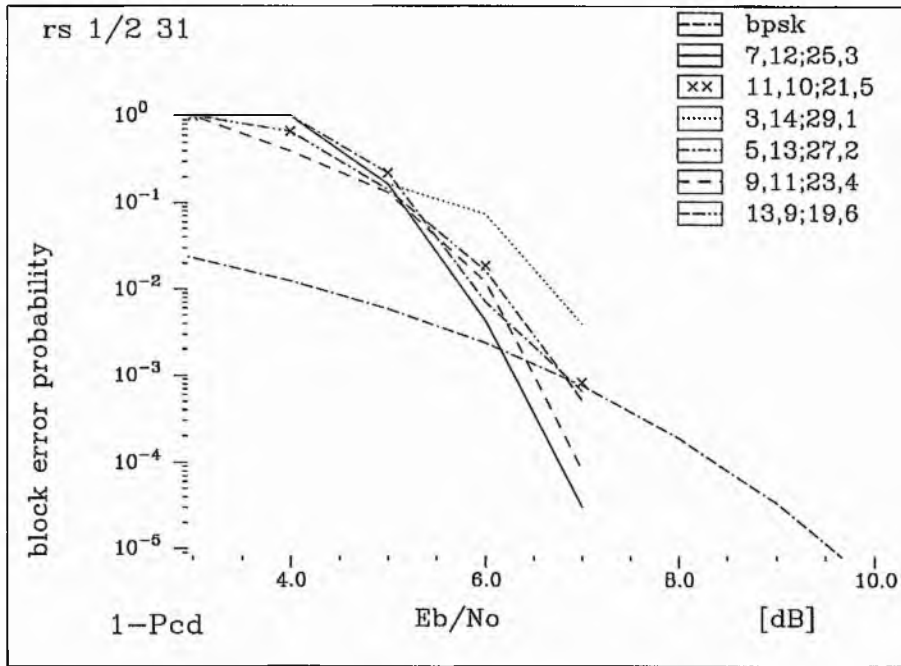
Figure 4.6 The error performances of various configurations of set-partitioned RS coded QPSK modulation with code length of 31.

Figure 4.7 The error performances of various configurations of set-partitioned RS coded QPSK modulation with code length of 63.

Figures 4.8 shows the error performances of Reed Solomon codes with code length of 63 combined with 8-PSK modulation using various component-code configurations, and Figure 4.9 shows the error performances of Reed Solomon codes with code length of 127 combined with 8-PSK modulation also using various component-code configurations. Label k_1, t_1; k_2, t_2; k_3, t_3 denotes that the first level component-code has information length of k_1 and t_1 error-correcting capability, then the second level component-code has information length of k_2 and t_2 error-correcting capability, and finally the third level component-code has information length of k_3 and t_3 error-correcting capability.

The overall code rate of partitioned Reed Solomon coded 8-PSK modulation, whose first level component code is an RS(n, k_1) code, the second level component code an RS(n, k_2) code and the third level component code an RS(n, k_3) code, is

$$R_c = \frac{\sum_{i=1}^{m} k_i}{\sum n} \qquad , m = 3 \text{ for coded 8-PSK modulation}$$

$$= \frac{k_1 + k_2 + k_3}{3n}$$

where each level component-code has the same code length, n, and m is number of bits defining a MPSK symbol, assuming all component codes have same size symbols. The throughput of partitioned Reed Solomon coded 8-PSK modulation is $m \cdot R_c$ bit sec^{-1} Hz^{-1}.

For example, the curve with label 7, 28; 59, 2; 61, 1 in Figure 4.8 is the error performance of partitioned Reed Solomon coded 8-PSK modulation with code length of 63 where the information length and error-correcting capability of the first level component code are 7 and 28, the information length and error-correcting capability of the second level component code are 59 and 2 and the information length and error-correcting capability of the third level component code are 61 and 1. The first level component-code has minimum Hamming distance of $2t_1 + 1 = 2 \times 28 + 1 = 57$, the second level component code has minimum Hamming distance of $2t_2 + 1 = 2 \times 2 + 1 = 5$ and the third level component code has minimum Hamming distance of $2t_3 + 1 = 2 \times 1 + 1 = 3$. This scheme gives a code rate of $R_c = {(7+59+61)}/{63 \times 3} = 0.672$ which translates into a throughput of $3 \times R_c = 3 \times 0.672 = 2.01$ bit sec^{-1} Hz^{-1} which is comparable to that of uncoded QPSK.

It is seen that the best error performance of partitioned Reed Solomon coded QPSK modulation with code length of 63 in Figure 4.8 is the error performance with label 7, 28;

59, 2; 61, 1. The properties of this component-code configuration have been explained in the previous paragraph.

The best error performance of partitioned Reed Solomon coded 8-PSK modulation with code length of 127 in Figure 4.9 is the error performance with label 11, 58; 119, 4; 125, 1. The information length and error-correcting capability of the first level component code are 11 and 58, the information length and error-correcting capability of the second level component code are 119 and 4 and the information length and error-correcting capability of the third level component code are 125 and 1. The first level component-code has minimum Hamming distance of $2t_1 + 1 = 2 \times 58 + 1 = 117$, the second level component code has minimum Hamming distance of $2t_2 + 1 = 2 \times 4 + 1 = 9$ and the third level component code has minimum Hamming distance of $2t_3 + 1 = 2 \times 1 + 1 = 3$. This scheme gives a code rate of $R_c = \frac{(11+119+125)}{127 \times 3} = 0.669$ which translates into a throughput of $3 \times R_c = 3 \times 0.669 = 2.007$ bit sec^{-1} Hz^{-1} which is comparable to that of uncoded QPSK.
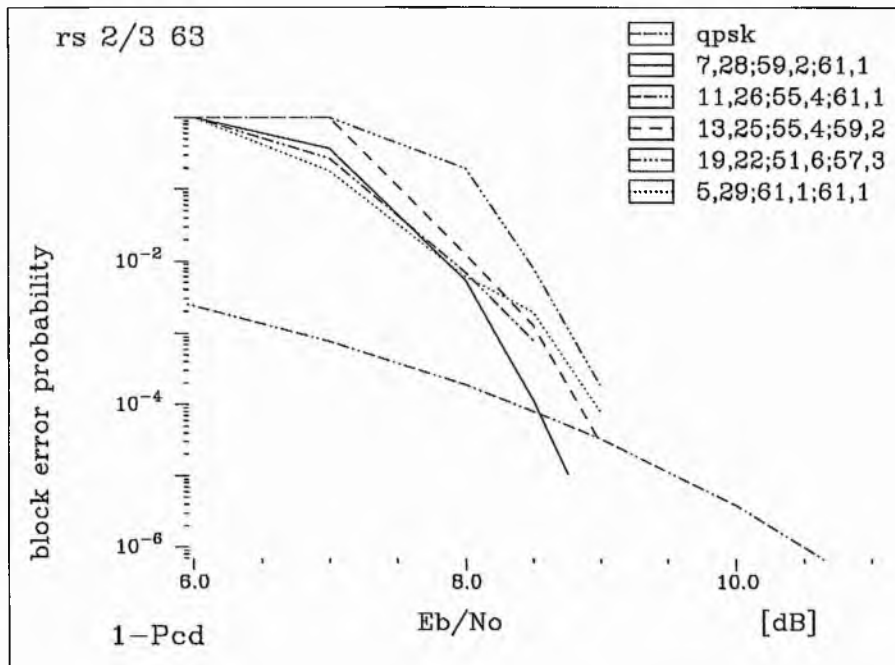
Figure 4.8 The error performances of various configurations of set-partitioned RS coded 8-PSK modulation with code length of 63.
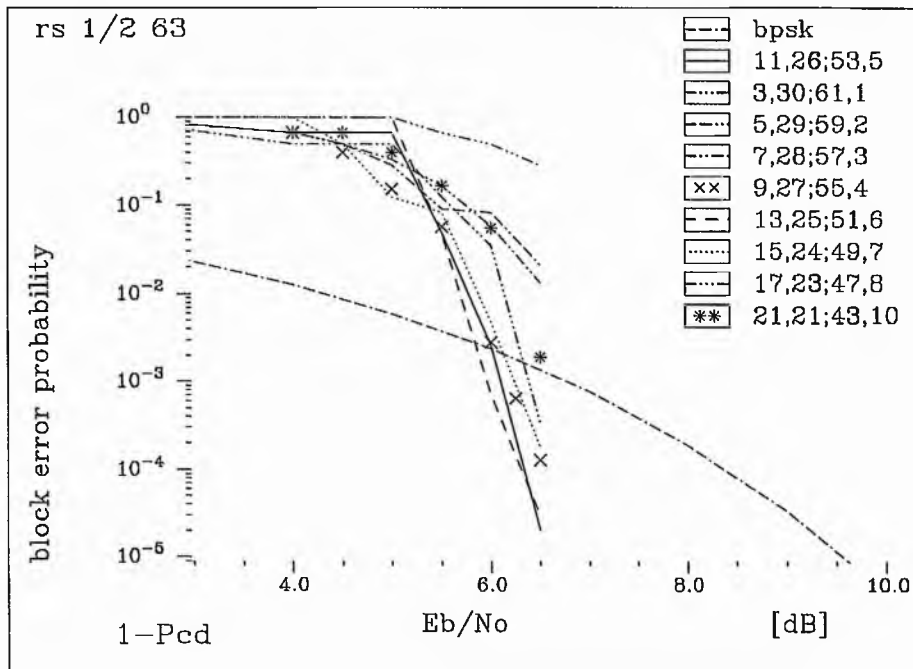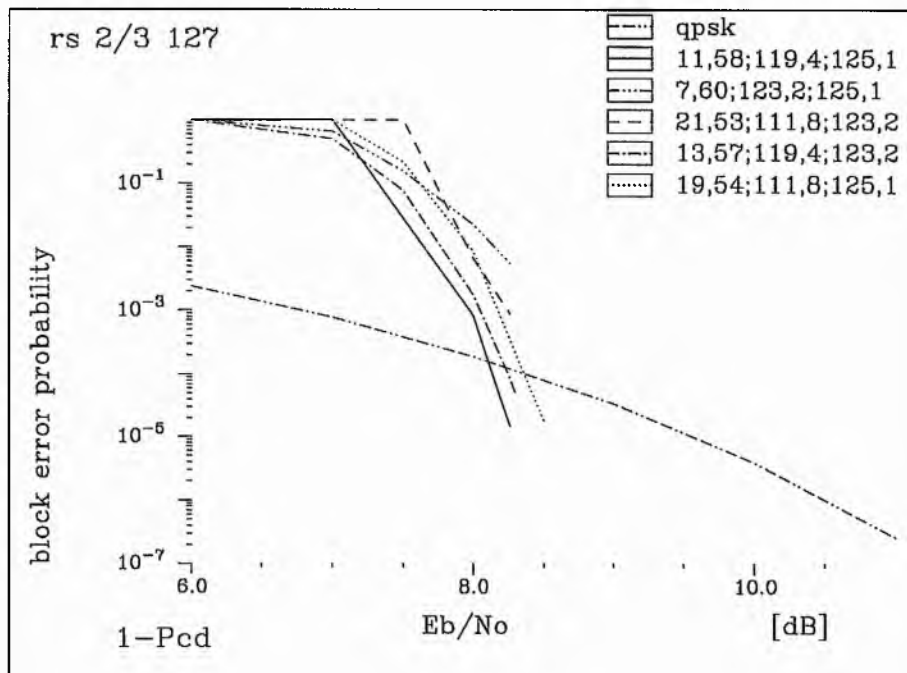
Figure 4.9 The error performances of various configurations of set-partitioned RS coded 8-PSK modulation with code length of 127.

level	$n = 63$		$n = 127$	
	k	d_{min}	k	d_{min}
1	7	57	11	117
2	59	5	119	9
3	61	3	125	3
throughput ($bit\ s^{-1}\ Hz^{-1}$)	2.01		2.007	
information-bit length	$(7+59+61) \cdot 6 = 762$		$(11+119+125) \cdot 7 = 1785$	

Table 4.1 Configuration of good schemes for RS coded 8-PSK modulation for code length of 63 and 127

level	$n = 31$		$n = 63$	
	k	$d_{\min}$	k	$d_{\min}$
1	7	25	11	53
2	25	7	53	11
throughput (bit s^{-1} Hz^{-1})	1.03		1.01	
information-bit length	$(7+25)\cdot5 = 160$		$(11+53)\cdot6 = 384$	

Table 4.2 Configuration of good schemes for RS coded QPSK modulation for code length of 31 and 63.

A list of component-code configurations, which have the best error performance for specific code length, for coded 8-PSK modulation can be seen in Table 4.1 and a list of component-code configurations, which have the best error performance for specific code length, for coded QPSK modulation can be seen in Table 4.2. These schemes are emerged from trials of a range of schemes with different code configurations.

As previously mentioned before, Equations 4.1 and 4.2 do not hold for Reed Solomon coded modulation; for example, for a good code of length 63 from Table 4.1:

$$\Delta_0{}^2 \cdot d_{\min 1} = 0.586 \times 57 = 33.4$$

$$\Delta_1{}^2 \cdot d_{\min 2} = 2 \times 5 = 10$$

$$\Delta_2{}^2 \cdot d_{\min 3} = 4 \times 3 = 12$$

and for a good scheme of length 31 from Table 4.2:

$$\Delta_0{}^2 \cdot d_{\min 1} = 1 \times 25 = 25$$

$$\Delta_1{}^2 \cdot d_{\min 2} = 2 \times 7 = 14$$

From these results we can see that the minimum Hamming distance of each level component code for Reed Solomon coded modulation based on set partitioning can not be determined from Equations 4.1 and 4.2. This is in line with our predictions in section 4.3.

4.3.1. Comparisons with Reed Solomon Coded Modulation not Based on Set Partitioning

Here, we compare the error performances of partitioned Reed Solomon coded modulation with those of non-partitioned. Figures 4.10 - 4.11 show block error probability for several schemes for coded QPSK modulation and Figures 4.12 - 4.13 for coded 8-PSK modulation. In these figures, the block error probability performance of Reed Solomon coded modulation schemes are compared with that of uncoded reference modulation systems for transmitting the same (or almost the same) number of information bits.

In Figure 4.10, the partitioned coded QPSK modulation of length 31, listed in Table 4.2, has component codes of RS(31,7) and RS(31,25) resulting in an information length of (7 + 25) symbols or $(7+25)\cdot v$ bits, where v is number of bits for one code symbol. The v of partitioned coded QPSK modulation of length 31 is 5, thus the information length is $(7+25)\cdot v = (7+25)\cdot 5 = 160$ bits.

In this picture, block error probability performance of partitioned Reed Solomon coded QPSK modulation of length 31 is compared with that of non-partitioned RS(63,33) which has information length of 33 symbols or $33\cdot v$ bits. The number of bits for one code symbol (v) of RS(63,33) is 6, thus the information length is $33\cdot v = 33\times6 = 198$ bits which is almost the same as the information length of partitioned Reed Solomon coded QPSK modulation (160 bits). The reference is the block error probability performance of uncoded 160-bit block BPSK.

In Figure 4.11, the partitioned coded QPSK modulation of length 63, listed in Table 4.2, has component codes of RS(63,11) and RS(63,53) resulting in an information length of (11 + 53) symbols or $(11+53)\cdot v$ bits. The number of bits of one code symbol (v) of partitioned coded QPSK modulation of length 63 is 6, thus the information length is $(11+53)\cdot v = (11+53)\cdot 6 = 384$ bits.

In this figure, block error probability performance of partitioned Reed Solomon coded QPSK modulation of length 63 is compared with that of non-partitioned RS(127, 65) which has information length of 65 symbols or $65\cdot v$ bits. The number of bits for one code symbol (v) of RS(127, 65) is 7, thus the information length is $65\cdot v = 65\times7 = 455$ bits which is almost the same as the information length of partitioned Reed Solomon coded QPSK modulation (384 bits). The reference is the block error probability performance of uncoded 384-bit block BPSK.

Next in Figure 4.12, the partitioned coded 8-PSK modulation of length 63, listed in Table 4.1, has component codes of RS(63,7), RS(63,59) and RS(63,61) resulting in an information length of (7 + 59 + 61) symbols or $(7+59+61)\cdot v$ bits. The number of bits of one code symbol (v) of partitioned coded 8-PSK modulation of length 63 is 6, thus the information length is $(7+59+61)\cdot v = (7+59+61)\cdot 6 = 762$ bits.

In this figure, block error probability performance of partitioned Reed Solomon coded 8-PSK modulation of length 63 is compared with that of non-partitioned RS(127, 85) which has information length of 85 symbols or $85\cdot v$ bits. The number of bits for one code symbol (v) of RS(127, 85) is 7, thus the information length is $85\cdot v = 85\times7 = 595$ bits which is almost the same as the information length of partitioned Reed Solomon coded 8-PSK modulation (762 bits). The reference is the block error probability performance of uncoded 762-bit block QPSK.

Finally in Figure 4.13, the partitioned coded 8-PSK modulation of length 127, listed in Table 4.1, has component codes of RS(127,11), RS(127,119) and RS(127,125) resulting in an information length of (11 + 119 + 125) symbols or $(11+119+125)\cdot v$ bits. The number of bits of one code symbol (v) of partitioned coded 8-PSK modulation of length 127 is 7, thus the information length is $(11+119+125)\cdot v = (11+119+125)\cdot 7 = 1785$ bits.

In this figure, block error probability performance of partitioned Reed Solomon coded 8-PSK modulation of length 127 is compared with that of non-partitioned RS(255, 171) which has information length of 171 symbols or $171\cdot v$ bits. The number of bits for one code symbol (v) of RS(255, 171) is 8 thus, the information length is $171\cdot v = 171\times8 = 1368$ bits which is almost the same as the information length of partitioned Reed Solomon coded 8-PSK modulation (1785 bits). The reference is the block error probability performance of uncoded 1786-bit block QPSK.

We can see in Figure 4.10 that at a block error probability of 10^{-4}, the partitioned coded QPSK modulation of length 31 is just 0.1 dB worse than non-partitioned coded QPSK modulation of length 63. In Figure 4.11, at a block error probability of 10^{-4}, the partitioned coded QPSK modulation of length 63 is just 0.1 dB worse than non-partitioned coded QPSK modulation of length 127. Therefore, we can conclude that for coded QPSK modulation, partitioned Reed Solomon coded modulation has an improvement over non-partitioned by an amount approximating to that obtained by doubling code length.

We also can see from Figure 4.12 that at a block error probability of 10^{-2}–10^{-4}, the partitioned coded 8-PSK modulation of length 63 is 1 dB better than non-partitioned coded 8-PSK modulation of length 127. In Figure 4.13, at a block error probability of 10^{-2}–10^{-4}, the partitioned coded 8-PSK modulation of length 127 is 1 dB better than non-partitioned coded 8-PSK modulation of length 255. Therefore, we can conclude that for coded 8-PSK modulation, set partitioning produces 1dB more coding gain than doubling the code length.
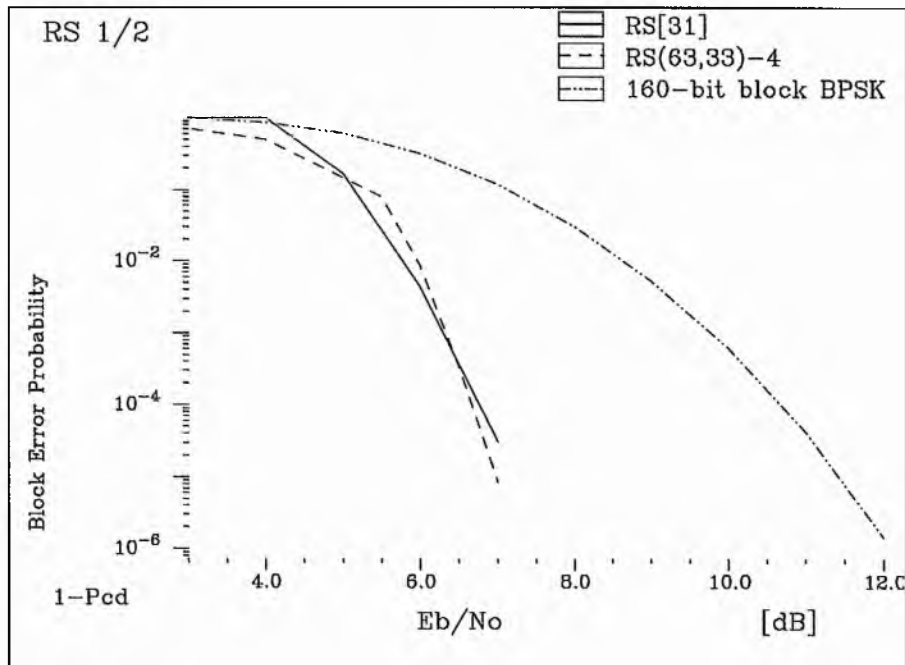
Figure 4.10 Error performances of RS coded QPSK modulation based on set partitioning **RS[31]** of length 31 and not based on set partitioning RS(63, 33).
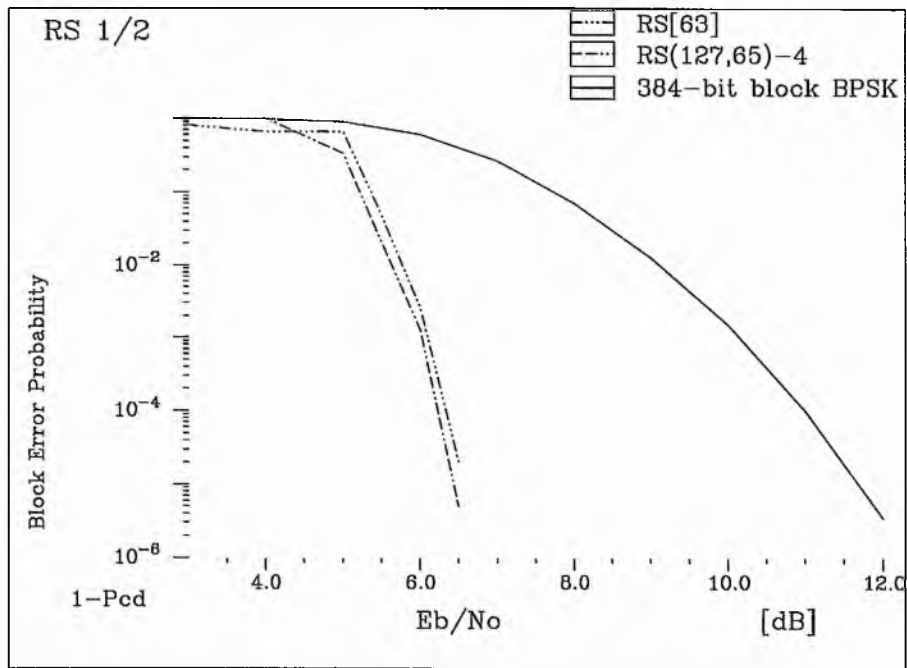
Figure 4.11 Error performances of RS coded QPSK modulation based on set partitioning **RS[63]** of length 63 and not based on set partitioning RS(127, 65).
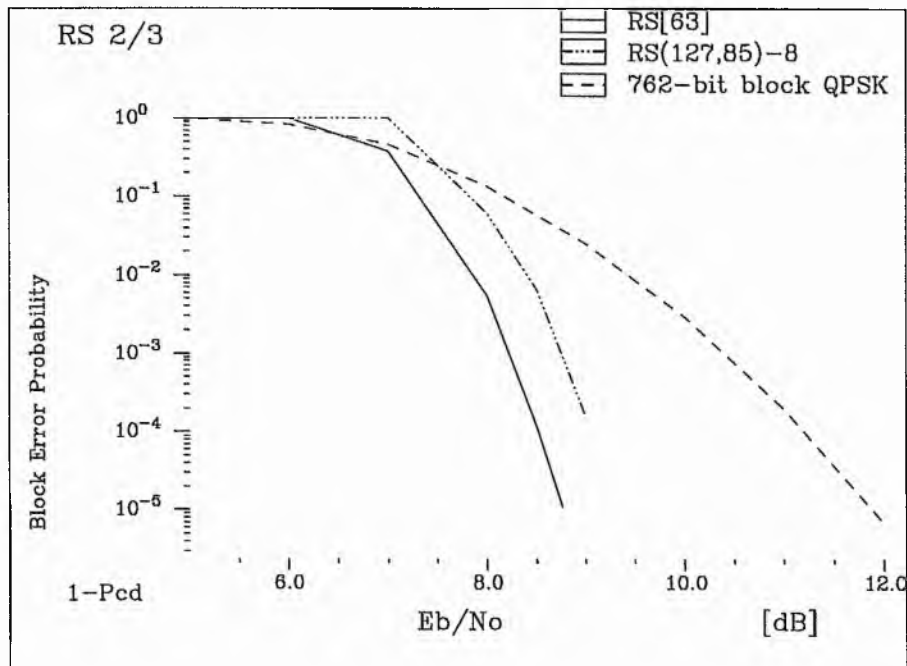
Figure 4.12 Error performances of RS coded 8-PSK modulation based on set partitioning **RS[63]** of length 63 and not based on set partitioning RS(127,85).
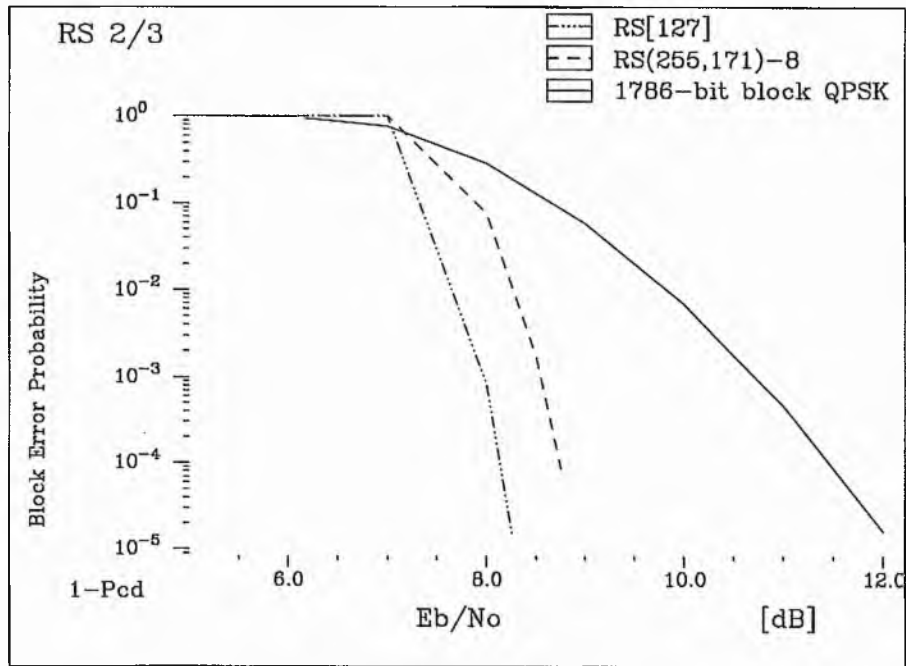
Figure 4.13 Error performances of RS coded 8-PSK modulation based on set partitioning **RS[127]** of length 127 and not based on set partitioning RS(255,171).
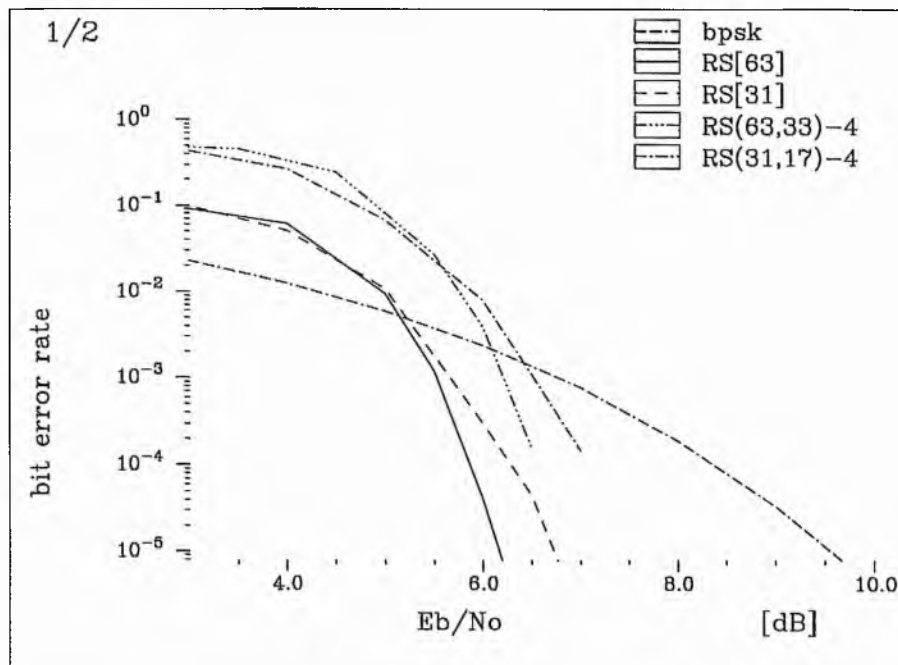
Figure 4.14 Bit error rates of various schemes of Reed Solomon coded QPSK modulation.

80
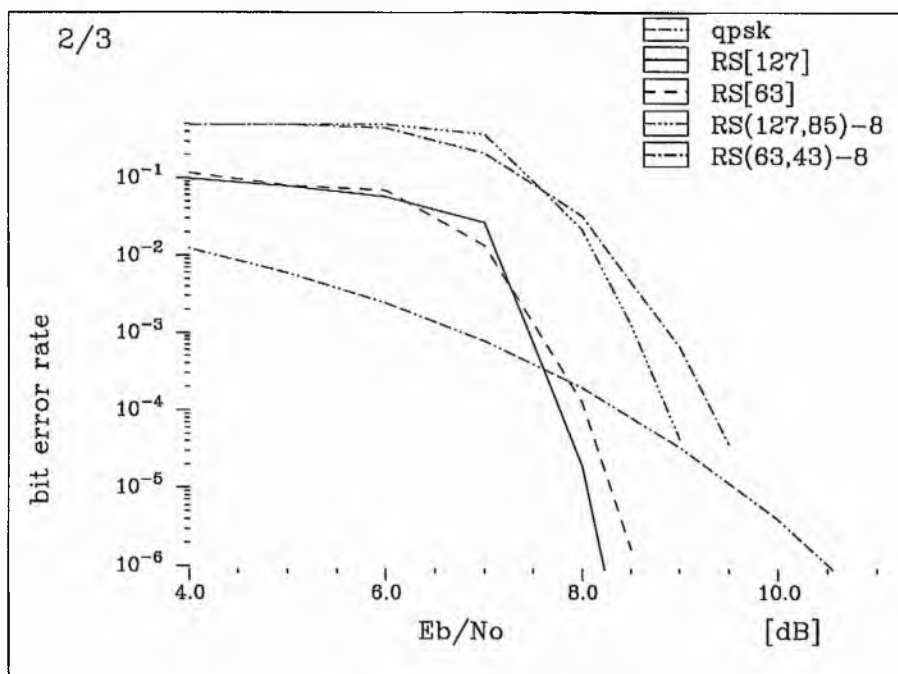
Figure 4.15 Bit error rates of various schemes of Reed Solomon coded 8-PSK modulation.

Figure 4.14 shows bit error rate performance of various schemes for Reed Solomon coded QPSK modulation. At a bit error probability of 10^{-5}, partitioned Reed Solomon coded modulation with code length of 63 has 0.5 dB more coding gain than partitioned RS coded modulation with code length of 31. At a bit error probability of 10^{-4}, non-partitioned Reed Solomon coded modulation with code length of 63 has 0.5 dB more coding gain than non-partitioned RS coded modulation with code length of 31. It is seen that at a bit error probability of 10^{-4}, partitioned Reed Solomon coded modulation has 0.75 dB more coding gain than non-partitioned with the same code length.

Figure 4.15 shows bit error rate performance of various schemes for Reed Solomon coded 8-PSK modulation. For partitioned coded 8-PSK modulation, it is seen that a code with length of 63 has 0.25 dB coding gain more than a code with length of 31 at a bit error probability of 10^{-4}-10^{-6}. At a bit error rate of 10^{-4}-10^{-5}, coded modulation based on set partitioning has at least 1 dB coding gain over non-partitioned coded modulation for the same code length.

81

4.3.2. Comparisons with Multilevel Reed Solomon Coded Modulation based on Gray Mapping

In this approach, each of the m bits defining an MPSK symbol is coded and decoded by different Reed Solomon codecs, where $M = 2^m$. The bits-to-signal mapping is achieved through Gray Mapping. Multistage decoding schemes are not used in this approach. At the output of demodulator, symbols are converted to binary signals using Gray Mapping. Then, the signals are divided to m Reed Solomon decoders by serial to parallel conversion. The decoding method of this approach for coded 8-PSK modulation is illustrated in Figure 4.16.

The Gray mapping from binary 3-tuples to 8-PSK channel symbols shown in Figure 4.17. Figure 4.17 also shows partitions of the signal set to subsets for Gray mapping. In this approach, we set the minimum Hamming distance of each of m Reed Solomon encoders the same because bit 1, bit 2 and bit 3 have the same minimum Euclidean distances which is different from Ungerboeck's partitioned signal sets.
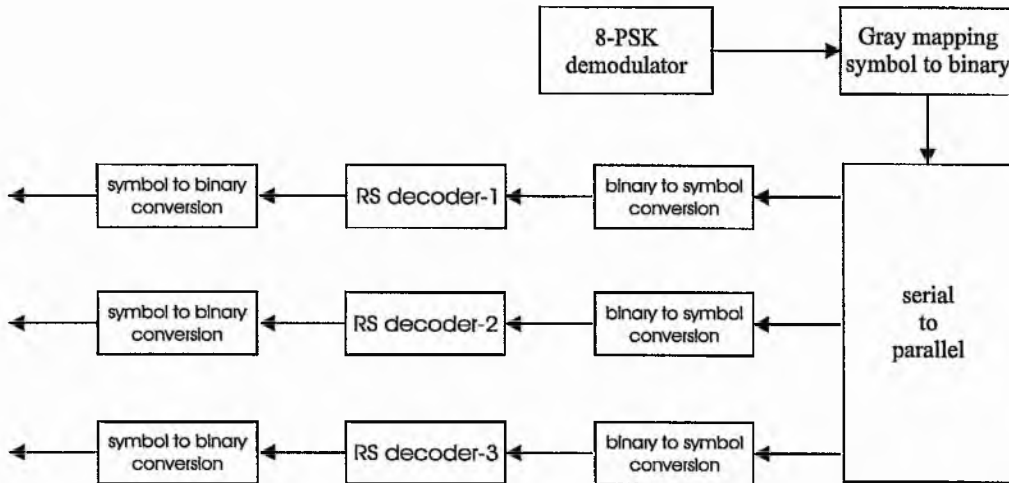
Figure 4.16 The Decoding block diagram of multilevel Reed Solomon coded 8-PSK modulation based on Gray mapping.

Bit 1

Bit 2

Bit 3
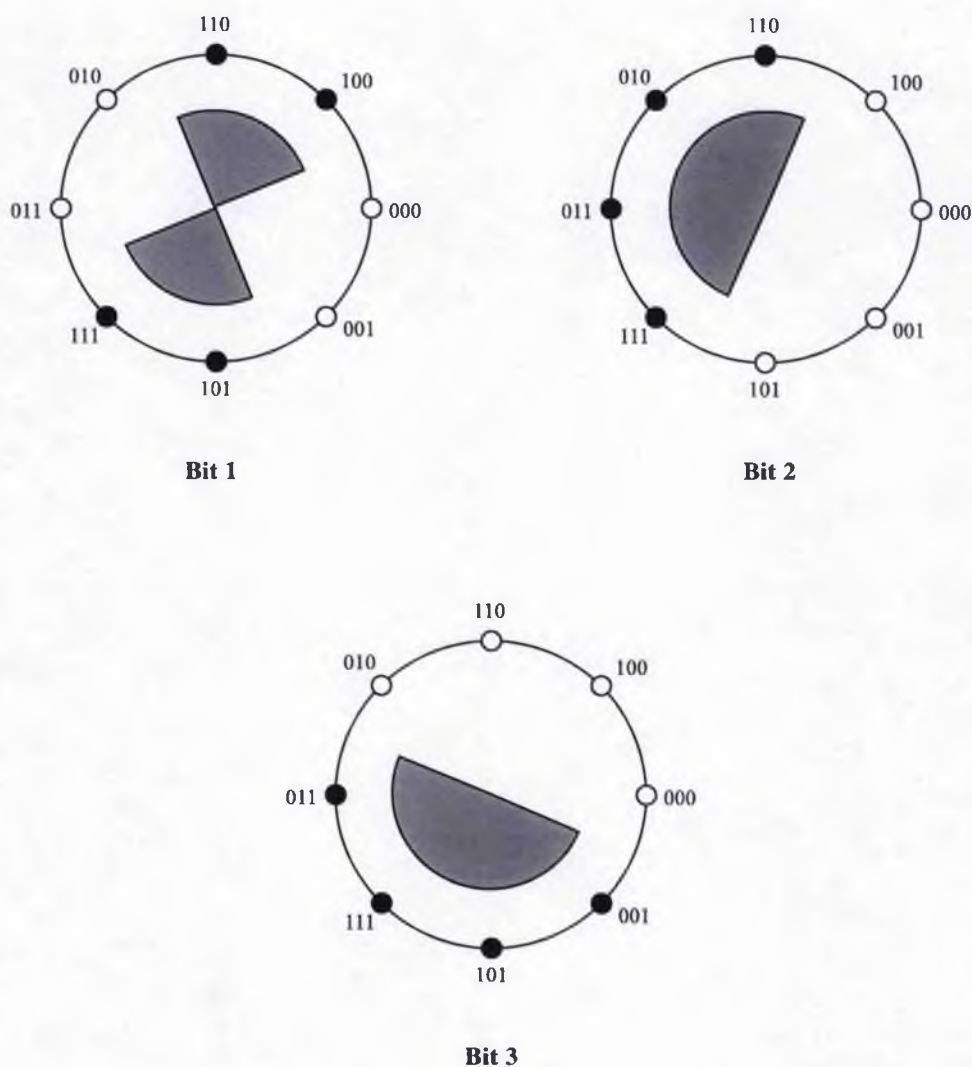
Figure 4.17 Partitions of signal set to subset for Gray Mapping

The minimum Euclidean distance of bit 1 is the distance between signal point 000 and signal point 100. Then, the minimum Euclidean distance of bit 2 is the distance between signal point 100 and signal point 110. And finally, the minimum Euclidean distance of bit 3 is the distance between signal point 001 and 000. It is seen that bit 1, bit 2, and bit 3 have the same minimum Euclidean distance.

Figure 4.18 shows the error performances of partitioned, non-partitioned, and multilevel Gray-mapped Reed Solomon coded QPSK modulation with code symbol length of 31 and

83

63. At a bit error probability of 10^{-4}, partitioned schemes have about 0.5 dB more coding gain than multilevel Gray-mapped Reed Solomon coded modulation. It appears that non-partitioned is slightly worse than Gray-mapped Reed Solomon coded modulation.

The component codes of multilevel Gray-mapped Reed Solomon coded QPSK modulation for code length of 31 are all RS(31, 15) which results in a code rate of $R_c = {(k_1+k_2)}/{2n} = {(15+15)}/{2 \times 31} = 0.484$ and throughput of $m \cdot R_c = 2 \times 0.484 = 0.968$ bit $\text{sec}^{-1} \text{Hz}^{-1}$. The component codes of multilevel Gray-mapped Reed Solomon coded QPSK modulation for code length of 63 are all RS(63, 31) which results in a code rate of $R_c = {(k_1+k_2)}/{2n} = {(31+31)}/{2 \times 63} = 0.492$ and throughput of $m \cdot R_c = 2 \times 0.492 = 0.984$ bit $\text{sec}^{-1} \text{Hz}^{-1}$. Their throughputs are comparable with those of BPSK.

The component codes of the multilevel Gray-mapped Reed Solomon coded 8-PSK modulation for code length of 63 are all RS(63, 43) which results in a code rate of $R_c = {(k_1+k_2+k_3)}/{3n} = {(3 \cdot 43)}/{3 \times 63} = 0.683$ and throughput of $m \cdot R_c = 3 \times 0.683 = 2.05$ bit $\text{sec}^{-1} \text{Hz}^{-1}$. The component codes of the multilevel Gray-mapped Reed Solomon coded 8-PSK modulation for code length of 127 are all RS(127,85) which results in a code rate of $R_c = {(k_1+k_2+k_3)}/{3n} = {(3 \cdot 85)}/{3 \times 127} = 0.669$ and throughput of $m \cdot R_c = 3 \times 0.669 = 2.0$ bit $\text{sec}^{-1} \text{Hz}^{-1}$. Their throughputs are comparable with those of QPSK.

Figure 4.19 shows the error performances of partitioned, non-partitioned, and multilevel Gray-mapped Reed Solomon coded 8-PSK modulation with code symbol length of 63 and 127. At a bit error probability of 10^{-4}, partitioned has about 2 dB more coding gain than multilevel Gray-mapped Reed Solomon coded modulation. It is seen that at a bit error probability of 10^{-4}, non-partitioned has about 0.5 dB more coding gain than multilevel Gray-mapped Reed Solomon coded modulation for the same code length.

From Figure 4.18, it is seen that multilevel Gray-mapped Reed Solomon coded QPSK modulation is better than non-partitioned but in Figure 4.19, multilevel Gray-mapped Reed Solomon coded 8-PSK modulation is worse than non-partitioned. This is thought to be because QPSK is different from other multilevel modulations in that it is essentially two orthogonal BPSK signals.
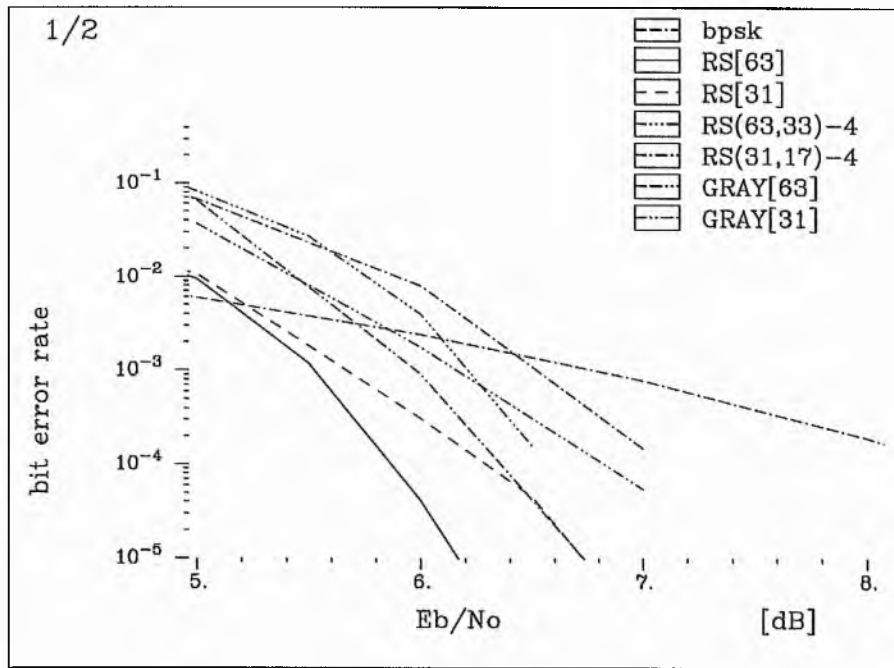
Figure 4.18 Error performances of partitioned **RS[n]**, non-partitioned **RS(n,k)**, and multilevel Gray-mapped **GRAY[n]** Reed Solomon coded QPSK modulation with code symbol length of 31 and 63.
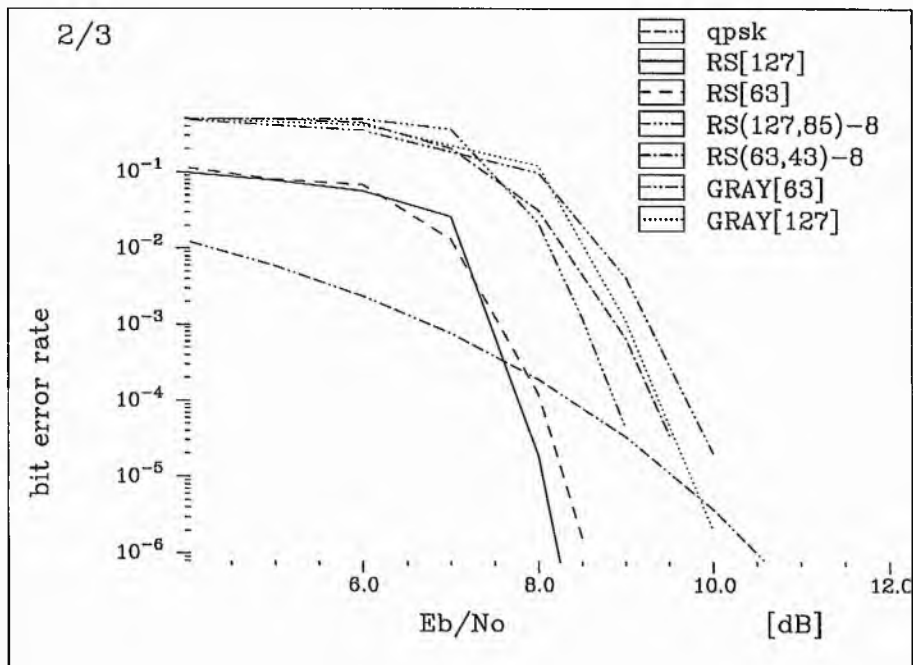
Figure 4.19 Error performances of partitioned **RS[n]**, non-partitioned **RS(n,k)**, and multilevel Gray-mapped **GRAY[n]** Reed Solomon coded 8-PSK modulation with code symbol length of 63 and 127.

85

4.3.3. Comparisons with Reed Muller Coded Modulation

Here, we compare error performances of Reed Solomon Coded Modulation schemes with those of coded modulation schemes using binary codes, namely Reed Muller codes. The explanation of Reed Muller codes was given in section 2.4. Block coded modulation using Reed Muller codes requires the same approaches as Reed Solomon coded modulation.

In the first approach, Reed Muller coded modulation not based on set partitioning, a Reed Muller code having code rate $R_c = \frac{m}{(m+1)}$ combined with a 2^{m+1}-PSK signal set. In this combination, the code rate is chosen such that the rate of coded scheme is the same as the uncoded one (2^m-PSK).

In the second approach, Reed Muller coded modulation based on set partitioning, each of the m bits defining an MPSK symbol, where $M = 2^m$, is coded by different Reed Muller component-code encoders. The set partitioning principle is applied to define subsets with distance Δ_i, ($i = 1$ to m) that are nondecreasing with i. Here, we use a similar multistage decoding procedure for decoding the received codewords. The explanation of binary block coded modulation was given in section 2.2; here we use Reed Muller codes as component codes.

In binary coded schemes, we can find the minimum Hamming distance of each component code of the signal space 8-PSK code using Equations 4.1 and 4.2, that is by setting:

$$0.586 d_{\min 1} \cong 2 d_{\min 2} \cong 4 d_{\min 3}$$

and

$$d_{\min 1} \cong 2 d_{\min 2}$$

for the signal space QPSK code, where $\cong$ denotes the same or almost the same.

A Reed Muller code RM(r, m) has the following properties:

Code length	$n = 2^m$
Information bits	$k = 1 + \binom{m}{1} + \cdots + \binom{m}{r}$
Minimum distance	$d_{\min} = 2^{m-r}$

Using Equation 4.2, we found that Reed Muller coded QPSK modulation of code length 256 (2^8) bits has component codes:

1. RM(3, 8) with minimum distance of $2^{(8-3)} = 32$ and with information length of 93.
2. RM(4, 8) with minimum distance of $2^{(8-4)} = 16$ and with information length of 163.

This scheme has $d_{\min 1} = 2 d_{\min 2}$ and the code rate of $R_c = \frac{(k_1 + k_2)}{2n} = \frac{(93+163)}{2 \times 256} = 0.5$.

Using Equation 4.1, we find that Reed Muller coded 8-PSK modulation of code length 128 (2^7) bits has component codes:

1. RM(2, 7) with minimum distance of $2^{(7-2)} = 32$ and with information length of 29.
2. RM(4, 7) with minimum distance of $2^{(7-4)} = 8$ and with information length of 99.
3. RM(5, 7) with minimum distance of $2^{(7-5)} = 4$ and with information length of 120.

This scheme has

$$0.586 d_{\min 1} = 0.586 \times 32 = 18.752$$

$$2 d_{\min 2} = 2 \times 8 = 16$$

$$4 d_{\min 3} = 4 \times 4 = 16$$

which gives $0.586 d_{\min 1} \cong 2 d_{\min 2} \cong 4 d_{\min 3}$. The code rate of this scheme is $R_c = \frac{(k_1 + k_2 + k_3)}{3 \cdot n} = \frac{(29+99+120)}{3 \cdot 128} = 0.64$.

Figure 4.20 shows the error performances of coded QPSK modulation: partitioned, non-partitioned Reed Solomon coded modulation, partitioned Reed Muller coded modulation with code length of 256, and non-partitioned Reed Muller coded modulation RM(3, 7) with code length of 128 and information length of 64 which results in a code rate of $R_c = {}^{64}\!/_{128}$.

It is seen that at a bit error rate of 10^{-4}, non-partitioned Reed Muller coded modulation using RM(3, 7) is 0.75 dB worse than partitioned Reed Solomon coded modulation with code length of 63 and 0.25 dB worse than partitioned Reed Solomon coded modulation with code length of 31. It appears that for coded QPSK modulation, Reed Muller coded modulation based on set partitioning is worse than Reed Muller coded modulation not based on set partitioning. For example, at a bit error rate 10^{-4}, Reed Muller coded modulation based on set partitioning with code length of 256 is 0.5 dB worse than Reed Muller coded modulation not based on set partitioning with code length of 128.
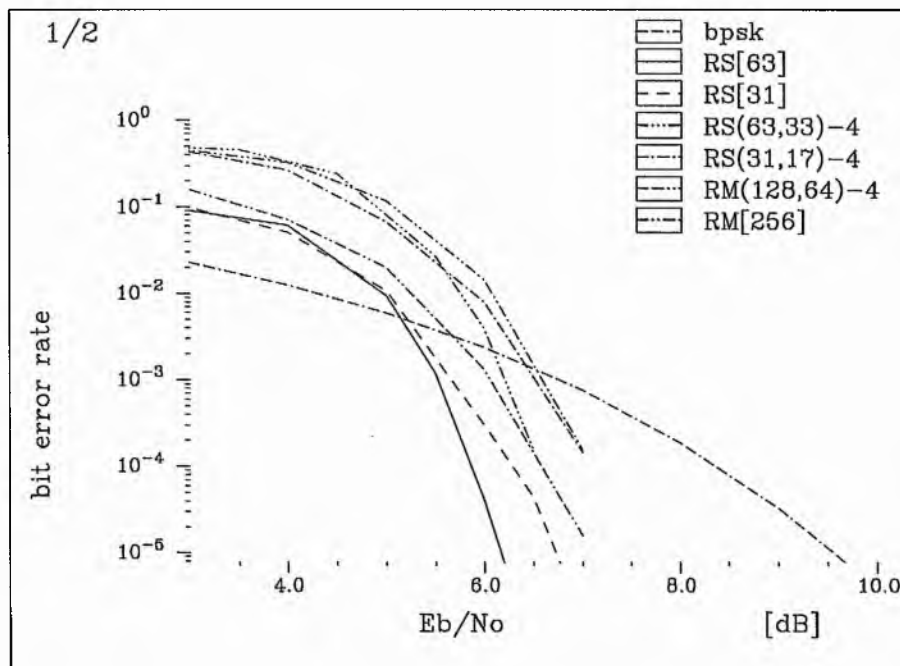
Figure 4.20 Error performances of partitioned **RS[n]**, non-partitioned **RS(n,k)** RS coded QPSK modulation with code symbol length of 31 and 63 and RM coded QPSK modulation based on set partitioning **RM[256]**, not based on set partitioning using RM(3, 7), **RM(128,64)**.

Figure 4.21 shows the error performances of coded 8-PSK modulation: partitioned, non-partitioned Reed Solomon coded modulation, partitioned Reed Muller coded modulation with code length of 128, and non-partitioned Reed Muller coded modulation RM(4, 7) with code length of 128 and information length of 99 which results in a code rate of $R_c = {}^{99}\!/_{128} = 0.77$. With code length of 128, we cannot have a Reed Muller code which gives a code rate of 2/3.

At a bit error rate of $2 \cdot 10^{-5}$, partitioned Reed Solomon coded modulation with code length of 63 has 0.25 dB coding gain over partitioned Reed Muller coded modulation. Different from coded QPSK modulation, the error performance of partitioned Reed Muller coded 8-PSK modulation is better than non-partitioned Reed Muller coded 8-PSK modulation. And the error performances of non-partitioned Reed Solomon coded modulation are much better than those of non-partitioned Reed Muller coded modulation.
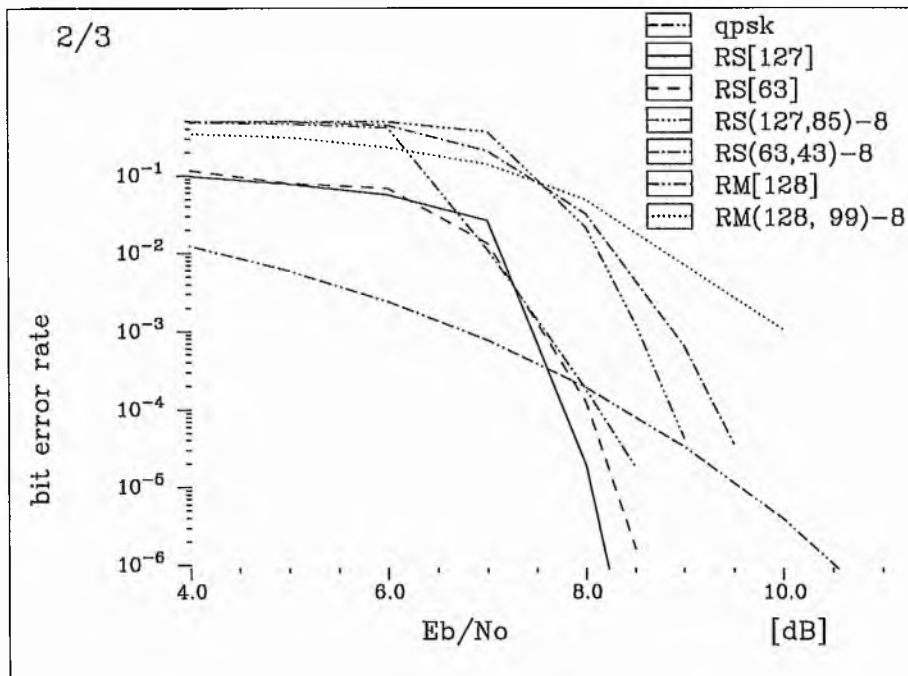
Figure 4.21 Error performances of partitioned **RS[n]**, non-partitioned **RS(n,k)** RS coded 8-PSK modulation with code symbol length of 63 and 127 and RM coded QPSK modulation based on set partitioning **RM[128]**, not based on set partitioning using RM(4, 7), **RM(128,99)**.

4.3.4. Multi-Iteration Approach of Multistage Decoding

As previously mentioned in subsection 3.3.1., either one or two iterations may be used for multistage decoding. In the first iteration for coded 8-PSK modulation, level 1 is first decoded, then level 2 is estimated based on the result of level 1. Finally level 3 is determined based on levels 1 and 2. For the second (optional) iteration, level 2 is again decoded using the result of levels 1 and 3 from the first iteration. then level 1 is estimated based on the result of levels 2 and 3. Finally level 3 is determined based on levels 1 and 2.

Figure 4.22 compares error performances between one iteration and two iteration multistage decoding for Reed Solomon coded QPSK modulation, and Figure 4.23 for Reed Solomon coded 8-PSK modulation. It appears that both kinds of iterations have the same error performances.
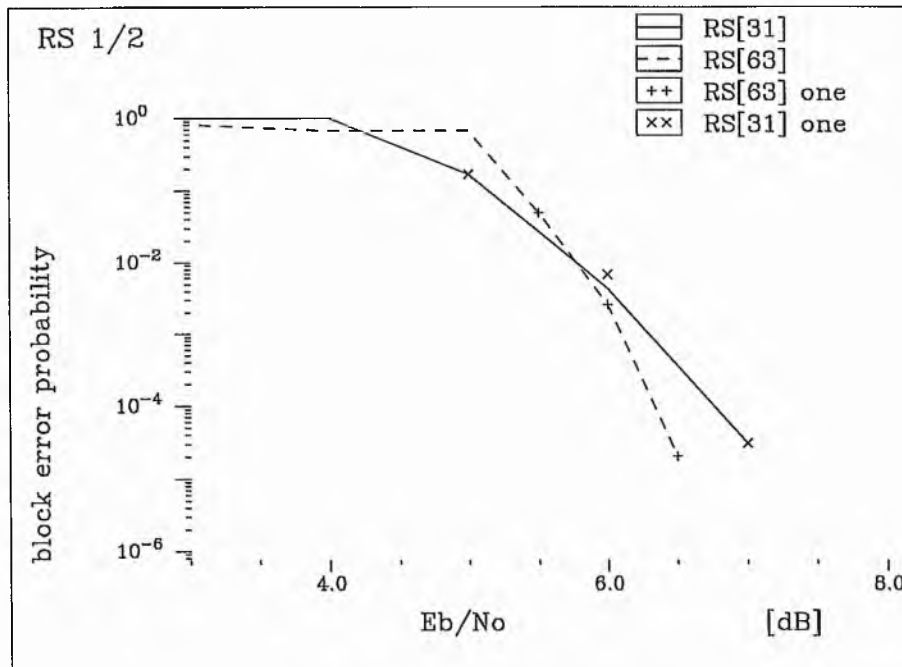
Figure 4.22 Error performances of RS coded QPSK modulation based on set partitioning using two-iteration multistage decoding: **RS[*n*]**, and one iteration multistage decoding: **RS[*n*] one** with code length of 31 and 63.
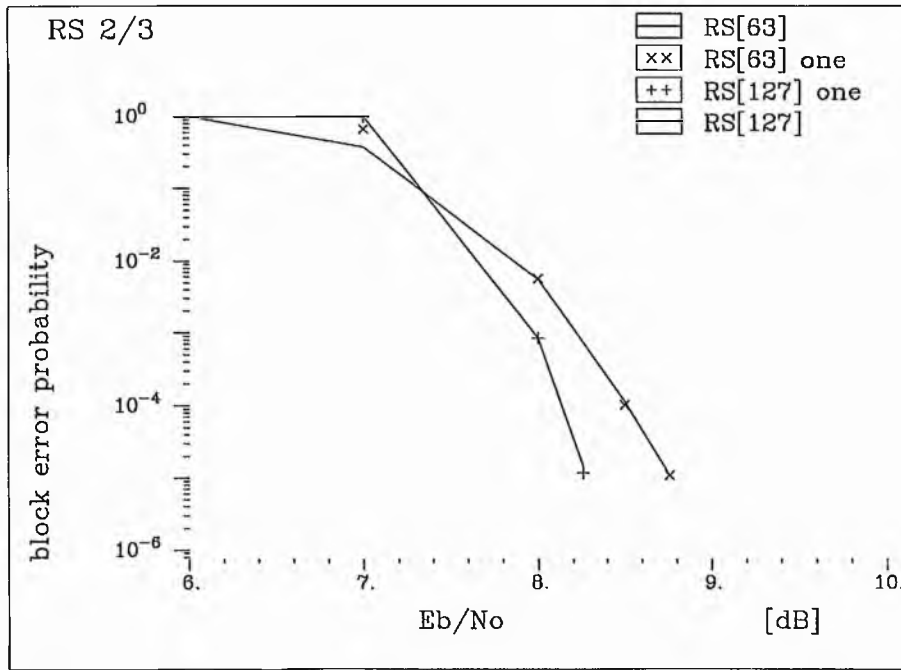
Figure 4.23 Error performances of RS coded 8-PSK modulation based on set partitioning using two-iteration multistage decoding: **RS[*n*]**, and one iteration multistage decoding: **RS[*n*] one** with code length of 63 and 127.

In [Woerz & Fazel, 1992], it was claimed that on the AWGN channel, two iterations will give better performance than one iteration if there is an interleaver between the coded bits of all stages or we use modified generalised-minimum-distance-decoding. They used a three-dimensional block interleaver for three levels coded modulation as illustrated in Figure 4.24. Every memory cell contains one coded bit from every level. The following list describes the rule in order to write the output of component-code encoder into the interleaver:

- The coded bits of the first level are written row-wise into the interleaver as illustrated in Figure 4.25 (a).
- The coded bits of the second level are written column-wise into the interleaver as illustrated in Figure 4.25 (b).
- The coded bits of the third level are written diagonally into the interleaver as illustrated in Figure 4.25 (c).
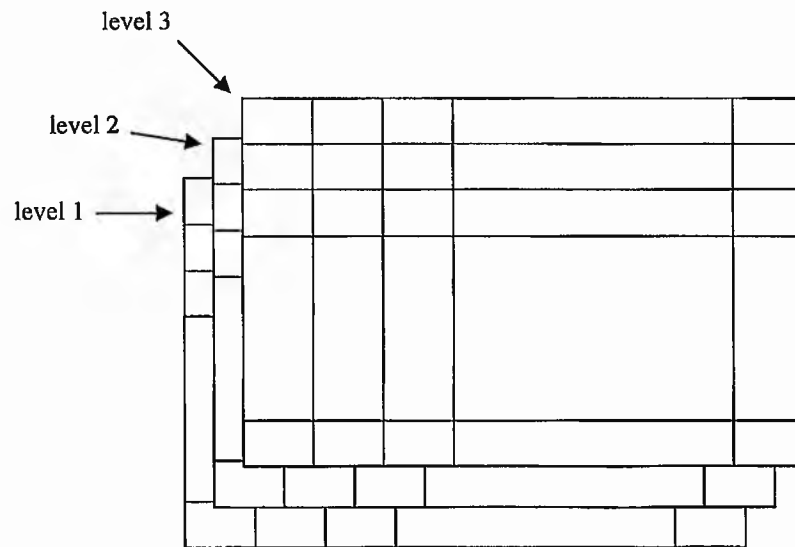
Figure 4.24 Three-dimensional block interleaver for three level coded modulation

(a)   (b)

(c)
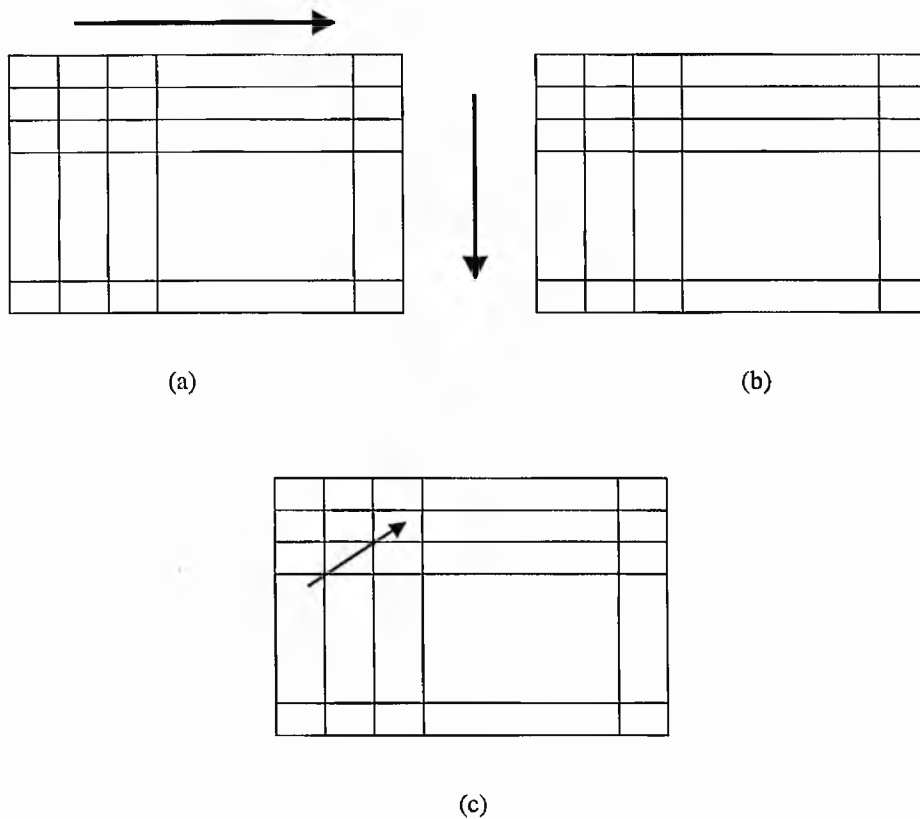
Figure 4.25 Each block interleaver of three-dimensional block interleaver

They used binary convolutional codes for the first and second levels and a single parity check for the third level. If we use the Viterbi algorithm for decoding, the estimated information bit sequence is liable to contain error bursts. This sequence is re-encoded and fed into the decoder of the next level. Thus, the re-encoded sequence also contains error bursts. If this decoder also uses the Viterbi algorithm then it is very sensitive to these error bursts, because the algorithm is designed to deal with independent errors in the input stream.

In order to avoid this error propagation effect, they introduced interleaving between the coded bit streams of each level as explained above. The interleaving spreads the re-encoded bit streams of any two decoders for the third decoder. So it will be hardly influenced by error bursts from any of the other two decoders.

Reed Solomon codes have powerful error detection capability which are different from binary convolutional codes. In the simulations if the decoder detected the errors but it could not correct the errors, the decoder passed the input sequence to the decoder output. Therefore, the possibility of an error propagation effect because of undetected errors is very small.

In the code configurations of Reed Solomon coded modulation based on set partitioning, the first level component code is much more powerful than other level component codes. If we use the interleaving technique as explained above and there are undetected errors when decoding at the first level, the errors will affect several input sequences of decoders at other levels. Thus, the interleaving technique which was proposed in [Woerz & Fazel, 1992] and [Woerz & Hagenauer, 1993] is not advisable for Reed Solomon coded modulation based on set partitioning.

4.4. CONCLUSIONS FOR THE GAUSSIAN CHANNEL

In this section, the error performance over the Gaussian channel of Reed Solomon coded modulation based on set partitioning was analysed and compared with Reed Solomon coded modulation not based on set partitioning, multilevel Reed Solomon coded modulation based on Gray mapping, and Reed Muller coded modulation.

For coded QPSK modulation, partitioned Reed Solomon coded modulation has improvement on non-partitioned by an amount approximately equivalently to doubling

code length. At a BER of 10^{-4}, partitioned Reed Solomon coded modulation has about 0.5 dB more coding gain than multilevel Gray-mapped Reed Solomon coded modulation and non-partitioned is slightly worse than multilevel Gray-mapped Reed Solomon coded modulation. Finally, the error performance of partitioned Reed Solomon coded modulation with code length of 31 is slightly better than that of Reed Muller coded modulation. It appears that for coded QPSK modulation, Reed Muller coded modulation based on set partitioning is worse than Reed Muller coded modulation not based on set partitioning.

For coded 8-PSK modulation, at a block error probability of 10^{-4}, partitioned Reed Solomon coded modulation has 1 dB more coding gain than doubling the code length of non-partitioned RS coded modulation. At a BER of 10^{-4}, partitioned has about 2 dB coding gain than multilevel Gray-mapped RS coded modulation and non-partitioned have about 0.5 dB more coding gain than multilevel Gray-mapped Reed Solomon coded modulation. Finally the error performances of partitioned RS coded modulation are slightly better than those of partitioned Reed Muller coded modulation and much better than those of non-partitioned RM coded modulation.

Overall, for the Gaussian channel, Reed Solomon coded modulation based on set partitioning is better than not based on set partitioning, multilevel Reed Solomon coded modulation based on Gray mapping and Reed Muller coded modulation.

CHAPTER 5

CODE DESIGN AND PERFORMANCE FOR A RAYLEIGH FADING CHANNEL

In this chapter, the designs of coded modulation schemes for a Rayleigh fading channel are studied and the error performance over a Rayleigh fading channel of Reed Solomon coded modulation schemes is analysed. The performance of Reed Solomon coded modulation based on set partitioning is compared with Reed Solomon coded modulation not based on set-partitioning, then multilevel Reed Solomon coded modulation using Gray mapping and finally with coded modulation schemes using binary codes, Reed Muller codes. The results of Reed Solomon coded modulation not based on set-partitioning schemes are also compared with bit-interleaved coded modulation which is proposed in [Zehavi, 1992] and with robust coded modulation proposed in [Sundberg & Seshadri, 1993]. We need to establish whether comparison between the many different methods previously described indicates if there are any general conclusions to be drawn about which is best.

5.1. FADING CHANNELS

Fading channels have randomly time-variant impulse responses which are a consequence of the constantly changing physical characteristics of the medium. If we transmit an extremely short pulse, ideally an impulse, over a time varying multipath channels, the

received signal might appear as a train of pulses. Hence one characteristic of a multipath medium is the time spread introduced in the signal. A second characteristic is the time variations the nature of the multipath varies with time. That is, there would be changes in the received pulse train, which include changes in the size of the individual pulses, changes in the relative delays among the pulses, and, quite often, changes in the number of pulses. Therefore, since the time delays of the fading channel are not predictable the time varying channel has to be represented statistically. A transmitted signal may be represented as

$$s(t) = \text{Re}\left[u(t)e^{j2\pi f_c t}\right]$$ 5.1

We assume that there are multiple propagation paths. Each path has an associated propagation delay and an attenuation factor which are time-variant. Thus the received bandpass signal is

$$x(t) = \sum_n \alpha_n(t)s\left[t - \tau_n(t)\right]$$ 5.2

where $\alpha_n(t)$ is the attenuation factor for the signal received on the n-th path and $\tau_n(t)$ is the propagation delay for the n-th path. Substitution of s(t) into Equation 5.2 yields the result

$$x(t) = \text{Re}\left(\left\{\sum_n \alpha_n(t)e^{-j2\pi f_c \tau_n(t)}u\left[t - \tau_n(t)\right]\right\}e^{j2\pi f_c t}\right)$$ 5.3

From observation of Equation 5.3, the equivalent lowpass received signal is

$$r(t) = \sum_n \alpha_n(t)e^{-j2\pi f_c \tau_n(t)}u\left[t - \tau_n(t)\right]$$ 5.4

Since r(t) is the response of the equivalent lowpass channel to the equivalent lowpass signal u(t) then the equivalent lowpass channel is described by the time-variant impulse response

$$c(\tau;t) = \sum_n \alpha_n(t)e^{-j2\pi f_c \tau_n(t)}\delta[t - \tau_n(t)] \qquad 5.5$$

This definition holds for a channel that contains discrete multipath component.

For some channels, such as the tropospheric scatter channel, it is more appropriate to view the received signal as consisting of a continuum of multipath components. A similar expression for the equivalent lowpass impulse response for a channel that contains continuous multipath is

$$c(\tau;t) = \alpha_n(\tau;t)e^{-j2\pi f_c \tau} \qquad 5.6$$

where $c(\tau;t)$ represents the response of the channel at time t due to an impulse applied at time $t-\tau$.

Now we consider the transmission of an unmodulated carrier at frequency f_c. Then $u(t) = 1$ for all t, therefore the received signal for the discrete multipath case, Equation 5.4, simplifies to

$$r(t) = \sum_n \alpha_n(t)e^{-j2\pi f_c \tau_n(t)}$$
$$= \sum_n \alpha_n(t)e^{-j\theta_n(t)} \qquad 5.7$$

where $\theta_n(t) = 2\pi f_c \tau_n(t)$. Thus the received signal is composed of the sum of a number of time-variant vectors having amplitudes $\alpha_n(t)$ and phases $\theta_n(t)$. The effects of the channel on the received signal are as follows: large dynamic changes in the medium are required for $\alpha_n(t)$ to change sufficiently to cause a significant change in the received signal. For variations of the phase of the received signal $\theta_n(t)$ will change by 2π radians whenever τ_n changes by $1/f_c$. But $1/f_c$ is a small number hence θ_n can change by 2π radians with relatively small motions of the medium. The delays $\tau_n(t)$ of the different paths will change at different rates in a random manner. This implies that the received signal $r(t)$ in Equation 5.7 can be modelled as a random process. When there is a large number of paths, the central limit theorem can be applied. That is, $r(t)$ can be modelled as complex-valued Gaussian random process. Therefore the time-variant impulse response $c(\tau;t)$ is a complex valued Gaussian random process in the t variable.

The multipath propagation model for the channel embodied in the received signal $r(t)$, Equation 5.7, results in signal fading. The fading is caused by the variations of the phase $\theta_n(t)$. If each vector $\left\{\alpha_n(t)e^{-j\theta_n(t)}\right\}$ has different phases, then at different times it will be seen that the vectors can add destructively, so reducing the amplitude of the received signal. At other times the vectors can add constructively and thus increase the amplitude of the signal. These amplitude variations are termed signal fading and are caused by the time-variant multipath characteristics of the channel.

When the impulse response $c(\tau;t)$ is modelled as a zero mean complex valued Gaussian process, the envelope $|c(\tau;t)|$ at any instant t is Rayleigh distributed. In this case the channel is said to be a Rayleigh fading channel.

5.1.1. Multipath Intensity Profile

We assume that $c(\tau;t)$ is a *wide-sense stationary*. A random process is said to be *stationary* if all its statistical properties do not change with time, and a random process $X(t)$ is the *wide-sense stationary* if two conditions are true:

$$E[X(t)] = \overline{X} = \text{constant}$$

$$E[X(t)X(t+\tau)] = R_{XX}(\tau)$$

where $R_{XX}(t_1,t_1+\tau) = E[X(t_1)X(t_1+\tau)] = R_{XX}(\tau)$ and $R_{XX}(t_1,t_1+\tau)$ is the *autocorrelation function* of the random process $X(t)$.

Then we define the autocorrelation function of $c(\tau;t)$ as

$$\phi_c(\tau_1,\tau_2;\Delta t) = \tfrac{1}{2} E\left[c^*(\tau_1;t)c(\tau_2;t+\Delta t)\right] \qquad 5.8$$

In most radio transmission media, the attenuation and phase shift of the channel associated with path delay τ_1 is uncorrelated with the attenuation and phase shift associated with path delay τ_2. This is usually called uncorrelated scattering. If we assume that the scattering at two different delays is uncorrelated, we can incorporate it into Equation 5.8 to obtain

$$\tfrac{1}{2}E\big[c^*(\tau_1;t)c(\tau_2;t+\Delta t)\big]=\phi_c(\tau_1;t)\delta(\tau_1-\tau_2)\qquad\text{5.9}$$

If $\Delta t = 0$, the resulting autocorrelation function $\phi_c(\tau;0)\equiv\phi_c(\tau)$ is simply the average power output of the channel as a function of the time delay τ. For this reason, $\phi_c(\tau)$ is called the multipath intensity profile or the delay power spectrum of the channel. In general, $\phi_c(\tau;\Delta t)$ gives the average power output as a function of the time delay τ and the difference Δt in observation time. Typically, the measured function $\phi_c(\tau)$ may appear as shown in Figure 5.1. The range of values of τ, over which $\phi_c(\tau)>0$, is called the multipath spread of the channel and is denoted by T_m.

In the frequency domain, the characteristics of the time-variant multipath channel can be taken from the Fourier transform,

$$C(f;t)=\int_{-\infty}^{\infty}c(\tau;t)e^{-j2\pi f\tau}d\tau\qquad\text{5.10}$$

where $C(f;t)$ is the time-variant transfer function. Since $c(\tau;t)$ is a complex-valued zero mean Gaussian random process in the t variable, it follows that $C(f;t)$ also has the same statistics.
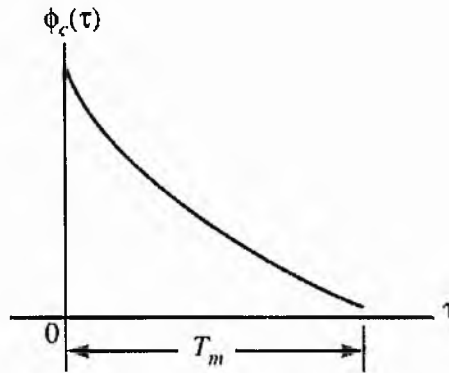
Figure 5.1 Multipath intensity profile

Since $C(f;t)$ is the Fourier transform of $c(\tau;t)$, it is not surprising to find that $\phi_C(f_1,f_2;\Delta t)$ is related to $\phi_c(\tau;\Delta t)$ by the Fourier transform. Furthermore, the assumption of uncorrelated scattering implies that the autocorrelation function of $C(f;t)$ in frequency is a function of only the frequency difference $\Delta f = f_2 - f_1$. Therefore it is

appropriate to call $\phi_C(f_1, f_2; \Delta t)$ the spaced-frequency spaced-time correlation function of the channel.

Suppose we set $\Delta t = 0$. Then, with $\phi_C(\Delta f; 0) \equiv \phi_C(\Delta f)$ and $\phi_c(\tau; 0) \equiv \phi_c(\tau)$, the transform relationship is simply

$$\phi_C(\Delta f) = \int_{-\infty}^{\infty} \phi_c(\tau) e^{-j2\pi\Delta f\tau} d\tau \qquad\qquad 5.11$$

The relationship is graphically depicted in Figure 5.2. Since $\phi_C(\Delta f)$ is an autocorrelation function in the frequency variable, it provides us with a measure of the frequency coherence of the channel. As a result of the Fourier transform relationship between $\phi_C(\Delta f)$ and $\phi_c(\tau)$, the reciprocal of the multipath spread is a measure of the coherence bandwidth of the channel. That is,

$$(\Delta f)_c \approx \frac{1}{T_m} \qquad\qquad 5.12$$

where $(\Delta f)_c$ denotes the coherence bandwidth. Thus two sinusoids with frequency separation greater than $(\Delta f)_c$ are affected differently by the channel. When an information-bearing signal is transmitted through the channel, if $(\Delta f)_c$ is small in comparison to the bandwidth of the transmitted signal, the channel is said to be frequency-selective. In this case the signal is severely distorted by the channel. On the other hand, if $(\Delta f)_c$ is large in comparison to the bandwidth of the transmitted signal the channel is said to be frequency-nonselective.
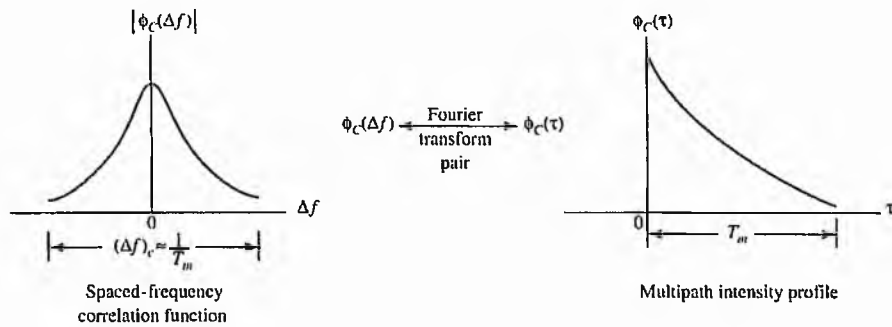
Figure 5.2 Relationship between $\phi_C(\Delta f)$ and $\phi_c(\tau)$

We now focus our attention on the time variations of the channel as measured by the parameter Δt in $\phi(\Delta f;\Delta t)$. The time variations in the channel are evidenced as a Doppler broadening and, perhaps, in addition as a Doppler shift of a spectral line. In order to relate the Doppler effects to the time variations of the channel, we define the Fourier transform of $\phi(\Delta f;\Delta t)$ with respect to the variable Δt to be the function

$$S_C(\Delta f;\lambda) = \int_{-\infty}^{\infty} \phi_C(\Delta f;\Delta t)e^{-j2\pi\lambda\Delta t}d\Delta t \qquad 5.13$$

with Δf set to zero $S_C(0;\lambda) \equiv S_C(\lambda)$

The function $S_C(\lambda)$ is a power spectrum that gives the signal intensity as a function of the Doppler frequency λ. Hence, we call $S_C(\lambda)$ the Doppler power spectrum of the channel.

The range of values of λ over which $S_C(\lambda)$ is essentially nonzero is called the Doppler spread B_d of the channel. Since $S_C(\lambda)$ is related to $\phi_C(\Delta t)$ by the Fourier transform, the reciprocal of B_d is a measure of the coherence time of the channel. That is,

$$(\Delta t)_c \approx \frac{1}{B_d} \qquad 5.14$$

where $(\Delta t)_c$ denotes the coherence time. Clearly, a slowly changing channel has a large coherence time or, equivalently, a small Doppler spread. Figure 5.3 illustrates the relationship between $\phi_C(\Delta t)$ and $S_C(\lambda)$.
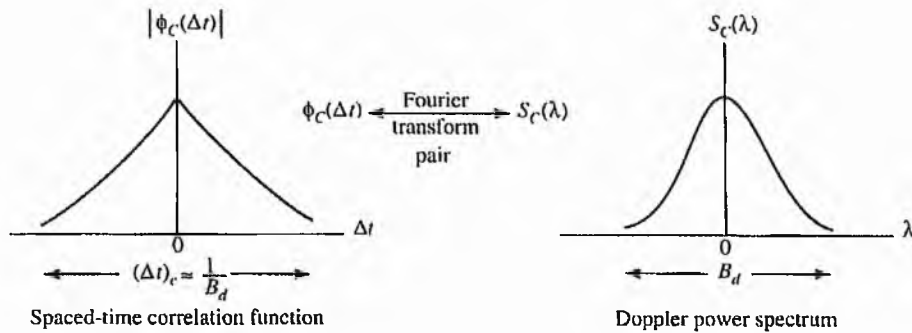
Figure 5.3 Relationship between $\phi_C(\Delta t)$ and $S_C(\lambda)$

5.1.2. Frequency-Nonselective, Slowly Fading Channels

The effect of the channel on the transmitted signal $s(t)$ is a function of the chosen signal bandwidth and signal duration. If the bandwidth of the signal pulse $s(t)$ is $W \approx 1/T$ where T is the signalling interval, the condition $T >> T_m$ implies that

$$W << \frac{1}{T} \approx (\Delta f)_c \qquad\qquad 5.15$$

That is, the signal bandwidth W is much smaller than the coherence bandwidth of the channel. Hence, the channel is frequency-nonselective. In other words, all of the frequency components in $S(f)$ undergo the same attenuation and phase shift in transmission through the channel.

The transfer function $C(0;t)$ for a frequency-nonselective channel may be expressed in the form

$$C(0;t) = \alpha(t)e^{-j\phi(t)} \qquad\qquad 5.16$$

where $C(f;t)$ is $c(\tau;t)$ in terms of the frequency function with its frequency content that concentrated in the vicinity of $f = 0$, $C(f;t) = C(0;t)$. When $C(0;t)$ is modeled as a zero-mean complex valued Gaussian random process, the envelope $\alpha(t)$ is Rayleigh-distributed for any fixed value of t and $\phi(t)$ is uniformly distributed over the interval $(-\pi, \pi)$.

Suppose it is possible to select the signal bandwidth W to satisfy the condition $W << (\Delta f)_c$ and the signalling interval T to satisfy the condition $T << (\Delta t)_c$. Since T is smaller than the coherence time of the channel, the channel attenuation and phase shift are essentially fixed for the duration of at least one signalling interval. When this condition holds, we call the channel a slowly fading channel. Furthermore, when $W \approx 1/T$, the conditions that the channel be frequency-nonselective and slowly fading imply that the product of T_m and B_d must satisfy the condition $T_m B_d < 1$. Consequently, the received equivalent lowpass signal in one signaling interval is

$$r(t) = \alpha e^{-j\phi} u(t) + z(t), \qquad 0 \le t \le T. \tag{5.17}$$

where $z(t)$ represents the complex-valued white Gaussian noise process corrupting the signal.

5.1.3. Simulation Model for Frequency-Nonselective, Slowly Fading Channels

We assume that $s(t)$ is transmitted signal

$$s(t) = \cos(2\pi f_c t). \tag{5.18}$$

The received signal (apart from any additive noise) can be obtained by summing different signal components which are arriving via different paths at the receiver as shown below

$$\begin{aligned} r(t) &= \sum_i \alpha_i(t) \cos\left(2\pi f_c t - \theta_i(t)\right) \\ &= a_I(t) \cos(2\pi f_c t) + a_Q \sin(2\pi f_c t) \end{aligned} \tag{5.19}$$

$$\begin{aligned} a_I(t) &= \sum_i \alpha_i(t) \cos\left(\theta_i(t)\right) \\ a_Q(t) &= \sum_i \alpha_i(t) \sin\left(\theta_i(t)\right) \end{aligned} \tag{5.20}$$

The central limit theorem arguments lead to the conclusion that the in-phase and quadrature components, $a_I(t)$ and $a_Q(t)$, are two statistically independent Gaussian random processes.

In fading channels with only a diffused multipath signal, these Gaussian processes have zero mean and the fading envelope, defined as

$$a = \sqrt{a_I{}^2 + a_Q{}^2} \tag{5.21}$$

has a Rayleigh distribution with a probability density function (pdf)

$$p_A(a) = \frac{a}{\sigma_a^2} e^{-\frac{a^2}{2\sigma_a^2}} \qquad\qquad 5.22$$

The fading phase defined as

$$\phi = \tan^{-1}\frac{a_Q}{a_I}, \qquad\qquad 5.23$$

is a uniformly distributed random process with a pdf of

$$p_\Phi(\phi) = \frac{1}{2\pi}, \qquad\qquad 5.24$$

where $0 \le \phi < 2\pi$.

In this simulation, we assume that the phase recovery, for the cancellation of the phase variations introduced by the channel, is perfect. The solution is to represent only the envelope variation; the real and imaginary parts of the input signal are multiplied by the complex fading process, a, in Equation 5.21, instead of the complex fading value. We also assume that the channel fading is sufficiently slow therefore, the phase shift ϕ can be estimated from the received signal without error.

The main case of interest here is using a normalised Rayleigh fading channel with

$$\sigma_a^2 = 1 \qquad\qquad 5.25$$

hence,

$$\sigma_{a_I}^2 = \sigma_{a_Q}^2 = \frac{1}{2}. \qquad\qquad 5.26$$

The block diagram of a Rayleigh fading channel model is illustrated in Figure 5.4. The complex channel gain is generated by two independent zero mean Gaussian random variables (GRV) which consist of in-phase and quadrature components. This model was used in simulations to assess the proposed block coded modulations.
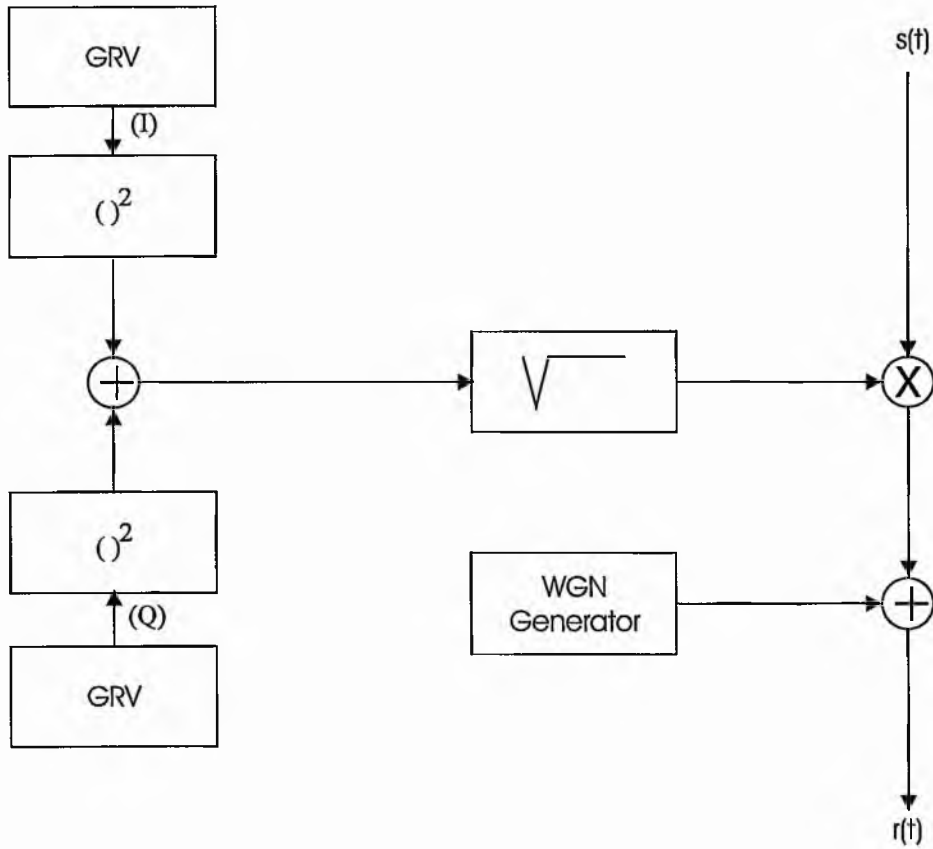
Figure 5.4 A Rayleigh fading channel model

5.2. REED SOLOMON CODED MPSK MODULATION NOT BASED ON SET PARTITIONING

Here, the results of methods 1 and 3 of this approach explained in section 3.1 are given. the results of method 2 are not given in this thesis because method 2 has limited configurations. In the first method, the MPSK signal set used for modulation does not correspond with the finite field over which the code is defined. Then in the second method, a Reed Solomon code, defined over $GF(2^m)$, is combined with a 2^m-PSK signal set. And in the third method, each symbol of the Reed Solomon code consists of the concatenation of y channel symbols. The results of method 2 can be seen in [Jamali and Le-Ngoc, 1994] in which Methods 2 and 3 were proposed for fading channels. Several Reed Solomon codes are used in these simulations. For all non-partitioned Reed Solomon coded modulation schemes, the code symbols are interleaved to a depth of 100 blocks before modulation in order to destroy the memory of the fading channel.

105

Figure 5.5 The error performances of RS(31, 17) and RS(63, 33) codes combined with a QPSK signal set.
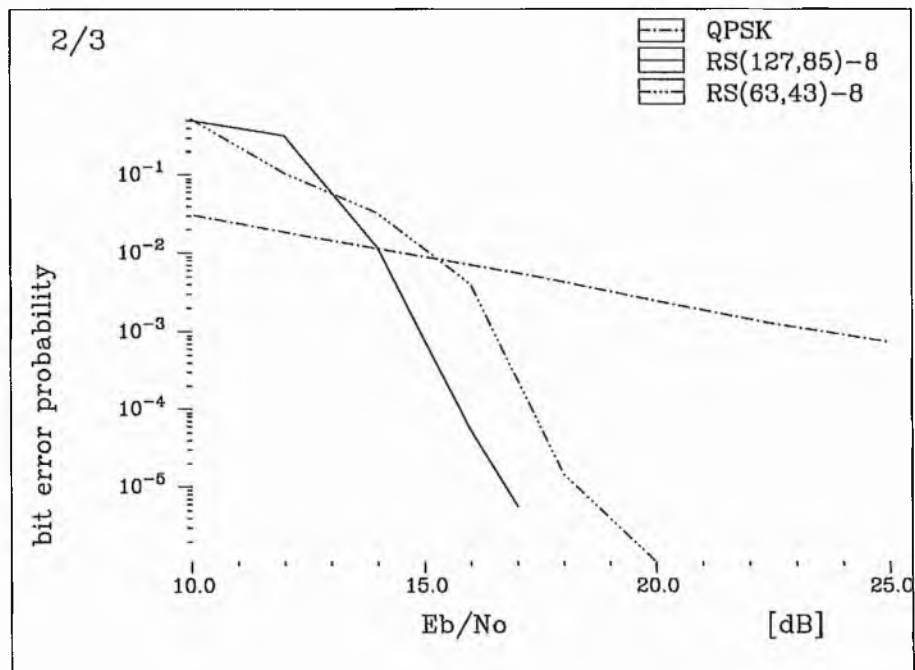
Figure 5.6 The error performances of RS(63, 43) and RS(127, 85) codes combined with an 8-PSK signal set.

Figure 5.5 shows the error performances of RS(31, 17) and RS(63, 33) codes combined with a QPSK signal set. The first code is an implementation of the first method. This code has code rate $R_c = {}^{17}\!/_{31} = 0.548$, which translates into a throughput of $m \cdot R_c = 2 \times {}^{17}\!/_{31} = 1.1$ bit sec^{-1} Hz^{-1} which is comparable to that of uncoded BPSK.

The second code is an implementation of the third method in which each code symbol consists of the concatenation of three channel symbols. This code is defined over GF(2^6), therefore each code symbol consists of three concatenated QPSK symbols. The code rate is 33/63 which translates into a throughput of 1.05 bit sec^{-1} Hz^{-1}.

Figure 5.6 shows the error performances of RS(63, 43) and RS(127, 85) codes combined with an 8-PSK signal set. The first code is defined over GF(2^6) and each code symbol consists of a concatenation of two 8-PSK symbols. The code rate is 43/63 which translates into a throughput of 2 bit sec^{-1} Hz^{-1} which is comparable to that of uncoded QPSK. The second code has code rate $R_c = {}^{85}\!/_{127}$, which translates into a throughput of $3 \times {}^{85}\!/_{127} = 2.008$ bit sec^{-1} Hz^{-1} which is comparable to that of uncoded QPSK.
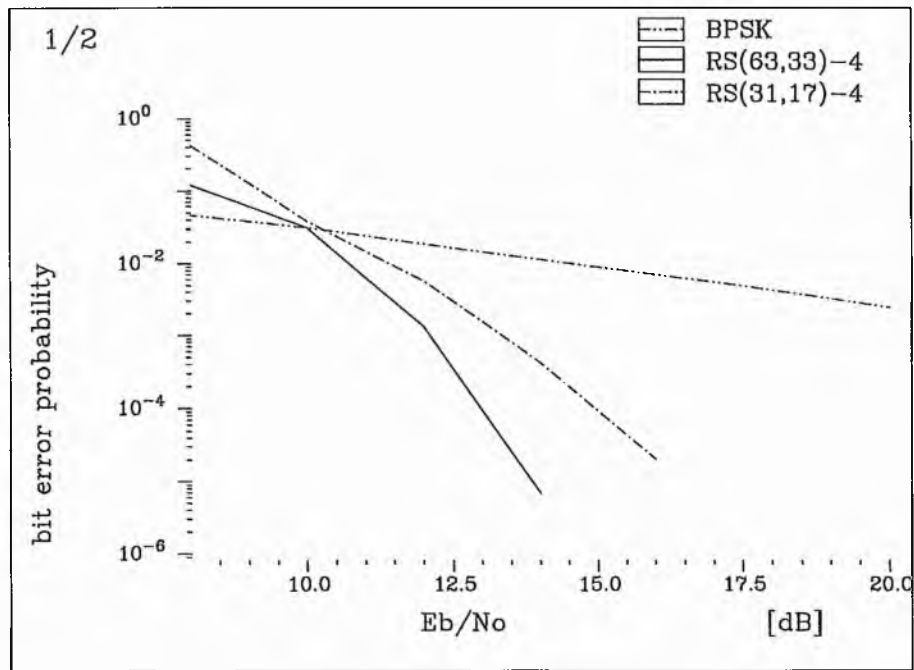
The first code is an implementation of the third method in which one code symbol consists of the concatenation of two channel symbols. The second code is an implementation of the first method in which the MPSK signal set used for modulation does not correspond with the finite field over which the code is defined. The results shows that the longer the code we use the better the performance becomes.

5.3. REED SOLOMON CODED MPSK MODULATION BASED ON SET PARTITIONING

For all partitioned Reed Solomon coded modulation schemes, the code symbols are interleaved to a depth of 100 blocks before modulation in order to destroy the memory of the fading channel. Figure 5.7 shows the error performances of good schemes for partitioned Reed Solomon coded QPSK modulation with code lengths of 31 and 63. The first scheme has component codes that are all RS(31, 15) with code rate $R_c = {}^{2 \times 15}\!/_{2 \times 31} = 0.484$, which translates into a throughput of $2 \times 0.484 = 0.968$ bit sec^{-1} Hz^{-1} which is comparable to that of uncoded BPSK. The second scheme's component codes are all RS(63, 31). The code rate is 31/63 which translates into a throughput of 0.984 bit sec^{-1} Hz^{-1} which is comparable to that of uncoded BPSK.
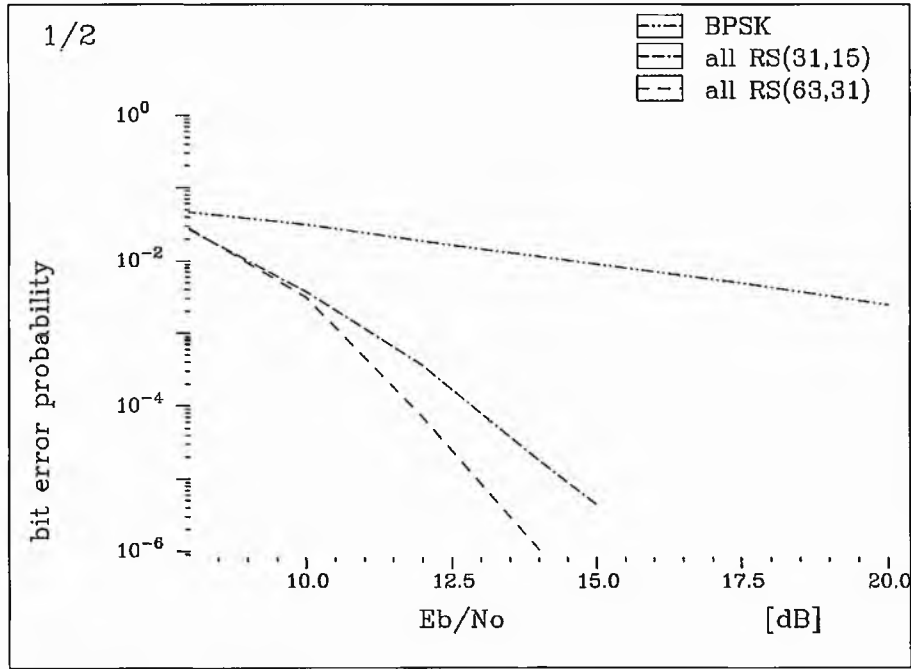
Figure 5.7 The error performances of partitioned RS coded QPSK modulation, **all RS(n,k)**, with code lengths of 31 and 63.

Figure 5.8 shows the error performances of partitioned Reed Solomon coded 8-PSK modulation with code lengths of 63 and 127. The first scheme has component codes that are all RS(63, 43) with code rate $R_c = {}^{43}\!/_{63}$, which translates into a throughput of $3 \times {}^{43}\!/_{63} = 2.05$ bit sec^{-1} Hz^{-1} which is comparable to that of uncoded QPSK. The second scheme's component codes are all RS(127, 85). The code rate is 85/127 which translates into a throughput of 2.01 bit sec^{-1} Hz^{-1} which is comparable to that of uncoded QPSK.

These schemes are different from those over the Gaussian channel in that good schemes have configurations in which all component codes have the same minimum Hamming distance. Partitioned Reed Solomon coded modulation schemes have these configurations because the fading phase is uniformly distributed random process over a Frequency-Nonselective, Slowly Fading Channels. We can conclude that the code performance depends strongly on its minimum Hamming distance (the *code diversity*), rather than on the minimum Euclidean distance of the code (as it does over the AWGN channel).

Figure 5.8 The error performances of partitioned RS coded 8-PSK modulation, **all RS(*n*,*k*)**, with code length of 63 and 127.

5.3.1. Multi-Iteration Approach of Multistage Decoding

In partitioned Reed Solomon coded modulation schemes, each of the m bits defining an MPSK symbol was coded and decoded by different Reed Solomon codecs. The set partitioning principle was applied to define subsets with distances Δ_i, ($i = 0$ to ($m-1$)) that were nondecreasing with i. We can see from Figure 2.2 that the minimum Euclidean distances between the signal points of the first and second subsets for a QPSK signal set are $\Delta_0 = \sqrt{2}\sqrt{E}$ and $\Delta_1 = 2\sqrt{E}$ and the minimum Euclidean distances between the signal points of the first, second and third subsets for a 8-PSK signal set are $\Delta_0 = 0.765\sqrt{E}$, $\Delta_1 = \sqrt{2}\sqrt{E}$ and $\Delta_2 = 2\sqrt{E}$.

For the Gaussian channel, the code performance depends strongly on the minimum Euclidean distance of the schemes. It was seen in chapter 4 that to maximise the minimum Euclidean distance, the partitioned Reed Solomon coded modulation schemes have component code configurations with minimum Hamming distances $d_{\min i}$, ($i = 1$ to m) that were nonincreasing with i, $d_{\min 1} > d_{\min 2} > d_{\min 3} > \cdots$.

Configurations of good schemes for partitioned Reed Solomon coded modulation which have component code configurations with minimum Hamming distances $d_{\min i}$, ($i = 1$ to m) that were nonincreasing with i, $d_{\min 1} > d_{\min 2} > d_{\min 3} > \cdots$, are given below. These schemes emerged from trials of a range of schemes with different component-code configurations.

A good scheme for partitioned Reed Solomon coded QPSK modulation with code length of 31 has component codes RS(31, 11) and RS(31, 21), with code rate $R_c = {}^{(11+21)}\!/\!_{2\times31} = {}^{16}\!/\!_{31}$ which translates into a throughput of $2 \times {}^{16}\!/\!_{31} = 1.03$ bit sec^{-1} Hz^{-1}, comparable to that of uncoded BPSK.

A good scheme for partitioned Reed Solomon coded QPSK modulation with code length of 63 has component codes: RS(63, 21) and RS(63, 43), with code rate $R_c = {}^{(21+43)}\!/\!_{2\times63} = {}^{64}\!/\!_{126}$ which translates into a throughput of $2 \times {}^{64}\!/\!_{126} = 1.01$ bit sec^{-1} Hz^{-1}, comparable to that of uncoded BPSK.

A good scheme for partitioned Reed Solomon coded 8-PSK modulation with code length of 63 has component codes RS(63, 19), RS(63, 51) and RS(63, 57), with code rate $R_c = {}^{(19+51+57)}\!/\!_{3\times63} = {}^{127}\!/\!_{189}$, which translates into a throughput of $3 \times {}^{127}\!/\!_{189} = 2.02$ bit sec^{-1} Hz^{-1}, comparable to that of uncoded QPSK.

Finally, a good scheme for partitioned Reed Solomon coded 8-PSK modulation with code length of 127 has component codes: RS(127, 37), RS(127, 103), and RS(127, 115), with code rate $R_c = {}^{(37+103+115)}\!/\!_{31\times127} = {}^{255}\!/\!_{381} = {}^{85}\!/\!_{127}$ which translates into a throughput of $3 \times {}^{85}\!/\!_{127} = 2.01$ bit sec^{-1} Hz^{-1}, comparable to that of uncoded QPSK.

However, we can see from two-iteration multistage decoding error performances at a bit error rate of 10^{-4} in Figures 5.9 and 5.10 that the schemes given above are 0.5 dB worse than the schemes given in section 5.3 in which all component codes have the same minimum Hamming distance. As explained before, partitioned Reed Solomon coded modulation schemes have these configurations because the fading phase is uniformly distributed random process over a frequency-nonselective, slowly Rayleigh fading channel. Therefore again, we can conclude that the code performance depends strongly on its minimum Hamming distance (the *code diversity*), rather than on the minimum Euclidean distance of the code (as it does on the AWGN channel).
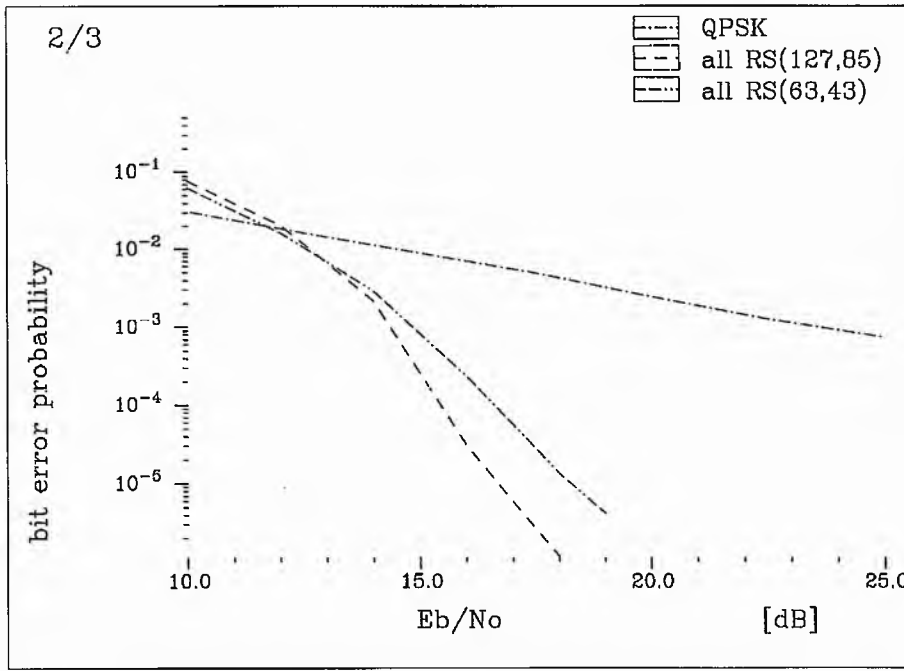
Figure 5.9 Error performances of partitioned RS coded QPSK modulation with code length of 31 using two-iteration multistage decoding: **all (31,15)** whose component codes are all RS(31,15), **31,11;31,21** whose component codes are RS(31,11) and RS(31,21), and one iteration multistage decoding: **all (31,15) one, 31,11;31,21 one**.

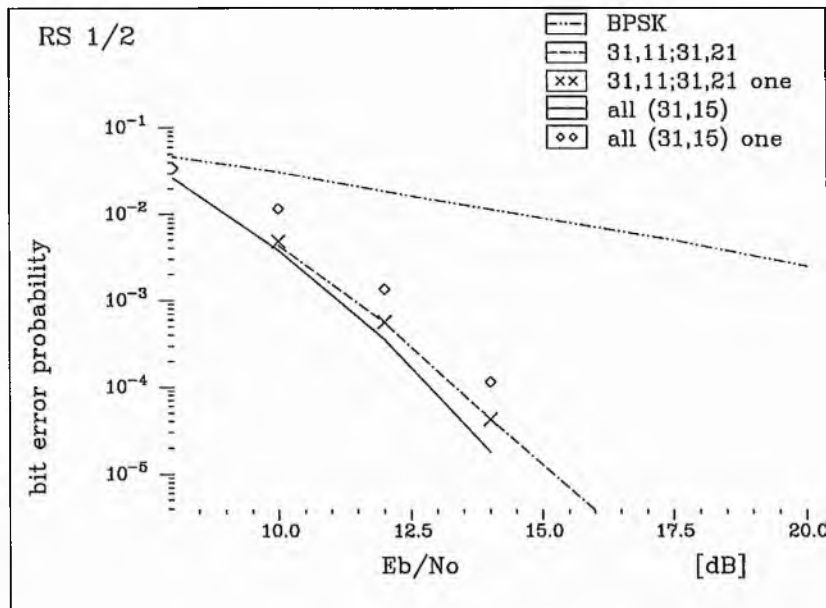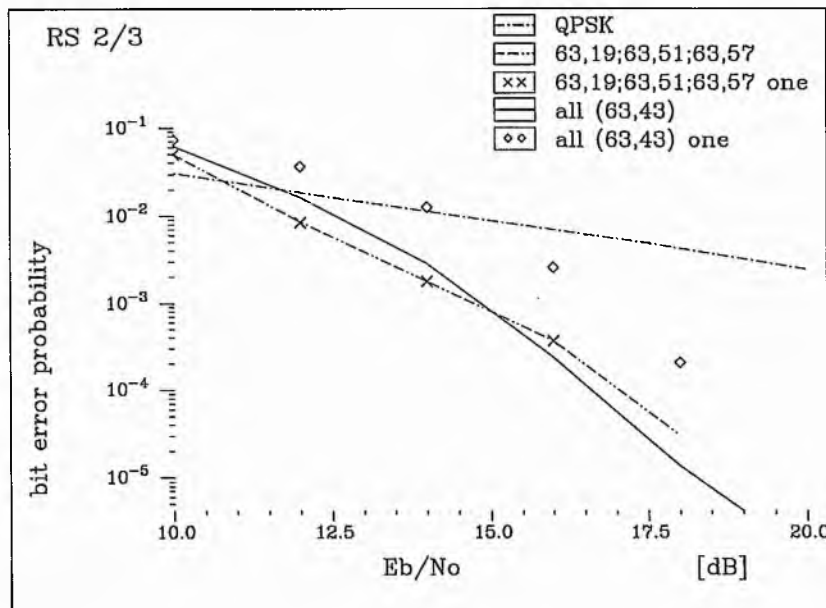

Figure 5.10 Error performances of partitioned RS coded 8-PSK modulation with code length of 63 using two-iteration multistage decoding: **all (63,43)** whose component codes are all RS(63,43), **63,19;63,51;63,57** whose component codes are RS(63,19), RS(63,51), and RS(63,57), and one iteration multistage decoding: **all (63,43) one, 63,19;63,51;63,57 one**.

111

Figures 5.9 and 5.10 also compare error performances of one iteration multistage decoding with those of two-iteration multistage decoding. We can see in Figure 5.9 that the error performances of a scheme with component codes RS(31, 11) and RS(31, 21) using one iteration and two-iteration multistage decoding are similar. Also, we see in Figure 5.10 that the error performances of a scheme with component codes RS(63, 19), RS(63, 51) and RS(63, 57) using one iteration and two-iteration multistage decoding are similar.

Therefore, we can conclude that the error performances of good schemes for partitioned Reed Solomon coded modulation which have component code configurations with minimum Hamming distances $d_{\min i}$, ($i = 1$ to m) that were nonincreasing with i, $d_{\min 1} > d_{\min 2} > d_{\min 3} > \cdots$, using one iteration and two-iteration are similar.

On the other hand, it is seen in Figure 5.9 that the error performance of a coded QPSK scheme in which all component codes have the same minimum Hamming distance using one iteration multistage decoding is 1 dB worse than that of the scheme using two-iteration multistage decoding. Similarly, in Figure 5.10, the error performance of a coded 8-PSK scheme in which all component codes have the same minimum Hamming distance using one iteration multistage decoding is 1.75 dB worse than that of using two-iteration multistage decoding.

Therefore we can conclude that good schemes for this channel must use two-iteration multistage decoding to have better error performance. This is because the good schemes have the same component codes; thus the first level component code also needs decoded codewords of other levels.

5.3.2. Comparisons with Reed Solomon Coded Modulation not Based on Set Partitioning

Figure 5.11 shows bit error rates of various schemes for Reed Solomon coded QPSK modulation. At a bit error probability of 10^{-4}, partitioned Reed Solomon coded modulation of length 31 has 1 dB more coding gain than non-partitioned and partitioned RS coded modulation with code length of 63 has 2 dB coding gain than non-partitioned.
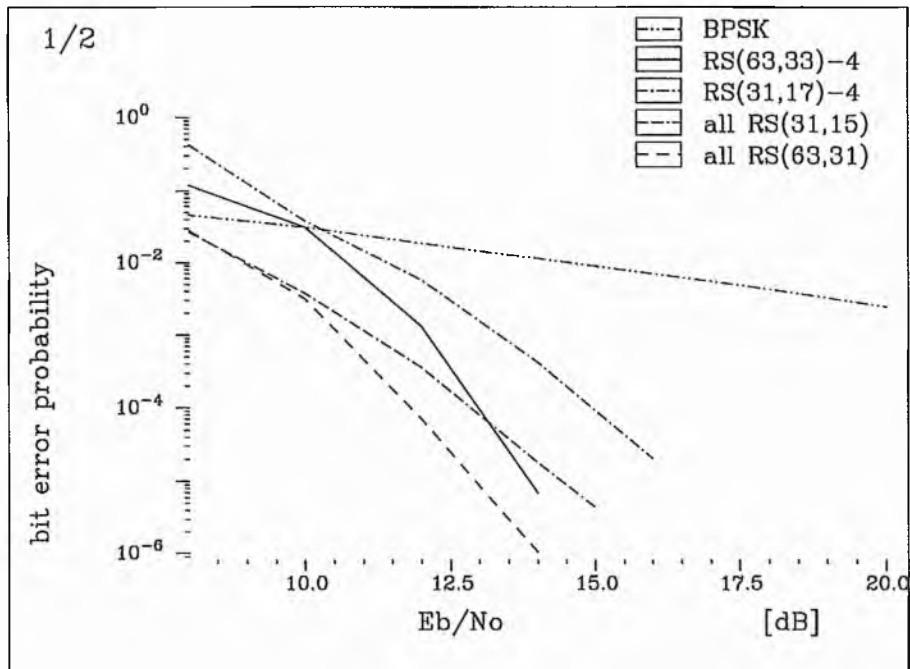
Figure 5.11 Bit error rates of various schemes for Reed Solomon coded QPSK modulation.
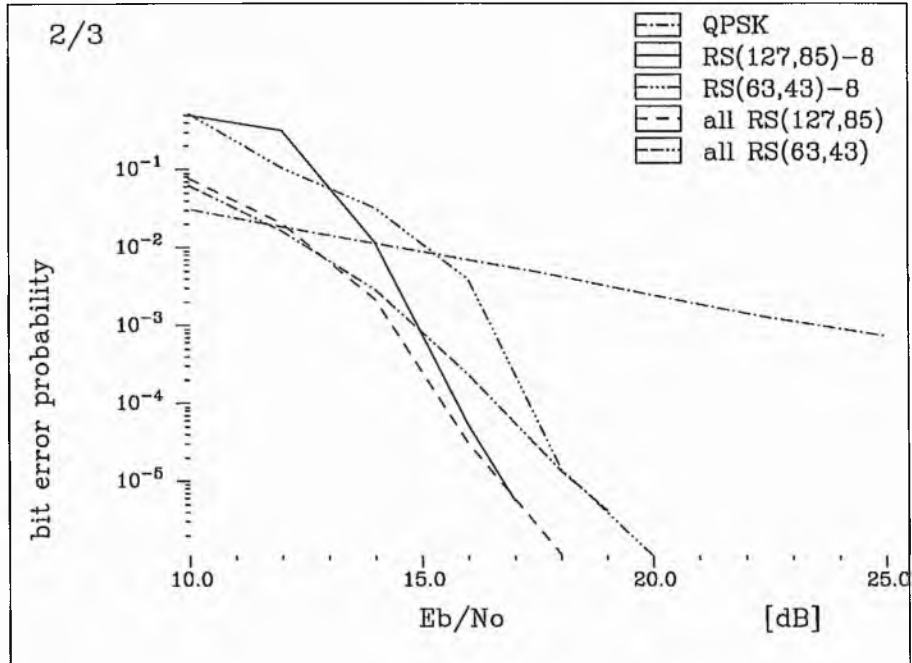
Figure 5.12 Bit error rates of various schemes for Reed Solomon coded 8-PSK modulation.

113

Figure 5.12 shows bit error rates of various schemes for Reed Solomon coded 8-PSK modulation. We see that error performances of partitioned RS coded 8-PSK modulation are better than those of non-partitioned at high BER, and finally they become the same at low BER. Therefore, the error performances of partitioned Reed Solomon coded modulation are never worse than those of non-partitioned RS coded modulation for the same code length.

5.3.3. Comparisons with Multilevel Reed Solomon Coded Modulation based on Gray Mapping

Here, the schemes used the same configurations of component codes as those over the Gaussian channel in which all component codes have the same minimum Hamming distance. The component-code configurations are suitable for a Rayleigh fading channel where the code performance depends strongly on its minimum Hamming distance. The code symbols are interleaved to a depth of 100 blocks before modulation in order to destroy the memory of the fading channel.

Figure 5.13 shows the error performances of partitioned and multilevel Gray-mapped Reed Solomon coded QPSK modulation with code length of 31 and 63. At a bit error probability of 10^{-4}, partitioned have about 1.25 dB more coding gain than multilevel Gray-mapped Reed Solomon coded modulation for the same code length.

Figure 5.14 shows the error performances of partitioned and multilevel Gray-mapped Reed Solomon coded 8-PSK modulation with code length of 63 and 127. At a bit error probability of 10^{-4}, partitioned has about 1.25 dB more coding gain than multilevel Gray-mapped Reed Solomon coded modulation for the same code length.

It is seen that at a bit error probability of 10^{-4}, all partitioned Reed Solomon coded QPSK and 8-PSK modulation schemes have about 1.25 dB more coding gain than multilevel Gray-mapped Reed Solomon coded modulation schemes.
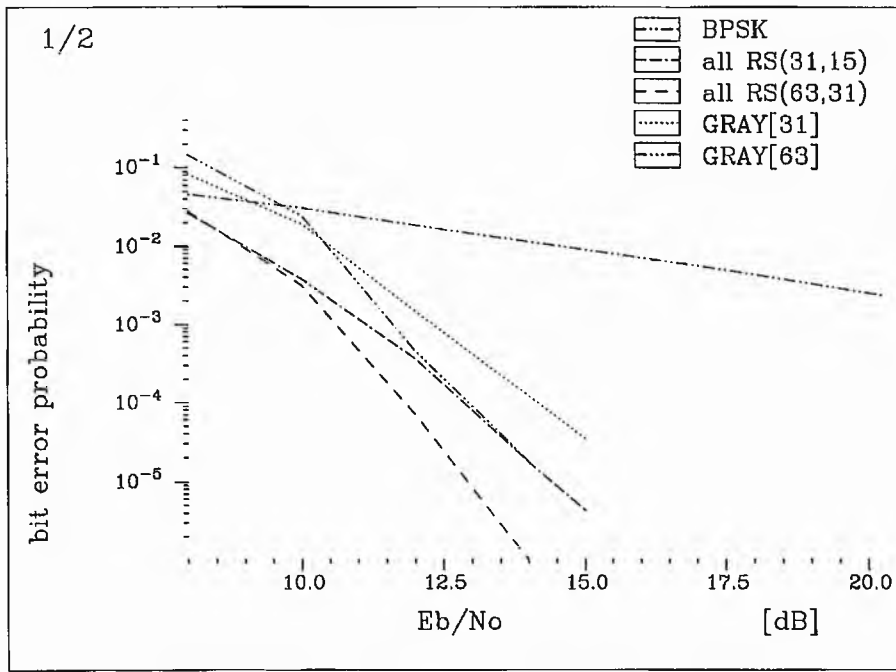
Figure 5.13 Error performances of partitioned **all RS(*n,k*)** and multilevel Gray-mapped **GRAY[*n*]**
Reed Solomon coded QPSK modulation with code length of 31 and 63.
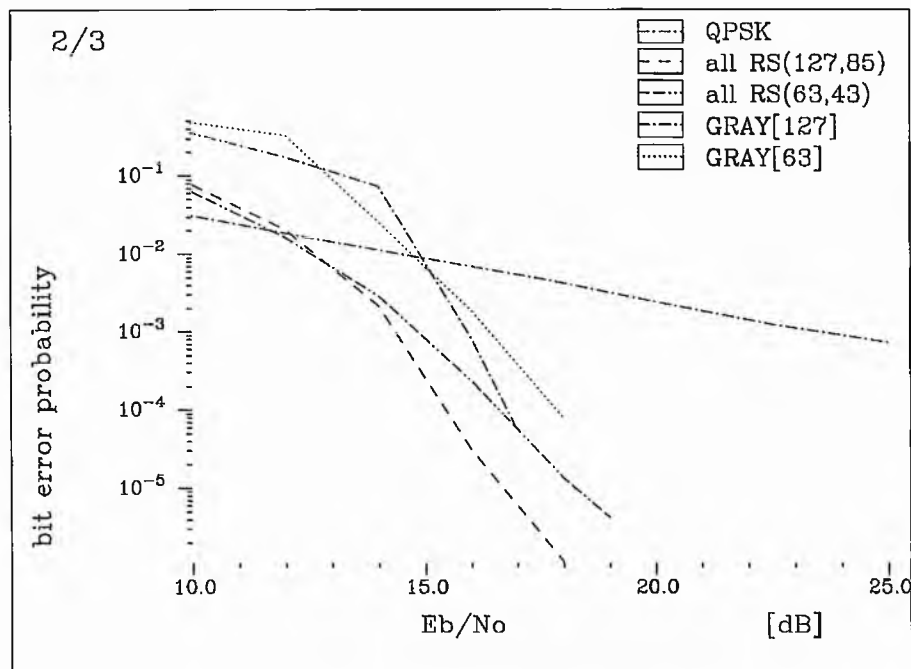
Figure 5.14 Error performances of partitioned **all RS(*n,k*)** and multilevel Gray-mapped **GRAY[*n*]**
Reed Solomon coded 8-PSK modulation with code length of 63 and 127.

115

5.3.4. Comparisons with Reed Muller Coded Modulation

Figure 5.15 shows error performances for coded QPSK modulation: partitioned Reed Solomon coded modulation, non-partitioned Reed Solomon coded modulation, partitioned Reed Muller coded modulation with code length of 256, and non-partitioned Reed Muller coded modulation RM(4, 9) with code length of 512 and information length of 256.

Here, the component-code configuration of partitioned RM coded modulation for code length of 256 is the same as that over the Gaussian channel because there is no Reed Muller code with code length of 256 which has code rate of 1/2. In other words, Reed Muller codes have limited configurations. For all Reed Muller coded modulation schemes, the coded bits are interleaved to a depth of 100 blocks before modulation in order to destroy the memory of the fading channel.

Reed Muller coded QPSK modulation of code length 256 (2^8) bits has component codes:

1. RM(3, 8) with minimum distance of $2^{(8-3)} = 32$ and with information length of 93.
2. RM(4, 8) with minimum distance of $2^{(8-4)} = 16$ and with information length of 163.

This scheme has $d_{\min 1} = 2d_{\min 2}$ and the code rate of $R_c = \frac{(k_1 + k_2)}{2 \cdot n} = \frac{(93+163)}{2 \cdot 256} = 0.5$.

It is seen that all Reed Muller coded modulation schemes have almost the same error performances. At a bit error probability of 10^{-4}, they are 0.5 dB worse than non-partitioned Reed Solomon coded modulation with code length of 31 and 2.5 dB worse than partitioned Reed Solomon coded modulation with code length of 31.

Figure 5.16 shows error performances for coded 8-PSK modulation: partitioned Reed Solomon coded modulation, non-partitioned Reed Solomon coded modulation, partitioned Reed Muller coded modulation with code length of 512, and non-partitioned Reed Muller coded modulation RM(5, 9) with code length of 512 and information length of 382. The non-partitioned Reed Muller coded modulation scheme results in a code rate of 0.75. Reed Muller codes with code length of 512 do not have a code whose code rate is 2/3 because Reed Muller codes have limited configurations.

The partitioned Reed Muller coded 8-PSK modulation of code length 512 (2^9) bits has component codes:

1. RM(3, 9) with minimum distance of $2^{(9-3)} = 64$ and with information length of 130.
2. RM(5, 9) with minimum distance of $2^{(9-5)} = 16$ and with information length of 382.
3. RM(6, 9) with minimum distance of $2^{(9-6)} = 8$ and with information length of 466.

This scheme results the code rate of $^{(130+382+466)}/_{3\times512} = 0.64$.

We can also see that all Reed Muller coded modulation schemes have the almost the same error performances. But at a bit error probability of 10^{-4}, they are much worse (at least 6 dB) than Reed Solomon coded modulation.
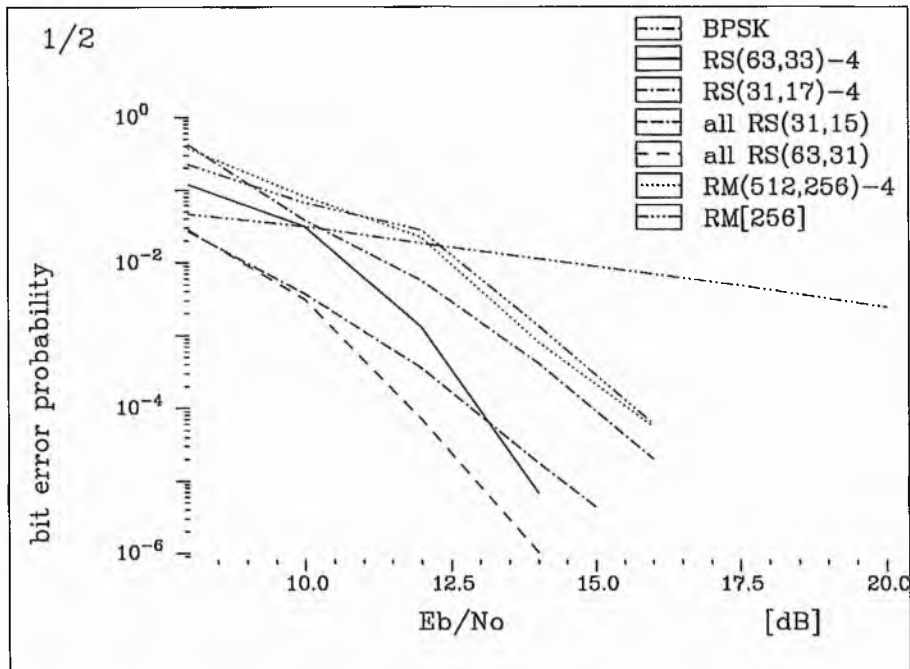
Figure 5.15 Error performances of partitioned **all RS(*n,k*)**, non-partitioned **RS(*n,k*)** RS coded QPSK modulation with code length of 31 and 63 and RM coded QPSK modulation based on set partitioning **RM[256]**, not based on set partitioning **RM(512, 256)**.
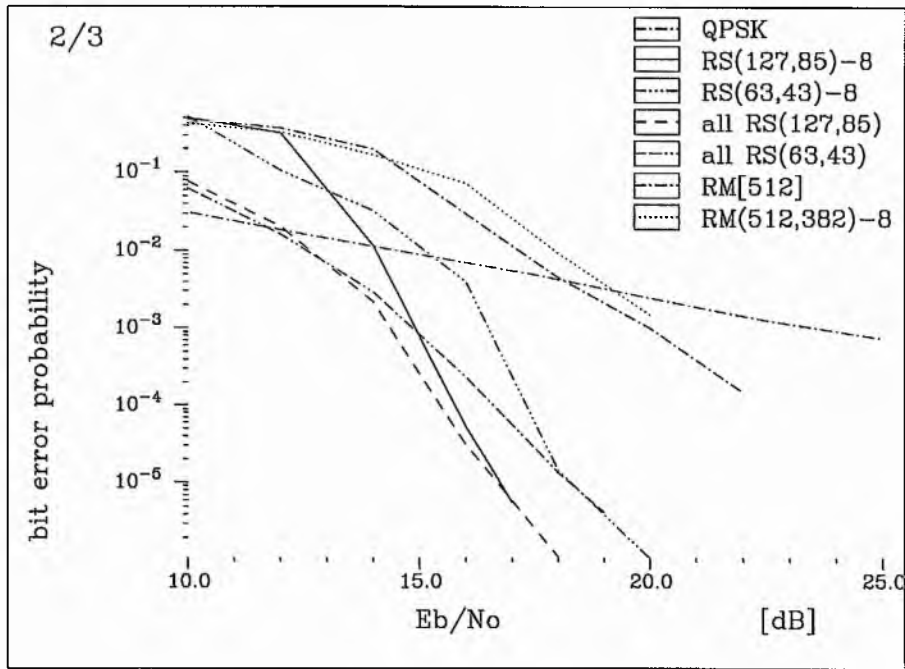
Figure 5.16 Error performances of partitioned **all RS(n,k)**, non-partitioned **RS(n,k)** RS coded 8-PSK modulation with code length of 63 and 127 and RM coded 8-PSK modulation based on set partitioning **RM[512]**, not based on set partitioning **RM(512, 382)**.

5.4. COMPARISON WITH BIT-INTERLEAVED CODED MODULATION

[Zehavi, 1992] and [Biglieri *et al.*, 1996] recognised that the code diversity, and consequently the reliability of coded modulation over a Rayleigh fading channel, could be further improved. He used a regular convolutional code followed by three bit-interleavers (not a channel-symbol interleaver), a Gray labelling for bits-to-signal mapping and an appropriate soft-decision bit metric as an input to the Viterbi decoder. This approach yields a coded system with high diversity, which is proportional to d_{free} of the code, where d_{free} is the free binary Hamming distance of the code. This is because the combined interleavers and mapping can be viewed as three statistically independent communication modulators and channels, assuming that we use ideal interleavers and deinterleavers.

Figure 5.17 shows a block diagram of a system proposed by Zehavi. Let $C = (C_1, C_2, C_3)$ be the vector of the three binary sequences at the encoder outputs. The sequences are fed into three independent ideal interleavers, resulting in a binary vector $C' = (C_1', C_2', C_3')$. A

group of 3 bits at the output of the interleavers is mapped into the 8-PSK signal set according to Gray mapping. The mapping signal points are digitally pulse shaped, and transmitted over the channel.
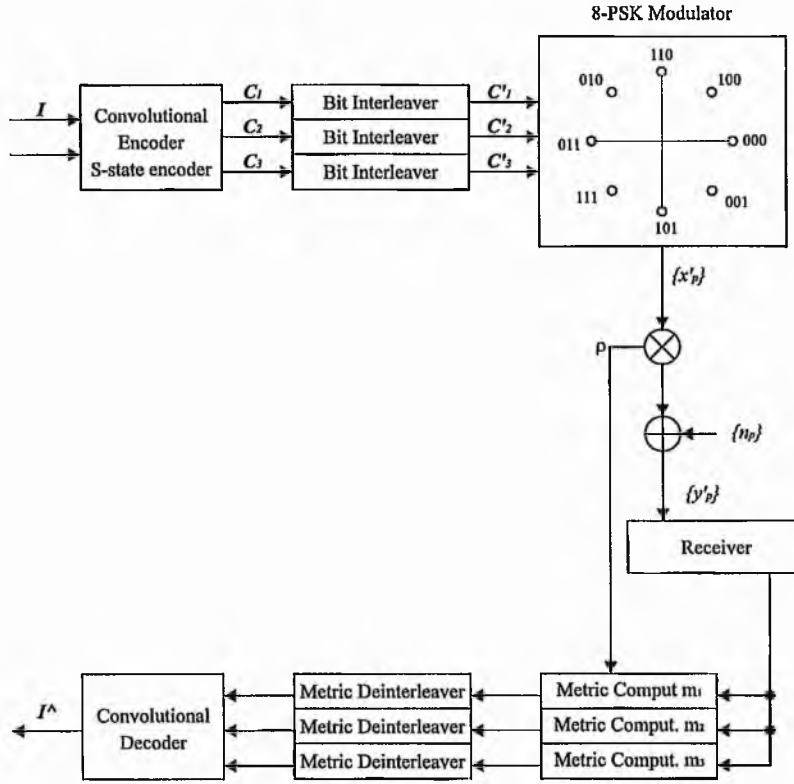
Figure 5.17 Block diagram of a bit-interleaved coded modulation system

At the receiver, the faded noisy version of the transmitted channel signal is passed through a demodulator, then the demodulator output is fed into three metric computation units. Finally, output bits of metric computation units are fed into the Viterbi decoder.

An analysis model of the Zehavi system is shown in Figure 5.18. Here, ideal interleavers and deinterleavers are assumed, so that the combined interleavers and mapping can be viewed as three statistically independent communication modulators and channels. The output of the encoder , $C_p = \left(c_p^1, c_p^2, c_p^3\right)$ the 3-tuple output of the encoder at time p, are transmitted by three random modulators. There are three channel symbols, x_p^i, $i = 1, 2, 3$, carrying the encoder output bits c_p^i. The mapping from binary 3-tuples to 8-PSK channel symbols, S_i^c, $i = 1, 2, 3$ and $c = 0, 1$, is done using Gray mapping.
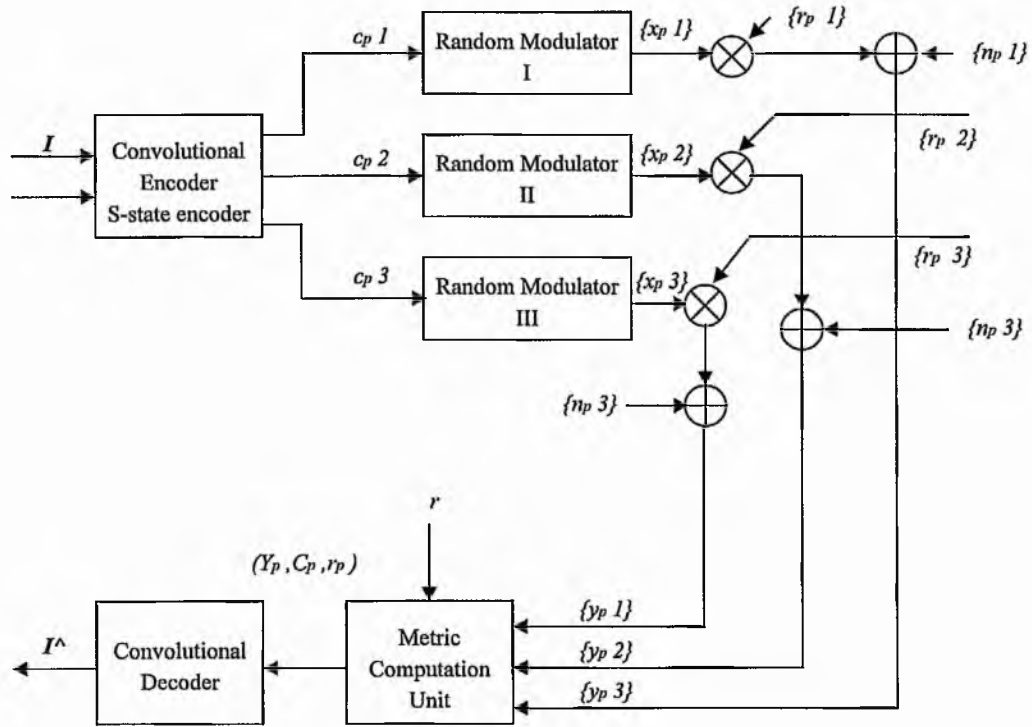
Figure 5.18 Analysis model of a bit-interleaved coded modulation system

At the receiver, the faded, noisy version of the transmitted channel symbol is passed through three metric computation units. Instead of a complicated metric which takes account the apriori probabilities of transmission of all possible four channel symbols from the set S_i^0 or S_i^1 associated with the output bit c_p^i, the receiver uses the suboptimal metric

$$m_i\left(y_p^i, S_i^c, r_p^i\right) = -\min_{x \in S_i^c}\left\|y_p^i - r_p^i x\right\|^2, c = 0,1, i = 1,2,3$$

where y_p^i is the received signal at the i-th channel at time p. The i-th metric computation unit produces two metrics corresponding to the two possible values of the bit c_p^i, at time p. The decoder input unit computes the branch metrics corresponding to all possible values of $C_p = \left(c_p^1, c_p^2, c_p^3\right)$. For each such value the decoder input unit computes the sum

$$m\left(Y_p, C_p, r_p\right) = \sum_{i=1}^{3}\left(1 - c_p^i\right)m_i\left(y_p^i, S_i^0, r_p^i\right) + c_p^i m_i\left(y_p^i, S_i^1, r_p^i\right), \quad r_p = \left(r_p^1, r_p^2, r_p^3\right).$$

Finally, these metrics are fed to the decoder, which employs the Viterbi algorithm to find the binary data sequence C with the highest cumulative sum of metrics, $m\left(Y_p, C_p, r_p\right)$.

The BER performance of partitioned Reed Solomon coded 8-PSK modulation with code length of 127 has been compared with upper bounds on the bit error rate versus E_b/N_0 of the bit-interleaved coded 8-PSK modulation in [Zehavi, 1992]. At a BER of 10^{-5}, partitioned Reed Solomon coded 8-PSK modulation with code length of 127 has similar BER performance to bit-interleaved coded 8-PSK modulation with a 16-state decoder. Because of the limited set of results he reported, we cannot compare other results with Zehavi's.

5.5. COMPARISON WITH SUNDBERG-SESHADRI CODED MODULATION

Figure 5.19 shows the basic block diagram of a transmitter for coded modulation proposed by [Sundberg & Seshadri, 1993] using coherent 8-PSK. Ungerboeck's signal mapping is used to label each signal point, where each binary digit is independently addressed by the output of a binary convolutional code. They found that the minimum Hamming distance between any two transmitted 8-PSK code sequences is

$$d_{\min} = \min\left(d_{\min 1}, d_{\min 2}, d_{\min 3}\right)$$

Therefore, they use the configuration where each component code has the same minimum Hamming distance which is the same configuration as we used.
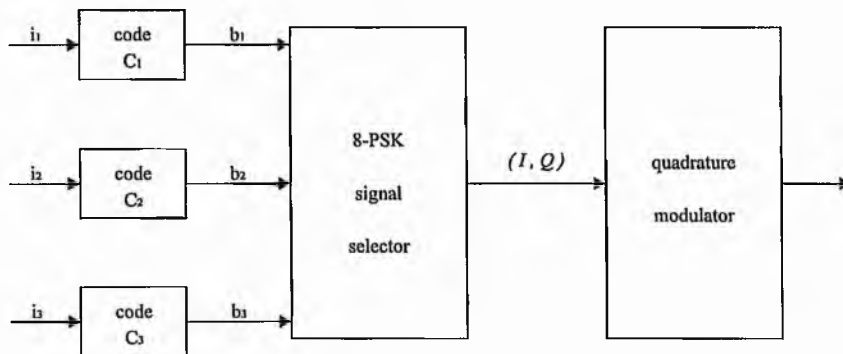
Figure 5.19 Block diagram of the encoder

At the receiver, they proposed an alternative multistage decoding algorithm; our multistage decoding procedure is impractical for the component code configurations used in their schemes. The decoder at every stage performs the task of decoding using the soft-Viterbi algorithm which computes the per symbol Euclidean metrics.

Decoding at the first stage proceeds as follows. For every received symbol y_p, the decoder finds the closest point in each of the two subsets at the first level of set partitioning. These two signal subsets are shown in Figure 5.20. Within each subset, there are four signal points, all of which have the same first bit b_1. Let the four points for which $b_1 = 0$, and $b_1 = 1$ be labelled as $S_p(k / b_1 = 0)$ and $S_p(k / b_1 = 1)$ respectively. The index k is given by $4b_3 + 2b_2 + b_1$. where p denotes the time. The decoder at the first stage performs the task of decoding using the Viterbi algorithm. The decoder trellis is determined only by code C_1. The decoder at time p compute the per symbol Euclidean metrics

$$M_p(i) = \min_{k, b_1 = i} \left| y_p - S_p(k / b_1 = i) \right|^2, \quad i = 0,1 \qquad 5.27$$

These metrics enter the branch metric calculations of the Viterbi algorithm. If a state transition results in bit 0 (or 1) at time p, then $M_p(0)$ (or $M_p(1)$) is used in the branch metric calculations. Decoding is achieved by finding the path through the trellis with the best accumulated Euclidean metric. Figure 5.21 shows the Trellis decoder at the first stage. In decoding code C_2, the Viterbi decoder as determined by C_2 uses the per symbol Euclidean metrics at time p

$$M_p(i) = \min_{k, b_2 = i, b_1 = \hat{b}_{1p}} \left| y_p - S_p(k / b_2 = i, \hat{b}_{1p}) \right|^2, \quad i = 0,1 \qquad 5.28$$

where $\hat{b}_{1p}$ corresponds to the p-th output of encoder of C_1. Also the Euclidean distance is calculated using the signals at the second level of set partitioning as in Figure 5.20. The input to the encoder is the decoded information sequence $\hat{i}_p$ that is obtained after the first stage of decoding. Decoding is performed in a similar manner for code C_3. The per symbol Euclidean metrics used by the Viterbi decoder at time p are now given by

$$M_p(i) = \left| y_p - S_p(k / b_3 = i, \hat{b}_{1p}, \hat{b}_{2p}) \right|^2, \quad i = 0,1 \qquad 5.29$$

122
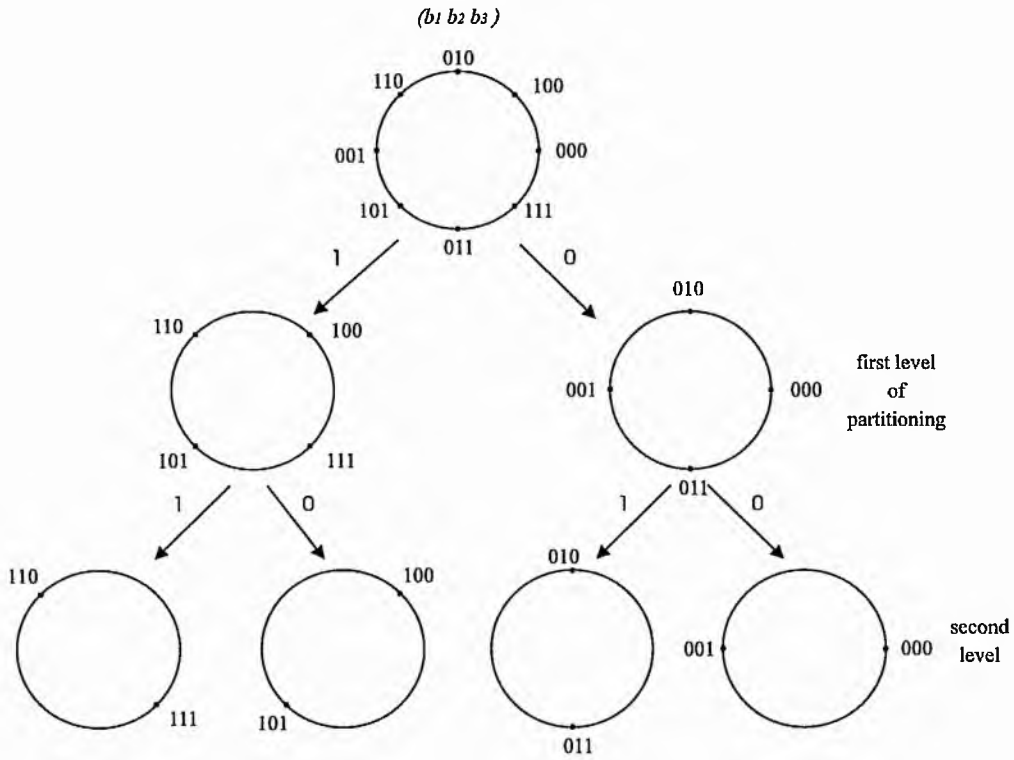
Figure 5.20 The 8-PSK signal constellation and its set partitions

In the Viterbi decoding algorithm, the estimated information bit sequence is liable to contain error bursts. In order to avoid the error propagation effect, they used interleaving between the coded bit streams of each level. At the second iteration of decoding, C_1 is decoded assuming that decisions on C_2 and C_3 are correct. The per symbol Euclidean metric is now given by

$$M_p(i) = \left| y_p - S_p\left(k \,/\, \hat{b}_{3p}, \hat{b}_{2p}, b_1 = i\right) \right|^2, \quad i = 0,1 \qquad 5.30$$

The difference may be compared to Equation 5.27; using the metrics in Equation 5.30, Viterbi decoding is performed. This results in an updated decoding of component code C_1. C_2 is now decoded assuming that the decision on C_3, obtained after first stage of decoding, and the updated decisions on C_1, obtained after second stage of decoding, are correct.

123
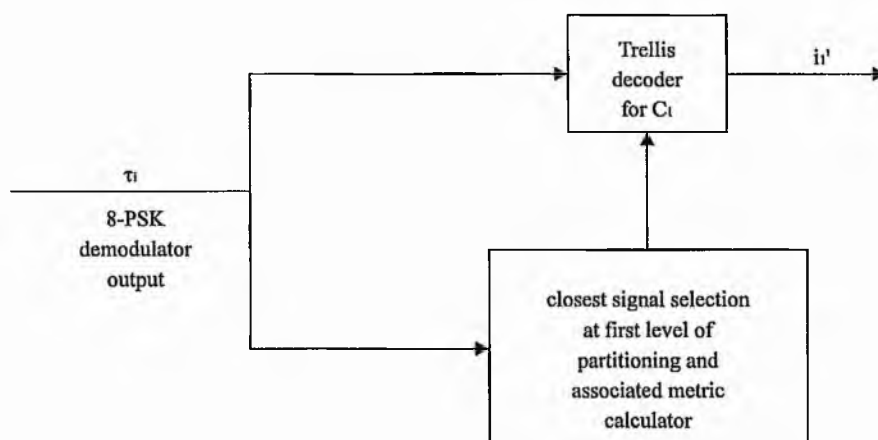
Figure 5.21 The Trellis decoder at the first stage

Here, the error performance of partitioned Reed Solomon coded 8-PSK modulation with code length of 127 is compared with the simulated BER performance of coded modulation proposed by [Sundberg & Seshadri, 1993]. They used three component codes which are all rate $R_c = 2 / 3$, rate-compatible punctured binary convolutional codes. Two iterations of multistage decoding was used.

The number of component-code decoder states is 16, and the component code's free distance (d_{free}) is 4. The overall optimal $R_c = 2 / 3$ code with number of decoder states = 16. They were looking at BER performance of every bit (b_1, b_2 and b_3). At a BER of 10^{-5}, BER performance of partitioned Reed Solomon coded 8-PSK modulation with code length of 127 is 1 dB better than that of b_1, but 1 dB worse than that of b_2 and 1.5 dB worse than that of b_3.

Note that Reed Solomon codes have powerful error detection capability which are different from binary convolutional codes. In the simulations of partitioned Reed Solomon coded modulation, if the decoder detected the errors but it could not correct the errors, the decoder passed the input sequence to the decoder output.

5.6. CONCLUSION FOR THE RAYLEIGH FADING CHANNEL

In this section, the error performance over a Rayleigh fading channel of Reed Solomon coded modulation based on set partitioning has been analysed and compared with Reed Solomon coded modulation not based on set partitioning, multilevel Reed Solomon coded modulation based on Gray mapping, and Reed Muller coded modulation.

For coded QPSK modulation: at a BER of 10^{-4}, partitioned Reed Solomon coded modulation has at least 1 dB more coding gain than non-partitioned. At a BER of 10^{-4}, partitioned RS coded modulation has about 1.25 dB more coding gain than multilevel Gray-mapped RS coded modulation. And finally, the error performances of partitioned RS coded modulation are better (at least 0.5 dB) than those of Reed Muller coded modulation.

For coded 8-PSK modulation: the error performances of partitioned Reed Solomon coded modulation are never worse than those of non-partitioned RS coded modulation for the same code length. At a BER of 10^{-4}, partitioned has about 1.25 dB coding gain than multilevel Gray-mapped RS coded modulation. And finally the error performances of partitioned RS coded modulation are much better (at least 6 dB) than those of partitioned Reed Muller coded modulation and much better than those of non-partitioned RM coded modulation.

Overall over a Rayleigh fading channel, Reed Solomon coded modulation based on set partitioning performs better than, or at least as well as not based on set partitioning, performs better 1.25 dB than multilevel Gay-mapped RS coded modulation, and performs better or much better than Reed Muller coded modulation.

These schemes are different from those over the Gaussian channel in that good schemes have configurations in which all component codes have the same minimum Hamming distance because the fading phase is a uniformly distributed random process.

Compared with bit-interleaved coded modulation proposed in [Zehavi, 1992], at a BER of 10^{-5}, partitioned Reed Solomon coded 8-PSK modulation with code length of 127 has almost similar BER performance to bit-interleaved coded 8-PSK modulation with 16 state decoder. Then compared with Sundberg-Seshadri coded modulation, at a BER of 10^{-5}, the BER performance of partitioned Reed Solomon coded 8-PSK modulation with code length of 127 is comparable to three-level component codes using a 16-state decoder.

Finally, we can see that by matching the configuration of component codes with the channel characteristics, it is shown that Reed Solomon coded modulation based on set partitioning is robust for the Gaussian and a Rayleigh fading channel.

CHAPTER 6

APPLICATION TO ORTHOGONAL FREQUENCY DIVISION MULTIPLEXING SYSTEMS

In this chapter, Reed Solomon coded modulation is used for concatenated schemes in which Reed Solomon codes are used both as inner code and outer codes and applied to OFDM systems. Firstly, we describe several approaches to OFDM systems, then develop an approach to an OFDM problem in mobile communications, namely peak-to-mean envelope power ratio. Finally, we study the designs of Reed Solomon-Reed Solomon concatenated schemes which are applied to an OFDM system.

The channel for mobile communication has a particularly hostile transmission environment, simultaneously containing multiple paths, interference and impulsive parasitic noise. It will simply be taken that the impulse response of the channel can be represented as the sum of pulses having different delays. Each of these pulses will be subject to a multiplying factor of which the amplitude generally follows a Rayleigh law and which corresponds to the effect of local diffraction in the region near the mobile receiver. Typically, this pulse train extends over several microseconds, so that the transmission of high bit-rates (several Mbit sec^{-1}) is a risky process.

The techniques sometimes used to resolve this problem are based on an extension of the duration of the symbols by increasing the dimension of the symbol alphabet. Among

these techniques, the most widely used is that of spectrum-spreading, where the emitted symbols have a wide spectrum and a narrow autocorrelation function. This approach has a problem that the spectral efficiency of this type of system is always relatively low.

Another approach consists in splitting the information to be transmitted into a large number of elementary sub-channels each carrying a low bit-rate. This transforms a highly-selective wide band channel into a large number of non-selective narrow-band channels which are frequency-multiplexed, Frequency Division Multiplexing (FDM). There remains the problem of fading, the amplitude of each of the sub-channels following a Rayleigh law or a Rice-Nakagami law if there is a direct path. The use of a coding system adapted to the fading nature of the channel permits the performance to be considerably improved.

The principles of an FDM system which is particularly effective from the point of view of the spectrum is known as Orthogonal Frequency Division Multiplexing (OFDM). In a normal FDM system, the many carriers are spaced apart in such a way that the signals can be received using conventional filters and demodulators. In such receivers, guard bands have to be introduced between the different carriers, and this results in a lowering of the spectral efficiency. It is possible, however, to arrange the carriers in OFDM signal so that the sidebands of the individual carriers overlap and the signals can still be received without adjacent carrier interference. In order to do this the carriers must be mathematically orthogonal.

The first use of OFDM signals over the bandlimited transmission medium was proposed in [Chang, 1966]. The system using such signals has the following properties:

1. The maximum signalling rate for the given channel (Nyquist rate) can be approached without the use of sharp cutoff filters. This is probably the most important property in high-speed data transmission.

2. With the entire frequency band divided into a number of narrow channels, the frequency division multiplexing system (parallel system) is less sensitive to narrow-band fading and interference than is the ordinary time division multiplexing system (serial system).

3. For the same reason, the parallel system is less sensitive to channel distortion. This has been shown quantitatively in [Saltzberg, 1967]

4. As in the serial system, the parallel system provides maximum signal-to-noise for analog data transmission and minimum probability of error for digital data

transmission in the presence of bandlimited white Gaussian noise under the constraint of no intersymbol or interchannel interference.

5. In serial transmission, certain types of noise (such as time variable tone interference) may cause the entire system to be disabled. This can be avoided in the parallel system by adaptively dropping out only the channels affected. Thus, like a special serial transmission scheme, the flexibility of the parallel system enables it to adapt to a variety of noise environments.
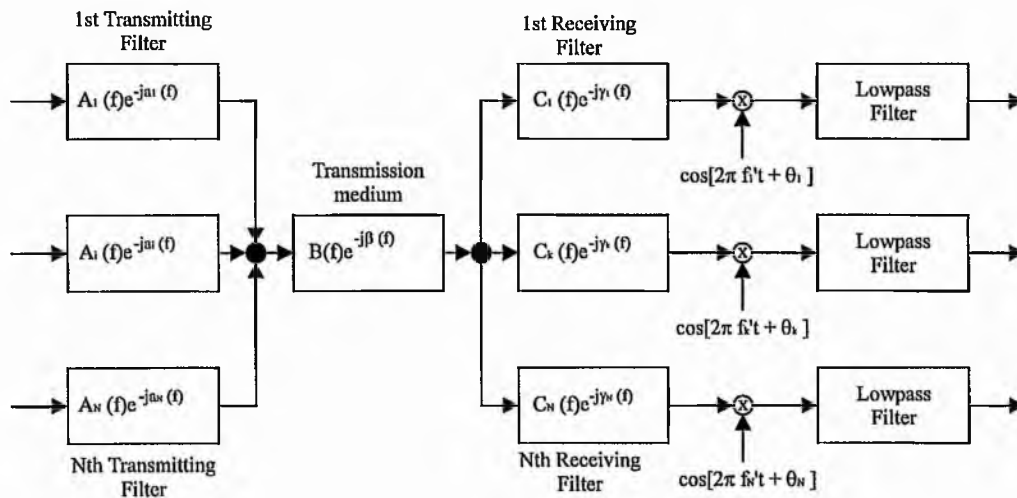
(a)
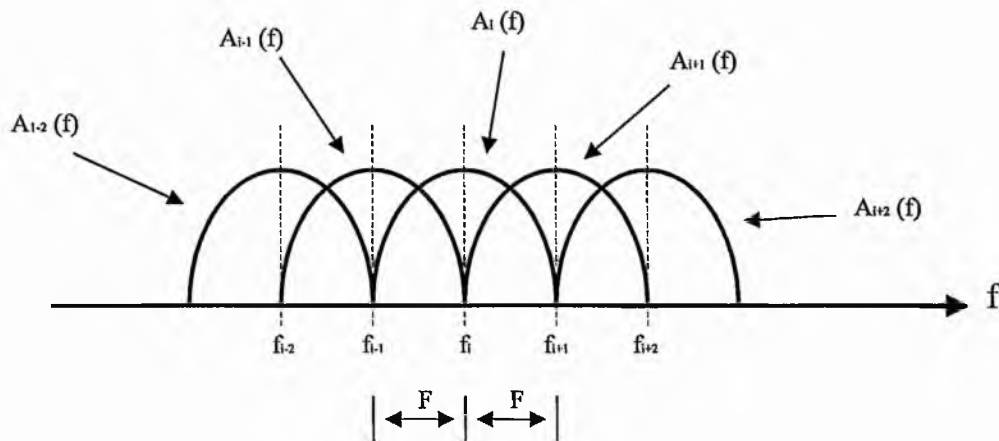
(b)

Figure 6.1 Block diagram of parallel data transmission

Figure 6.1 illustrates the block diagram of the parallel transmission system considered. The N parallel channels operate on equally spaced centre frequencies and transmit at the same data rate. The signalling intervals of the channels are synchronised. Let

$f_k \triangleq$ centre frequency of the k-th channel

$F \triangleq$ difference between two adjacent centre frequencies

$f_k' \triangleq$ demodulating carrier frequency of the k-th channel

$R \triangleq$ data rate per channel $= 2F$ baud

$T_0 \triangleq$ baud interval of each channel $= \dfrac{1}{2F}$ seconds.

Each channel is capable of transmitting either binary or multilevel signals. As is shown in Figure 6.1 (b), the transmitting filter $A_i(f)e^{-j\alpha_i(f)}$ of the i-th channel is bandlimited from $f_i - F$ to $f_i + F$. (Note particularly that adjacent channels overlap in frequency.) It is also shown in Figure 6.1 (b) that if the system consists of N channels, the overall bandwidth required is $(N+1)F$. For this bandwidth, the maximum baud rate that is theoretically possible to transmit (Nyquist rate), is $R_{\max} = 2(N+1)F$ bauds without intersymbol interference. However, this rate cannot be achieved in practice since it requires filters with perpendicular cutoffs and linear phases. In the present system, where each channel transmits at a data rate of $2F$ bauds, the overall data rate is $R = 2FN$ bauds $= N/(N+1) \cdot R_{\max}$. Thus, as N increases, the overall data rate of the present system approaches the theoretical maximum rate $R_{\max}$.

For a large number of channels, the arrays of sinusoidal generators and coherent demodulators required in parallel systems become unreasonably expensive and complex. However, it can be seen in [Salz & Weinstein, 1969] that an OFDM data signal is effectively the Fourier transform of the original serial data train, and that the bank of coherent demodulators is effectively an inverse Fourier transform generator. This idea suggests a completely digital modem built around a special-purpose computer performing the fast Fourier transform (FFT) and is the key to its current popularity.

To develop OFDM schemes using the Fourier transform, three approaches are considered: Weinstein and Ebert's approach, Proakis' approach and complex-signal approach. They will be discussed in the following sections.

6.1. WEINSTEIN AND EBERT'S APPROACH TO OFDM

The block diagram of the OFDM system proposed in [Weinstein & Ebert, 1971] is shown in Figure 6.2. They used the discrete Fourier transform (DFT) at both the transmitter and receiver.
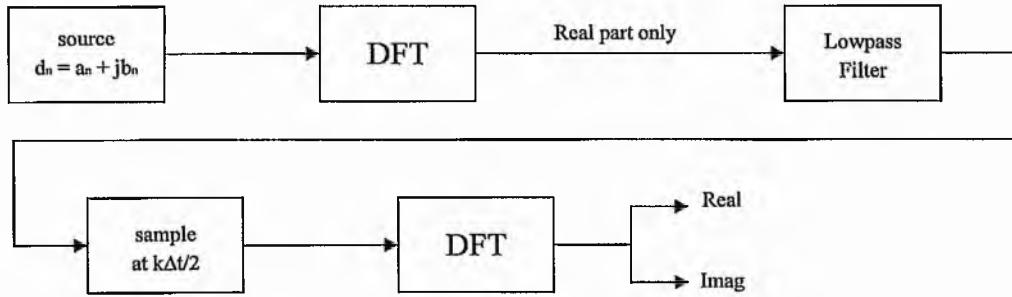
Figure 6.2 OFDM block diagram as proposed by Weinstein and Ebert

Consider a data sequence $(d_0, d_1, \cdots, d_{N-1})$, where each d_n is a complex number $d_n = a_n + jb_n$. Assuming that DFT is performed on $2d_n$, the result is a vector $S = (S_0, S_1, \cdots, S_{N-1})$, with

$$S_m = \sum_{n=0}^{N-1} 2d_n e^{-j(2\pi nm/N)} = 2\sum_{n=0}^{N-1} d_n e^{-j2\pi f_n t_m} , \qquad m = 0, 1, \cdots, N-1$$

where $f_n = \dfrac{n}{N\Delta t}$ and $t_m = m\Delta t$.

The transmitted signals are the real part of S

$$Y_m = 2\sum_{n=0}^{N-1} (a_n \cos 2\pi f_n t_m + b_n \sin 2\pi f_n t_m)$$

If these components are applied to a lowpass filter at time interval Δt, a signal is obtained that closely approximates the frequency division multiplexed signal

131

$$y(t) = 2 \sum_{n=0}^{N-1} \left(a_n \cos 2\pi f_n t + b_n \sin 2\pi f_n t \right), \qquad 0 \leq t \leq N\Delta t$$

At the receiver we sample with interval $\dfrac{\Delta t}{2}$ (two time faster) and the DFT will operate at the $2N$ samples. When there is no channel distortion:

$$y_k = y\left(k\frac{\Delta t}{2} \right) = 2 \sum_{n=0}^{N-1} \left(a_n \cos\frac{2\pi nk}{2N} + b_n \sin\frac{2\pi nk}{2N} \right), \qquad k = 0,1,\cdots,2N-1.$$

and the output of the DFT will be:

$$
\begin{aligned}
z_l &= \frac{1}{2N} \sum_{k=0}^{2N-1} Y_k e^{-j\frac{2\pi lk}{2N}} \\
&= \frac{1}{2N} \sum_{k=0}^{2N-1} 2\left[\sum_{n=0}^{N-1} a_n \cos\left(\frac{2\pi nk}{2N}\right) + b_n \sin\left(\frac{2\pi nk}{2N}\right) \right] e^{-j\frac{2\pi lk}{2N}} \\
&= \frac{1}{N} \sum_{k=0}^{2N-1} \left[a_n \sum_{n=0}^{N-1} \cos\left(\frac{2\pi nk}{2N}\right) + b_n \sum_{n=0}^{N-1} \sin\left(\frac{2\pi nk}{2N}\right) \right] e^{-j\frac{2\pi lk}{2N}} \\
&= \frac{1}{N} \sum_{k=0}^{2N-1} \left[a_n \sum_{n=0}^{N-1} \frac{e^{j\frac{2\pi nk}{2N}} + e^{-j\frac{2\pi nk}{2N}}}{2} e^{-j\frac{2\pi lk}{2N}} + b_n \sum_{n=0}^{N-1} \frac{e^{j\frac{2\pi nk}{2N}} - e^{-j\frac{2\pi nk}{2N}}}{2j} e^{-j\frac{2\pi lk}{2N}} \right] \\
&= \frac{1}{2N} \sum_{k=0}^{2N-1} \left[a_n \sum_{n=0}^{N-1} \left(e^{j\frac{2\pi k}{2N}(n-l)} + e^{-j\frac{2\pi k}{2N}(n+l)} \right) + \frac{b_n}{j} \sum_{n=0}^{N-1} \left(e^{j\frac{2\pi k}{2N}(n-l)} - e^{-j\frac{2\pi k}{2N}(n+l)} \right) \right]
\end{aligned}
$$

where the equality

$$\sum_{n=0}^{N-1} e^{-j\frac{2\pi n(k-m)}{N}} = \begin{cases} 0, & m \neq k \\ N, & m = k \end{cases}$$

has been employed. Thus, we have the following outputs:

$$z_l = \begin{cases} z_0 = \frac{1}{2N}\left[a_0(2N+2N) - jb_n(2N-2N) \right] = 2a_0, & l = 0 \\ z_l = \frac{1}{2N}\left[a_l(2N) - jb_l(2N) \right] = a_l - jb_l, & 0 < l \leq N-1 \\ \text{irrelevant}, & l > N-1 \end{cases}$$

We can see that the original data a_l and b_l are available (except for $l = 0$).

132

6.2. PROAKIS' APPROACH TO OFDM

A block diagram of OFDM systems proposed in [Proakis, 1995] is shown in Figure 6.3. A serial to parallel buffer segments the information sequence into frames of N_f bits. In each frame, the N_f bits are divided into $\tilde{N}$ groups, where the i-th group is assigned $\tilde{n}_i$ bits, thus

$$\sum_{i=1}^{\tilde{N}} \tilde{n}_i = N_f$$

Each group may be encoded separately, so that the number of output bits from the encoder for the i-th group is $n_i \geq \tilde{n}_i$.
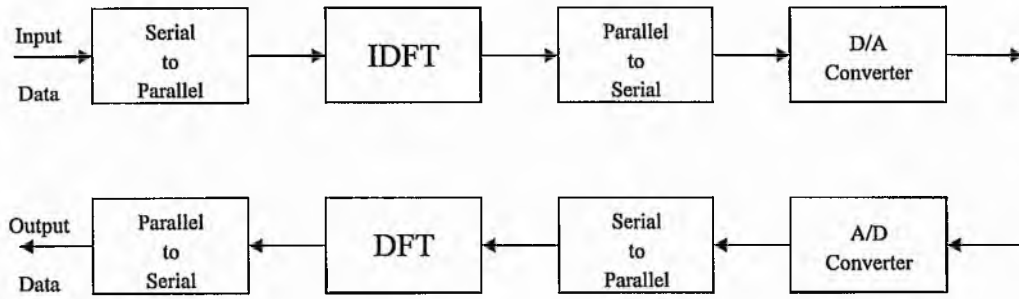
Figure 6.3 OFDM block diagram as proposed by Proakis

It is convenient to view the OFDM system as consisting of $\tilde{N}$ independent QAM channels, each operating at the same symbol rate $1/T$ but each channel having a distinct QAM constellation, as an example the i-th channel will employ $M_i = 2^{n_i}$ signal points. We denote the complex-valued signal points corresponding to the information symbols on the subchannels by X_k, $k = 0, 1, \ldots, \tilde{N} - 1$. In order to modulate the $\tilde{N}$ subcarriers by the information symbols $\{X_k\}$, we employ inverse DFT (IDFT).

However, if we compute the $\tilde{N}$-point IDFT of $\{X_k\}$ we shall obtain a complex-valued time series. Instead we create $N = 2\tilde{N}$ information symbols by defining

$$X_{N-k} = X_k^*, \qquad k = 1, \ldots, \tilde{N} - 1$$

and $X_0' = \mathrm{Re}(X_0)$, $X_{\tilde{N}} = \mathrm{Im}(X_0)$. Thus, the symbol X_0 is split into two parts, both real. Then, the N-point IDFT yields the real-valued sequence

$$x_n = \frac{1}{\sqrt{N}} \sum_{k=0}^{N-1} X_k e^{j2\pi nk/N}, \qquad n = 0,1,\ldots,N-1$$

where $1/\sqrt{N}$ is simply a scale factor.

The sequence $\{x_n, 0 \le n \le N-1\}$ corresponds to the samples of the sum $x(t)$ of $\tilde{N}$ subcarrier signals, which is expressed as

$$x(t) = \frac{1}{\sqrt{N}} \sum_{k=0}^{N-1} X_k e^{j2\pi kt/T}, \qquad 0 \le t \le T$$

where T is the symbol duration. We observe that the subcarrier frequencies are $f_k = k/T$, $k = 0,1,\ldots,\tilde{N}$. Furthermore, the discrete-time sequence $\{x_n\}$ represents the samples of $x(t)$ taken at times $t = nT/N$ where $n = 0,1,\ldots,N-1$.

To obtain a better view of this multiplexing scheme works and indeed produces real valued OFDM signals, a simple example is given. Let us assume that square 16-QAM constellation is used for this OFDM system and that the output signals of modulator of $\tilde{N}$ subcarrier are

$$X_0 = (1+j), \ X_1 = (3+j3), \ X_2 = (3-j) \text{ and } X_3 = (3-j3)$$

Then we create $N = 2\tilde{N}$ information symbols

$$X_0' = (1+j0), \ X_1' = (3+j3), \ X_2' = (3-j) \text{ and } X_3' = (3-j3)$$
$$X_4' = (1+j0), \ X_5' = (3+j3), \ X_6' = (3+j) \text{ and } X_7' = (3-j3)$$

The N-point IDFT yields the real-valued sequence

$$x_0 = 7.0711$$
$$x_1 = 0.7071$$
$$x_2 = -5.6568$$
$$x_3 = -0.7071$$
$$x_4 = -1.4142$$
$$x_5 = 0.7071$$
$$x_6 = 2.8284$$
$$x_7 = -0.7071$$

As we can see from the IDFT output, the imaginary parts of the OFDM signal samples are zero. This verifies that the proposed multiplexing yields real signals.

6.3. COMPLEX–SIGNAL OFDM

In this chapter, the complex-signal OFDM approach is used for OFDM simulations. Mathematically, each carrier of the OFDM can be described as a complex wave:

$$s_c(t) = A_c(t)e^{j[\omega_c t + \phi_c(t)]}$$

The real signal is the real part of $s_c(t)$. Both $A_c(t)$ and $\phi_c(t)$, the amplitude and phase of the carrier, can vary on a symbol by symbol basis.

In OFDM we have many carriers. Thus the complex signal $s_s(t)$ is represented by

$$s_s(t) = \frac{1}{N} \sum_{n=0}^{N-1} A_n(t)e^{j[\omega_n t + \phi_n(t)]}$$

where

$$\omega_n = \omega_0 + n\Delta\omega$$

This is of course a continuous signal. If we consider the waveforms of each component of the signal over one symbol period, the variables $A_c(t)$ and $\phi_c(t)$ take on fixed values which depend on the frequency of that particular carrier, and so can be rewritten

$$\phi_c(t) = \phi_n$$
$$A_c(t) = A_n$$

135

If the signal is sampled using a sampling frequency of $1/\Delta t$, then the resulting signal is represented by

$$s_s(k\Delta t) = \frac{1}{N} \sum_{n=0}^{N-1} A_n e^{j\left[(\omega_0 + n\Delta\omega)k\Delta t + \phi_n\right]}$$ 6.1

Here, we have restricted the time over which we analyse the signal to N samples. It is convenient to sample over the period of one data symbol. Thus we have a relationship

$$T = N\Delta t$$

If we now simplify Equation 6.1 without loss of generality by letting $\omega_0 = 0$, then the signal becomes

$$s_s(k\Delta t) = \frac{1}{N} \sum_{n=0}^{N-1} A_n e^{j\phi_n} e^{j(n\Delta\omega)k\Delta t}$$ 6.2

Now, Equation 6.2 can be compared with the general form of the inverse Fourier transform

$$g(k\Delta t) = \frac{1}{N} \sum_{n=0}^{N-1} G\left(\frac{n}{N\Delta t}\right) e^{j2\pi nk/N}$$ 6.3

In Equation 6.2, the function $A_n e^{j\phi_n}$ is no more than a definition of the signal in the sampled frequency domain, and $s(k\Delta t)$ is the time domain representation. Equations 6.2 and 6.3 are equivalent if

$$F = \frac{1}{N\Delta t} = \frac{1}{T}$$

This is the same condition that was required for orthogonality. Thus, one consequence of maintaining orthogonality is that the OFDM signal can be defined by using Fourier transform procedures.

The receiver acts as a bank of demodulators, translating each carrier down to DC, the resulting signal then being integrated over a symbol period to recover the raw data. If the other carriers all beat down to frequencies which, in the time domain, have a whole number of cycles in the symbol period (T), then the integration process results in zero contribution from all these other carriers. Thus the carriers are linearly independent (i.e. orthogonal) if the carrier spacing is a multiple of $1/T$.

136

As previously mentioned, complex-signal OFDM has been used here for OFDM simulations. Figure 6.4 shows the error performance of OFDM transmission using 8-PSK modulation which is compared with that of single-carrier transmission using 8-PSK modulation over the Gaussian channel. It is seen that single-carrier and OFDM transmission have the same error performance.
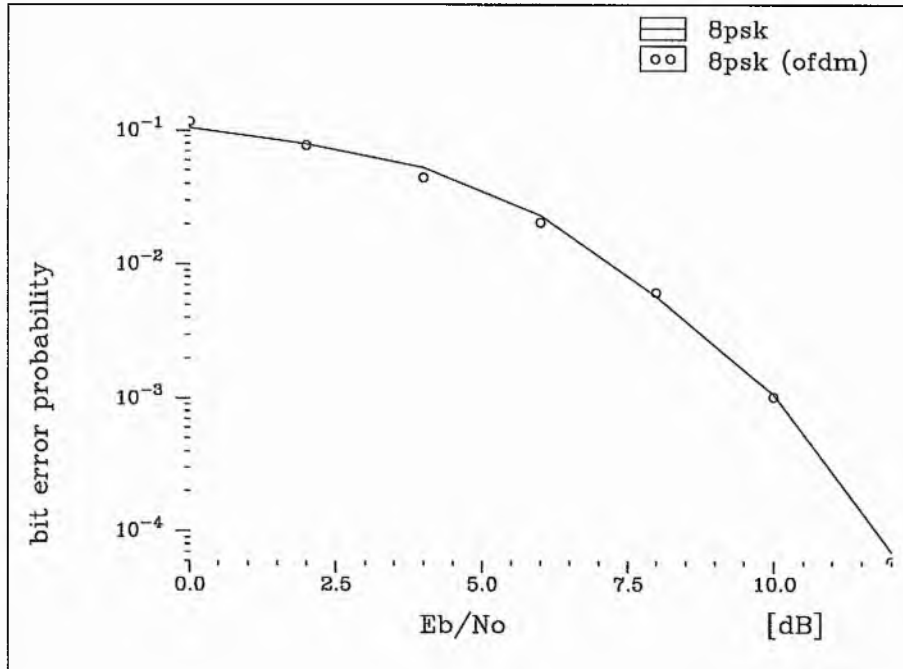
Figure 6.4 The error performance of OFDM transmission compared with that of single-carrier transmission over the Gaussian channel

Figure 6.5 shows the error performance of OFDM transmission using QPSK modulation which is compared with that of single carrier transmission using QPSK modulation over a Rayleigh fading channel. It is also seen that single-carrier and OFDM transmission have the same error performance over a non-selective Rayleigh fading channel. These results confirm that we can use OFDM transmission instead of single-carrier transmission without affecting the error performance.
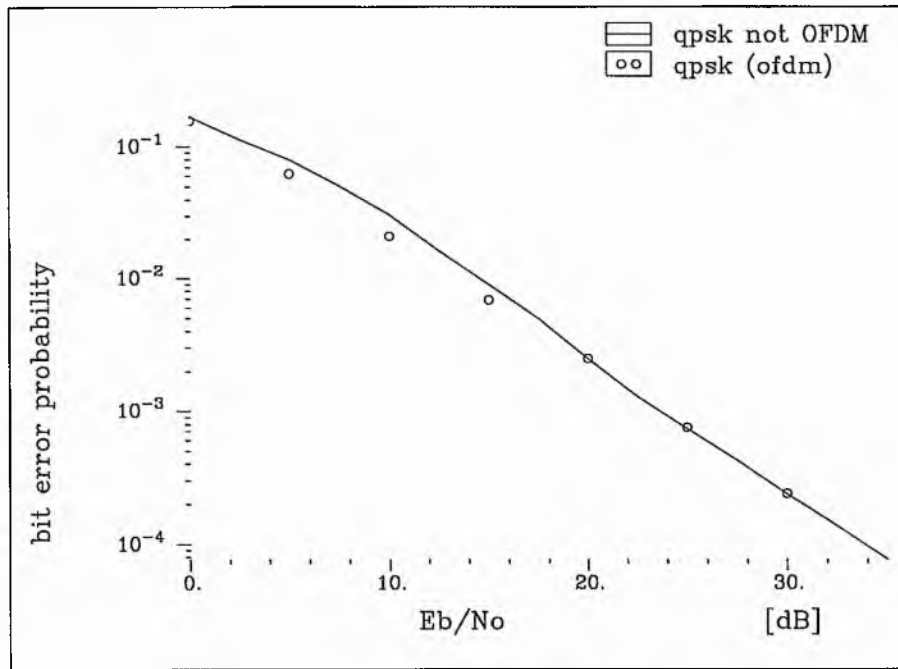
Figure 6.5 The error performance of OFDM transmission compared with that of single-carrier transmission over a Rayleigh fading channel
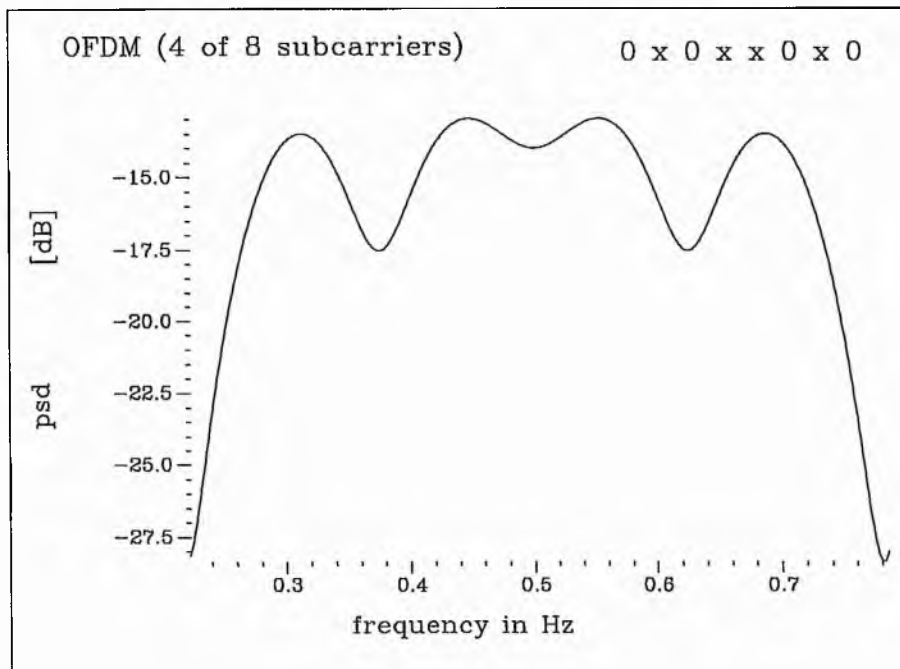
Figure 6.6 Power spectral density of OFDM signals in which 4 out of 8 carriers are used

138

Figure 6.6 shows the power spectral density (PSD) of OFDM signals with 8 carriers in which only 4 carriers are used, and Figure 6.7 shows the PSD of OFDM signals with 8 carriers in which all carriers are used. We can see that adjacent channels are overlapped in frequency. In Figure 6.7 the PSD curve is flat because all carriers are used but in Figure 6.6, we can see that there are empty spaces in frequency because not all carriers available are used.
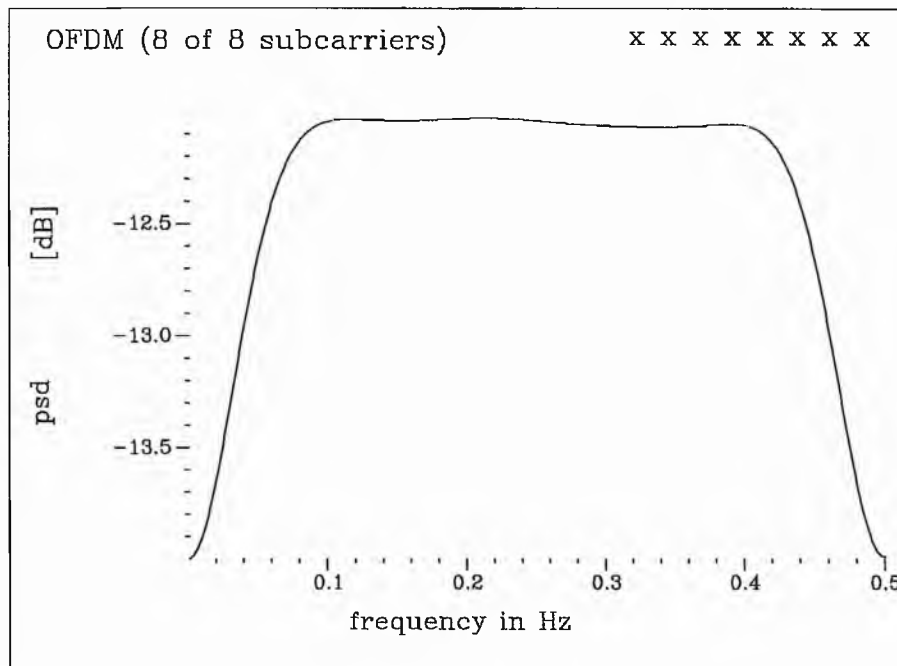
Figure 6.7 Power spectral density of OFDM signals with 8 carriers

Here, we consider that the FFT in the receiver is performing conventional demodulation of each of the carriers followed by a baseband matched filter, which is implemented as an integrate-and-dump. The frequency separation, $1/T$, of the carriers is such that, if the rectangular pulses are not distorted the baseband signals are orthogonal. The problem, therefore, is to maintain or restore this orthogonality if the channel distorts the pulses.

The theoretically ideal multicarrier system would use an infinitesimally small frequency spacing between carriers and, consequently, an infinite-length symbol. It would be immune to distortion because the (finite) length of the impulse response of the channel (the transient at the beginning of each set of data symbols) would be negligible compared to the length of the symbol over which the integration is performed. Most systems,

however, have a maximum tolerable delay from data input to output (latency), and since the end-to-end delay through a multicarrier transceiver is typically three symbols, this defines a maximum symbol length.

If, as is usual, the duration of the impulse response of the channel is not negligible compared to the permissible symbol duration, there are three fairly straightforward ways of avoiding ISI (interference between successive symbols modulated onto the same carrier) [Chow *et al.*, 1993]:

1. Fully equalise the channel with a conventional adaptive tapped delay line; this has the disadvantage that the amount of computation may be too great for programmable DSP implementation at high data rates.

2. Use a symbol (baseband pulse) length, T', that is greater than T, and perform the integration (i.e., collect samples for the FFT) over only the latter T of each symbol, when the transient response of the channel is assumed to have subsided to a negligible level; that is, $T' = (1 + v/N)T$, where N is the FFT length.

   This extending of the baseband pulses can be easily implemented by cyclically prefixing the block of N samples of the output of the IFFT by a repeat of the last v samples. Since these added samples are redundant this reduces the throughput efficiency to $N/(N + v)$.

3. Use a combination of methods 1 and 2: that is, by using a fairly short (i.e., computationally feasible) equaliser to constrain the impulse response of the channel to just $v + 1$ samples, and using a cyclic prefix, guard interval, of v samples.

6.4. OFDM APPLICATIONS

OFDM schemes have been proposed for many different types of digital communication systems. The OFDM applications to Digital Audio Broadcasting and to Asymmetric Digital Subscriber Line will be briefly discussed below.

6.4.1. The Application of OFDM to Digital Audio Broadcasting

Digital Audio Broadcasting (DAB) offers the potential to give every radio in Europe the sound quality of a compact disc and is seen by many as the logical progression in sound

transmission for the next century. Eureka DAB - the European version of digital audio broadcasting - is an impressive attempt at tackling the technical shortcomings of present day FM radio broadcasts. The process used by Eureka DAB to send data over the radio transmission path is known as coded OFDM.

Let us use the DAB system as an example of an OFDM system and consider the choice of parameters. First there is the question of what bandwidth to use for the OFDM system. The wider the bandwidth, the more likely that the system exceeds the correlation bandwidth of the channel. Short delay echoes are the main problem to overcome, and as these are always present, there is no hard bound. The narrower the bandwidth, the more likely it is that the whole signal will be affected. There is a trade-off between bandwidth and transmitter power.

From the experiment in [Shelswell, 1995], a bandwidth of about 7 MHz showed few problems. At a bandwidth of 1.5-2 MHz, there is a degradation equivalent to about 1 dB in performance. If the bandwidth is reduce to the 200 KHz used for FM sound, then the margin required would be an additional 6 dB or so. Thus a figure of about 1.5 MHz for the bandwidth of the system is a good compromise for the type of propagation conditions that apply to mobile and portable radio reception.

One of the parameters that is directly affected by the bandwidth is the available bit-rate. The modulation system on each carrier is QPSK. The carriers are separated in frequency by about the inverse of their symbol period. Thus the maximum bit-rate available is 2 bit sec^{-1} Hz^{-1} of bandwidth. This figure is reduced by the inefficiency of the guard interval, the null symbol and the error coding; in the DAB system the main channel code is a convolutional code, with a Viterbi decoder. For DAB, this brings the useful bit-rate down to about 1 bit sec^{-1} Hz^{-1} of bandwidth. Thus a DAB system will provide just under 1.5 Mbit sec^{-1} of useful data. This is considerably more than the 256 Kbit sec^{-1} that is needed for a high-quality stereophonic programme, so the implication is that several broadcast programmes will share the same multiplex.

For differential demodulation to work properly, the multipath environment must change slowly from symbol to symbol. Thus there is a limit to the symbol period and hence the number of carriers. For mobile reception, the motion of the vehicle leads to changes in multipath environment. Over a symbol period, a vehicle moving at v m sec^{-1} will travel $vT \times f/c$ wavelengths. This is $f_d T$ wavelengths, where f_d is the maximum Doppler shift. To produce negligible phase distortion, the function $f_d T$ must be small. A figure of $f_d T < 0.02$ has been proposed as suitable for general use. The Eureka 147 system has

141

been specified so that reception is not significantly impaired unless vehicles are travelling in excess of 100 mph.

To minimise the power loss by this mechanism, it is desirable to keep the guard interval to as low a percentage as possible of the symbol period. In practice a guard interval of the order of 25% of the symbol period has been found to be a good compromise. This lead to a symbol period of 1 ms and hence to a carrier spacing of about 1 KHz. Thus about 1500 carriers are accommodated in the minimum bandwidth desirable for one OFDM transmission. Within the multiplex we are achieving about one programme per 250 KHz of bandwidth

For DAB, the number of carriers defined is 1536 (not 1500) because the FFT works most effectively if the number of samples is a power of 2. Now, however, technology has advanced to the point where higher order FFTs are being proposed for digital television applications.

6.4.2. The Application of OFDM to Asymmetric Digital Subscriber Line (ADSL)

ADSLs are used to deliver high-rate digital data over existing ordinary phone-lines. An OFDM system allows the transmission of high speed data. ADSL facilitates the simultaneous use of normal telephone services, ISDN, and high speed data transmission, e.g., video. OFDM-based ADSL can be seen as the transition from existing copper-lines to the future fibre-cables. This makes ADSL economically interesting for the local telephone companies. They can offer customers high speed data speed data services even before switching to fibre-optics.

The excellent high-performance/cost tradeoff of multitone modulation also makes it a strong candidate for the transceiver implementation for high-bit-rate digital data transmission, a 1.6 Mbit sec^{-1} digital subscriber service on twisted-pair channels of up to two miles. [Chow, 1991] generally found that, even on worst-case channels, a 1.6 Mbit sec^{-1} (1.536 Mbit sec^{-1} user data plus 64 kbit sec^{-1} control channel) data rate is achievable at an error rate of 10^{-7} on a single twisted pair.

6.5. LOW PEAK-TO-MEAN ENVELOPE POWER RATIO OFDM

OFDM system have advantages for signalling at high data rates over time dispersive channels. However, the main disadvantage of OFDM systems is that they have high Peak-to-Mean Envelope Power Ratio (PMEPR). This leads to non-linear effects in the RF amplification stages which will give rise to intermodulation products that may interfere with signals in adjacent bands on wireless communications.

The complex envelope of an OFDM signal at $t = k\Delta t$ is given by

$$y(k\Delta t) = \frac{1}{\sqrt{N}} \sum_{n=0}^{N-1} x_{o,n} e^{j2\pi nk/N} \qquad\qquad 6.4$$

where $x_{o,n}$ is a complex symbol in frame o and N is the number of carriers. where $1/\sqrt{N}$ is a scale factor which normalises the envelope power in the individual carriers of MPSK-OFDM to 1 W. The composite envelope of the OFDM signal is given by

$$r(k\Delta t) = \sqrt{y(k\Delta t) y^*(k\Delta t)} \qquad\qquad 6.5$$

where $(\cdot)^*$ denotes complex conjugate. From Equation 6.5, the PMEPR is defined by

$$\text{PMEPR} = \frac{\max(r)^2}{\frac{1}{u}\sum_{k=0}^{u} r^2(k)}$$

where u is the maximum number of samples performed in the calculation, and $\max(r)$ selects the largest value corresponding to the peak voltage in the sampled composite envelope vector.

When N signals in MPSK-OFDM are added with the same phase, they produce the maximum Peak Envelope Power (PEP) which is N^2 W. For example, if 4 input signals of IDFT are all $1 + j0$ the output signals will be:

IDFT Input	IDFT Output
$1 + j0$	$2 + j0$
$1 + j0$	$0 + j0$
$1 + j0$	$0 + j0$
$1 + j0$	$0 + j0$

which produces PEP of $2^2 = 4$ W. The envelope power in the individual carriers is normalised to 1 W, thus the PMEPR is 6.02 dB. If 8 input signals of the IDFT are all $1 + j0$ the output signals will be:

IDFT Input	IDFT Output
$1 + j0$	$\sqrt{8} + j0$
$1 + j0$	$0 + j0$
$1 + j0$	$0 + j0$
$1 + j0$	$0 + j0$
$1 + j0$	$0 + j0$
$1 + j0$	$0 + j0$
$1 + j0$	$0 + j0$
$1 + j0$	$0 + j0$

which produces PEP of $\left(\sqrt{8}\right)^2 = 8$ W. Thus, the PMEPR is 9.03 dB. In the second example, the length of the DFT is doubled, which increases the PMEPR by 3.01 dB. Usually the FFT length used in the applications is large; this produces high PMEPR which leads to non-linear effects. There is clearly a necessity to limit the PMEPR of OFDM signals.

6.5.1. Coding for Minimising the PMEPR

Much work has been done on design of schemes for reducing the PMEPR of OFDM systems: [O'Neil & Lopes, 1994] and [O'Neil & Lopes, 1995] proposed a method which is amplitude limiting the OFDM signals at the point of generation. In [Jones et al. 1994], [Wilkinson & Jones, 1995], [Van Eetvelt et al., 1995] and [Jones & Wilkinson, 1996], block coding schemes are proposed with various code rates for reducing the PMEPR of

MPSK-OFDM. [Friese, 1996] proposed a scheme which results in a PMEPR of < 3.3 dB for the case of a 32 carrier OFDM using 2-DPSK (differential phase shift keying) by adding 16-carrier redundancy. [Boyd, 1986] and [Popovic, 1991] investigated the possibility of using Golay complementary sequences for reducing the PMEPR of BPSK-OFDM. Subsequently, [Van Nee, 1996] proposed multiphase complementary codes for reducing the PMEPR and error correction of MPSK-OFDM. He produced a PMEPR of 3 dB for the case of 8-carrier 8-PSK OFDM with code rate of 1/2.

6.5.2. Complementary Codes for Reducing PMEPR MPSK and QAM OFDM

The main case of interest here is using multiphase complementary code pairs of length 2 which can be used to reduce the PMEPR of MPSK and QAM OFDM. The complementary sequences have specific autocorrelation properties so that after an IDFT the transmitted power is affected. The resulting transmissions are unlike anything that could be produced from the original data without the codes, and various authors [Boyd, 1986], [Popovic, 1991] and [Van Nee, 1996], have identified complementary sequences as a candidate approach to reducing PMEPR in OFDM. Complementary sequences are pairs of sequences for which the sum of autocorrelation functions is zero except for the main peak at zero shift.

Let $[S_{N+1}]$ be a discrete phase-coded sequence of length $N + 1$, consisting of complex number with unit modulus and arbitrary phases as elements:

$$[S_{N+1}] = [s_0, s_1, \cdots, s_N].$$ 6.6

The n-th element as a function of time is given by

$$s_n = A(t - n\tau_s)e^{j(\omega_0 t + \Phi_n)}$$ 6.7

where τ_s is elemental time duration,

$$A(t) = \begin{cases} 1, & \text{for } t_s \geq t \geq 0 \\ 0, & \text{otherwise,} \end{cases}$$

and $\Phi_n = \sum\limits_{p=0}^{n} \phi_p$.

The complex autocorrelation function of $[S_{N+1}]$ is given by

$$\chi(\tau) = \sum_{n=0}^{N+1-\tau} s_n \cdot s_{n+\tau}^* \qquad \tau \geq 0 \qquad\qquad 6.8$$

Let $[C_{N+1}]$ be second sequence similar to $[S_{N+1}]$ such that

$$[C_{N+1}] = [c_0, c_1, \cdots, c_N] \qquad\qquad 6.9$$

and

$$c_n = A(t - n\tau_s)e^{j(\omega_0 t + \Theta_n)}, \qquad \Theta_n = \sum_{p=0}^{n} \theta_p. \qquad\qquad 6.10$$

The autocorrelation function of $[C_{N+1}]$ is

$$\psi(\tau) = \sum_{n=0}^{N+1-\tau} c_n \cdot c_{n+\tau}^* \qquad \tau \geq 0. \qquad\qquad 6.11$$

The sequences $[S_{N+1}]$ and $[C_{N+1}]$ are termed *complementary* if

$$\chi(\tau) + \psi(\tau) = \begin{cases} 0, & \text{for all } \tau > 0 \\ 2(N+1), & \text{for } \tau = 0 \end{cases} \qquad\qquad 6.12$$

If $N=1$ the length will be 2. From Equations 6.6 and 6.7

$$[S_{N+1}] = \left[e^{j\phi_0}, e^{j(\phi_0 + \phi_1)}\right]$$

and from Equations 6.9 and 6.10

$$[C_{N+1}] = \left[e^{j\theta_0}, e^{j(\theta_0 + \theta_1)}\right].$$

$[S_{N+1}]$ gives the autocorrelation of $\chi(\tau) = \left[e^{-j\phi_1} \right]$ and $[C_{N+1}]$ gives the autocorrelation of $\psi(\tau) = \left[e^{-j\theta_1} \right]$.

From Equation 6.12, $e^{j\phi_1} + e^{j\theta_1} = 0$, and thus $\theta_1 = (\phi_1 + l\pi)$, where l is an odd integer. Hence

$$[S_2] = \left[e^{j\phi_0}, e^{j(\phi_0 + \phi_1)} \right] \qquad [C_2] = \left[e^{j\theta_0}, e^{j(\theta_0 + \phi_1 + l\pi)} \right]$$

Here s_0, s_1, c_0, c_1 are complex valued to represent MPSK signal points. We choose $\phi_0 = \theta_0$

$$[C_2] = [c_0, c_1] = [s_0, -s_1]$$

where $[S_2]$ and $[C_2]$ are information and redundancy symbol sequences respectively. The matrix representation of this complementary sequence scheme is

$$\begin{bmatrix} S_2 \\ C_2 \end{bmatrix} = \begin{bmatrix} s_0 \\ s_1 \\ c_0 \\ c_1 \end{bmatrix} = \begin{bmatrix} 1 & 0 \\ 0 & 1 \\ 1 & 0 \\ 0 & -1 \end{bmatrix} \begin{bmatrix} s_0 \\ s_1 \end{bmatrix}$$

These sequences are then fed to an Inverse DFT (IDFT) to produce OFDM signals

$$y_n = \frac{1}{\sqrt{N}} \sum_{k=0}^{N-1} X_k e^{j2\pi kn/N}, \qquad N = 4; n = 0, 1, 2, 3 ; k = 0, 1, 2, 3$$

where X_k and y_n are input and output sequences of an IDFT respectively. Here, the input sequence of an IDFT is the complementary sequence explained above

$$[X_0, X_1, X_2, X_3] = [s_0, s_1, c_0, c_1]$$

The matrix representation of an IDFT output sequence is:

$$\begin{bmatrix} y_0 \\ y_1 \\ y_2 \\ y_3 \end{bmatrix} = \frac{1}{2} \begin{bmatrix} 1 & 1 & 1 & 1 \\ 1 & e^{j\frac{\pi}{2}} & e^{j\pi} & e^{j\frac{3}{2}\pi} \\ 1 & e^{j\pi} & e^{j2\pi} & e^{j\pi} \\ 1 & e^{j\frac{3}{2}\pi} & e^{j\pi} & e^{j\frac{\pi}{2}} \end{bmatrix} \begin{bmatrix} 1 & 0 \\ 0 & 1 \\ 1 & 0 \\ 0 & -1 \end{bmatrix} \begin{bmatrix} s_0 \\ s_1 \end{bmatrix}$$

$$= \begin{bmatrix} 1 & 0 \\ 0 & e^{j\frac{\pi}{2}} \\ 1 & 0 \\ 0 & -e^{j\frac{\pi}{2}} \end{bmatrix} \begin{bmatrix} s_0 \\ s_1 \end{bmatrix}$$

$$\qquad\qquad 6.13$$

$$= \begin{bmatrix} s_0 \\ e^{j\frac{\pi}{2}}s_1 \\ s_0 \\ -e^{j\frac{\pi}{2}}s_1 \end{bmatrix} = \begin{bmatrix} s_0 \\ js_1 \\ s_0 \\ -js_1 \end{bmatrix}$$

The matrix in Equation 6.13 shows the relation between an input sequence of a complementary code encoder, $[s_0, s_1]$, and an output sequence of IDFT, $[y_0, y_1, y_2, y_3]$. It can be seen that the IDFT output sequence is an MPSK complementary sequence. Therefore, the PMEPR of the OFDM signals is equal to 0 dB.

The IDFT output has a characteristic that $y_0 = y_2$ and $y_1 = -y_3$. Thus, we can transmit just y_0 and y_1

$$\begin{bmatrix} y_0 \\ y_1 \end{bmatrix} = \begin{bmatrix} s_0 \\ e^{j\frac{\pi}{2}}s_1 \end{bmatrix} = \begin{bmatrix} s_0 \\ js_1 \end{bmatrix} \qquad\qquad 6.14.$$

This results in an OFDM system of low PMEPR without redundancy. This transmission method does not affect the OFDM PMEPR because the OFDM signals are still MPSK signal sequences.

Equations 6.13 and 6.14 can be used not only with MPSK, but also with QAM signal sets. If the input sequence of a complementary code encoder in Equation 6.13 is a QAM signal-point sequence, $s_0, s_1 \in \{\text{QAM signal points}\}$, the IDFT output sequence will be $[s_0, js_1, s_0, -js_1]$ which results in $y_0, y_1, y_2, y_3 \in \{\text{QAM signal points}\}$. Therefore, Equations 6.13 and 6.14 can be used with QAM signal sets.

It can be seen that the IDFT output sequence is a QAM complementary sequence. Therefore, the PMEPR of OFDM with a square 16-QAM signal set (in Figure 6.8) applying complementary code pairs of length 2 can be calculated as the PMEPR of square 16-QAM.

Here, we assume that every signal point of the 16-QAM signal set (in Figure 6.8) has the same probability to be transmitted. Therefore, the mean envelope power

$$= \frac{1}{n} \sum_{k=0}^{n-1} r_k r_k^* \qquad , \; r_k \text{ is a complex value of a } n\text{-QAM signal point}$$

$$= \frac{1}{16}\left(4 \times (1+j)(1-j) + 8 \times (1+j3)(1-j3) + 4 \times (3+j3)(3-j3)\right)$$

$$= \frac{1}{16}\left(4 \times 2 + 8 \times 10 + 4 \times 18\right)$$

$$= 10$$

and the peak envelope power (PEP)

$$= \max\left(rr^*\right)$$

$$= 18$$

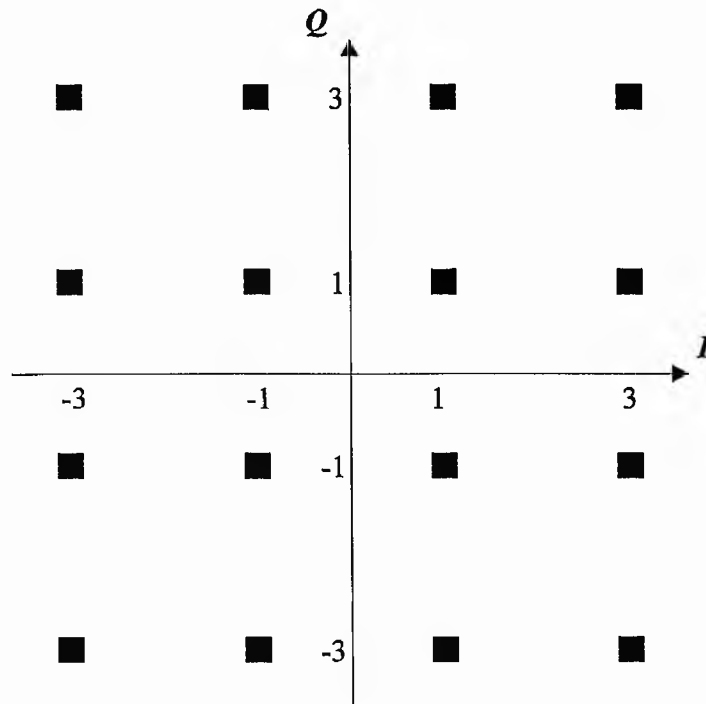This gives the PMEPR of $\frac{18}{10} = 1.8 = 2.55$ dB.

Figure 6.8 A square 16-QAM constellation

6.5.3. Larger Number of Carriers

Equations 6.13 and 6.14 can be extended in the time-domain without loss of orthogonality. If the input of a complementary encoder is $[s_0, s_1]$, the IDFT output will be $[s_0, js_1, s_0, -js_1]$. Then we have another input of a complementary encoder of $[s_0, s_2]$ which give the IDFT output of $[s_0, js_2, s_0, -js_2]$. From those two output sequences we can see that s_0, js_1, s_0 are orthogonal each others and s_0, js_2, s_0 are also orthogonal each others, so we can conclude that the IDFT output signals can be extended become

$$[s_0, js_1, s_0, js_2, s_0, js_3, \cdots]$$ 6.15

without loss of orthogonality. If we have other inputs $[s_2, s_1]$ to a complementary encoder, the IDFT output will be $[s_2, js_1, s_2, -js_1]$. We also can see from the last IDFT output sequence that js_1, s_2 are orthogonal to each other. Therefore, s_0 in Equation 6.15 is not necessarily a constant and the extended IDFT output signals will be

$$[s_0, js_1, s_2, js_3, s_4, js_5, \cdots]$$ 6.16

without loss of orthogonality. A sequence in Equation 6.16 is a combination of several IDFT output sequences of DFT length 4 using complementary code pairs of length 2 in which the last 2 signals of an IDFT output sequence in Equation 6.13 are truncated. In other words, a sequence in Equation 6.16 is a combination of several sequences in Equation 6.14.

This section gives a preliminary investigation into reducing the PMEPR of OFDM systems using complementary code pairs of length 2 in which the IDFT output signals can be extended. There is still work to do in building a complete system for this scheme.

6.6. CONCATENATED REED SOLOMON-REED SOLOMON SCHEMES FOR OFDM SYSTEMS

Here, concatenated schemes with Reed Solomon coded modulation as an inner code and a Reed Solomon code as an outer code are proposed as coding schemes for OFDM systems.

A concatenated scheme is one that uses two levels of coding, an inner code and an outer code, to achieve the desired error performance. Concatenated coding was introduced by [Forney, 1966]. Figure 6.9 illustrates the order of encoding and decoding. The inner code, the one that interfaces with the modulator/demodulator and channel, is usually configured to correct most of the channel errors. The outer code, usually a higher-rate (lower-redundancy) code, then reduces the probability of error to the specified level. The primary reason for using a concatenated scheme is to achieve a low error rate with an overall implementation complexity which is less than that which would be required by a single coding operation. We can see in Figure 6.9 that an interleaver is used between the two coding steps. This is required to spread any error bursts that may appear at the output of the inner coding operation.
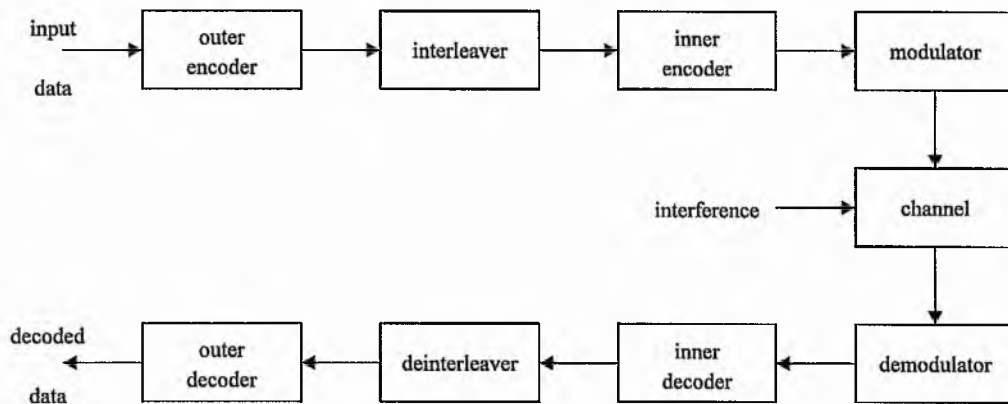
Figure 6.9 Block diagram of a concatenated coding system

One of the most popular concatenated coding systems uses a Viterbi-decoded convolutional inner code and a Reed Solomon outer code, with interleaving between the two coding steps [Odenwalder, 1976]. In this system, the demodulator outputs soft quantised code symbols to the inner convolutional decoder, which in turn outputs hard quantised code symbols with bursty errors to the Reed Solomon decoder (in a Viterbi decoder, the output errors tend to occur in bursts). However, the concatenated system performance is severely degraded by correlated errors among successive symbols. Hence the interleaving between codes needs to take place at the symbol level (not at the bit level).

151

The main case of interest here is using Reed Solomon codes for both inner and outer codes. Reed Solomon coded modulation based on set partitioning and not based on set partitioning schemes are used as an inner code. A high rate Reed Solomon code is used as an outer code which reduces an overall code rate. With small code rate reduction, a concatenated code will have large coding gain over non-concatenated code usually at very low bit error probabilities. Here, we study concatenated code designs using Reed Solomon codes for both inner and outer codes.

A concatenated Reed Solomon-Reed Solomon code system called CIRC [Sklar, 1988] has been used for the *compact disc* (CD) *digital audio system*. These concatenated schemes are used over the channel, which has several sources of errors:

1. Small unwanted particles or air bubbles in the plastic material or pit inaccuracies arising in manufacturing.

2. Fingerprints or scratches during handling. The channel mainly has a burstlike error behavior, since a scratch or fingerprint will cause several consecutive data samples to be in error.

In this application, error control depends mostly on Reed Solomon coding and multiple layers of interleaving. The digital information is protected by adding parity bytes derived from two Reed Solomon encoders. In digital audio applications, an undetected decoding error is very serious since it results in clicks, while occasional detected failures are not so serious because they can be concealed. The CIRC involves both correction and concealment of errors.

6.6.1. Concatenated Schemes for a Rayleigh Fading Channel

In this application, an RS(511, 443) code is used for the outer code. Reed Solomon coded modulation based on set partitioning and not based on set partitioning with configuration codes explained in Chapters 4 and 5 are used as inner codes.

Figure 6.10 shows a block diagram of a concatenated scheme for a Rayleigh fading channel. An RS(511, 443) code is used as an outer code and Reed Solomon coded QPSK modulation based on set partitioning with code length of 31 as an inner code.
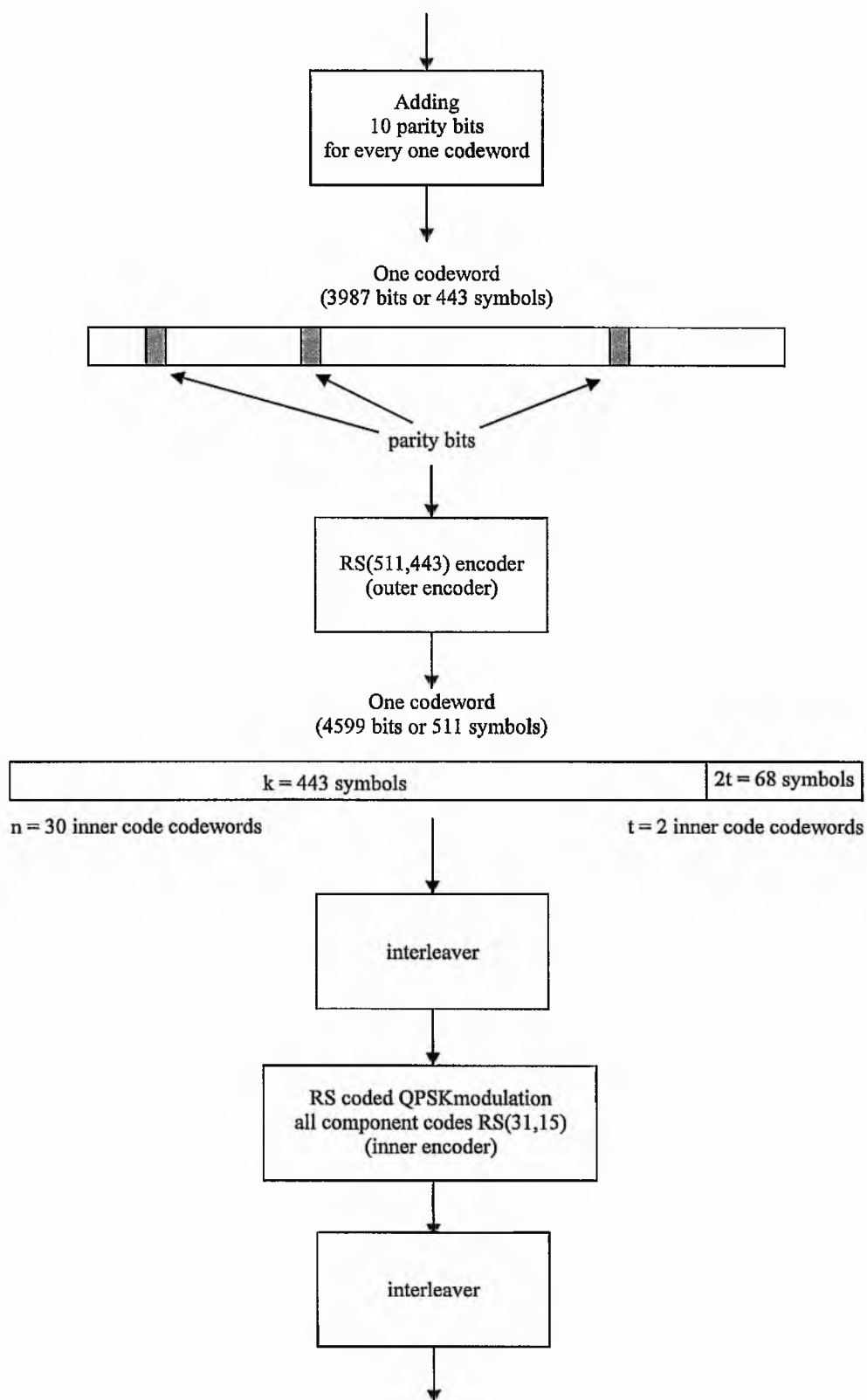
Figure 6.10 Block diagram of concatenated Reed Solomon-Reed Solomon schemes for a Rayleigh fading channel

The inner code has two component codes which are all RS(31, 15) codes. The inner code has information length of 15×2 = 30 symbols or 30×5 = 150 bits (the input length of the inner code). The outer code has information length 433 symbols, or $433 \times 9 = 3897$ bits, and code length 511 symbols, or $511 \times 9 = 4599$ bits. Thus one codeword of the outer code consists of $\lfloor 4599/150 \rfloor = 30$ codewords of the inner code, where $\lfloor c \rfloor$ means the largest integer no greater than c. The outer code can correct

$$\left\lfloor \frac{(n_o - k_o) \cdot v_o \Big/ 2}{n_i \cdot v_i} \right\rfloor = \left\lfloor \frac{(511-443)9 \Big/ 2}{(15 \times 2) \times 5} \right\rfloor = 2 \text{ codewords}$$

of the inner code, where n_o is the code length, k_o the information length, v_o the number of bits in the code symbol of the outer code and n_i is the code length and v_i the number of bits in the code symbol of the inner code. This is the reason why we use an RS(511, 443) code as the outer code. However, the errors appearing at the output of the inner decoding operation are bursty. Hence interleaving between the inner and outer codes is required to spread any error bursts.

In addition, the digital information is protected by adding parity bits at the outer code in order to protect the error performance from undetected decoding errors. If the decoder decodes incorrectly, the decoder can give more errors than those at the decoder input. 10 parity check bits are added to the outer code. Figure 6.11 shows error performances of concatenated schemes, with partitioned Reed Solomon coded 8-PSK modulation as the inner code, using parity bits at the outer code. These are compared with error performances of concatenated schemes not using parity bits at the outer code. At a bit error probability of 10^{-4}, concatenated schemes using parity bits at the outer code are 0.3 − 0.4 dB better than concatenated schemes not using parity bits.

The rate of the outer code is (443×9 − 10)/(511×9) = 0.865 and the rate of the inner code 15/31 = 0.48. This results in an overall code rate of 0.865×15/31 = 0.42. Hence the code rate of partitioned Reed Solomon coded QPSK modulation is reduced from 0.48 to 0.42.
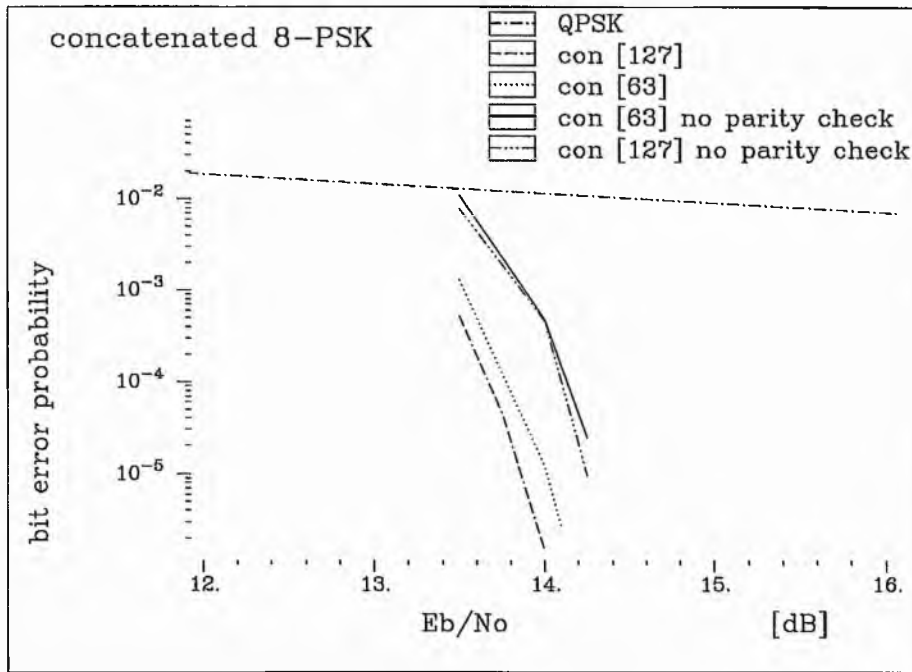
154

Figure 6.11 Error performances of concatenated schemes using parity bits at the outer code with partitioned RS coded 8-PSK modulation as the inner code, **con[n]**, compared with those of concatenated schemes not using parity bits at the outer code, **con[n] no parity check**, over the Rayleigh fading channel

6.6.1.1. Concatenated Schemes with Reed Solomon Coded QPSK modulation

Figure 6.12 shows error performances of concatenated schemes using an RS(511, 443) code as the outer code and partitioned Reed Solomon coded QPSK modulation as the inner code. These are compared with error performances of partitioned Reed Solomon coded QPSK modulation with code length of 63 and 31 over a Rayleigh fading channel.

The first concatenated scheme has, as its inner code, partitioned Reed Solomon coded QPSK modulation with code length of 31. We can see that at a BER of 10^{-5}, the concatenated scheme has 3.75 dB coding gain over the non-concatenated scheme. The second concatenated scheme has, as its inner code, partitioned Reed Solomon coded QPSK modulation with code length of 63 whose component codes are all RS(63, 31). The rate of the inner code is $31/63 = 0.492$ which results in an overall code rate of $0.865\times$ $(31/63) = 0.425$. Hence the code rate of partitioned Reed Solomon coded QPSK

155

modulation is reduced from 0.492 to 0.425. At a BER of 10^{-5}, the concatenated scheme has 2.75 dB coding gain over the non-concatenated scheme.

For a concatenated scheme using, as its inner code, partitioned Reed Solomon coded QPSK modulation with code length of 63, the outer code can correct less than one inner codeword. To have an outer code which can correct more than one inner codeword with the same code rate, the outer code length must be longer than 511. However, the concatenated scheme becomes more complex. If we use an outer code with the code length less than 511 and the code rate of $R_c = \frac{443}{511}$, the error performances of the concatenated schemes will be worse than those of concatenated schemes using an RS(511, 443) code. This is because the error performance of a concatenated scheme is very influenced by the choice of the outer code. Therefore, an RS(511, 443) code is a compromise choice for the outer code. All concatenated schemes used in this thesis have a RS(511, 443) code as the outer code.
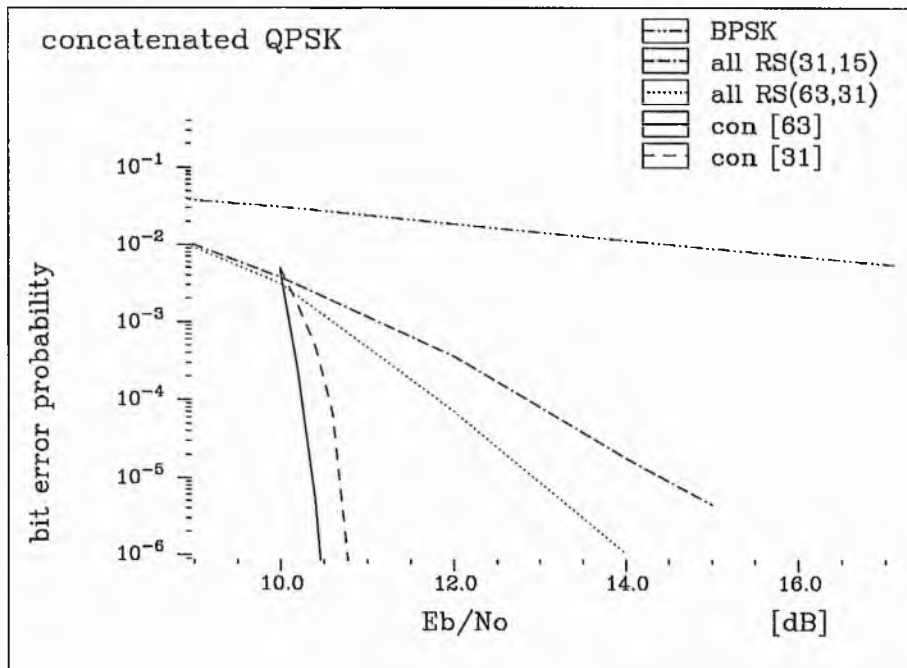
Figure 6.12 Error performances of concatenated schemes with partitioned RS coded QPSK modulation as the inner code, **con[*n*]**, compared with those of partitioned RS coded QPSK modulation, **all RS(*n,k*)**, with code length of 63 and 31 over a Rayleigh fading channel

The curves of BER against E_b/N_0 for concatenated schemes have very sharp cut-off; the BER reduces from $5.0 \cdot 10^{-3}$ to $2.0 \cdot 10^{-7}$ in less than 1 dB E_b/N_0 difference. Thus, concatenated schemes will have large coding gain at a very low BER. At a BER of 10^{-5}- 10^{-6}, a concatenated scheme with an inner code of length 63 has 0.25 dB coding gain over a concatenated scheme with an inner code of length 31.

Figure 6.13 Error performances of concatenated schemes with non-partitioned RS coded QPSK modulation as the inner code, **con(*n,k*)**, compared to those of non-partitioned RS coded QPSK modulation, **RS(*n,k*)**, with code length of 63 and 31 over a Rayleigh fading channel

Figure 6.14 Error performances of all concatenated schemes using Reed Solomon coded QPSK modulation as the inner code with code length of 63 and 31 over a Rayleigh fading channel

Figure 6.13 shows error performances of concatenated schemes with an RS(511, 443) code as the outer code and non-partitioned Reed Solomon coded QPSK modulation as the inner code. These are compared with error performances of non-partitioned Reed Solomon coded QPSK modulation with code length of 63 and 31.

The first concatenated scheme has an inner code for non-partitioned Reed Solomon coded QPSK modulation with an RS(63, 31) code. The rate of the inner code is 31/63 = 0.492 which reduces an overall code rate of 0.865×(31/63) = 0.425. Hence the code rate of non-partitioned Reed Solomon coded QPSK modulation is reduced from 0.492 to 0.425. At a BER of 10^{-5}, the concatenated scheme has 3.5 dB coding gain over the non-concatenated scheme.

The second concatenated scheme has an inner code for non-partitioned Reed Solomon coded QPSK modulation with an RS(31, 15) code. The rate of the inner code is 15/31 = 0.48 which results in an overall code rate of 0.865×(15/31) = 0.42. Hence the code rate of non-partitioned Reed Solomon coded QPSK modulation is reduced from 0.48 to 0.42. At a BER of 10^{-5}, the concatenated scheme has 6 dB coding gain over non-concatenated scheme.

As can be seen from the results in Figure 6.13, the curves of BER against E_b/N_0 for concatenated schemes have very sharp cut-off. At BER of 10^{-5}-10^{-6}, a concatenated scheme with the inner code of length 63 has 0.25 dB coding gain over a concatenated scheme with the inner code of length 31.
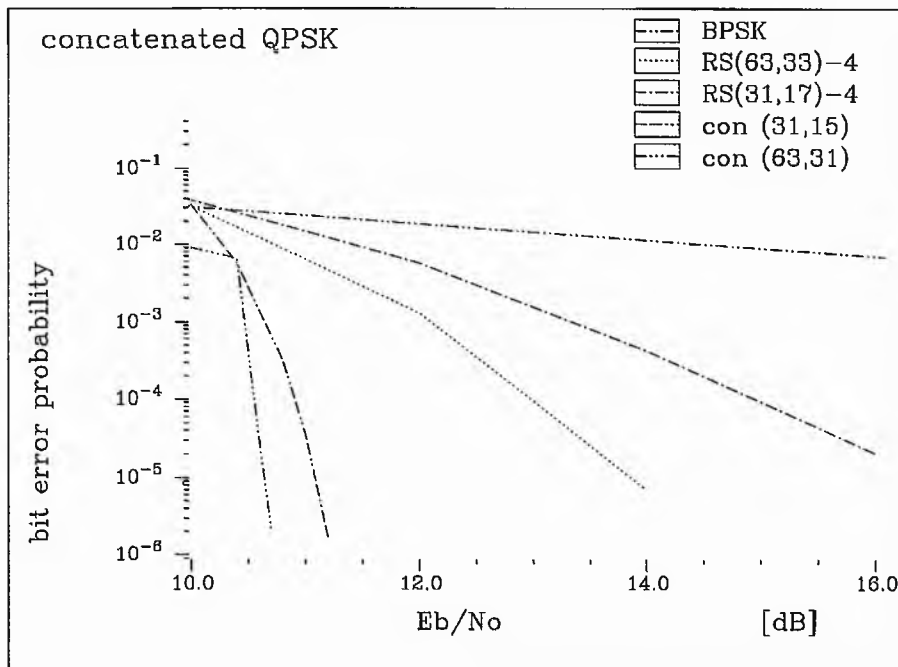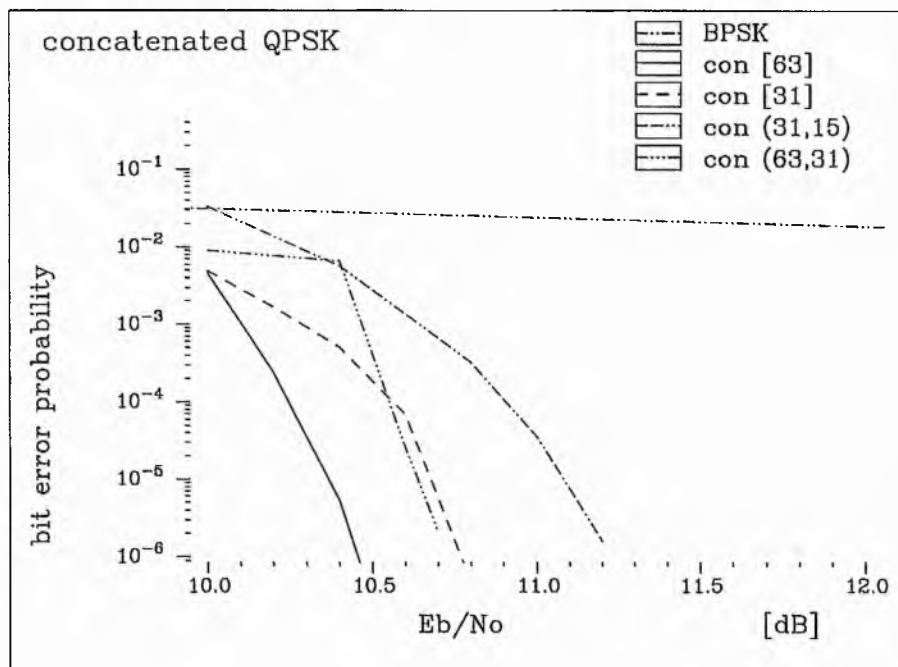
Figure 6.14 shows error performances of concatenated schemes with an RS(511, 443) code as the outer code and Reed Solomon coded QPSK modulation as the inner code with code length of 63 and 31. We can see that at a BER of 10^{-5}-10^{-6}, a concatenated scheme using partitioned Reed Solomon coded QPSK modulation as the inner code has 0.25 dB coding gain over non-partitioned with the same code length. Thus, the performance of concatenated schemes is very influenced by the outer codes.

6.6.1.2. Concatenated Schemes with Reed Solomon Coded 8-PSK modulation

Figure 6.15 shows error performances of concatenated schemes using an RS(511, 443) code as the outer code and partitioned Reed Solomon coded 8-PSK modulation as the

inner code. these are compared with error performances of partitioned Reed Solomon coded 8-PSK modulation with code length of 127 and 63.

For the first concatenated scheme, partitioned Reed Solomon coded 8-PSK modulation whose the component codes are all an RS(127, 85) code is used as an inner code. The rate of the inner code is $85/127 = 0.67$ which reduces an overall code rate of $0.865 \times (85/127) = 0.59$. Hence the code rate of partitioned Reed Solomon coded 8-PSK modulation is reduced from 0.67 to 0.59. At a BER of 10^{-5}, the concatenated scheme has 3 dB coding gain over the non-concatenated scheme.

The second concatenated scheme has, as its inner code, partitioned Reed Solomon coded 8-PSK modulation whose the component codes are all an RS(63, 43) code. The rate of the inner code is $43/63 = 0.68$ which reduces an overall code rate of $0.865 \times (43/63) = 0.59$. Hence the code rate of partitioned Reed Solomon coded 8-PSK modulation is reduced from 0.68 to 0.59. At a BER of 10^{-5}, the concatenated scheme has 4 dB coding gain over the non-concatenated scheme.

The concatenated schemes will give large coding gain over the non-concatenated schemes at a very low BER because curves of BER against E_b/N_0 for concatenated schemes have much sharper cut-off than non-concatenated schemes. At BER of 10^{-5}-10^{-6}, a concatenated scheme with an inner code of length 127 has only less than 0.25 dB coding gain over a concatenated scheme with an inner code of length 85.

Figure 6.16 shows error performances of concatenated schemes using an RS(511, 443) code as the outer code and non-partitioned Reed Solomon coded 8-PSK modulation as the inner code. These are compared with error performances of non-partitioned Reed Solomon coded QPSK modulation with code length of 127 and 63.

The first concatenated scheme has an inner code for non-partitioned Reed Solomon coded 8-PSK modulation with an RS(127, 85) code. The rate of the inner code is $85/127 = 0.67$ which results in an overall code rate of $0.865 \times (85/127) = 0.59$. Hence the code rate of partitioned Reed Solomon coded 8-PSK modulation is reduced from 0.67 to 0.59. At a BER of 10^{-5}, the concatenated scheme has 2.5 dB coding gain over the non-concatenated scheme.

The second concatenated scheme has an inner code for non-partitioned Reed Solomon coded 8-PSK modulation with an RS(63, 43) code. The rate of the inner code is $43/63 = 0.68$ which results in an overall code rate of $0.865 \times (43/63) = 0.59$. Hence the code rate of

159

partitioned Reed Solomon coded 8-PSK modulation is reduced from 0.68 to 0.59. At a BER of 10^{-5}, the concatenated scheme has 3.5 dB coding gain over the non-concatenated scheme.

As can be seen from the results in Figure 6.16, the curves of BER against E_b/N_0 for concatenated schemes have much sharper cut-off than non-concatenated schemes. Thus, the concatenated schemes will have large coding gain over the non-concatenated schemes at a very low BER. At a BER of 10^{-5}, a concatenated scheme with the inner code of length 127 has only 0.25 dB coding gain over a concatenated scheme with the inner code of length 85.

Figure 6.15 Error performances of concatenated schemes with partitioned RS coded 8-PSK modulation as the inner code, con[n], compared with those of partitioned RS coded 8-PSK modulation, all RS(n,k), with code length of 127 and 63 over a Rayleigh fading channel

Figure 6.17 shows error performances of concatenated schemes with an RS(511, 443) code as the outer code and Reed Solomon coded 8-PSK modulation as the inner code with code length of 127 and 63. We can see that at a BER of 10^{-5}, a concatenated scheme using partitioned Reed Solomon coded QPSK modulation as the inner code has less than 1 dB coding gain over non-partitioned with the same code length. Here, we also can see that the performance of concatenated schemes is very influenced by the outer codes.
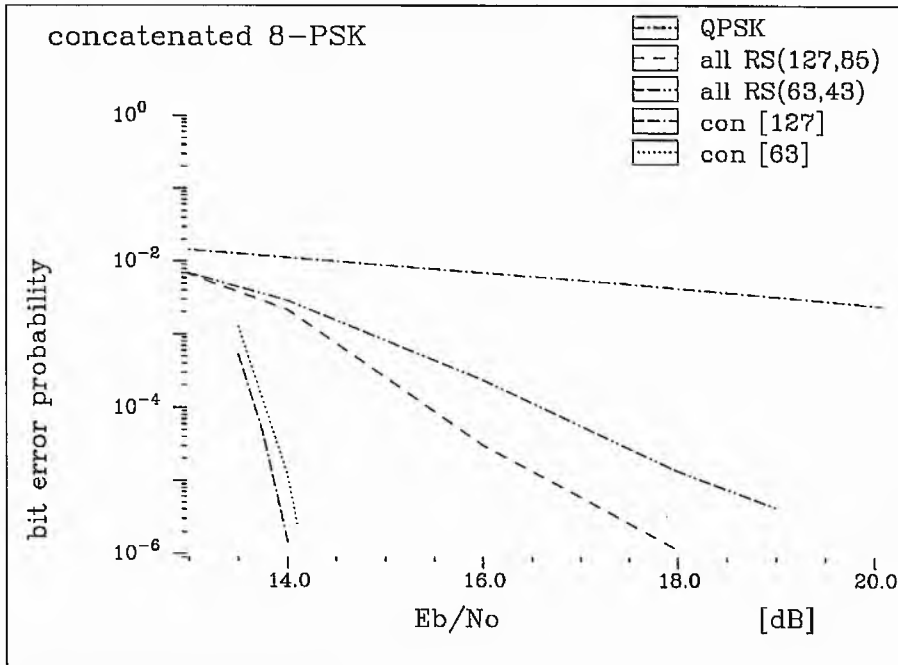
Figure 6.16 Error performances of concatenated schemes with non-partitioned RS coded 8-PSK modulation as the inner code, **con(*n,k*)**, compared to those of non-partitioned RS coded 8-PSK modulation, **RS(*n,k*)**, with code length of 127 and 63 over a Rayleigh fading channel

Figure 6.17 Error performances of all concatenated schemes using Reed Solomon coded 8-PSK modulation as the inner code with code length of 127 and 63 over a Rayleigh fading channel

6.6.2. Concatenated Schemes for the Gaussian Channel

Figure 6.18 shows a block diagram of a concatenated scheme for the Gaussian channel. An RS(511, 443) code is used as an outer code and Reed Solomon coded modulation as an inner code. Here, we did not add parity check bits to the inner-encoder's input. Over the Gaussian channel we do not need the interleaver at the output of the inner code.

Figure 6.18 Block diagram of concatenated Reed Solomon-Reed Solomon schemes for the Gaussian channel

6.6.2.1. Concatenated Schemes with Reed Solomon Coded QPSK modulation

Error performances of concatenated schemes using an RS(511, 443) code as the outer code and partitioned Reed Solomon coded QPSK modulation as the inner code are shown

in Figure 6.19. These are compared with error performances of partitioned Reed Solomon coded QPSK modulation with code length of 63 and 31 over the Gaussian channel.

Partitioned Reed Solomon coded QPSK modulation with code length of 63 is used as an inner code. The component-code configuration of the inner code can be seen in Table 4.2. The rate of the inner code is $(11 + 53)/(2 \times 63) = 0.508$ and the rate of the outer code is $443/511 = 0.873$ which result in an overall code rate of $0.873 \times 0.508 = 0.443$. Hence the code rate of partitioned Reed Solomon coded QPSK modulation is reduced from 0.508 to 0.443. The error performance of the concatenated scheme is better than that of the non-concatenated scheme at BER below $2 \cdot 10^{-4}$.

The second concatenated scheme has, as its inner code, partitioned Reed Solomon coded QPSK modulation with code length of 31. The component-code configuration of the inner code can be seen in Table 4.2. The rate of the inner code is $(7 + 25)/(2 \times 31) = 0.516$ which results in an overall code rate of $0.873 \times 0.516 = 0.45$. Hence the code rate of partitioned Reed Solomon coded QPSK modulation is reduced from 0.516 to 0.45. The error performance of the concatenated scheme is better than that of the non-concatenated scheme at BER below 10^{-3}.
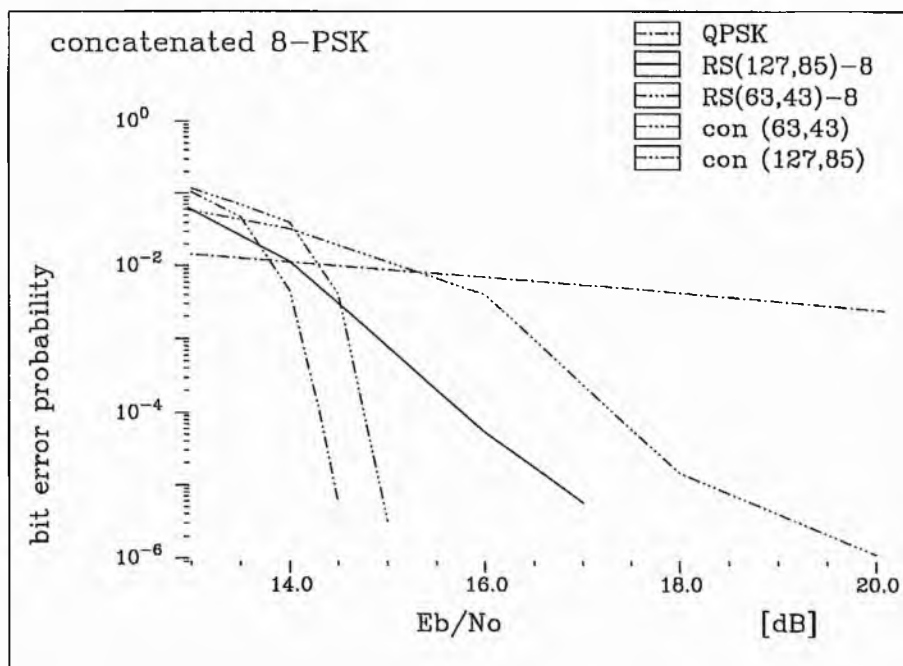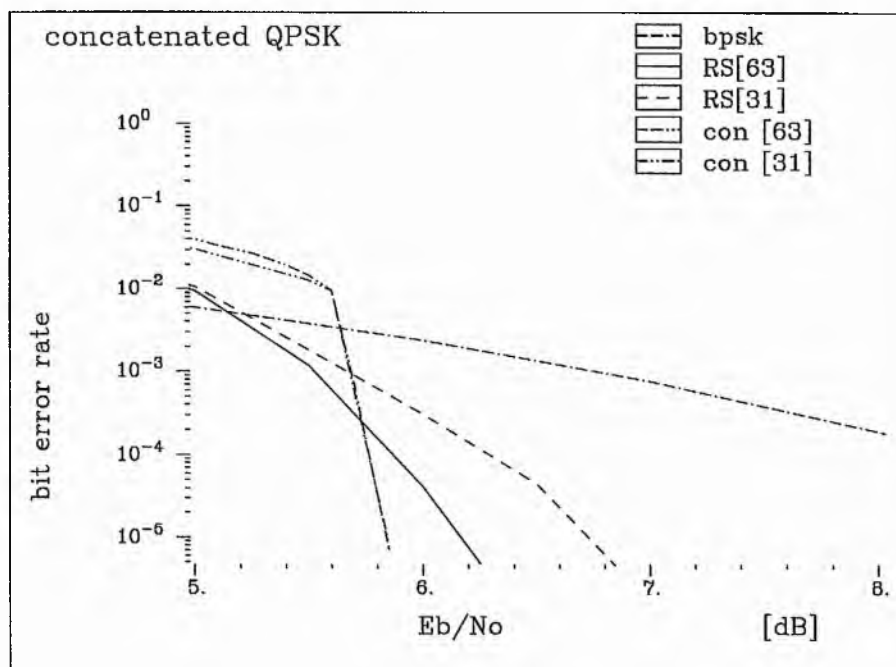

Figure 6.19 Error performances of concatenated schemes with partitioned RS coded QPSK modulation as the inner code, con[n], compared with those of partitioned RS coded QPSK modulation, RS[n], with code length of 63 and 31 over the Gaussian channel
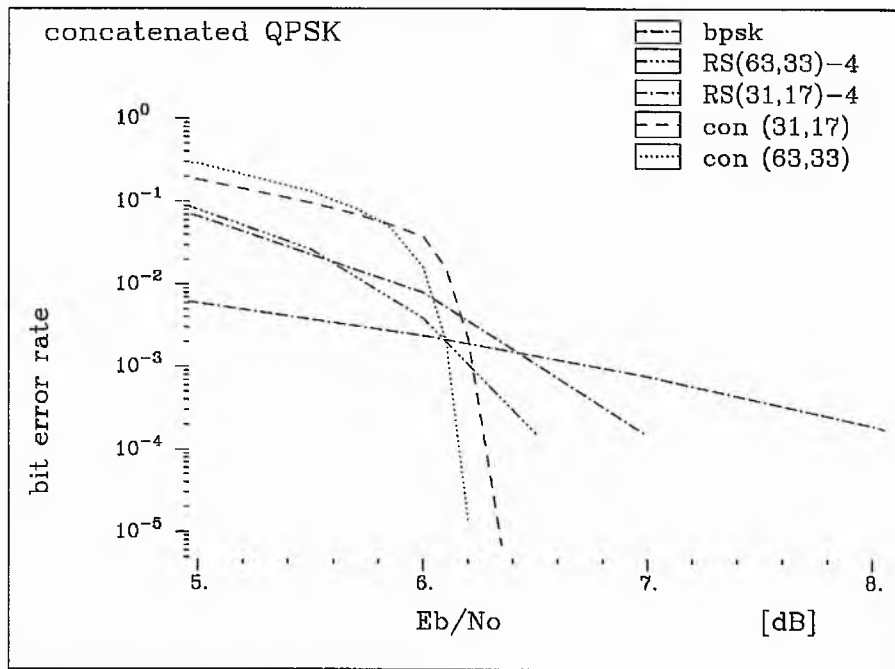
Figure 6.20 Error performances of concatenated schemes with non-partitioned RS coded QPSK modulation as the inner code, **con(*n,k*)**, compared to those of non-partitioned RS coded QPSK modulation, **RS(*n,k*)**, with code length of 63 and 31 over the Gaussian channel
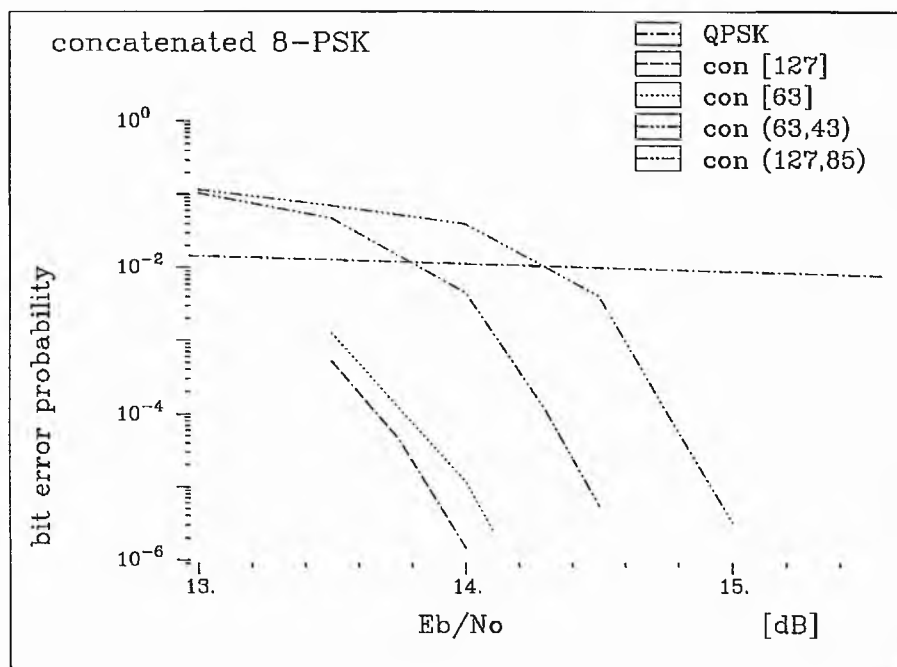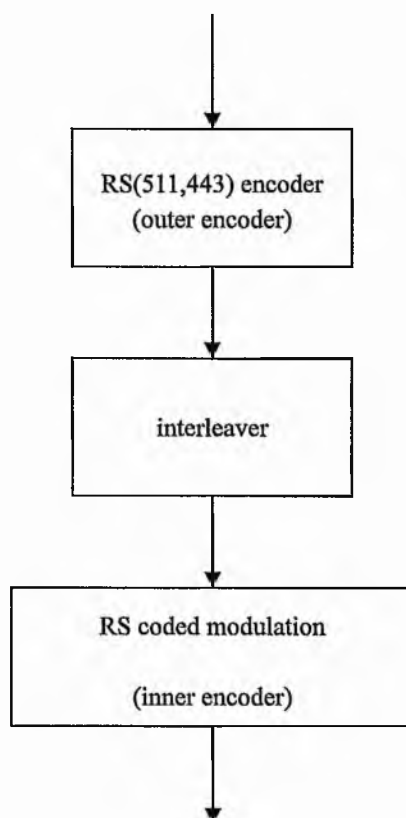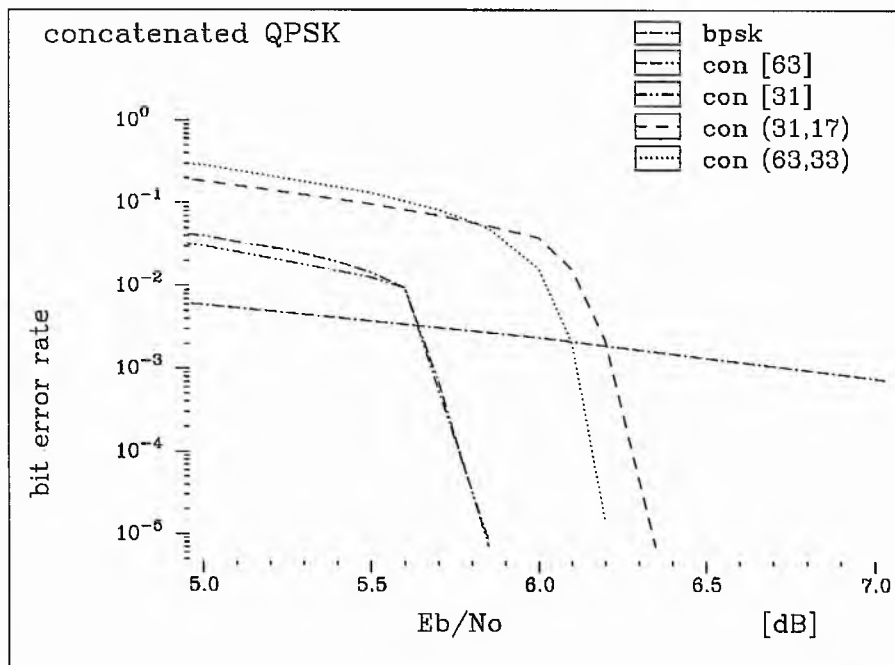

Figure 6.21 Error performances of all concatenated schemes using Reed Solomon coded QPSK modulation as the inner code with code length of 63 and 31 over the Gaussian channel

164

The curves of BER against E_b/N_0 for concatenated schemes have very sharp cut-off, the BER reduces from 10^{-2} to 10^{-5} with an increase of 0.25 dB in E_b/N_0. From these results, we can say that concatenated schemes will have large coding gain over non-concatenated schemes at very low BER. At a BER of 10^{-2}-10^{-5}, a concatenated scheme with the inner code of length 63 has similar error performance to a concatenated scheme with the inner code of length 31. A concatenated scheme with the inner code of length 63 will be better than a concatenated scheme with the inner code of length 31 at very low BER.

Figure 6.20 shows error performances of concatenated schemes using an RS(511, 443) code as the outer code and non-partitioned Reed Solomon coded QPSK modulation as the inner code. These are compared with error performances of non-partitioned Reed Solomon coded QPSK modulation with code length of 63 and 31 over the Gaussian channel.

The first concatenated scheme has an inner code of non-partitioned Reed Solomon coded QPSK modulation with an RS(63, 33) code. The rate of the inner code is 33/63 = 0.52 which results in an overall code rate of 0.873×0.52 = 0.45. Hence the code rate of non-partitioned Reed Solomon coded QPSK modulation is reduced from 0.52 to 0.45. The error performance of a concatenated scheme is better than that of a non-concatenated scheme at BER below $2 \cdot 10^{-3}$.

The second concatenated scheme has an inner code of non-partitioned Reed Solomon coded QPSK modulation with an RS(31, 17) code. The rate of the inner code is 17/31 = 0.55 which results in an overall code rate of 0.873×0.55 = 0.48 Hence the code rate of non-partitioned Reed Solomon coded QPSK modulation is reduced from 0.55 to 0.48. The error performance of the concatenated scheme is better than that of the non-concatenated scheme at BER below $4 \cdot 10^{-3}$.

The concatenated schemes will have large coding gain over the non-concatenated schemes at a very low BER because curves of BER against E_b/N_0 for concatenated schemes have very sharp cut-off, the BER reduces from 10^{-2} to 10^{-5} with an increase of 0.25 dB in E_b/N_0. At a BER of 10^{-2}-10^{-5}, a concatenated scheme with the inner code of length 63 has 0.2 dB coding gain over a concatenated scheme with the inner code of length 31.

Figure 6.21 shows error performances of concatenated schemes with an RS(511, 443) code as the outer code and Reed Solomon coded QPSK modulation as the inner code with

code length of 63 and 31. We can see that at a BER of 10^{-3}-10^{-5}, a concatenated scheme using partitioned Reed Solomon coded QPSK modulation as the inner code has at least 0.4 dB coding gain over that using non-partitioned with the same code length. Here, we also can see that the performance of concatenated schemes is very influenced by the outer codes.

6.6.2.2. Concatenated Schemes with Reed Solomon Coded 8-PSK modulation

Error performances of concatenated schemes using an RS(511, 443) code as the outer code and partitioned Reed Solomon coded 8-PSK modulation as the inner code are shown in Figure 6.22. These are compared to error performances of partitioned Reed Solomon coded 8-PSK modulation with code length of 127 and 63 over the Gaussian channel.

The first concatenated scheme has, as its inner code, partitioned Reed Solomon coded 8-PSK modulation with code length of 127. The component-code configuration of the inner code can be seen in Table 4.1. The rate of the inner code is $(11 + 119 + 125)/(3 \times 127) = 0.67$ which results the overall code rate of $0.873 \times 0.67 = 0.58$. Hence the code rate of partitioned Reed Solomon coded 8-PSK modulation is reduced from 0.67 to 0.58. The error performance of the concatenated scheme is better than that of the non-concatenated scheme at BER below $2 \cdot 10^{-5}$.

The second concatenated scheme has, as its inner code, partitioned Reed Solomon coded 8-PSK modulation with code length of 63. The component-code configuration of the inner code can be seen in Table 4.1. The rate of the inner code is $(7 + 59 + 61)/(3 \times 63) = 0.67$ which results the overall code rate of $0.873 \times 0.67 = 0.58$. Hence the code rate of partitioned Reed Solomon coded 8-PSK modulation is reduced from 0.67 to 0.58. The error performance of the concatenated scheme is better than that of the non-concatenated scheme at BER below $2 \cdot 10^{-4}$.

The curves of BER against E_b/N_0 for concatenated schemes have very sharp cut-off; the BER reduces from 10^{-3} to 10^{-5} in 0.1 dB E_b/N_0 difference. From these results we can see that the concatenated schemes will have large coding gain over the non-concatenated schemes at very low BER. At a BER of 10^{-2}-10^{-5}, a concatenated scheme with the inner code of length 63 is better than a concatenated scheme with the inner code of length 127. Compared to other results, we can say that a concatenated scheme with the inner code of

length 127 will be better than a concatenated scheme with the inner code of length 63 at very low BER.
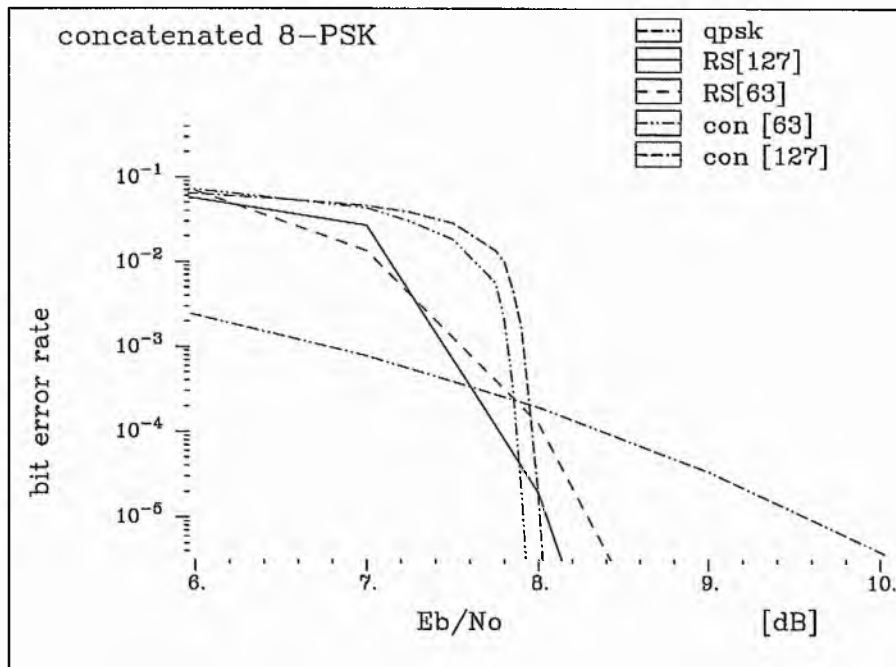
Figure 6.22 Error performances of concatenated schemes with partitioned RS coded 8-PSK modulation as the inner code, **con[n]**, compared with those of partitioned RS coded 8-PSK modulation, **RS[n]**, with code length of 127 and 63 over the Gaussian channel

Figure 6.23 shows error performances of concatenated schemes using an RS(511, 443) code as the outer code and non-partitioned Reed Solomon coded 8-PSK modulation as the inner code. These are compared with error performances of non-partitioned Reed Solomon coded 8-PSK modulation with code length of 127 and 63 over the Gaussian channel.

Non-partitioned Reed Solomon coded 8-PSK modulation with an RS(127, 85) code is used as an inner code. The rate of the inner code is $85/127 = 0.67$ which results in an overall code rate of $0.874 \times 0.67 = 0.58$. Hence the code rate of non-partitioned Reed Solomon coded 8-PSK modulation is reduced from 0.67 to 0.58. The error performance of the concatenated scheme is better than that of the non-concatenated scheme at BER below $4 \cdot 10^{-4}$.

Figure 6.23 Error performances of concatenated schemes with non-partitioned RS coded 8-PSK modulation as the inner code, **con(*n,k*)**, compared to those of non-partitioned RS coded 8-PSK modulation, **RS(*n,k*)**, with code length of 127 and 63 over the Gaussian channel

Figure 6.24 Error performances of all concatenated schemes using Reed Solomon coded 8-PSK modulation as the inner code with code length of 127 and 63 over the Gaussian channel

The second concatenated scheme has an inner code of non-partitioned Reed Solomon coded 8-PSK modulation using an RS(63, 43) code. The rate of the inner code is 43/63 = 0.68 which results the overall code rate of 0.873×0.68 = 0.59. Hence the code rate of non-partitioned Reed Solomon coded 8-PSK modulation is reduced from 0.68 to 0.59. The error performance of the concatenated scheme is better than that of the non-concatenated scheme at BER below $2 \cdot 10^{-3}$.

The curves of BER against E_b/N_0 for concatenated schemes have also very sharp cut-off; the BER reduce from 10^{-2} to 10^{-5} in 0.25 dB E_b/N_0 difference. From these results, we can say that concatenated schemes will have large coding gain over non-concatenated schemes at very low BER. At a BER of 10^{-4}, a concatenated scheme with the inner code of length 127 has 0.2 dB coding gain over a concatenated scheme with the inner code of length 63.
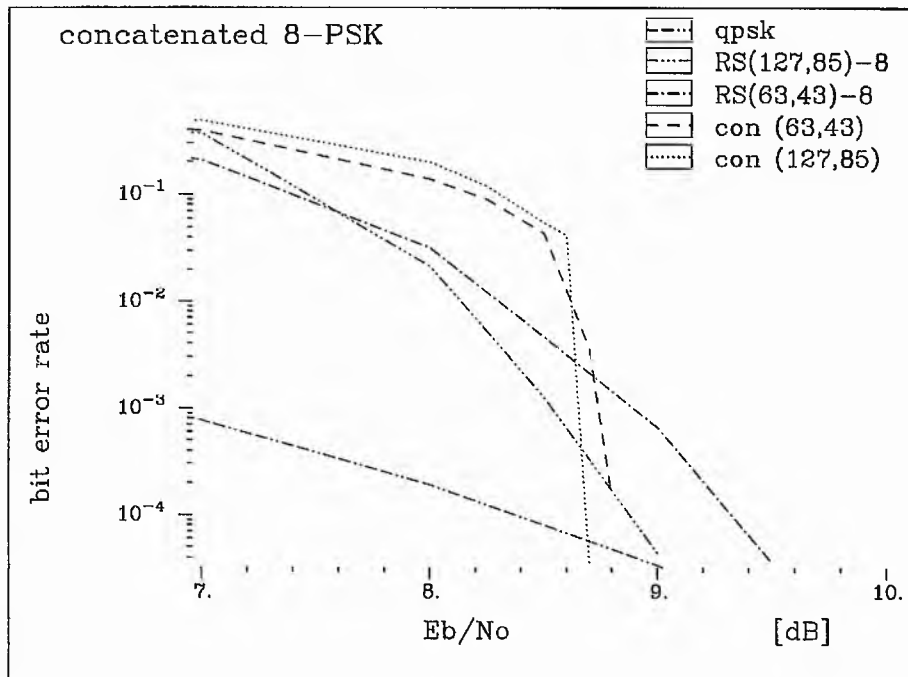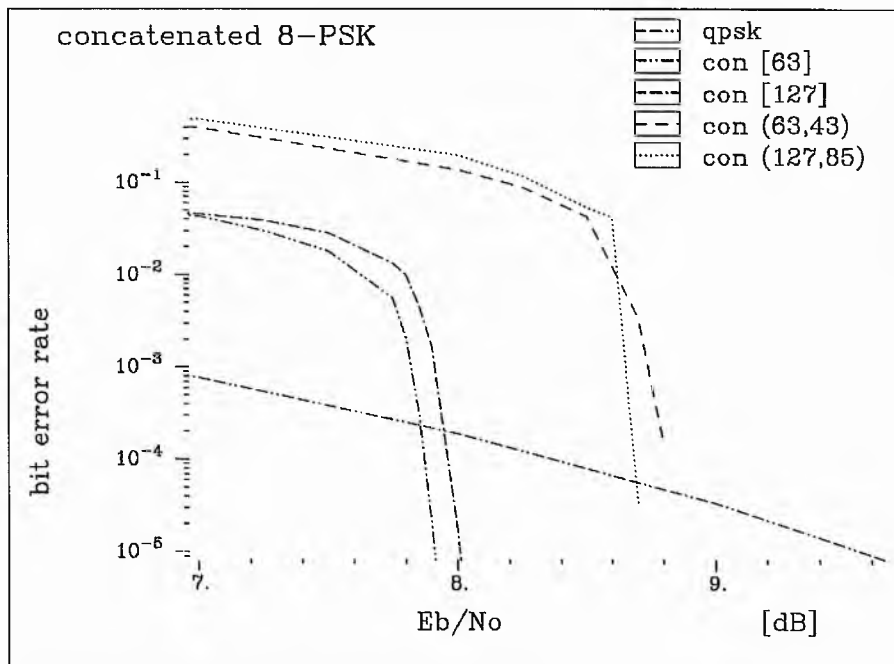
Figure 6.24 shows error performances of concatenated schemes with an RS(511, 443) code as the outer code and Reed Solomon coded 8-PSK modulation as the inner code with code length of 127 and 63. We can see that at a BER of 10^{-3}-10^{-5}, a concatenated scheme using partitioned Reed Solomon coded QPSK modulation as the inner code has at least 0.75 dB coding gain over that using non-partitioned with the same code length. Here, we also can see that the performance of concatenated schemes is very influenced by the outer codes.

6.6.3. Conclusion for Concatenated Schemes

Over a Rayleigh fading channel:

At a BER of 10^{-5}, the concatenated schemes have at least 2.5 dB coding gain over the non-concatenated schemes.

Concatenated schemes using, as the inner code, Reed Solomon coded QPSK modulation with code length of 63 have less than 0.5 dB coding gain over concatenated schemes using an inner code with code length of 31. Also concatenated schemes using, as the inner code, Reed Solomon coded 8-PSK modulation with code length of 127 have less than 0.5 dB coding gain over concatenated schemes using an inner code with code length of 63.

At a BER of 10^{-5}-10^{-6}, a concatenated scheme using partitioned Reed Solomon coded QPSK modulation as the inner code has 0.25 dB coding gain over non-partitioned with

the same code length. At a BER of 10^{-5}, a concatenated scheme using partitioned Reed Solomon coded QPSK modulation as the inner code has less than 1 dB coding gain over non-partitioned with the same code length. From these results, we can see that the performance of concatenated schemes is very influenced by the outer code.

The curves of BER against E_b/N_0 for concatenated schemes have much sharper cut-off than non-concatenated schemes. Thus, the concatenated schemes will have large coding gain over the non-concatenated schemes at very low BER.

Over the Gaussian channel:

At a BER of 10^{-5}, the concatenated schemes using, as an inner code, partitioned Reed Solomon coded modulation have less than 1 dB coding gain over the non-concatenated schemes. Concatenated schemes using, as an inner code, non-partitioned Reed Solomon coded modulation have less than 1 dB coding gain over the non-concatenated schemes at a BER of 10^{-4}.

However, the curves of BER against E_b/N_0 for concatenated schemes have much sharper cut-off than non-concatenated schemes. Thus, the concatenated schemes will have large coding gain over the non-concatenated schemes at very low BER.

At BER above 10^{-5}, the concatenated schemes using, as an inner code, partitioned Reed Solomon coded modulation with the same signal set have almost the same performance. Therefore, the performance of concatenated schemes is very influenced by an outer code.

At a BER 10^{-4}-10^{-5}, the concatenated schemes using, as an inner code, partitioned Reed Solomon coded QPSK modulation have 0.5 dB coding gain over the concatenated codes using, as an inner code, non-partitioned Reed Solomon coded QPSK modulation, with the same code length.

At a BER 10^{-4}-10^{-5}, the concatenated schemes using, as an inner code, partitioned Reed Solomon coded 8-PSK modulation have 0.8 dB coding gain over the concatenated codes using, as an inner code, non-partitioned Reed Solomon coded 8-PSK modulation with the same code length.

CHAPTER 7

CONCLUDING REMARKS

This thesis has examined the construction of Reed Solomon coded modulation which is robust for the Gaussian channel and a Rayleigh fading channel. Coded modulation is an attractive proposition for improving the performance of digital transmission systems without increasing the transmitted power or the required bandwidth, with the first such schemes having been designed for the Gaussian channel by maximising Euclidean distance. More recently, the increasing interest in digital mobile-radio systems has led to the consideration of coded modulation for fading channels. Analysis of coded modulation for fading channels has shown that the code performance depends strongly on its minimum Hamming distance (the *code diversity*) rather than on the minimum Euclidean distance of the code.

The designs of Reed Solomon coded modulation for the Gaussian channel and a Rayleigh fading channel have been studied. Then the error performance of these schemes has been analysed using simulation. The performance of Reed Solomon coded modulation was compared with other coded modulation schemes. We need to establish comparisons between the many different methods described to see if there are any general conclusions to be drawn about which is best.

Section 7.1 summarises the achievements of this research, then in section 7.2 the comparison of the proposed schemes with other coded modulation schemes is represented. Finally in section 7.3, some further work is suggested.

7.1. SUMMARY OF THE RESEARCH

Two approaches have been applied to Reed Solomon coded modulation. The first approach was that a Reed Solomon code was combined with an MPSK signal set using Gray code mapping. This approach is called Reed Solomon Coded modulation not based on set partitioning. There were three methods generalising this approach: in the first method, the MPSK signal set used for modulation does not correlate with the finite field over which the code is defined. then in the second method, a Reed Solomon code, defined over $GF(2^m)$, is combined with a 2^m-PSK signal set. Finally in the third method, each symbol of the Reed Solomon code consists of the concatenation of y channel symbols. This approach was the baseline schemes which would be compared with the proposed schemes, Reed Solomon coded modulation based on set partitioning.

The second approach to coded MPSK with $M = 2^m$ was multilevel Reed Solomon coding which is called Reed Solomon coded modulation based on set partitioning. In this case each of the m bits defining an MPSK symbol was coded and decoded by different Reed Solomon codecs (called component codes). The set partitioning principle which was proposed by Ungerboeck was applied to define subsets with distances Δ_i, $(i = 1$ to $m)$ that are nondecreasing with i. The component-code configuration for specific code length must be find to have a code rate of $R_c = {}^{m-1}\!/_m$.

Each of the m bits defined a subset and was decoded in multistage decoding schemes. In these methods component codes were decoded sequentially stage by stage and with decoded information passed from one stage to the next stage. The main case of interest here was using a block encoder and a block decoding algorithm for each component code of a multilevel modulation code. The novel idea was that in the receiver, a rotated 2^{m+1}-PSK detector will be used if the transmitter uses a 2^m-PSK modulator. The advantage of using the rotated 2^{m+1}-PSK signal set is that the signal point gives additional information of direction to determine the closest 2^m-PSK region having a required sublabel to another 2^m-PSK region in which the received rotated 2^{m+1}-PSK signal point falls in if a decoder detects a bit error.

Approaches for multistage decoding of Reed Solomon codes have been considered. The time domain technique would be better than the frequency domain technique for multistage decoding if we assume that the frequency domain and the time domain techniques have the same degree of computational complexity. Frequency domain decoding technique must convert the frequency domain output-codeword to time domain codeword to pass information from one stage to the next stage.

The designs of Reed Solomon coded modulation schemes for the Gaussian channel (i.e. choice of the code configurations which were suitable for this channel) have been studied. Unlike block coded modulation using binary codes, the minimum Hamming distance of each level component-code could not determined using an equation which was used to find the minimum squared Euclidean distance, D_{min}^2. Therefore, the error performances of many component-code configurations were used to find good component-code configurations for specific code length.

The designs of Reed Solomon coded modulation schemes for a Rayleigh fading channel have also been studied. It was found that these schemes were different from those for the Gaussian channel in that good codes have configurations in which all component codes had the same minimum Hamming distance because the fading phase is uniformly distributed random process.

Reed Solomon coded modulation schemes were applied to Orthogonal Frequency Division Multiplexing (OFDM) transmissions. In OFDM signals, the sidebands of the individual carriers are overlapped and the signals can still be received without adjacent carrier interference. This results in a lowering of the spectrum efficiency compared with Frequency Division Multiplexing. This approach consists in splitting the information to be transmitted into a large number of elementary sub-channels each carrying a low bit-rate. This approach could resolve the problem in mobile-communication environment in which transmission of high bit-rates (several Mbit sec^{-1}) is a risky process.

Concatenated schemes with Reed Solomon coded modulation as an inner code and an RS(511, 443) code as an outer code were proposed as coding schemes for OFDM systems. An RS(511, 443) code was chosen as an outer code so that it could correct several sequences of the inner code for some Reed Solomon coded modulation schemes. The error performance of these concatenated codes has been analysed over the Gaussian channel and a Rayleigh fading channel. It was seen that over the Gaussian channel, the concatenated schemes were suitable for very low bit error rate requirements and over a Rayleigh fading channel, the concatenated schemes had large coding gain over the non-concatenated at BER of 10^{-4}-10^{-5}.

As the last step of this research, a design of a scheme for reducing the Peak-to-Mean Envelope Power Ratio (PMEPR) of OFDM systems was investigated. The main disadvantage of OFDM systems is that they have high PMEPR. This leads to non-linear effects in the RF amplification stages which will give rise to intermodulation products that may interfere with signals in adjacent bands on wireless communications.

Multiphase complementary code pairs of length 2 have been proposed to reduce the PMEPR of MPSK and QAM OFDM. Complementary sequences are pairs of sequences for which the sum of autocorrelation functions is zero except for the main peak at zero shift. The complementary sequence results in 0 dB PMEPR of MPSK OFDM systems and low PMEPR of QAM OFDM systems without redundancy. The IDFT output signals using multiphase complementary code pairs of length 2 can be extended to have a large number of carriers.

7.2. COMPARISONS OF CODED MODULATION SCHEMES

The error performance over the Gaussian channel of Reed Solomon coded modulation schemes has been analysed. The performance of Reed Solomon coded modulation based on set partitioning was compared with Reed Solomon coded modulation not based on set-partitioning, then multistage Reed Solomon coded modulation using Gray mapping and finally with coded modulation schemes using binary codes, Reed Muller codes. Performance for coded QPSK and 8-PSK modulation was evaluated.

In multistage Reed Solomon coded modulation using Gray mapping, each of the m bits defining an MPSK symbol was coded and decoded by different Reed Solomon codecs, where $M = 2^m$. The bits-to-signal mapping was achieved through Gray Mapping. Multistage decoding schemes were not used in this approach. At the output of demodulator, symbols were converted to binary signals using Gray Mapping. Then, the signals were divided to m Reed Solomon decoders by serial to parallel converter.

Block coded MPSK modulation using Reed Muller codes required the same approaches. At the first approach, Reed Muller code having code rate $R_c = \frac{m}{(m+1)}$ was combined with a 2^{m+1}-PSK signal set. In this combination the code rate was chosen such that the rate of the coded scheme was the same as the uncoded one (2^m-PSK). At the second approach, Reed Muller codes were used for component codes. It used similar multistage decoding procedure for decoding the received codewords.

Reed Solomon coded modulation based on set partitioning was better than not based on set partitioning, multistage Reed Solomon coded modulation based on Gray mapping and Reed Muller coded modulation.

The performance of Reed Solomon coded modulation based on set partitioning has also been compared with Reed Solomon coded modulation not based on set-partitioning, then multistage Reed Solomon coded modulation using Gray mapping and finally with coded modulation schemes using binary codes, Reed Muller codes. The results of Reed Solomon coded modulation not based on set-partitioning schemes were also compared with bit-interleaved trellis coded modulation proposed by Zehavi and with robust trellis coded modulation proposed by Sundberg and Seshadri. Bit-interleaved trellis coded modulation schemes and robust trellis coded modulation schemes proposed by Sundberg and Seshadri are modification of trellis coded modulation schemes [Ungerboeck, 1982] which are designed by maximising the minimum Euclidean distance of the schemes. They are designed for the Rayleigh fading channel by maximising the code diversity of the schemes.

Reed Solomon coded modulation based on set partitioning performs better than, or at least as well as not based on set partitioning, performs better 1.25 dB than multistage Gay-mapped RS coded modulation, and performs better or much better than Reed Muller coded modulation.

Compared with bit-interleaved coded modulation proposed by Zehavi, the performance of partitioned Reed Solomon coded 8-PSK modulation with code length of 127 is comparable to that of bit-interleaved coded 8-PSK modulation with a 16-state decoder. Then compared with Sundberg-Seshadri coded modulation, the performance of partitioned Reed Solomon coded 8-PSK modulation with code length of 127 is comparable to that of three-level component codes using a 16-state decoder.

Finally, we can see that by matching the configuration of component codes with the channel characteristics, it is shown that Reed Solomon coded modulation based on set partitioning is robust for the Gaussian and a Rayleigh fading channel.

7.3. FURTHER WORK

[Shin, 1994] proposed Reed Solomon codes using soft decision trellis decoding which could give at least 2 dB coding gain over hard decision decoding at moderate bit error rates on the Gaussian channel. However, the complexity of such a decoder is often prohibitive. [Shin, 1994] and [Honary *et al.*, 1993] have done investigations on reducing the complexity of trellis decoding.

The error performance of Reed Solomon coded modulation using a soft decision trellis decoding method will have larger coding gain over using hard decision Reed Solomon codes for the Gaussian channel. However, we can use soft decision trellis decoding only if it is computationally feasible. At moderate bit error rates, non-partitioned Reed Solomon coded QPSK modulation using a soft decision trellis decoding method could give at least 2 dB coding gain over hard decision non-partitioned Reed Solomon coded QPSK modulation.

[Hagenaeur, 1980] proposed a method which could improve the performance of trellis decoding over fading channels by utilising the appropriate decoding metric which is calculated based on the channel state information. Further developments of Reed Solomon coded modulation using soft decision trellis decoding into application on time-varying channels by adapting Hagenauer's idea would be valuable.

This thesis gives a preliminary investigation into reducing the PMEPR of OFDM systems using complementary code pairs of length 2 in which the IDFT output signals can be extended. Further developments of OFDM systems using this approach would be valuable. This will give a solution to OFDM systems for mobile communications.

[Hirosaki, 1981] and [Vahlin & Holte, 1996] have done investigation on filter bank OFDM (without Fourier transform); thus the combination of OFDM using complementary code pairs of length 2 with Fourier transform and filter bank OFDM could be a subject for future work.

APPENDIX A - COSSAP

COSSAP is an advanced integrated design, simulation and implementation environment for communication systems. COSSAP provides facilities such as hierarchical block diagram editor, a stream driven simulation engine, an interactive data display utility and a simulation report generator.

Implementation of a system in COSSAP involves constructing the system using either the primitive models available in the libraries, or hierarchical models, or models created by the user (using the programming language C). These models are connected via signals, each model must also be appropriately configured. The system is then ready for simulation. The results of the simulation can then be viewed using the COSSAP CHART environment, this allows the results to be viewed in a number of ways, such as waveforms, graphs, eye diagram, scatter diagram etc.

The COSSAP operation is such that a model will only operate when sufficient signal elements are available at its input. It does not depend on a defined time base, but the stream driven simulation engine.

REFERENCES

Arai, T., "High Capability Error Correction LSI for CD Player and CD ROM," *IEEE Transactions on Consumer Electronics*, vol CE-30, no. 3, pp.353-359, August 1984.

Atungsiri, S. A., Smith, C. J., Asjadi, G. H., Kondoz, A. M. and Evans, B. G., "DSP Implementation of Soft RS Codes For Land Mobile Speech Communications," *Proceedings of International Symposium. on Communication Theory and Applications*, September 1991.

Beauchamp, K. G., *Transforms for Engineers: A Guide to Signal Processing*, Clarendon Press, Oxford, 1987.

Beauchamp, K. G., *Walsh Functions and Their Applications*, Academic Press, London, 1975.

Biglieri, E., Divsalar, D., McLane, P. J. and Simon, M. K., *Introduction to Trellis Coded Modulation with Applications*, Macmillan Publishing Company, 1991.

Biglieri, E., Caire, G., Taricco, G. and Ventura-Traveset, J., "Coding and modulation for the fading channel: the quest for robustness," *The Fifth ESA Intl. Workshop on DSP techniques Applied to Space Communication*, Barcelona, pp. 8.1-89, Oct 1996.

Blahut, R. E., *Theory and Practice of Error Control Codes*, Addison Wesley, Reading, Massachusetts, 1983.

Boyd, S., "Multitone Signals with Low Crest Factor," *IEEE Transactions on Circuits and Systems*, vol. CAS-33, no. 10, pp. 1018-1022, 1986.

Chang, R. W., "Synthesis of Band-limited Orthogonal Signals for Multichannel Data Transmission," *Bell Sys. Tech. J.*, vol. 45, December 1966

Chang, R. W. and Gibby, R. A., "A Theoretical Study of Performance of an Orthogonal Multiplexing Data Transmission Scheme," *IEEE Transactions on Communication Technology*, vol. COM-16, no. 4, pp. 529-540, 1968.

Chow, J. S., Cioffi, J. M. and Bingham, J. A. C., "Equalizer Training Algorithms for Multicarrier Mudulation Systems," *IEEE International Conference on Communications*, Piscataway, pp. 761-765, 1993.

Chow, J. S., Tu, J. C. and Cioffi, J. M., "A Discrete Multitone Transceiver System for HDSL Applications," *IEEE Journal on Selected Areas in Communications*, vol. 9, no. 6, pp. 895-908, 1991

Clark, G. C. and Cain, J. B., *Error-Correction Coding for Digital Communications*, Plenum Press, New York, 1981.

Cusack, E. L., "Error Control Codes for QAM Signalling," *Electronics Letters*, vol. 20, pp. 62-63, Jan. 1984.

Elias, P., "Coding for Noisy Channels," *IRE Conv. Rec.*, pt. 4, pp.37-46, 1955.

Farrell, P. G., "Coding As a Cure For Communication Camalities: The Successes and Failures of Error Control," *Electronic and Communications Engineering Journal*, vol. 6, no. 2, pp. 213-220, 1990.

Forney, G. D., *Concatenated Codes*, MIT Press, Cambridge, 1966.

Frank, R. L., "Polyphase Complementary Codes," IEEE Transactions on Information Theory, vol. IT-26, no. 6, pp. 641-647, 1980.

Friese, M., "Multicarrier Modulation with Low Peak-to-Average Power Ratio," *Electronics Letters*, vol. 32, pp. 713-714, 1996.

Hagenauer, J., "Viterbi Decoding of Convolutional Codes for Fading and Burst Channels," *Proc. Int. Zurich Seminar on Digital Communications*, Zurich, pp. G2.1-G2.7, 1980.

Hamming, R. W., "Error Detecting and Error Correcting Codes," *Bell Sys. Tech. J.*, 29(2), pp.147-160, 1950.

Hirosaki, B., "An Orthogonally Multiplexed QAM System Using the Discrete Fourier Transform," *IEEE Transactions on Communications*, vol. COM-29, no. 7, pp. 982-989, 1981.

Hodgart, M. S., "Efficient Coding and Error Monitoring For Spacecraft Digital Memory," *International Journal of Electronics*, vol. 73, no. 1, pp.1-36, 1992.

Honary, B. and Markarian, G., "Low Complexity Trellis Decoding," *Electronics Letters*, vol. 29, no. 12, pp. 1114-1116, 1993.

Imai, H. and Hirakawa, S., "A New Multilevel Coding Method Using Error Correcting Codes," *IEEE Transactions on Information Theory*, vol. IT-23, no. 3, pp.371-377, May 1977.

Jakes, W. C., *Microwave Mobile Communications*, John Wiley & Sons, New York, 1974.

Jamali, S. H. and Le-Ngoc, T., *Coded Modulation Techniques for Fading Channels*, Klower Academic Publishers, Boston, 1994.

Jones, A. E. and Wilkinson, T. A., "Combined Coding for Error Control and Increased Robustness to System Nonlinearities in OFDM," *IEEE VTC96*, pp. 904-908, 1996.

Jones, A. E., Wilkinson, T. A. and Barton, S. K., "Block Coding Scheme for Reduction of Peak to Mean Envelope Power Ratio of Multicarrier Transmission Schemes," Electronics Letters, vol. 30, pp. 2098-2099, 1994.

Liu, K. Y. and Lee, J., "Recent Results on the Use of Concatenated Reed-Solomon/Viterbi Channel Coding and Data Compression For Space Communications," *IEEE Transactions on Communications*, vol. COM-32, no. 5, pp.518-523, May 1984.

MacWilliams, F. J. and Sloane, N. J. A., *The Theory of Error-Correcting Codes*, North-Holland Publishing Co., London, 1977.

Maral, G. and Bousquet, M, *Satellite Communications Systems 2nd ed.*, John Wiley & Sons, London, 1993.

Massey, J. L., "Coding and Modulation in Digital Communications," *1974 International Zurich Seminar on Digital Communications*, Zurich, March 1974.

Michaelson, A. M. and Levesque, A. H, *Error-Control Techniques for Digital Communication*, John Wiley & Sons, New York, 1985.

Mortimer, B. C., et al., "The Design of a High-Performance Error-Correcting Coding Scheme for the Canadian Broadcast Telidon System Based on Reed Solomon Codes," *IEEE Transactions on Communications*, vol. COM-35, no.11, pp.1113-1123, November 1987.

Odenwalder, J. P., *Error Control Coding Handbook*, Linkabit Corporation, San Diego, 1976.

O'Neill, R. and Lopes, L. B., "Performance of Amplitude Limited Multitone Signals," *IEEE 44th VTC*, pp. 1675-1679, 1994.

O'Neill, R. and Lopes, L. B., "Envelope Variations and Spectral Splatter in Clipped Multicarrier Signals," IEEE VTC95, pp. 71-75, 1995.

Pollard, J. M., "Encoding and Error-Correction procedures for the Bose-Chaudhuri Codes," *Mathematics of Computation*, vol. 25, no. 114, pp.365-374, April 1971.

Popovic, B. M., "Synthesis of Power Efficient Multitone Signals with Flat Amplitude Spectrum," *IEEE Transactions on Communications*, vol. 39, no. 7, pp. 1031-1033, 1991.

Proakis, J. G., *Digital Communications 3rd ed.*, MacGraw-Hill Inc., New York, 1995.

Rajpal, S., *et al.*, "Multidimensional MPSK Trellis Codes," *Proc. 14th Symposioum. Infor. Theory and Its Applicat.*, Vol. 1, pp.393-396, December 1991.

Reed, I. S. and Solomon, G., "Polynomial Codes Over Certain Finite Fields," *Journal of the Society of Industrial Applied Mathematics*, vol. 8, no. 2, pp.300-304, June 1960.

Saltzberg, B. R., "Performance of an Efficient Parallel Data Transmission System," *IEEE Transactions on Communication Technology*, vol. COM-15, pp. 805-811, 1967.

Salz, J. and Weinstein, S. B., "Fourier Transform Communication System," Presented at the Ass. Comput. Machinery Conf. Computers and Communication, Pine Mountain, Ga., October 1969.

Sayegh, S. I., "A Class of Optimum Block Codes in Signal Space," *IEEE Transactions on Communications*, vol. COM-34, no. 10, pp.1043-1045, October 1986.

Shannon, C. E., "A Mathematical Theory of Information, " *Bell Sys. Tech. J.*,27, pp. 379-423 & 623-656, 1948.

Shelswell, P., "The COFDM Modulation System: the Heart of Digital Audio Broadcasting," *Electronics & Communication Engineering Journal*, pp. 127-136, June 1995.

Shin, S. K., *Trellis Decoding of Reed Solomon Codes*, Ph.D. Thesis, University of Surrey, Guildford, 1994.

Singleton, R. C., "Maximum Distance q-nary Codes," *IEEE Transactions on Information Theory*, IT-10, pp.116-118, 1964.

Sivaswamy, R., "Multiphase Complementary Codes," *IEEE Transactions on Information Theory*, vol. IT-24, no. 5, pp. 546-552, 1978.

Skar, B., *Digital Communications: Fundamentals and Applications*, Prentice-Hall International Inc., New Jersey, 1988.

Sundberg, C. W. and Seshadri, N., "Coded Modulations for Fading Channels: An Overview," *European Transaction on Telecommunications and Related Technologies*, vol. 4, no. 3, pp. 309-324, May-June 1993.

Sweeney, P., *Error Control Coding: An Introduction*, Prentice Hall Inc., 1991.

Takata, T., Ujita, S., Kasami, T. and Lin, S., "Multistage Decoding of Multilevel Block M-PSK Modulation Codes and Its Performance Analysis," *IEEE Transactions on Information Theory*, IT-39, no. 4, 1204-1218, July 1993.

Taubin, F. A. and Trofimov, A. N., "Pipeline Decoding of embeded Trellis Codes: Error Tolerance Analysis," *Probl. Peredach. Inform.*, vol. 26, no. 4, pp.56-70, October-December 1990.

Ungerboeck, G., "Channel Coding with Multilevel/phase Signals," *IEEE Transactions on Information Theory*, vol. IT-28, pp.56-67, January 1982.

Ungerboeck, G., "Trellis-Coded Modulation with Redundant Signal Sets. Part I: Introduction," *IEEE Communications Magazine*, vol. 25, pp.5-12, February 1987.

Ungerboeck, G. and Csajka, I., "On Improving Data-Link Performance by Increasing the Channel Alphabet and Introducing Sequence Coding," *1976 International Symposium on Information Theory*, June 1976.

Vahlin, A. and Holte, N., "Optimal Finite Duration Pulses for OFDM," *IEEE Transactions on Communications*, vol. 44, no. 1, pp. 10-14, 1996.

Van Eetvelt, P. W. J., Shepherd, S. J. and Barton, S. K., "Distribution of Peak Factor in QPSK Multi-Carrier Modulation, " *Wireless Personal Communications*, vol. 2, pp. 87-96, 1995.

Van Eetvelt, P. W. J., Wade, G. and Tomlinson, M., "Peak to Average Power Reduction for OFDM Schemes by Selective Scrambling," *Electronics Letters*, vol. 32, pp. 1963-1964, 1996

Van Nee, R. D. J., "OFDM Codes for Peak-to-Average Power Reduction and Error Correction," *1996 IEEE Global Telecom. Conf. Record*, pp. 740-744, 1996.

Watkinson, J., *The Art of Digital Audio*, Focal Press, London, 1988.

Weinstein, S. B. and Ebert, P. M., "Data Transmission by Frequency-Division Multiplexing Using the Discrete Fourier Transform," *IEEE Transactions on Communication Technology*, vol. COM-19, no. 5, pp. 628-634, 1971.

Wilkinson, T. A. and Jones, A. E., "Minimisation of the Peak to Mean Envelope Power Ratio in Multicarrier Transmission Schemes by Block Coding," *IEEE VTC95*, pp. 825-831, 1995.

Woerz, T. and Fazel, "Comparison of Different Decoding Strategies for Block Coded Modulation," *1992 URSI Int. Symp. Signals, Sys. and Electronics*, Paris, 1992, pp. 117-120.

Woerz, T. and Hagenauer, J., "Decoding of *M*-PSK-Multilevel Codes," *European Transaction on Telecommunications and Related Technologies*, vol. 4, no. 3, pp. 299-308, May-June 1993.

Woerz, T. and Hagenauer, J., "Multistage Coding and Decoding for a M-PSK System," *Proc. IEEE Global Telecommun. Conf.*, pp.698-703, December 1990.

Yamaguchi, K. and Imai, H, "Highly Reliable Multilevel Channel Coding System Using Binary Convolutional Codes," *Electronics Letters*, vol. 33, pp.939-943, August 1987.

Zehavi, E., "8-PSK Trellis Codes for a Rayleigh Channel", *IEEE Transactions on Communications*, vol. 40, no. 5, 1992.